

Master thesis

Quantitative paleoecology and gradient analysis of the Rytteråker Formation, Lower Silurian, Oslo region

Searching for ecosystem change across a spatially and temporally complex rock record

Audun Rugstad

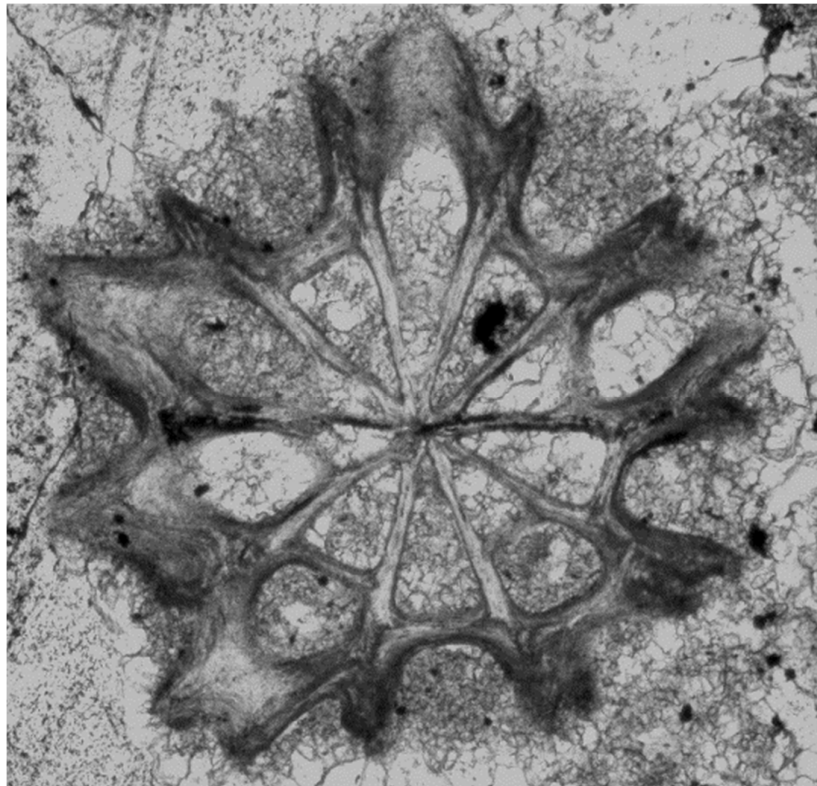
Bioscience: Ecology and evolution
60 credits

Institute for Bioscience / Norwegian Center for Paleontology
Faculty of Mathematics and Natural Sciences / Natural History Museum



Quantitative paleoecology and gradient analysis of the Rytteråker Formation, Lower Silurian, Oslo Region

Searching for ecosystem change across a spatially and temporally complex rock record



Audun Rugstad,
Institute for Bioscience / Natural History Museum
Master thesis, 60 credits

Supervisors: Øyvind Hammer, Hans Arne Nakrem, Glenn-
Peter Sætre

August, 2022



N Natural History
Museum

Dog hertil kræves så minutiøse undersøgelser, at et forsøg i denne retning endnu ikke kunde gøres.

–Johan Kiær (1908), in describing the need for high-resolution biological facies studies of the Silurian in the Oslo region

Acknowledgements

“Life can only be understood backwards, but must be lived forwards”, is an insight I find to be true not only for the science of our planet’s awe-inspiring history, but also for my own journey to become part of it. That I would end up following the dreams of my five-year old self was certainly not something I could have imagined only a few years ago, but I am nevertheless eternally grateful for doing so with this master thesis. The biggest thank you goes to my two main supervisors Øyvind Hammer and Hans Arne Nakrem, for opening my mind to the science of paleontology, providing me with a challenging and rewarding master project, always taking the time to answer my questions, and for giving extremely helpful feedback on my writing and research. I also owe a huge thanks to Rune Halvorsen from the GeCo-group at NHM for introducing me to the strange and wonderful land of ecological ordinations and gradient analysis, and for being extraordinarily helpful in the statistical part of this project. Thank you also to Glenn-Peter Sætre for being my co-supervisor and for constructive writing feedback, and to Salahalldin Akhavan at the Geology department for preparing my thin sections. Also Nicola Möller and Nils Martin Hanken, for taking the time to assist and inspire me with their great knowledge and enthusiasm for the fossils and geology of the Oslo region. In this regard I also have to mention Steinklubben and the passionate souls there that first helped spark and nurture my love for geology and paleontology many years ago, with their educational and memorable fieldtrips in the Oslo region. Your work certainly paid off in this case, I think.

Thanks also so much to everyone at Økern for a great studying environment, amazing facilities, and many lovely barbeque lunches. A special thank you to my fellow master students these two years: Mees Floris Auener, Synnøve Mo Saugen, Trym Ekhaugen, Thomas Bang Hansen, Emil Bang and Maren Stokke, for all the nice conversations, lunches, geology help, shared joys and frustrations, and some truly legendary boardgame nights.

Finally, thank you so much to my girlfriend Mari for always being there for me with your love and support, never failing to cheer me up when things got a bit overwhelming, and for enduring all my frustrated monologues about bryozoan growth forms over the breakfast table these last two years. And last but not least, to my mom and dad, for all your incredible support, and for always teaching me to be open and curious about the world around me, both in mind and heart. I love you all.



Paleontologist in the field, ca. 2003 (left), and paleontologist in the field, ca 2021 (right)

Abstract

In the present study, the temporal and spatial paleoecology of the Lower Silurian Rytteråker Formation in the Oslo region, is explored through multivariate gradient analysis of a novel dataset of stratigraphically collected acetate peels from two localities in the Oslo Region, as well as ordination-based reanalysis of two previously published datasets.

By applying up to four different ecological ordination methods in parallel in a comparative, integrated approach – on both raw and abundance-scale weighted data, a single robust high-level faunal and environmental gradient associated with ordination axis one was identified in both the newly sampled and historical datasets. In both the novel acetate peel dataset and the historical dataset of bedding plane point-count data, the gradient appeared to be primarily structured by the abundances of pentamerid brachiopods, and secondarily by overall fossil diversity and richness.

In-sample environmental proxy variables from the datasets, as well as newly gathered supplementary data in the form of elemental XRF measurements, magnetic susceptibility readings, brachiopod shell orientation measurements and field observations, seem to indicate storm frequency and/or high energy deposition as the most significant complex environmental variable structuring all three primary gradients. As such, the gradients are likely reflective both of real ecological change affecting species distribution, as well as a biases regarding preservation and taphonomy.

As such, the results from this study partially challenge previous interpretations of the fauna of the Rytteråker Formation as being primarily controlled by depositional depth. Although depth would in some cases also be correlated with benthic storm frequency, the prospect of a barrier patch reef/shoal-lagoonal system in the area does not make this connection a necessity. It also provides a strong case for the multiple parallel ordination approach as a useful tool for discerning ecologically interpretable gradients both from new and historic datasets. However, as indicated disparities in diversity and richness, the novel acetate peel study design applied here seems to be more appropriate for discerning faunal gradients in localities that are generally more fossil rich (i.e. higher depositional energy), while larger-scale macrofossil surveys akin to some of the historical datasets, might be more appropriate for energetically quieter depositional environments.

The link between periodic wave turbulence and faunal change also implies some interesting possible parallels between the underlying environmental factors influencing Paleozoic and modern benthic soft-substrate ecosystem gradients, which could provide a basis for future studies.

Table of contents

1	Introduction.....	1
1.1	<i>Background and motivation.....</i>	1
1.2	<i>Aim of thesis.....</i>	3
1.2.1	Methodological research questions.....	4
1.2.2	Paleoecological research questions.....	7
1.2.3	Preliminary hypotheses.....	10
1.3	<i>What is ordination-based gradient analysis?.....</i>	11
1.3.1	Underlying principles.....	11
1.3.2	Indirect ordination methods.....	12
1.3.3	Comparing ordinations.....	18
1.3.4	Interpretation and fitting of environmental variables.....	18
1.4	<i>Ecological setting.....</i>	19
1.4.1	Earth system dynamics in the Silurian.....	19
1.4.2	Taxonomic composition and diversity of marine faunas.....	21
1.4.3	Structure of benthic ecosystems.....	22
1.5	<i>Geological setting.....</i>	24
1.5.1	The Oslo Region.....	24
1.5.2	The Lower Silurian in the Oslo Region.....	24
1.5.3	Historical definition of the Rytteråker Formation.....	25
1.5.4	Current definition of the Rytteråker Formation.....	27
1.5.5	Regional variation.....	27
1.5.6	Paleogeographic and paleoenvironmental interpretation.....	29
2	Materials and methods.....	31
2.1	<i>Fieldwork.....</i>	31
2.1.1	Toverud farm, road-cutting.....	31
2.1.2	Ulvøya, north-west shoreface.....	31
2.1.3	Magnetic susceptibility readings.....	34
2.2	<i>Lab work.....</i>	34
2.2.1	Preparation of samples.....	34
2.2.2	Acetate peels.....	35
2.2.3	Thin sections.....	36
2.2.4	XRF scans.....	36
2.3	<i>Data handling and analysis.....</i>	36
2.3.1	Subplot frequency count of acetate peels.....	36
2.3.2	Bioturbation measurements.....	39
2.3.3	Lithological classification.....	40
2.3.4	Assignment of ecological categories.....	42
2.3.5	Shell orientations.....	42
2.3.6	Reanalysis of Malmøykalven and Jong macrofossil data.....	42
2.3.7	Reanalysis of Bjerkøya bedding plane point counts.....	43
2.4	<i>Statistics.....</i>	43

2.4.1	Shell orientation modelling	44
2.4.2	Abundance/diversity metrics	44
2.4.3	Ordinations	44
3	Results	46
3.1	<i>Toverud and Ulvøya supplementary data</i>	<i>46</i>
3.1.1	Macrofossil observations in the field	46
3.1.2	Magnetic susceptibility readings.....	49
3.1.3	Toverud XRF data.....	50
3.1.4	TOV2 Shell orientation analysis.....	51
3.1.5	Overview of taxon morphology in acetate peels and thin sections	52
3.1.6	Summary of organism abundance data	60
3.1.7	Diversity metrics	63
3.1.8	Ecological occupancy.....	64
3.1.9	Ordination of raw-data acetate peels.....	65
3.1.10	Ordination of abundance-scale weighted data	70
3.1.11	Lithological and faunistic variables measured in the plots.....	74
3.2	<i>Reanalysis of Malmøykalven and Jong macrofossil data</i>	<i>77</i>
3.2.1	Coral group abundance in the plots.....	77
3.2.2	Ordination of lithological matrix and growth form measurements	78
3.2.3	Correlation between ordinations.....	80
3.2.4	Correlation between ordinations and coral abundances	80
3.3	<i>Reanalysis of Holmestrand bedding plane point counts</i>	<i>82</i>
3.3.1	DCA and NMDS ordinations.....	82
3.3.2	Correlation between ordinations.....	84
3.3.3	Correlation with lithological/trace fossil variables.....	85
4	Discussion.....	86
4.1	<i>Toverud and Ulvøya supplementary data</i>	<i>86</i>
4.1.1	Macrofossil observations.....	86
4.1.2	Magnetic susceptibility readings.....	87
4.1.3	Toverud XRF data.....	88
4.1.4	Toverud shell orientation analysis.....	88
4.2	<i>Toverud and Ulvøya acetate peel study.....</i>	<i>90</i>
4.2.1	Comparison with thin sections.....	90
4.2.2	Morphotaxa abundances and diversity	90
4.2.3	Ecological occupancy.....	92
4.2.4	Comparison of raw-data ordinations	93
4.2.5	Effect of abundance-scale weighting on DCA and NMDS ordinations	97
4.2.6	Relationship to lithological and faunistic variables.....	99
4.2.7	Ordination axis 1 as a complex ecological and preservational gradient	100
4.3	<i>Malmøykalven and Jong macrofossils</i>	<i>105</i>
4.3.1	Stratigraphic abundances and proportions.....	105
4.3.2	PCA and NMDS gradients.....	106
4.4	<i>Holmestrand bedding plane study</i>	<i>107</i>
4.5	<i>Comparison between studies.....</i>	<i>109</i>
4.5.1	Methodological results.....	109
4.5.2	Paleoecological results.....	110

4.6	<i>Summary and conclusion</i>	111
4.6.1	Viability of novel sampling strategy and study design	111
4.6.2	Utility of multiple parallel ordination approach	112
4.6.3	Ordination-based evidence for a depth-controlled ecocline in the Rytteråker Formation...	113
4.6.4	Sources of error and bias	114
4.7	<i>Future perspectives</i>	114
References		117
Appendix		126

1 Introduction

1.1 Background and motivation

In our current century, the threats facing the natural and semi-natural ecosystems of planet Earth are greater than at any time before in human history. Overuse of resources and the destruction and fragmentation of natural habitats, coupled with drastic, rapid and accelerating anthropogenic greenhouse gas emissions and other changes to global biogeochemical cycles, has led to the extinction of animal and plant species at a rate orders of magnitude above what is considered Holocene “background levels” (Ceballos et al., 2015). Many scientists thus argue that we are on a trajectory to the sixth mass extinction event in the Phanerozoic eon (Dirzo et al., 2014). This in turn begs the question of how our current circumstances compare not only to the other “big five” Phanerozoic mass extinctions, but also to smaller climatic, environmental and biotic shifts in Earth’s history, of different magnitudes and characteristics. Scientists have noted that high resolution knowledge of how ecosystems in the deep past functioned and were affected by change, on both local and global levels, may prove to be vital reference points for the present (Schmidt, 2018). Even when their composition, structure and environmental setting differed fundamentally from recent systems, they might provide important insights on how ecosystem resilience, functional diversity and other ecological attributes vary under different biotic and abiotic regimes. The Early Paleozoic Silurian period, with its comparatively “unsettled” biogeochemical cycles and volatile sea-level and climate, has been suggested as an interesting case study in this regard (Calner, 2008).

To answer questions about ecosystem change in the deep past however, there is need for a quantitative framework for studying ecological gradients in the fossil record that allows comparison with present-day ecology, or at least one that speaks the same analytical language. Of all the tools in the paleoecologist’s toolbox, the means of exploratory, multivariate gradient analysis afforded by the various indirect ordination methodologies developed in the last fifty years, stand out as perhaps the most versatile and useful in this regard (Clapham, 2011; Holland, 2005; Shi, 1993). The ability of these methods to condense and display the structure of potentially very large and sprawling multivariate datasets in few dimensions make them well suited for analyzing and inferring hypotheses about the biotic and abiotic environmental factors structuring species distribution in the fossil record.

Fossil assemblages of benthic invertebrates are likely the most taxonomically complete proxies we have for ecosystems in the deep past (Speden, 1966), and are also the most well studied by paleoecologists. Where ordination-based analyses have been used in these studies, they have usually pointed to *relative water depth* as the primary environmental gradient controlling the distribution of taxa. This pattern appears to be consistent throughout the Phanerozoic (Amati & Westrop, 2006; Bush & Brame, 2010; Clapham, 2011; Hendy, 2013; Holland et al., 2001; Webber, 2002), and both confirms most of the assertions of older, more qualitative studies (Boucot, 1975, 1981; Ziegler et al., 1968), as well as studies of recent ecosystems (Tyler &

Kowalewski, 2014; van Son et al., 2014). This gradient also makes sense ecologically, since water depth is typically correlated with a number of other environmental factors such as light conditions, substrate composition, wave energy exposure (shear stress) and oxygen availability (Saeedi et al., 2022).

In this regard, an interesting find is that indirect ordination, and related forms of gradient analysis on species' composition, in some cases seem to be able to detect more subtle depth-related changes in the environment than more "traditional", classificatory schemes of bio- and lithofacies types (Cisne & Rabe, 1978; Hennebert & Lees, 1991; Holland, 2005; Holland et al., 2001; Miller et al., 2001).

However, several unique challenges, concerns and biases also present themselves when applying ordination methods to paleoecological data, as compared to the recent ecology (Alroy, 2015; Shi, 1993). Alroy (2015) mentions disparity between sample sizes, variation in preservation quality and difficulty of identifying taxa as some of the most important. Additionally, sediment lithology and outcrop properties from fossil collection sites also place significant constraints on sampling, as pointed out by Forcino and Stafford (2020). Particularly in the case of limestone successions, some sampling strategies may be unviable due to the hardness and alkalinity of the sediment. The most important of these are systematic pickup of disaggregated, weathered-out fossils, and body fossil identification from bulk-collected, acid-treated samples. Usually, the only workable options for carbonate deposits are either *in situ* studies of exposed bedding-planes and macrofossils (if these are present), or the analysis of stratigraphically collected rock samples in slabs, thin sections or acetate peels. Especially in the latter case, the identification of fossil fragments to a taxonomic resolution below class or order can be time-consuming, challenging and often impossible – which in turn may impact the ordination (Forcino, Stafford, et al., 2012).

Additionally, in many paleoecological studies, only one or at the most two ordination methods are typically used in parallel (with some notable exceptions, e.g. Clapham, 2011; Patzkowsky & Holland, 2016). The analytical tools for ordination comparison and assessment recommended by contemporary ecologists – i.e. multiple parallel ordinations (MPO) with different weighing of abundance scales, correlation tests between axes and ordinations, and assessment of outlier influence (Liu et al., 2008; Økland, 2007; van Son et al., 2014; van Son & Halvorsen, 2014), are rarely employed. While comparative assessments of different parallel (indirect) ordinations cannot in and of itself be used to assess a fit with the "true" underlying ecological gradients (as they are unknown *a priori*), they can still provide valuable insights into the robustness and consistency of the ordination axes' structure. If axis structure is more or less consistent among ordinations, there is a greater reason to assume that the results reflect actual ecological and environmental gradients in the data, rather than "noise" or statistical artifacts (van Son & Halvorsen, 2014). Moreover, when ordination results differ, the MPO approach may help shed light on which properties of the ordination methods and the data produce these differences.

Indeed, this comparative ordination approach may be particularly relevant in paleoecology, precisely due to the “noisiness”, uncertainty and locality-dependency of many paleoecological datasets. Not to mention that paleoecological data often are complex in the sense that they encompass both a spatial and a temporal dimension. Especially for limestone successions lacking in fossil-rich bedding plane exposures, where a limited range of sampling options typically are available (see above), investigating the degree to which comparative ordinations in these cases might nevertheless be able to produce robust and environmentally realistic (e.g. depth structured) gradients in fossil composition, seems to be well worth exploring. Ordination of thin-sections has already shown some promising results in this regard (Hennebert & Lees, 1991). The prospect of extracting more scientific insight from such resources might therefore in turn help us better understand the environmental and ecological factors that have structured some of the most biologically important and active habitats in Earth’s history, particularly in the Paleozoic . It would also provide an opportunity to better our understanding of how different sampling strategies and dataset decisions impact paleoecological ordinations, as they have been demonstrated to do (Forcino et al., 2013; Forcino, Leighton, et al., 2015; Forcino, Richards, et al., 2012).

1.2 Aim of thesis

The central aim of this master thesis is to explore the use of multiple parallel ordinations on a dataset of stratigraphically collected acetate peels from the early Silurian (Llandovery) Rytteråker Formation in the Oslo region – using every tool in the ordination toolbox, so to speak, to investigate whether it is possible to discern a spatial and temporal gradient in the abundances of different high-level morphotaxa identifiable from the samples. The Rytteråker Formation is a shallow marine carbonate succession historically assumed to have been deposited at different paleodepths in a submarine shoal-barrier system during a marine regression and subsequent transgression in the Oslo region approximately 430 Ma ago (Bruton et al., 2010; Möller, 1989). The deposition of the formation also coincides with the poorly understood “Sandvika event”, a relatively minor biodiversity crisis recorded in pelagic graptolites, which also seems to correspond to global $\delta^{13}\text{C}$ -excursion and changes in ocean chemistry around the Aeronian-Telychian boundary (Aldridge et al., 1993; Johnson, 2006; Zhang et al., 2017). To investigate the spatial gradient of species composition, samples will be collected stratigraphically from two different outcrops assumed to have been situated at different paleodepths (see Section 1.5).

In addition to the dataset collected for this study, two macrofossil datasets from previous studies of the Rytteråker Formation, (Keilen, 1985 and Mørk, 1978) will also be reanalyzed with current ordination methodology (Table 1.1). This is done for three reasons: 1) to provide a supplement and contrast to the smaller-scale samples examined in the acetate peels. 2) To provide data from other outcrop localities – namely the Holmestrand and Asker districts (see Section 1.5), and 3) to compare the viability of the ordination approach on different sampling scales and sampling strategies than the one collected for this study, as well as on historical data originally collected without multivariate gradient analysis in mind.

An overview of the main methodological and paleoecological research questions of the study will be outlined in the following sections (1.2.1 & 1.2.2), followed by the preliminary research hypothesis (Section 1.2.3).

Table 1.1. Overview of the different datasets used to perform ordinations in this study, and their most important methodological properties regarding sampling area and sampling strategy.

Dataset	Locality (district)	Sampling substrate	Sampling strategy
This study	Ulvøya (Oslo), Sylling (Ringerike)	Acetate peels from polished slabs (30x20 mm), semi-randomly collected	Subplot frequency counts (40 subplots) of high-level morphotaxa
Keilen (1985)	Malmøykalven (Oslo), Jong (Bærum)	1x2/1x1 m plots (1 meter bedding-parallel and 1 meter bedding-perpendicular) approx. every 5 meters stratigraphically.	Individual count of all tabulate corals (identified to order) and stromatoporoids in each plot, with growth form and surrounding matrix registered for each individual
Mørk (1978)	Bjerkøya (Holmestrand)	0.25x0.25 m squares on 4 adjacent bedding planes	Point count (100 points) of high-level morphotaxa and lithology (=shale, mudstone etc.)

1.2.1 Methodological research questions

1.2.1.1 Viability of morphotaxa categories

Fossil remains in thin sections and acetate peels (also known as *bioclasts* or *skeletal grains*) are only visible in a two-dimensional section, in addition to often being fragmented, disarticulated, and biologically or geologically eroded. This normally makes taxonomic identification of fossil fragments to anything lower than broad class- or order level (e.g.: Crinoidea or Rugosa) unviable. Some paleoecologists argue that such a coarse taxonomic resolution is insufficient to produce reliable, ecologically interpretable ordination axes, when compared to identifications to the genus or family level (Forcino, Stafford, et al., 2012). However, other studies seem to suggest that abundance-counts of fossil fragments identified to class or similar high-level taxonomic categories in thin sections and slabs nevertheless makes it possible to differentiate between different depth-structured Paleozoic carbonate environments, both by graphing the raw data (Klug et al., 2018; Watkins, 1996), and through the inference of depth-related environmental gradients from ordination axes (Hennebert & Lees, 1991).

In this study, a combination of broad taxonomic and easily distinguishable morphological traits assumed to have ecological significance (i.e. brachiopod shell morphology or bryozoan growth form) was used to distinguish 18 fossil organism groups (hereby referred to as *morphotaxa*), in an attempt to capture as much variation in the samples as practically possible. This approach is relatively similar to the concept of *constituent analysis* in carbonate sedimentology (Flügel,

2004), which typically operates with a similar taxonomic resolution of fossil fragments. However, constituent analyses also often include inorganic components of the peels/thin sections (i.e. cement, siliciclastic particles etc.) in the abundance counts, which will not be done in this study (although they will be used to an extent as explanatory environmental variables). A central research question is therefore whether our organismal categories alone are sufficient to produce robust ordinations.

1.2.1.2 Sampling strategy

Two aspects of the paleoecological sampling procedure applied on the samples collected in this study may be considered novel, and will therefore receive special attention. These are: 1) the use of *acetate peels* rather than thin sections as the primary 2D-sampling substrate, and 2) the use of *subplot frequency* as the measure of morphotaxa abundances, rather than raw fossil abundance counts or point counts.

The acetate peel technique is a cheaper and much less time-consuming way of preparing two-dimensional microscopy slides from sedimentary rocks than thin sections (Wilson & Palmer, 1989), and has been recognized as highly effective in studies of carbonate rocks in particular (Brown, 1986; Gutteridge, 1985). Thus, the potential of this method to easily provide large and acceptable quality micro-scale paleoecological datasets from carbonate deposits seems to be worth exploring. The thesis will therefore also contain a short, qualitative comparison between selected acetate peels and thin sections in terms of the ability to describe and identify organism groups.

Similarly, the subplot frequency (SF) counting method is explored here as a potential alternative to the two most common abundance-counting methods otherwise used in paleoecology: raw abundance counts (AC, i.e. count of raw number of visual specimens in an area/plot) and point-intercept counts (PC, i.e. number of intersections of an overlain grid that come into contact with a taxon). AC has been proven effective when counting relatively unfragmented fossils in the same size range, and is also applicable to bulk-sampled fossils as well as bedding planes/microfacies. However, it is argued to be ill-suited when faced with colonial and/or easily disarticulated or fragmented taxa, and in cases with large size-differences between individuals (Bush, Kowalewski, et al., 2007).

With PC, taxa are in principle represented more proportionally to their (calcified) biomass, and it is often the method preferred in microfacies/constituent analysis studies (Bialik et al., 2021; Bonelli Jr. et al., 2006; Watkins, 1996). However, the method is relatively time-consuming, and might easily miss taxa with small individuals in the samples completely. This is because the likelihood of coming into contact with a “grid cross” is proportional with the size of the individual. However, some versions of the methods have addressed this issue by giving all taxa that are present, but not represented by a point-interception, an abundance count of 1 (Mamet et al., 2016). Due to their inherent differences, AC and PC have been shown to produce substantially dissimilar ordination results when applied to bedding-plane point counts in limestone formations (Forcino et al., 2013).

In the SF method, taxon abundance is registered as the sum of presence-absence occurrences in a grid of subplots (in this study: 40 15mm² plots per acetate peel). As such, it might be seen as providing better representation of rare taxa and total presence of individuals, at the cost of being less representative of total biomass. SF is frequently used in vegetation ecology, where it in some nature types has been shown to be less time-consuming and perform equally well or better than PC and other abundance measures when describing overall abundance and species richness (Mamet et al., 2016; Prosser et al., 2003), as well as in producing robust ordination gradients (Økland et al., 2001).

Due to the few and broad morphotaxa categories used in the acetate peel study, as well as the large size difference between organisms in the samples – often on an order of magnitude (e.g. a 5 mm diameter brachiopod and a 0.2 mm diameter ostracod), this “compromise” is assumed to allow as much biotic variation as possible to be represented in the samples. If the SF approach is proven to work successfully here, it might provide an argument for developing the approach to be used more extensively in future paleoecological studies with similar sampling challenges. It might also be interesting to contrast the results from this approach with the point-counts obtained by Mørk (1978) (see Table 1.1), although these were done on a completely different scale (and using slightly different morphotaxa categories), making a direct comparison impossible.

Another important conceptual difference between the PC, SF and AC methods, is that the latter two methods produce topologically open datasets, while PC results are topologically closed datasets, provided all points in the grid are accounted for (Bialik et al., 2021). However, these distinctions involve quite complex mathematical theory which is outside the scope of this thesis and will subsequently not be discussed.

1.2.1.3 Ordination assessment

This study will compare the ordination results obtained by the four most widely used indirect ordination methods in ecology and paleoecology: Principal Component Analysis (PCA), Correspondence analysis (CA), Detrended Correspondence Analysis (DCA) and Non-metric multidimensional scaling (NMDS). As these methods both employ fundamentally different algorithms and different numerical/statistical basis (see Section 1.3), the relative correlation of axis scores between the resulting ordinations on the same dataset may be used as a measure of the robustness of the gradients observed. On the dataset collected for this study, all four methods will be compared on the raw, normalized SF data, and DCA and NMDS compared on abundance-weighted data aimed at assessing the impact of the quantitative versus qualitative aspect of the SF data. For the Malmøykalven/Jong and Holmestrand data, a smaller, dual comparison of ordination methods will be performed. The principal means of comparing the ordinations will be:

- 1) Visual comparison of the ordination scores, both in two-dimensional (ordination axis 1 and 2) ordination plots and biplots (with both plot positions and morphotaxa

- optima shown), color coded by location, and by plotting ordination axis 1 against sampling position, exploring the spatial and temporal dimensions respectively.
- 2) Correlation of the complete ordinations using the Procrustes correlation test statistic (*protest*) (as done by Forcino, Ritterbush, et al., 2015; Peres-Neto & Jackson, 2001)
 - 3) Correlation between the axes, measured using the Kendall's rank correlation coefficient (Kendall's τ) – the non-parametric rank-order coefficient that has been argued to be best fitted to ordination comparison (van Son & Halvorsen, 2014).
 - 4) The influence of outlier plots on the ordination axes, assessed using the *relative core length* (RCL) metric (Liu et al., 2008), defined as the shortest interval of the ordination axis containing 90% of the plots, divided by the total length of the axis.
 - 5) How well the axes correspond to environmental proxy variables such as the convex-concave orientation of brachiopod shells, elemental composition, magnetic susceptibility, bioturbation and lithology – which are assumed to be indicative of the substrate composition, sedimentation and wave energy of the original paleoenvironment (see Section 1.2.2.2).

The important methodological research questions here are therefore both 1) to what degree the multiple parallel ordination approach is capable of producing gradients that are robust and comparable across ordinations 2) what impact the quantitative versus the qualitative properties of the samples have on the ordination results (measured through differing abundance weighting), and 3) which ordination methods of the four provides the most ecologically interpretable ordination. Based on the underlying properties of the different ordination methods (see Section 1.3), and comparisons from the literature (Økland, 1990, 2007; ter Braak & Prentice, 1988), DCA and NMDS are assumed to be the most suited to representing species-plot data with unimodal responses of species along environmental gradients. However, if the species-response gradients are short enough to approximate a linear response, PCA could in fact prove to be equally robust and accurate, due to its underlying statistical basis (see Section 1.3). The assessment of the different ordinations might therefore also be informative of the nature of the species-environment relationship found in the samples.

1.2.2 Paleoeological research questions

1.2.2.1 Temporal versus spatial variation

The central paleoeological research question in this thesis is how the variation in morphotaxa abundances is structured spatially versus temporally in the Rytteråker Formation. In previous studies, the formation has been interpreted as primarily representing a marine regression sequence, especially in the areas sampled in this study (see Section 1.4), with evidence of a subsequent transgression in the upper part of the sequence in some areas. The study localities in question are also presumed to have been deposited in different parts of a complex onshore-offshore shelf environment including an offshore carbonate bank/patch reef barrier to the west and a deeper, possibly lagoonal area to the east (Möller, 1989, see also Section 1.5 and Figure 1.2). In light of this, we would therefore expect – under the assumption that depositional depth is the most important environmental gradient structuring species distribution – to observe a depth-related gradient in abundances both between and within the localities. If such a gradient

is found, it is expected to be the primary gradient in the dataset and thus reflected in ordination axis 1 (see Section 1.2.1). This result would also be in accordance with the sedimentological principles of Walter’s Law of Facies (López, 2013).

Yet, whether such a double gradient is actually observable in this study is still an open question. And if it is, the same goes for which signal (spatial or temporal) will be the most decisive for the gradient observed (i.e. whether the (idealized) ordination looks most like Figure 1.1A or 1.1B, or something in between). One species-level study from a Devonian shale formation found that even when depositional depth was similar across different localities, localities separated markedly in ordination space when sampled at the same (short) stratigraphic intervals (Forcino, Richards, et al., 2012). However, when the sampling was expanded to a longer stratigraphic succession which also included a substantial qualitative shift in species composition, the spatial signal disappeared. In this study, where the localities are assumed to be more qualitatively different than in the above example (see Section 1.4), factors other than depositional depth, both paleo-environmental and also taphonomic, could easily influence the separation of the samples and the structure of the ordination axis even more, in addition to the depth gradient. This also ties into the question of whether the broad morphotaxa categories employed in the study are sufficient to discern the potentially complex and multifaceted double-layered gradient hypothesized.

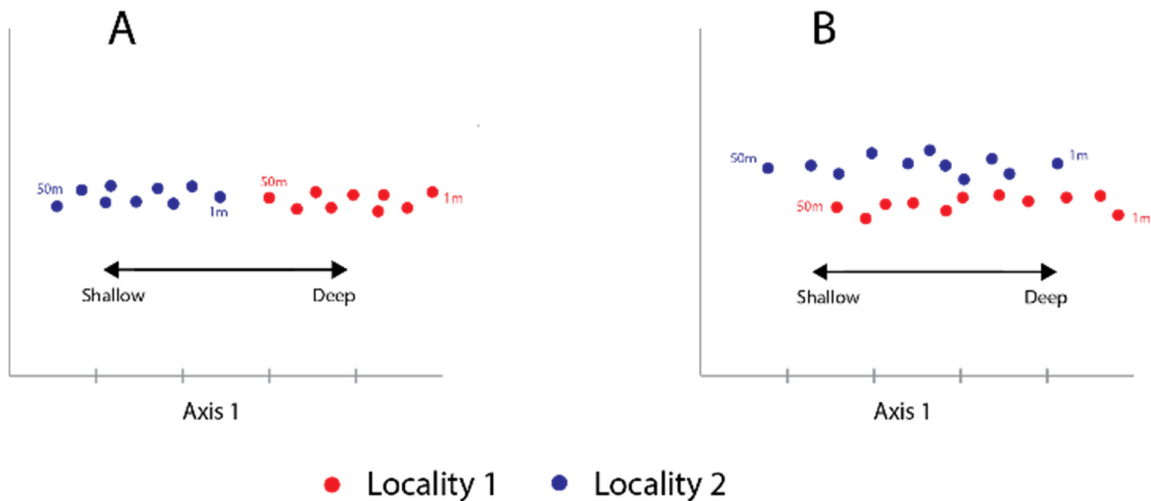


Figure 1.1. Theoretical example of how site scores from two localities (with 50m stratigraphic samples for each locality) will separate along an ordination axis 1 corresponding to depositional depth, depending on whether the spatial signal (A) or the temporal/stratigraphic signal (B) is the most dominant.

1.2.2.2 Relationship between environmental variables and faunal composition

To better understand the paleoecological nature and interpretability of any eventual gradients observed in the ordinations, the study is also interested in exploring the relationship between the ordination results and different proxy variables for the paleoenvironment. Namely depth and wave energy (carbonate lithofacies types, brachiopod shell orientation), biological activity in the sediment (degree of bioturbation), and chemical composition of the sediments (magnetic

susceptibility and elemental composition). As some of these variables, in particular the carbonate lithofacies types (see Section 2.3.3), by definition are strongly connected to the fossil content of the samples, as well as wave energy (see Figure 1.2), they might be especially important as a measure of the qualitative difference between the samples, and by extension the effect of sampling within temporally and spatially heterogeneous sedimentary setting. Even though these divisions may be somewhat subjective and uncertain.

Assessment of these variables will be done through correlation testing of the environmental variables measured in the acetate peels (carbonate lithofacies types and degree of bioturbation), as well as correlation and fitting of these environmental variables to the ordination results. The magnetic susceptibility readings, elemental composition data and shell orientations measured parallel to the acetate peel samples, will also be correlated with each other to the gradient observed in the data, but in a more qualitatively manner.

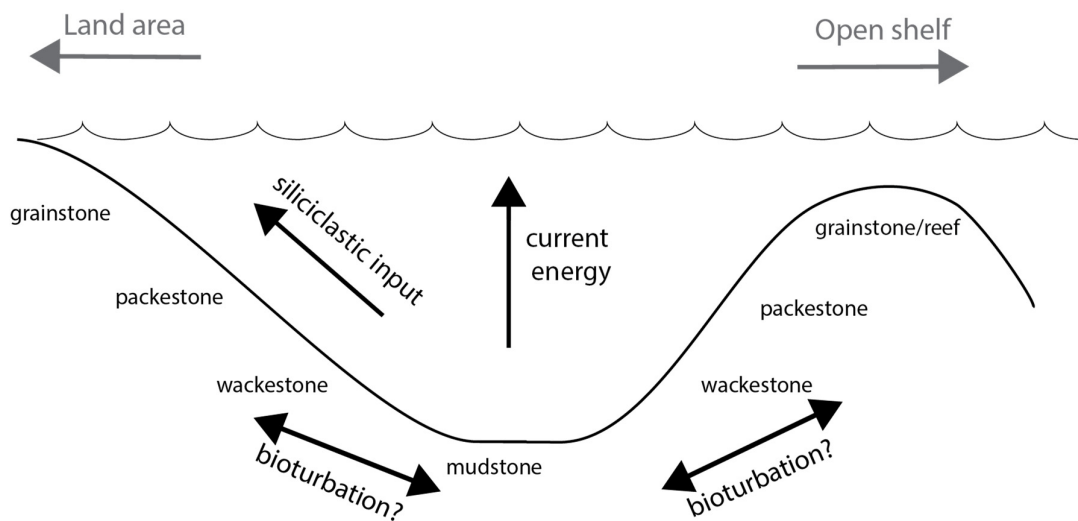


Figure 1.2. Simplified schematic of proposed depositional setting of the Rytteråker Formation, with approximate relative “optima” of the lithofacies categories used in this study (Dunham, 1962, see Section 2.3.3), and their proposed relationship to wave energy, which again could be a partial proxy for depositional depth (Flügel, 2004)

1.2.2.3 Ecological occupancy

The last research question is what the ecological implications of the spatiotemporal gradients of the samples are. The abundances of the different morphotaxa groups in the samples will therefore be analyzed within the framework of the generalized three-dimensional eco-space model devised by Bush et al. (2007) (also referred to as the “Bush cube”, and more or less analogue to the “megaguild” concept employed by Bambach (2002)), in which all benthic organisms occupy a triple grouping according to their feeding mechanism, motility level and tiering relative to the seafloor (table 2). This model has been shown to be flexible and effective in capturing and describing several major qualitative structural changes in benthic ecosystems from the Ediacaran to the Cenozoic (Bush, Bambach, et al., 2007; Bush et al., 2011). As such, it might be interesting to view the results, as well as in a comparison to more recent ecosystems. However, the broadness of the morphotaxa categories, as well as the general uncertainties

surrounding the autecology of some Silurian organisms, makes assignment to one definitive “cube” uncertain and debatable in several cases. This will be discussed in more detail in Section 2.3.4, as well as in the discussion.

Table 1.2. Ecological categories for feeding mechanism, tiering and motility level. Modified from [Bush et al. \(2007\)](#).

Ecological category	Description	Silurian example taxa
Tiering		
1. Pelagic	In the water column	Graptolites, cephalopods
2. Erect	Benthic, extending into the water mass	Crinoids, some tabulate corals
3. Surficial	Benthic, not extending significantly upward	Most corals and brachiopods
4. Semi-infaunal	Partly infaunal, partly exposed	Many ostracods, possibly tentaculitoids
5. Shallow infaunal	Living in the top ~5 cm of the sediment	Some bivalves
6. Deep infaunal	Living more than ~5 cm down in the sediment	Some bivalves
Motility level		
1. Freely, fast	Regularly moving, unencumbered	Most arthropods and vertebrates
2. Freely, slow	As above, but strongly bound to the substrate	Gastropods
3. Facultative, unattached	Moving only when necessary, free-lying	Many bivalves (i.e. clams)
4. Facultative, attached	Moving only when necessary, attached	Many bivalves (i.e. mussels)
5. Non-motile, unattached	Not capable of movement, free-lying	Pentamerid brachiopods
6. Non-motile, attached	Not capable of movement, attached	Pedunculate brachiopods, crinoids
Feeding mechanism		
1. Suspension	Capturing food particles from the water	Brachiopods, bryozoans, crinoids
2. Surface deposit	Capturing loose particles from a substrate	Many trilobites
3. Mining	Recovering buried food	Many bivalves (i.e. nuculids)
4. Grazing	Scraping or nibbling food from a substrate	Many gastropods
5. Predatory	Capturing prey capable of resistance	Cephalopods, some trilobites
6. Other	e.g. photo- or chemosymbiosis	Calcareous algae

1.2.3 Preliminary hypotheses

To summarize the most important points discussed in sections 1.2.1 and 1.2.2, the most important preliminary hypotheses of this study can be expressed as follows:

- 1) The sampling strategy used in the novel data collection for this study suitable for robustly capturing a primary gradient of faunal compositional change in the Rytteråker Formation, if it exists.
- 2) The Multiple Parallel Ordination approach described here will similarly be useful for robustly discerning ecologically interpretable faunal gradients in the data, as well as evaluating the numerical/statistical properties of these gradients, both in the newly sampled data and the reanalyses
- 3) Depositional depth is the most important environmental gradient controlling faunal composition in the Rytteråker Formation both in time (stratigraphically) as well as spatially between different localities, as has been suggested by previous studies on the stratigraphy (Baarli et al., 1999; Johnson, 1989; Keilen, 1985; Möller, 1989; Mørk, 1978; Worsley et al., 1983).
- 4) If the above are true, a gradient in faunal change controlled by depositional depth will be reflected in axis 1 of the ordinations, both spatially (between localities) and temporally (by stratigraphic position) in the ordination diagrams. This gradient will be correlated with both quantitative and semi-qualitative environmental proxy variables measured in the samples and in parallel samples. And a comparable spatio-temporal

gradient will also be observable in the reanalyzed data, using the same comparative ordination approach.

1.3 What is ordination-based gradient analysis?

1.3.1 Underlying principles

Unlike the more qualitative and classificatory approaches traditionally employed in paleoecology (in the tradition of [Boucot, 1981](#); [Ziegler et al., 1968](#); etc.), ecological gradient analysis rests on the assumption that each individual species' abundance or likelihood of occurrence is best explained as a continuous function of one or more environmental variables (ter Braak & Prentice, 1988). This is formalized in the *species-response model* (shown in Figure 1.3).

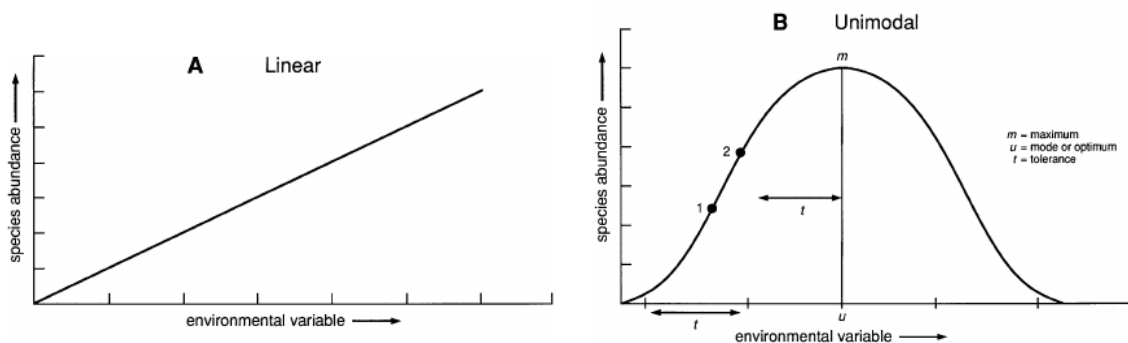


Figure 1.3. A) Linear species-response model, B) Unimodal species-response model with Gaussian distribution. (Reprinted from Ter Braak & Prentice, 1988). The segment between points 1 and 2 in figure B exemplifies that under a unimodal species-response model, a linear response might be observed if the environmental gradient sampled is short enough.

A general assumption of the species response model is that along a sufficiently long ecological- or complex-gradient (see overview of terminology in Table 1.3), a species' abundance-response to this gradient will be a *unimodal*, often bell-shaped (Gaussian) distribution ([Austin, 1985](#); [Gauch Jr. & Whittaker, 1972](#), exemplified in Figure 1.3B). Along shorter intervals of the environmental gradient however, the species-response may approximate linearity (Figure 1.3a). An example of a theoretical ecocline following the species-response model is shown in figure 1.4.

Table 1.3. Terminology of ecological gradient analysis (as defined by [Whittaker 1967](#)).

Concept	Definiton	Examples
<i>Ecological gradient</i>	Gradual change in an environmental variable	Change in pH or water temperature
<i>Coenocline</i>	Gradual change in species composition	Change from moss- to heather dominated pine forest, or composition of benthic Foramenifera
<i>Complex-gradient</i>	More or less parallel change in several ecological gradients	Change in soil nutrient status, water depth etc.
<i>Ecocline</i>	Variation in species composition along a complex-gradient	Change from one depth-controlled benthic community to another

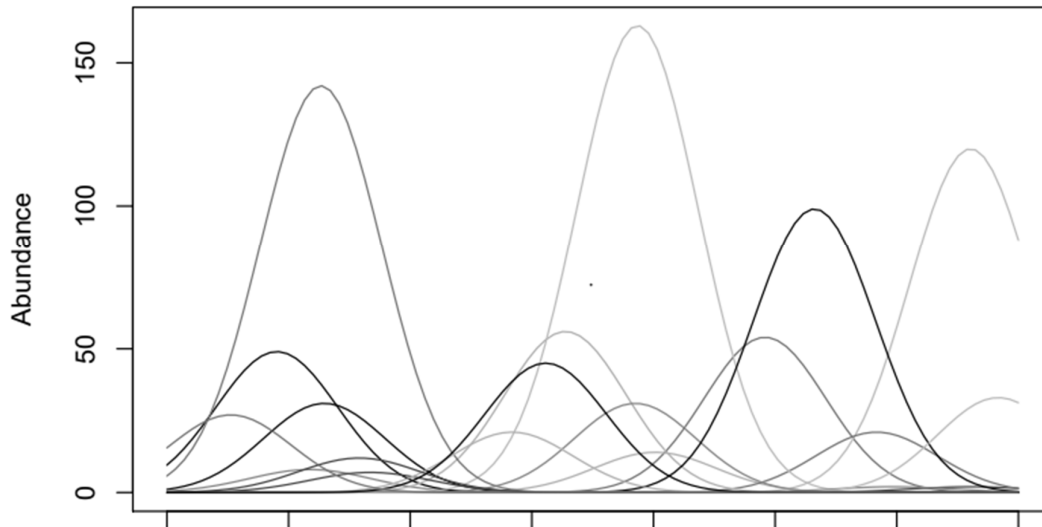


Figure 1.4. Hypothetical ecocline with independent, gaussian response curves of species' abundances (y-axis) along a complex-gradient (x-axis) (reprinted from Simpson et al., 2021).

1.3.2 Indirect ordination methods

Generally, indirect ordination methods can be defined as exploratory, multivariate techniques that aim to find the underlying variables (commonly called *ordination axes*) best explaining the *patterns in variation* between samples in a multivariate dataset – normally with the aim to construct hypotheses and summarize the main structure of the data (Austin, 1985; Dale, 1975). When used on species-abundance or environmental data in an ecological framework, the goal is typically to identify ordination axes that can be interpreted as reflecting the primary *compositional gradients* (i.e. the coenoclines or complex-gradients) in the environments sampled (Legendre & Legendre, 1998).

To this end, several different ordination methods have been developed for use in ecology over the last 50 years. These methods differ often quite substantially in their theoretical basis and iteration algorithm, and can be both statistically based as well as heuristic or geometric. There is also a key difference between *indirect* and *direct* (also called *constrained*) ordination methods. In direct ordination methods (such as Canonical Correspondence analysis), ordination axes are optimized to fit a set of separate explanatory variables (e.g. environmental variables), while indirect methods only condense the variation in the primary dataset. As such, direct ordination might be the most suited to test more specific hypotheses about species-environment relationships, while indirect ordination methods should be preferred for exploratory analysis and hypothesis creation, as they contain fewer assumptions about the data (ref). Correlation between environmental variables and ordination scores may also still be done *a posteriori* in indirect ordinations, in order to create hypotheses about species-environment interaction (see Section 1.3.3). In the following sections, the central properties of the four indirect ordination methods explored in this thesis are outlined, and a short, comparative summary is provided in Table 1.4.

Table 1.4. Overview of the different ordination methods considered in this study, and their central properties. PCA=Principal component analysis, CA=Correspondence analysis, DCA=Detrended correspondence analysis, NMDS= Non-metric multidimensional scaling

	PCA	CA	DCA	NMDS
Short description	Extension of linear regression to m dependent (e.g. sample abundances) and s independent (e.g. species) variables, with assumption of normally distributed errors.	Weighted averaging regression to estimate plot positions around unimodal species optima.	CA with non-linear rescaling of axes and detrending of axes 2+ <i>a posteriori</i> .	Geometric positioning of samples according to their between-sample dissimilarity which minimizes stress in a monotone regression of dissimilarities
Statistical properties of axes	Eigenvalues based on variation (sum of squares) explained relative to total dataset variation	Eigenvalues based on contingency analysis, related to PCA eigenvalues.	None (heuristic).	None (geometric), stress value gives an indication of the fit of the data to the complete ordination.
Common artefacts	“Horseshoe” effect when response variables do not fit assumptions of linearity.	“Arch” and “edge” effects due to lack-of fit of model (similar to PCA)	“Tongue” effect due to distortion of “real” secondary axes in detrending	Polynomial distortion in higher ordination axes without real gradients

1.3.2.1 Principal component analysis

Principal Component Analysis (PCA) is one of the oldest multivariate statistical techniques in science. Originally formalized by Pearson (1901) and Hotelling (1933), it was widely adapted by ecologists in the 1950s and 60s, and has since been a standard tool for gradient analysis both in ecology as well as other scientific fields.

The perhaps most intuitive explanation of PCA is provided by Legendre & Legendre (1998). Here, the dataset is imagined as points in an m -dimensional space, where m is the number of response variables (e.g. species) observed in each sample (i.e. point). PCA is then understood as a *rotation* of the m -dimensional space to find the direction that display the most variation (i.e. sum of squares (SS) in statistical regression terms), which then become the first *axis* (or principal component) of the PCA. Higher axes (axis 2, 3 etc.) subsequently explain the maximum of variance left over that is unrelated (orthogonal) to the lower axes. In the example shown in Figure 1.5, three species are observed in each plot, meaning each point has a 3-dimensional coordinate according to the abundances of each species (axis). PCA axes 1 and 2 would thereby be found by rotating this 3D space to find the optimal 2D-“window” that displays the maximum variation of plot coordinates.

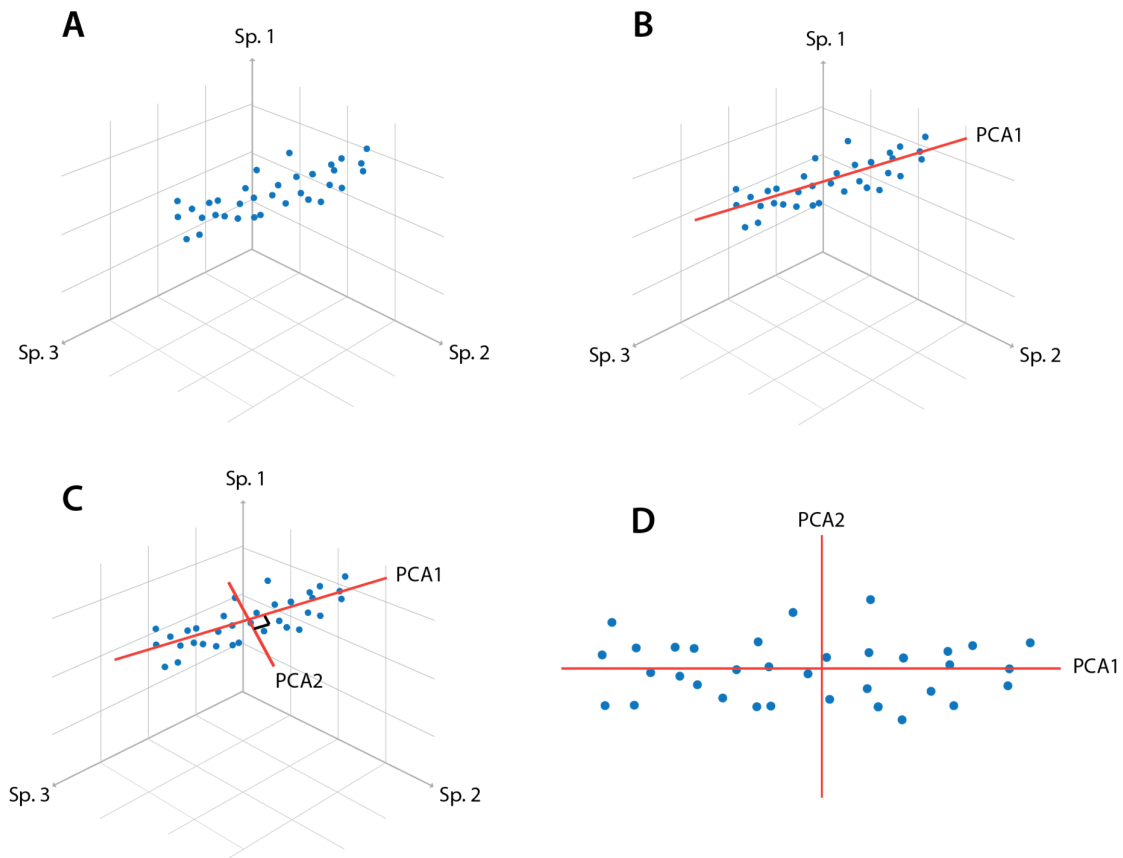


Figure 1.5. Geometric depiction of the PCA algorithm. A: samples are positioned in a 3-dimensional space according to their abundances of three different species (sp. 1, 2 and 3). B: PCA axis 1 is found as the line drawn through the point-cloud that captures the longest range of variation in point coordinates. C: Ordination axis 2 is found as the *orthogonal* axis relative to PCA1 that similarly captures the most variation possible. D: the resulting ordination diagram, showing the plot positions in a reduced, 2-dimensional space, which maximizes the variation shown.

An arguable strength of PCA is the fact that the ordination axes have a straightforward, statistical relationship with the amount of variation in the dataset they explain, represented by the eigenvalues of each axis as a fraction of the total variation in all axes (the *total inertia*). The method is also easy to compare to more “traditional” regression methods in biology, i.e. linear regression (Legendre & Legendre, 2012).

However, researchers have long noted several major problems with applying PCA to ecological species-abundance data. The most important of these is that the method’s assumption of a strict, linear relationship between the predictor variables (species) and response variables (plot abundances), is violated in cases where the coenoclines follow a version of the unimodal species-response model. This violation of the PCA model frequently results in a statistical artefact called the “horseshoe” effect, in which a coenocline with unimodal abundances in axis 1 is “pushed” and distorted into a horseshoe shape in axis 2, profoundly hindering interpretation of the gradients in the data. As such, PCA is usually not recommended for species-abundance data attempting to capture long or intermediate coenoclines (Beals, 1973). However, the method might perform better when the gradients sampled are short, or when the variables measured do not follow a unimodal distribution. Additionally, it is likely the most robust choice

for ordination of *environmental* variables in plots (e.g. pH, temperature etc.), which generally can be assumed to have a more linear relationship with each other. PCA also continues to be a widely used method in ecology, perhaps especially paleoecology (Barbacka et al., 2019; M. T. Dean et al., 2010; Huang et al., 2016), so the decision include it in this study is also done with this in mind.

1.3.2.2 Correspondence analysis

Correspondence Analysis (CA), also known as Reciprocal Averaging, was proposed in the 1970s as a solution to the problems inherent to PCA with regards to species abundance gradients (Hill, 1974). Rather than linear regression, the CA method is based on *weighted averaging regression* of species plot scores. As such, the algorithm estimates unimodal optima for each species on the axis, and plot scores as the weighted average of the optima of the species present in each plot (ter Braak, 1985). Axis have eigenvalues based on their contribution to the total weighted variation in the dataset, with the distribution of variation on the axes being closely related to contingency analysis (i.e. the χ^2 -distribution) (Greenacre, 2010).

Due to CAs unimodal basis, and its suitability to incidence data (i.e. count- or presence-absence data), it has been preferred by many ecologists and paleoecologists over PCA (notably for this thesis, Hennebert & Lees' (1991)). However, like PCA, the CA algorithm also frequently turns out to produce polynomial distortion artefacts when applied to coenocline data: namely the so-called “arch” and “edge” effects (Økland, 1990). The arch effect is analogous to the horseshoe effect in PCA, and is similarly caused by lack-of-fit of the model due to the orthogonalization step and variation partitioning between the axes being similar between the methods (Wagner, 2004). The edge effect refers to the fact that plot positions in primary coenocline axis tend to be spaced by the CA algorithm further apart near the middle of the axis, and closer together near the edges. This happens because the “species packing model” at the basis of CA – which assumes that species optima are evenly spaced along the whole gradient where species occur (and must occur within the range of plot scores) – is more or less always violated with ecological data (ter Braak & Looman, 1986).

1.3.2.3 Detrended correspondence analysis

As the name suggests, Detrended correspondence analysis (DCA) is a variant of CA. Specifically, it is a version developed with the explicit goal to more or less directly “fix” the distortion effects produced by the CA algorithm, by applying heuristic methods to a CA ordination *a posteriori* (Hill & Gauch, 1980). The DCA algorithm uses two such methods: *detrending by segments* and *non-linear rescaling*, to remove the arch effect and the edge effect respectively (see example in Figure 1.6). The detrending procedure is applied to all ordination axes higher than the first. It functions by dividing the previous axis into segments, then averaging the new axis scores around the first axis in each segment, which aims to ensure that there is no “systematic relationship” between the ordination axes (Hill & Gauch, 1980). Non-linear rescaling is a more complicated algorithmic step, in which each axis is divided into overlapping segments and their plot scores rescaled by weighted averaging into units of *relative*

compositional turnover (Økland, 1986). This means that one unit in the axis theoretically corresponds to one set amount of compositional change, relative to the average of the species in a given interval (Eilertsen et al., 1990).

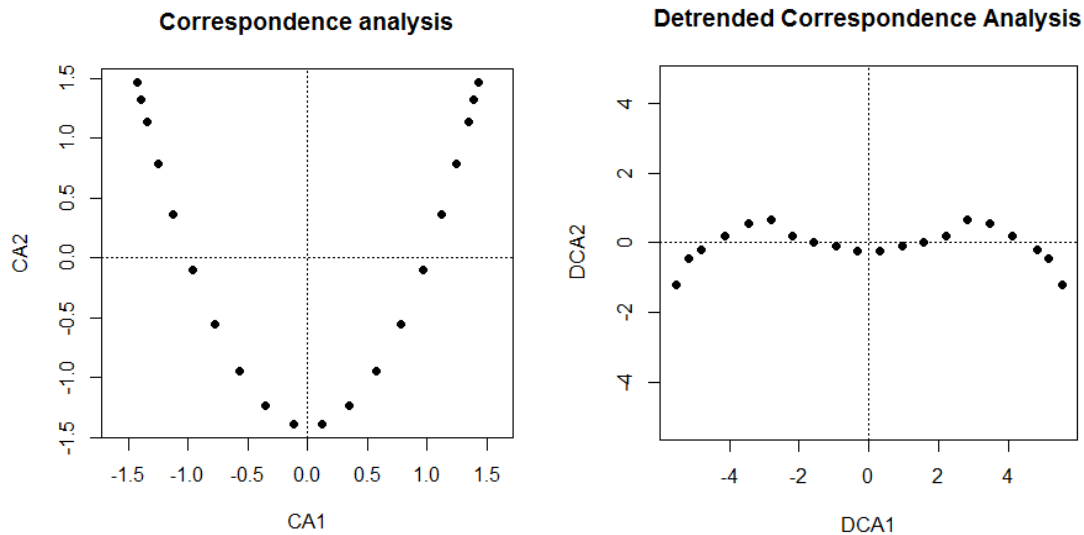


Figure 1.6. A simplified example of the results of detrending and non-linear rescaling procedure on a simulated, idealized test dataset with one gradient in species composition (axis 1). Reprinted from [Zdearveindy \(2014\)](#).

Due to the heuristic nature of the method, the axes in a DCA ordination have no real statistical relationships with each other and to the dataset, as opposed to with PCA and CA. This may limit interpretability with regards to variation partitioning, and has been criticized as a weakness of the method (Wartenberg et al., 1987). DCA is also demonstrated to produce a distortion artifact called the “tongue effect” in cases where axis above the first (almost always axis 2) contain real species-compositional gradients that are sampled unevenly along the underlying axis. These are subsequently “folded” by the detrending method, leading to distortion (Minchin, 1987; Økland, 1990).

Nevertheless, DCA consistently performs better than PCA and CA in studies of simulated coenocline studies, especially with the recovery of primary gradients in axis 1 through non-linear rescaling (Minchin, 1987). Units in the primary axis are also often ecologically well-interpretable as measures of species turnover along a coenocline (Eilertsen et al., 1990). Because of this, DCA, together with NMDS (see below), has become a standard method for ecological gradient analysis, both in ecology and paleoecology in the last 25 years, with many paleoecologists in particular lauding its ability to identify primary – often assumed to be depth-related – coenoclines in fossil assemblages (i.e. Ayoub-Hannaa et al., 2013; Miller et al., 2001; Turvey, 2005).

1.3.2.4 Non-metric multidimensional scaling

Non-metric multidimensional scaling is a purely geometric ordination method, which in contrast to the other methods discussed here, uses a matrix of *between-sample dissimilarities* to estimate plot positions in a predefined number of dimensions (usually between 2 and 4) (Mead, 1992). Sample dissimilarities are most commonly calculated using the floristic Bray-

Curtis dissimilarity measure (percent dissimilarity), although Euclidian distance is also sometimes used (e.g. Q.-N. Li et al., 2022). In cases where samples have very few or no shared species, the geodetic “stepacross” method is also often applied (as raw floristic dissimilarity cannot be higher than 1), replacing the direct dissimilarity values with the lowest sum of reliable distances (e.g. dissimilarities). This is argued to generally improve robustness and ecological interpretability of NMDS ordinations, especially for longer coenoclines (Mahecha et al., 2007)

The NMDS algorithm iterates by moving plot scores from a random start configuration in the chosen number of dimensions, until the configuration which minimizes the *stress* of the ordination is found. The stress is defined as the amount of residual variation in a monotonic regression of the distance between plot positions as a function of their floristic dissimilarity (a Shepard diagram). The stress value thus indicates the general “fit” of the geometric ordination to the compositional differences between samples. Many different varieties of NMDS exist, the most common of which are the local (LNMDs) and global (GNMDS) versions, differing with respect to how stress is calculated. Variations in performance between the two are generally thought to be small, however (Liu et al., 2008). Therefore, for simplicity’s sake, GNMDS will be used as the default method when referring NMDS in this study, unless otherwise stated.

Due to the properties of the method, the stress value will always be lowered the more starting dimensions are added. However, higher dimensions of NMDS also increase the likelihood of polynomial distortions (like the ones in PCA and CA), caused by lack of real compositional gradients. Determining the number of dimensions that best condenses and displays the gradients therefore normally represents a trade-off regarding the fit of the data. One rule of thumb proposed by Liu et al. (2008), is a “stress cutoff” at 0.2, above which more starting dimensions should be added to better capture the variation in the dataset.

The raw NMDS axes scores in and of themselves have no relationship to the variation-structure of the data, as the relative distance between the points is the only thing that is optimized. Most modern NMDS software therefore, by default, also perform a PCA rotation of the NMDS ordination *a posteriori*, making the final axes decreasingly summarize the variation of the “point cloud” created by NMDS. Species optima are also typically estimated *a posteriori*, using weighted averaging on the finished ordination (Oksanen et al., 2019).

Because the NMDS algorithm may easily converge on local stress minima, NMDS is usually run multiple times with different starting configurations to increase the likelihood that a global, stable solution is found. This makes NMDS a far more computer-intensive method than CA, PCA and DCA, and it is only in the last 25 years that it has become practical to use for many researchers, given the limited resources and computational time often available. Today however, NMDS – together with DCA – is considered one of the most robust ordination method both in ecology and paleoecology, and is subsequently used about equally with DCA (Chahouki, 2013). Comparisons on simulated coenoclines suggest that none of the two methods consistently performs better than the other. There is, however, some indication that NMDS

generally performs better at displaying multiple gradient structures in cases with more than one coenocline, while DCA being slightly better at retrieving the primary gradient (Minchin, 1987). Due to their inherent differences and similar performance on simulated gradients, parallel use of both ordinations is nevertheless usually recommended to assert the validity of gradient structures inferred from real data (Clapham, 2011; Økland, 1990, 1996).

However, like with DCA, NMDS is frequently the only method in studies which use ordination in paleoecology. Perhaps most importantly for the context of this thesis, this is true for the heavily referenced paleoecological sampling- and methodological studies of Forcino and associates (Forcino et al., 2010, 2013; Forcino, Leighton, et al., 2015; Forcino, Richards, et al., 2012; Forcino, Stafford, et al., 2012; Forcino & Stafford, 2020).

1.3.3 Comparing ordinations

Assessing the congruence of results from different indirect ordinations is commonly done in one of two ways: either by comparison of entire ordinations through Procrustes permutation testing (Peres-Neto & Jackson, 2001), or through correlation between individual axes. In the latter case, non-parametric metrics, primarily Kendall's rank-order correlation (Kendall's τ), is advocated, as it contains the fewest assumptions about the homogeneity and variance distribution of the data (van Son & Halvorsen, 2014). Additionally, the relative influence of outlier plots on the ordination axes may be assessed using the "relative core length" metric described by Liu et al. (2008), defined as the shortest interval along each axis containing 90% of the plots, divided by the length of the entire axis.

1.3.4 Interpretation and fitting of environmental variables

Interpreting ordination results in light of environmental factors, i.e. creating hypotheses about the *ecocline* structure of the plot distribution, is similarly done mainly through one of two numerical approaches: 1) correlation testing between the variables and individual axis scores (preferably using Kendall's τ), and 2) fitting of the variables to the first two or three axes simultaneously. The latter is either done by vector fitting of the variables, using multiple linear regression (represented by the *envfit* function in the *vegan* package in R, or through fitting a smoothing function (usually GAM) to the ordination (the *ordisurf* function in the *vegan* package), creating isolines in the diagram. Both correlation testing and vector fitting (through a Monte Carlo permutation test), can give a value for the strength and significance of the variables' relationship to the axes. On the other hand, isoline fitting may allow for better visual interpretation in the ordination diagram.

In order to use these methods however, the environmental variables need to be continuous, and standardized to equal range and variance, with some researchers also advocating standardization to minimize skewness (Økland, 1986). For binary and factor variables (e.g. study locality), visual coding by color, size and shape is often the only way of describing their dispersal in the ordination diagram. This approach might nevertheless be very informative in qualitatively describing the patterns observed, and is normally the primary exploratory way of displaying and interpreting ordinations.

1.4 Ecological setting

1.4.1 Earth system dynamics in the Silurian

The Silurian (443.8-419.2 Ma) is the shortest geologic period in the Paleozoic, as well as in the entire geologic record (Cohen et al., 2013). Traditionally, the period was thought to represent a timespan of relatively stable global greenhouse conditions, with high, slowly rising sea levels and a gradual, slow recovery of marine ecosystems following the Ordovician-Silurian Mass Extinction Event (Jia-Yu & Harper, 1999). However, the Silurian has received renewed scientific interest in the last three decades, as C and O isotope studies have suggested that global biogeochemical cycles in the period may in fact have been highly volatile, and punctuated by several extreme $\delta^{13}\text{C}$ excursions and sea-level changes of somewhat uncertain causes (Aldridge et al., 1993; Calner, 2008; Cramer & Saltzman, 2007; Johnson, 2006; Melchin et al., 2013; Munnecke et al., 2010). Munnecke et al. (2010) even posits that “fundamental changes in the global carbon cycle were much more frequent in the comparatively short Silurian Period than in any other system of the Paleozoic.” The early Silurian period might therefore be an interesting case study for how shallow-water benthic ecosystems in the Paleozoic responded to a highly volatile sea-level and geobiosphere, as well as the recovery from a major mass extinction.

1.4.1.1 Oceanic episodes and events

In their review, Calner (2008) specifically identify nine graptolite and conodont extinction events in the Silurian, most of them correlated with positive $\delta^{13}\text{C}$ excursions, later updated to 11 by Trotter et al. (2016). Of these, the most severe in terms of both carbon cycle perturbation and species turnover were the Ireviken event at the Llandovery-Wenlock boundary, the middle Wenlock Mulde event and the mid-Ludlow Lau event (shown in capitals in Figure 1.7). These events are primarily described from Silurian strata from Gotland, Sweden, while the aforementioned much smaller Sandvika Event is primarily based on conodont data from the Oslo Region and Estonia (Aldridge et al., 1993; Johnson et al., 1991).

Based on the oceanic model proposed by Jeppson (1990), researchers have interpreted the Silurian bioevents as connected to the switching between two different semi-stable states of ocean circulation and climate, dubbed “primo” and “secundo” episodes (Jeppson, 1997; Jeppson & Calner, 2002; Jeppsson, 1996; Johnson, 2006; Landing & Johnson, 1998; Munnecke et al., 2010). While this model has been refined and altered substantially over the years, it generally suggests, as summarized in Aldridge (1993), that primo episodes were characterized by “cool high-latitude climates, cold oceanic bottom waters, and high nutrient supply which supported abundant and diverse planktonic communities”, and that Secundo episodes were characterized by “warmer high-latitude climates, salinity-dense oceanic bottom waters, low diversity planktonic communities, and carbonate formation in shallow waters”. The fluctuation of climate-ocean states have also been attempted linked with fluctuations in sea level (Johnson, 2006), and to global temperature proxies in the form of $\delta^{18}\text{O}$ curves (Munnecke et al., 2010; Trotter et al., 2016). While the originally hypothesized link between low sea-levels and Primo episodes – and high sea-levels and Secundo episodes – has not been consistently found, many

Silurian bioevents have nevertheless been linked to sea level regressions/lowstands, $\delta^{18}\text{O}$ excursions (most often positive, indicating a colder climate), and glacial periods (Davies et al., 2016; Jeppson & Calner, n.d.; Jeppson, 1996; Johnson, 2006, see also Figure 7). In this regard, they are also hypothesized to be connected to the biogeochemical processes assumed to underlie the End-Ordovician extinction event, although below the climate change “threshold” hypothesized to have been exceeded then (Calner, 2008; Rothman, 2017).

In the correlation proposed by Trotter et al. (2016) (Figure 1.7), the deposition of the Rytteråker Formation in the central Oslo Region appears to coincide with the Sandvika event at the base of the formation, and a gradual warming during the Malmøykalven Secundo episode during most of the deposition, followed by the “S-P”-event around the transition to the overlying Vik formation (see Section 1.5), which has also been associated with a widespread oceanic oxygenation event in northern Europe (Hounslow et al., 2021).

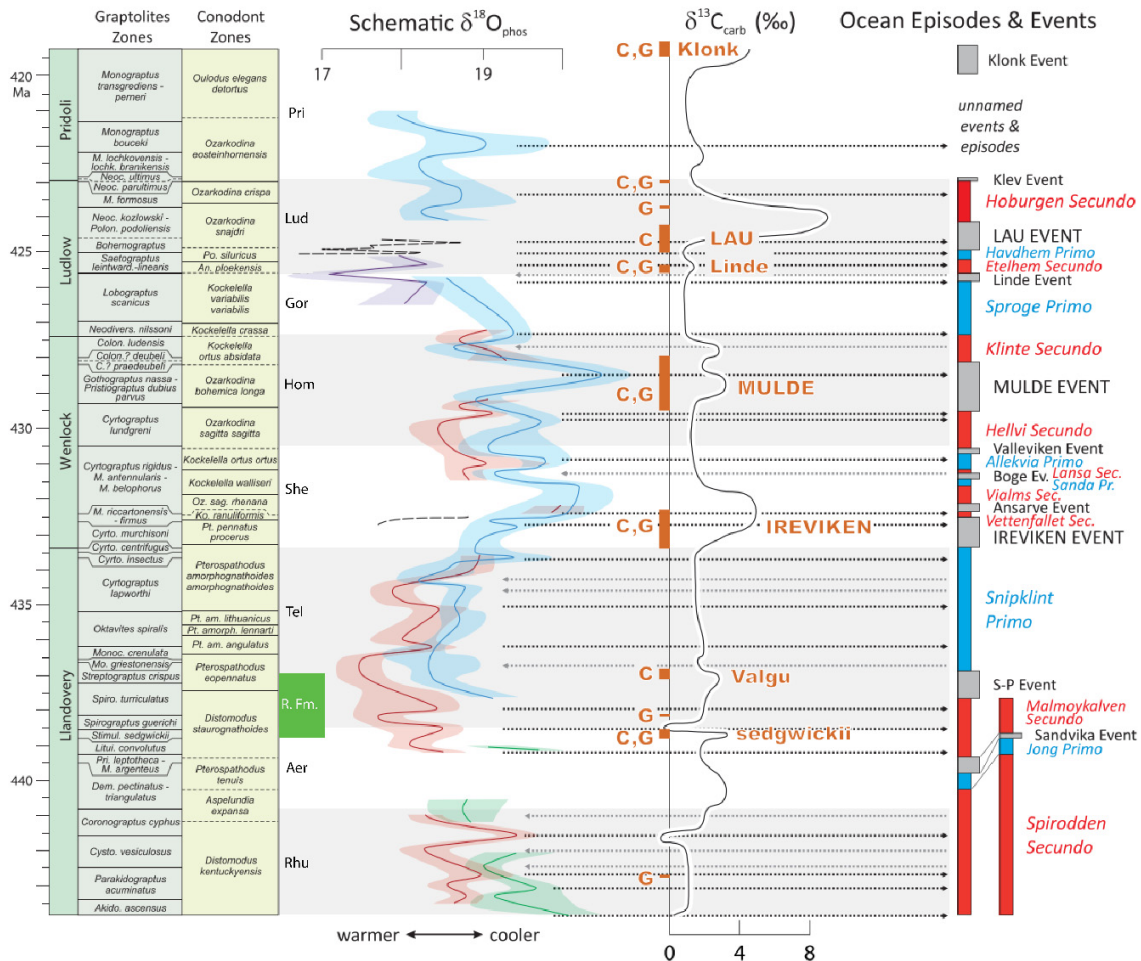


Figure 1.7. Correlation of global $\delta^{13}\text{C}$ (from Cramer et al., 2011), and regional conodont $\delta^{18}\text{O}$ curves from five different localities/paleocontinents (from Trotter et al., 2016. Red: Cornwallis Island, blue: Baltica, green: Anticosti island, purple: Avalonia, black dashed lines: Australia), correlated to global Graptolite- and Conodont biostratigraphy, global primo (blue) and secundo (red) episodes, and oceanic events (grey). Approximate temporal range of the Rytteråker Formation in the Oslo Region in green (correlation based on Graptolite biozones from Bruton et al. (2010)). G: Graptolite extinction event. C: Conodont extinction event. Arrows indicate $\delta^{18}\text{O}$ peaks and troughs. Figure modified from Trotter et al. (2016).

1.4.2 Taxonomic composition and diversity of marine faunas

In his famous 1981 study, Sepkoski introduced the idea of three distinct “evolutionary faunas” dominating successively in the Phanerozoic, based on patterns in family-level diversity of marine invertebrates observed by factor analysis – an ordination method related to PCA (Sepkoski, 1981). These faunas were identified as 1) A mostly trilobite-dominated *Cambrian* fauna, 2), a *Paleozoic* fauna dominated by brachiopods, crinoids, tabulate and rugose corals and other epibenthic suspension-feeders, rising to dominance in the wake of the Ordovician Biodiversification Event, and 3) The “modern” marine invertebrate fauna, characterized by mollusks, crustaceans and an increase in active, infaunal modes of life.

Despite heavy criticism and revisions of Sepkoski's original estimates of the total diversity difference between the Paleozoic and Meso-/Cenozoic faunas (Aberhan & Kiessling, 2012; Alroy et al., 2001, 2008), the regionality of the findings (McGowan & Smith, 2008), the relative ratios of the faunas through the Phanerozoic (Alroy, 2010), and the inability of the categories to account for major faunal dynamics within the “modern” fauna (Alroy, 2004), this basic tripartite pattern of faunal diversity has remained consistent in reanalysis (Rojas et al., 2021).

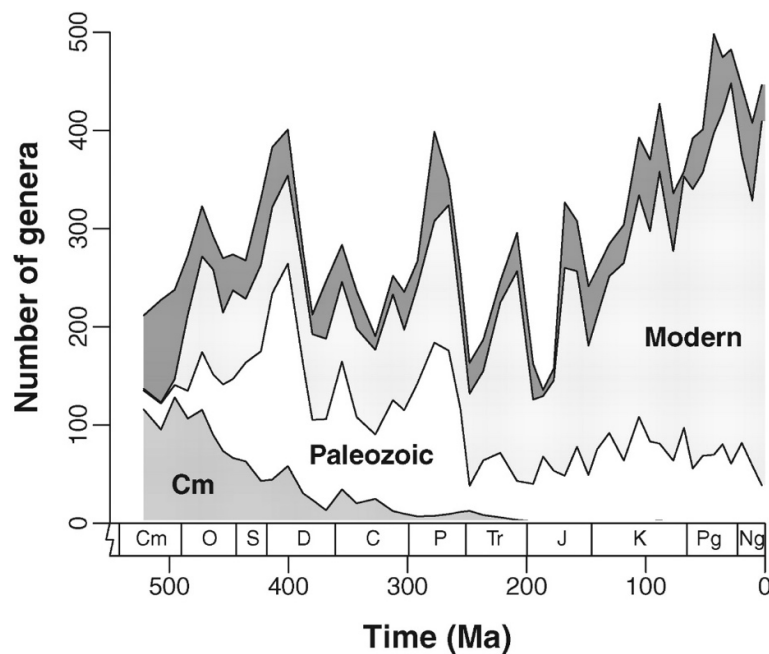


Figure 1.8. Sample-standardized curve of Phanerozoic generic diversity in 11 Ma bins, division into the Cambrian (Cm), Paleozoic and Modern faunas indicated. Taxa with no clear affiliation are in dark grey (reprinted from Alroy, 2010; fig. 3).

Within this macro-scale framework, the Silurian falls within the period most heavily dominated by the Paleozoic evolutionary fauna (see Figure 1.8). It is also interesting to observe that the End-Ordovician extinction event – as opposed to later Mass Extinction Events – did not substantially impact the relative evolutionary fauna composition of the Silurian, even though approximately 50% of marine invertebrate species are estimated to have gone extinct (McGhee et al., 2013).

1.4.3 Structure of benthic ecosystems

Together with the continued dominance of the “Paleozoic fauna”, the ecological impact of the End-Ordovician extinction event appear to have been decidedly smaller than that of later Mass Extinction Events, although the exact nature of the change is debated (Bush, Bambach, et al., 2007; Christie et al., 2013; M. Droser et al., 2000; M. L. Droser et al., 1997; Huang et al., 2017; McGhee et al., 2013; McGhee et al., 2012). The fundamental functional structure of benthic shelf ecosystems in the Silurian seems to have been broadly similar to that of the middle-late Ordovician, which had seen dramatic increases in ecospace utilization, community diversity and the establishment of the first eumetazoan (i.e. coral) reefs following the diversification of the “Paleozoic fauna” in the Great Ordovician Biodiversification Event (M. L. Droser et al., 1997; Servais et al., 2010).

1.4.3.1 Benthic communities and assemblages

Early Silurian benthic assemblages nevertheless appear to have been more cosmopolitan and less diverse than in the late-Ordovician, and showed a gradual recovery and re-diversification throughout the Rhuddanian (Gushulak & Jin, 2017; Huang et al., 2018). Silurian benthic assemblages have otherwise been described extensively using the *benthic community* framework originally introduced by Ziegler et al. (1968). In Ziegler’s model, five distinct benthic communities – usually characterized by one or more key brachiopod species – displace each other more or less gradually along a depth gradient from the intertidal to the open shelf.

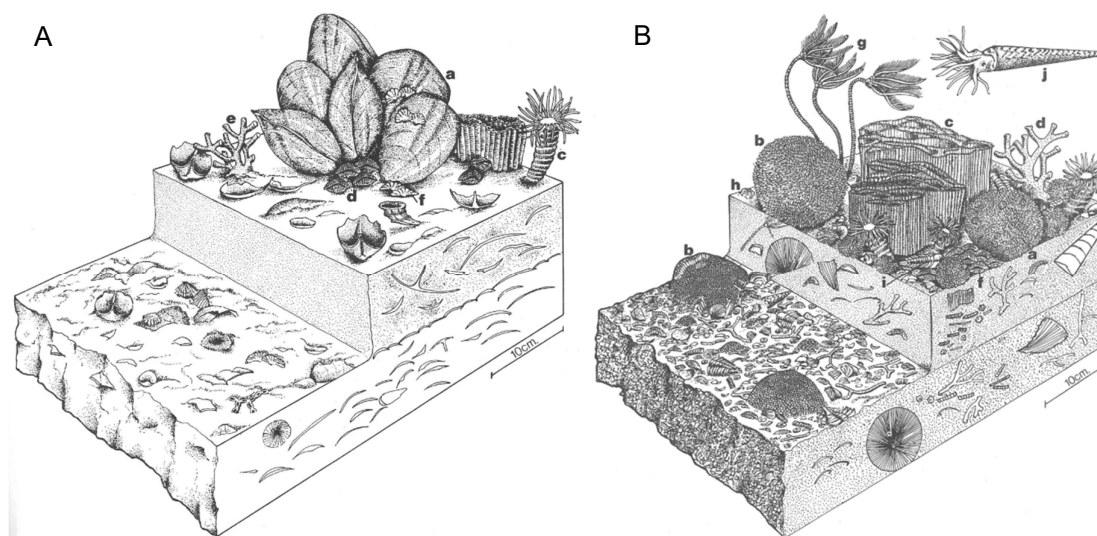


Figure 1.9. Artist’s rendition of proposed Silurian benthic communities (reprinted from McKerrow, 1978; figs. 22 & 24). 9A: Pentamerus Community, between storm and normal wave base. a: *Pentamerus* sp. (Brachiopoda: Pentamerida, b: *Halycites* sp. (Anthozoa: Tabulata), c: *Streptelasma* sp. (Anthozoa: Rugosa), d: *Atrypa* sp. (Brachiopoda: Spiriferida), *Hallopora* (Bryozoa: Trepostomata), f: *Eocoelia* (Brachiopoda: Rhynchonellida). 9B: Silurian reef assemblage, based on the Wenlock of England. a: *Heliolites* (Anthozoa: Tabulata), b: *Favosites* Sp. (Anthozoa: Tabulata), c: *Halycites* Sp., d: *Hallopora*, e: *Streptelasma*, f: *Atrypa*, g: crinoid (Echinodermata: Crinoidea), h: *Leptaena* Brachiopoda: Strophomenida), i: *Dalmanites* (Arthropoda: Trilobita), j: orthocone cephalopod (Cephalopoda).

These inferences were later expanded and generalized by Boucot (1975) to a system of *benthic assemblages* (BA), in which groups of benthic communities are tied to one of five zones along a bathymetric gradient, separated by environmental bounds such as the tidal zone, fair-weather

wave base, storm wave base and the lower limit of the photic zone (Boucot, 1975). Boucot and Lawson (1999) list more than 1200 primarily Silurian communities and community varieties described from Europe, North America and Asia. Even though this qualitative classification scheme is somewhat at odds with a gradient-based view of species distribution, and has been criticized for being ecologically essentialist (Hoffman, 1979), often showing weak statistical correlations (Bennington & Bambach, 1996) and being an uncertain indicator of depositional depth when compared to other proxies (Azmy et al., 2006), it may still provide valuable reference points for future research. Most previous paleoecological research from the Oslo region primarily uses this theoretical framework to describe and group different faunas stratigraphically and spatially (Baarli, 1981; Baarli et al., 1999), and in some cases even to make sea-level curves (Baarli et al., 2003). The fauna of the Rytteråker Formation has consistently been grouped as the *Pentamerus community* (figure 9a) within this framework – due to the prevalence of Pentamerid brachiopods in the formation, and placed between storm wave base and normal wave base (BA3) in Boucot’s BA scheme (Baarli et al., 1999).

1.4.3.2 Reefs

Reef formation in the Silurian is known to have resumed at least by the lower Aeronian (Yue & Kershaw, 2003), and phases of prolific reef formation by tabulate corals, stromatoporoids and to a lesser extent bryozoans, occurred throughout the rest of the period – possibly relating to the oceanic episode dynamic described in Section 1.4.1 (Cramer & Saltzman, 2007). In fact, the Silurian as a whole stands out as the perhaps most abundant reef-building period in the entire Paleozoic (Copper, 2002). Some shallow-water reef systems in Gotland appear to have been especially species-rich and productive, which is hypothesized to be connected to the evolution of zooxanthellate photosymbiosis in tabulate corals (Zapalski, 2014; Zapalski & Berkowski, 2019), although this is debated (Scrutton, 1998; Tornabene et al., 2017). The Silurian also saw first appearance of highly diverse pinnacle reef tracts on the edge of epicontinental seas, in the middle Telychian, assumed to be connected to a concurrent $\delta^{13}\text{C}$ excursion (McLaughlin et al., 2019).

1.4.3.3 Ecospace structure

Within the “Bushian” ecospace framework, the Silurian benthic faunas appear to be highly enriched in sessile, epifaunal suspension feeders, such as brachiopods, stenolemate bryozoans, rugose and tabulate corals and crinoids, when compared to modern benthic faunas (Bush, Bambach, et al., 2007; Bush & Bambach, 2011; Novack-Gottshall, 2007). Conversely, the modern fauna appear to overall contain greater ecological disparity and be more enriched in active molluscan and echinoderm predators and infaunal burrowers (Bush, Bambach, et al., 2007).

However, the well documented preservation bias of aragonitic (most modern, i.e. mollusks and Scleractinian corals) versus calcitic (most Paleozoic) taxa in the fossil records remains a substantial barrier to this comparison (Cherns et al., 2011), even as attempts are made to correct for it (as in Bush, Bambach, et al., 2007). For instance, the preservation bias seems to have

been uneven across habitats and oceanic conditions, and generally more severe in carbonate environments than with siliciclastic preservation (C. D. Dean et al., 2019; Foote et al., 2015).

More direct comparisons between mid-Paleozoic and modern shelf communities have also been attempted, mainly between Paleozoic epicontinental carbonate platforms and modern tropical reefs and carbonate banks such as the Java sea and the Bahama Banks (Edinger et al., 2002). However, as the extensive epicontinental oceans of the mid-Paleozoic have no direct modern analogues, such comparisons are also argued to be problematic (Cramer & Saltzman, 2007; Peters, 2007).

1.4.3.4 Macroevolutionary events

Despite the ecological continuity from the Ordovician, there also occurred significant evolutionary novelties during the Silurian, assumed to have been driven by changes in, and in turn profoundly impacted – the global biosphere and carbon cycle. The early to middle Silurian represent the first known terrestrialization of metazoans, in the form of mandibulate and chelicerate arthropods (Kenrick et al., 2012), and the first evidence of land plants with vascular tissue (tracheophytes) is also known from this period (Stemans et al., 2009)

The aforementioned Silurian oceanic events have also in one case been tied directly to macroevolutionary change. One recent study suggests that the middle-Silurian Mulde event was an important environmental driver of the origination of the brittle star (Ophiuroidea) body plan, through miniaturization and neotony in response to environmental stressors (Thuy et al., 2022).

1.5 Geological setting

1.5.1 The Oslo Region

The Oslo region – also known as the Oslo Graben – is an approximately 10 000 km² Permo-Carboniferous paleorift system extending from the Skien area in the southwest, to the Hadeland and Toten region in the north (Bruton et al., 2010) (see Figure 1.11). Here, a succession of fossil-bearing marine Paleozoic sediments from the Cambrian to the Silurian are exposed. The area has been extensively studied by geologists and paleontologists for over 200 years, and has yielded several unique species, particularly of brachiopods and trilobites. Størmer (1953) divided the Oslo region into 11 *districts* primarily based on paleontological and geological variation from the middle Ordovician (see Figure 1.11). A division which – in several different modifications – has been used by researchers ever since. As seen in Figure 1.11, this study will be primarily focused on the Oslo-Asker districts, the area where the Oslo-Asker, Modum and Ringerike districts intersect, and the Holmestrand district.

1.5.2 The Lower Silurian in the Oslo Region

The seafloor sediments of the Ordovician and early Silurian strata of the Oslo region were deposited as part of an epicontinental seaway on the western submarine shelf of the Baltica

paleocontinent, which is estimated to have been situated around or slightly below the paleoequator in the early Silurian (Baarli et al., 2003; Cocks & Torsvik, 2005). During the Llandovery and Wenlock, the Laurentian and Baltic continental plates collided, initiating the Caledonian orogeny and gradually closing the seaway between the continents. It was gone by the Ludlow, where deposition of floodplain/alluvial sandstone succeeds the marine sediments (Bruton et al., 2010, see also Figure 1.12). This leaves a period of approximately 20 Ma for marine deposition in the Silurian (Bruton et al., 2010). See Figure 1.10 for a generalized interpretation of the paleogeography of Baltica in the early Silurian.

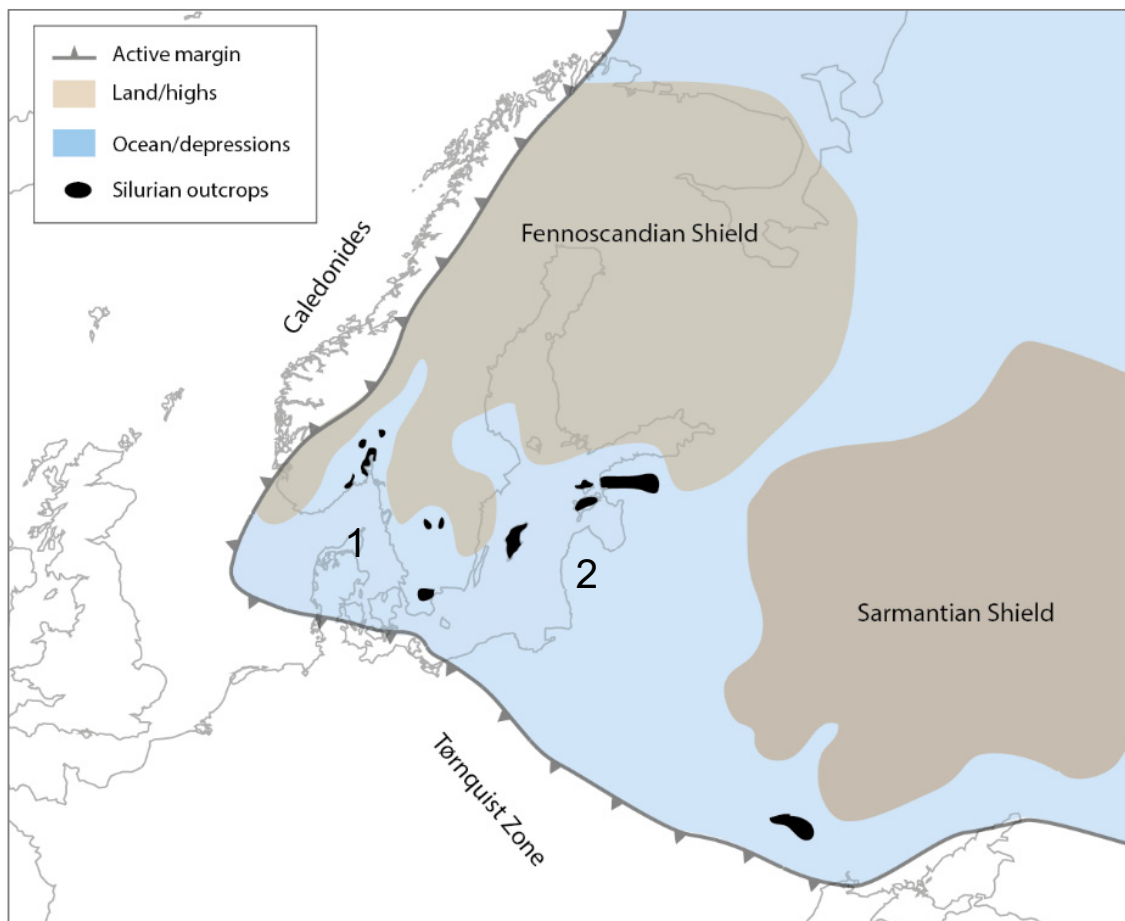


Figure 1.10. Continental configuration of western Baltica in the early Silurian, overlain of modern geography with known Silurian outcrops in black (redrawn from Baarli et al., 2003; fig. 1). 1: western shelf sea (incl. Oslo region). 2: eastern shelf sea (incl. Gotland and Estonia).

1.5.3 Historical definition of the Rytteråker Formation

The sedimentary succession that today corresponds to the Rytteråker Formation was first formally described by Kiær (1908), as stage (*Etagen*) 7a and 7b of the Silurian succession in the Oslo region (with stage 6-10 comprising the entirety of the Silurian system). Kiær's definition of stages 7a and 7b was based primarily on the high carbonate content in the succession, compared to the over- and underlying lithologies, as well as the presence of the brachiopod species *Pentamerus oblongus* and *P. borealis* (today *Borealis borealis* (Mørk,

1981)). The term “*Pentamerus* limestone” (*Pentameruskalk*) was also used by Kiær as a descriptor of this part of the succession, and the name has since been used semi-informally to refer to part or all of the Rytteråker Formation, primarily the sections containing abundant pentamerid brachiopods (e.g. Sneltorp, 2020).

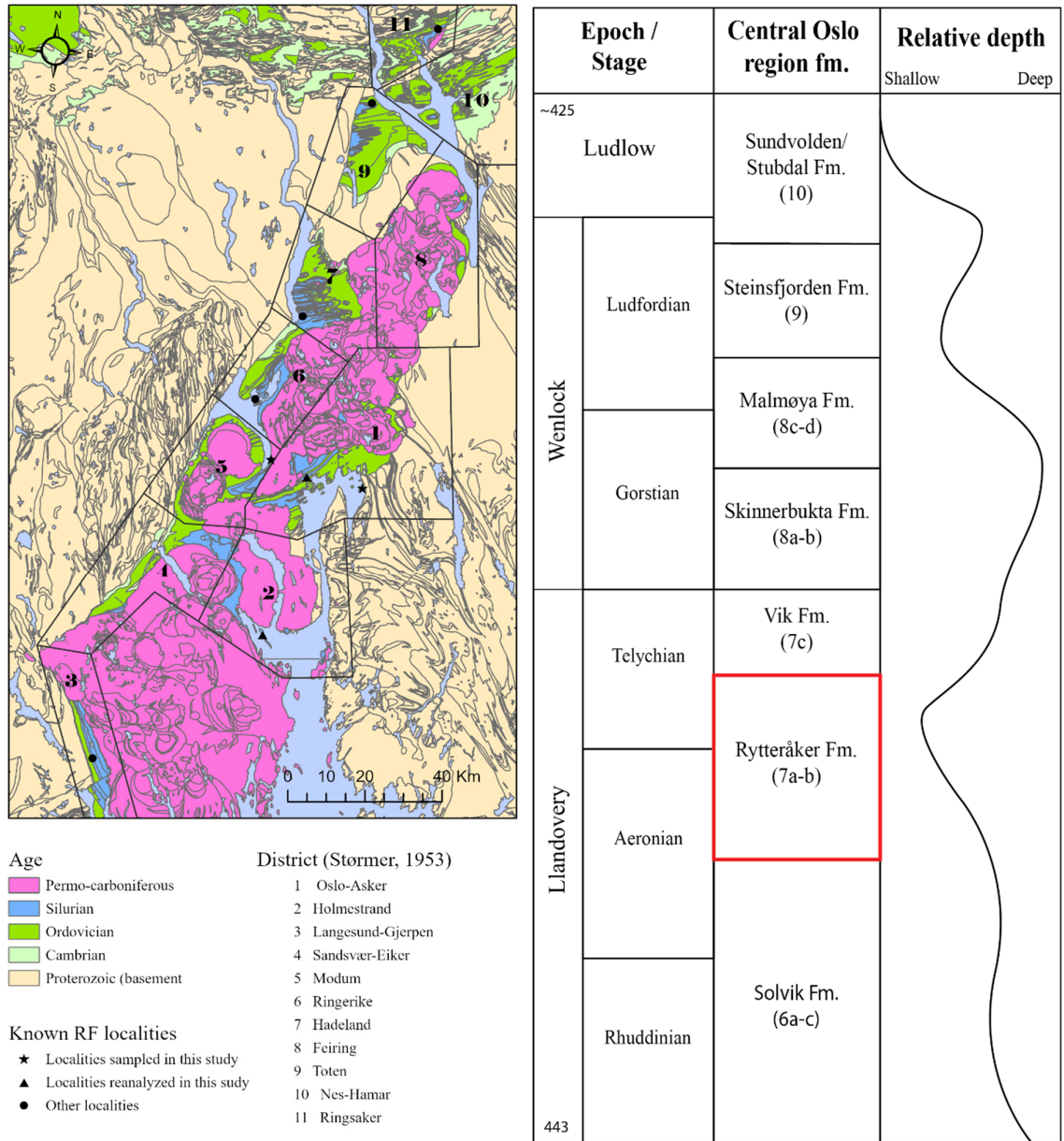


Figure 1.11 (left). Geologic map of the Oslo Region with all known localities of the Rytteråker Formation (RF) marked. Localities sampled in this study are marked with a star. Base topographic map (land outline) modified from Kartverket (2015). Geologic maps modified from Norges geologiske undersøkelse (2022b). Map created in ArcGis Pro (version 2.8.2).

Figure 1.12 (right). Simplified schematic of lithostratigraphic units and in the central Oslo Region, with the ICC Epoch and Stage names in the left column, and approximate corresponding formation, with the corresponding stages of Kiær (1908) in parenthesis, in the middle (adapted from Bruton et al., 2010), with the relative depositional depth curve to the right reported by Baarli et al., (2003) to the right.

1.5.4 Current definition of the Rytteråker Formation

Since the mid-1900s, formations have served as the primary standardized formal unit in geological stratigraphy. According to the definition by the North American Commission on Stratigraphic Nomenclature, a lithological formation is defined as “mappable, tracable succession” of sedimentary rock that “possess some degree of internal lithic homogeneity or distinctive lithic features” (North American Commission on Stratigraphic Nomenclature, 2005). Within this framework, the Rytteråker Formation was formally defined by Worsley et al. (1983) as one of 13 formations comprising the Silurian succession in the Oslo region. Its defining characteristics is the high carbonate content compared to over- and underlying lithologies. Two adjacent outcrops at Rytteråker Farm and Limovnstangen, located in Ringerike, were defined as the type area (indicated as the black dot in the Ringerike district in Figure 1.11). Notably, it is the only Silurian formation that is with known outcrops in all geological districts in the Oslo region as defined by Størmer (1953) (Möller, 1989).

The formation overlies the Sælabonn Formation in the Ringerike, Skien, Hadeland, Toten and Hamar districts, and the Solvik Formation in the rest of the Oslo area. In both cases, the underlying formations are primarily shale- and sandstone dominated, and the base of the Rytteråker Formation is defined as the point where the carbonate content reaches 50%, reflecting a gradual transition from the underlying lithology (Worsley et al., 1983).

Overlying formations are the Vik Formation in the central Oslo region, and the Ek Formation in the Hadeland and Toten districts. Both of these are predominately characterized by shales and carbonate nodules (Worsley et al., 1983). In the type area, the upper boundary of the Rytteråker Formation is defined by a sharp transition from carbonate to shale dominance, which occurs approximately 4 meters below the first occurrence of red shales in the Vik Formation, and the transition is generally similar in other regions (Worsley et al., 1983).

In the latest revision of Silurian lithostratigraphy of the Oslo region (Bruton et al., 2010), the Rytteråker Formation is approximated to have spanned the boundary between the Aeronian and Telychian stages in the upper half of the Llandovery, comprising a time interval of approximately 1-3 Ma, 438 Ma ago. However, it has been argued that the deposition of the Rytteråker Formation may also have been significantly diachronous across the Oslo region (Bruton et al., 2010; Möller, 1989).

1.5.5 Regional variation

Building on Kiær (1908) and Worsley et al. (1983), the majority of the primary research on the Rytteråker Formation consists of facies- and paleoecological studies by Mørk (1978), Keilen (1985), Johnson (1989) and Möller (1987, 1989), spanning the localities shown in Figure 1.11. In the review by Möller (1989), it was remarked that the thickness of the Rytteråker Formation varies significantly between outcrops in the Oslo region, from approximately 15 meters in the north (Hadeland, Toten) to 80-100 meters in the Asker area. Although the “core” area (the central Oslo Region) is typically 40-80 meters in thickness (Möller, 1989). Polynomial

interpolation of the thicknesses reported by Möller (1989) and Johnson (1989) suggest a roughly south-east gradient in increasing formational thickness (figure 1.13).

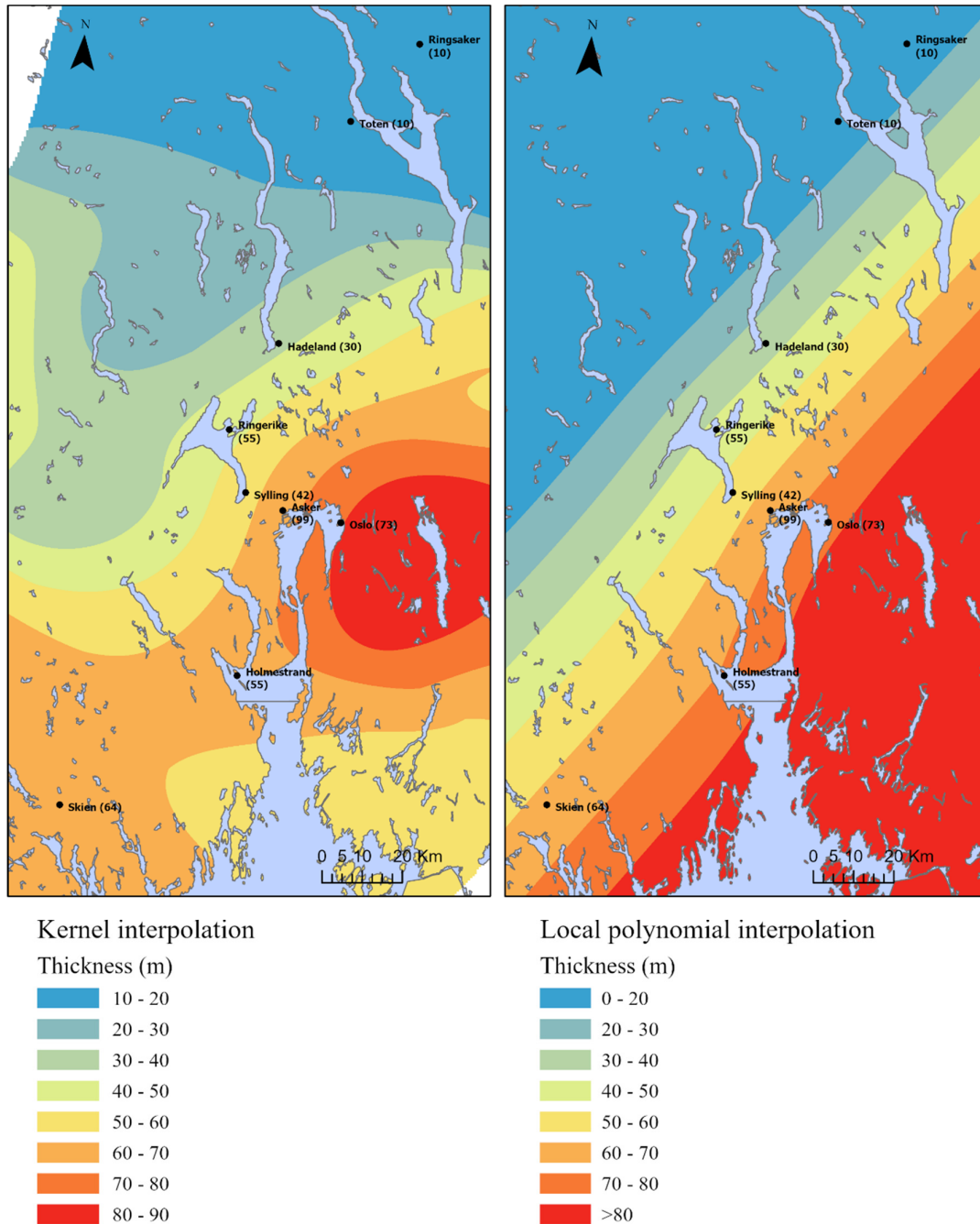


Figure 1.13. Interpolation of the thickness of the Rytteråker Formation in the Oslo region, using kernel interpolation (left) and local polynomial interpolation (right), made using the interpolation tool in ArcGIS Pro (version 2.8.2). Base topographic map (land outline) modified from Kartverket (2015).

While the unifying formational characteristic throughout the region is carbonate dominance, the lithology of the formation also varies substantially both stratigraphically and between regions/localities. A notable and unique feature of Rytteråker outcrops in the Ringerike and Asker districts is an interval containing small to medium coral-stromatoporoid bioherms in the

upper part of the formation, typically associated with a shoal/bank barrier environment (see Section 1.5.6), and interpreted as signs of a sea-level lowstand. At other localities, e.g. at Malmøykalven and Sylling, massive limestone layers are found in the upper part of the formation, and have been taken to be representative of a similar lowstand. Comparative logs, from Möller (1989) are shown in Figure 1.14.

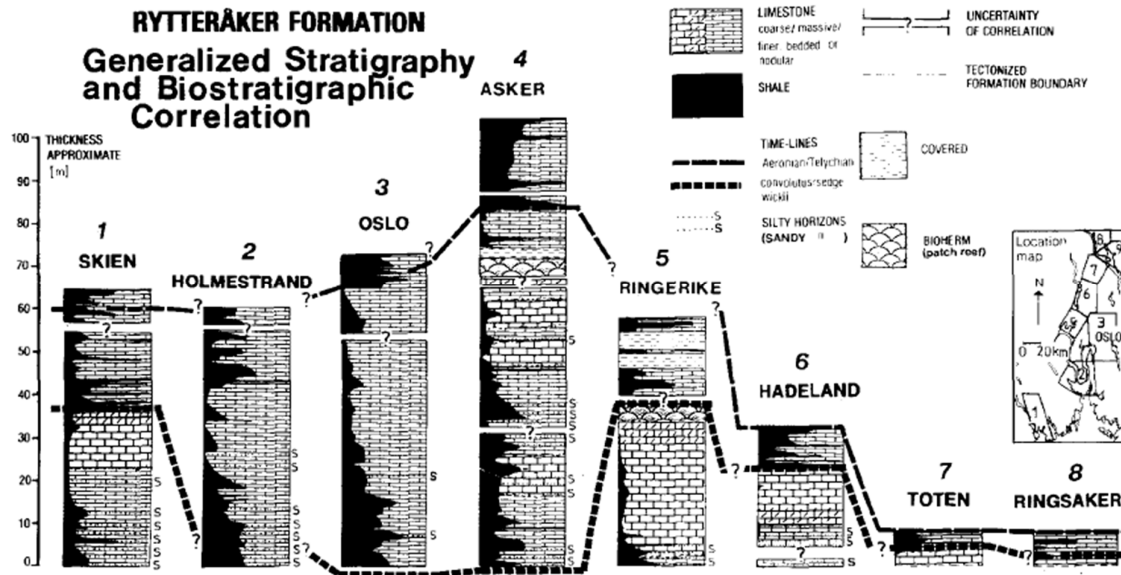


Figure 1.14. Comparative logs from eight different outcrops of the Rytteråker Formation. Reprinted from Möller (1989; fig. 1a).

1.5.6 Paleogeographic and paleoenvironmental interpretation

As a result of the Caledonian orogeny, the relative sea-levels and underwater topography of the Oslo region changed profoundly during the Silurian. Some studies nevertheless suggest that a number of these sea-level changes were consistent across the region, and that the perhaps clearest example of this was the regression-transgression represented in the Rytteråker Formation (Baarli et al., 2003; Johnson et al., 1991; Möller, 1989). However, whether this pattern actually represented a true, global eustatic sea-level change (see Section 1.4.1), or appeared as the result of carbonate buildup temporarily “overtaking” an ongoing transgression caused primarily by the Caledonian orogeny, is debated. Johnson et al. (1991), Baarli (1990b) and Baarli et al. (2003) mainly support the former position, while Möller (1989) advocates the latter.

Interpretation of the underwater topography of the area also differs substantially between studies. While Möller’s depositional model posits an offshore shoal/shell-bank barrier migrating east from Ringerike to Asker between the late Aeronian and the early Telychian, Baarli (1990b) attributes the same development to a foreland bulge from the Caledonian orogeny migrating southeast. The two models also differ with respect to whether they envision the Oslo area as a restricted (lagoonal) marine basin, with a land area to the southeast which

floods during the early Telychian (Möller, 1989), or as part of an open shelf (Baarli, 1990b). A simplified schematic of the two contrasting models are attempted shown in Figure 1.15.

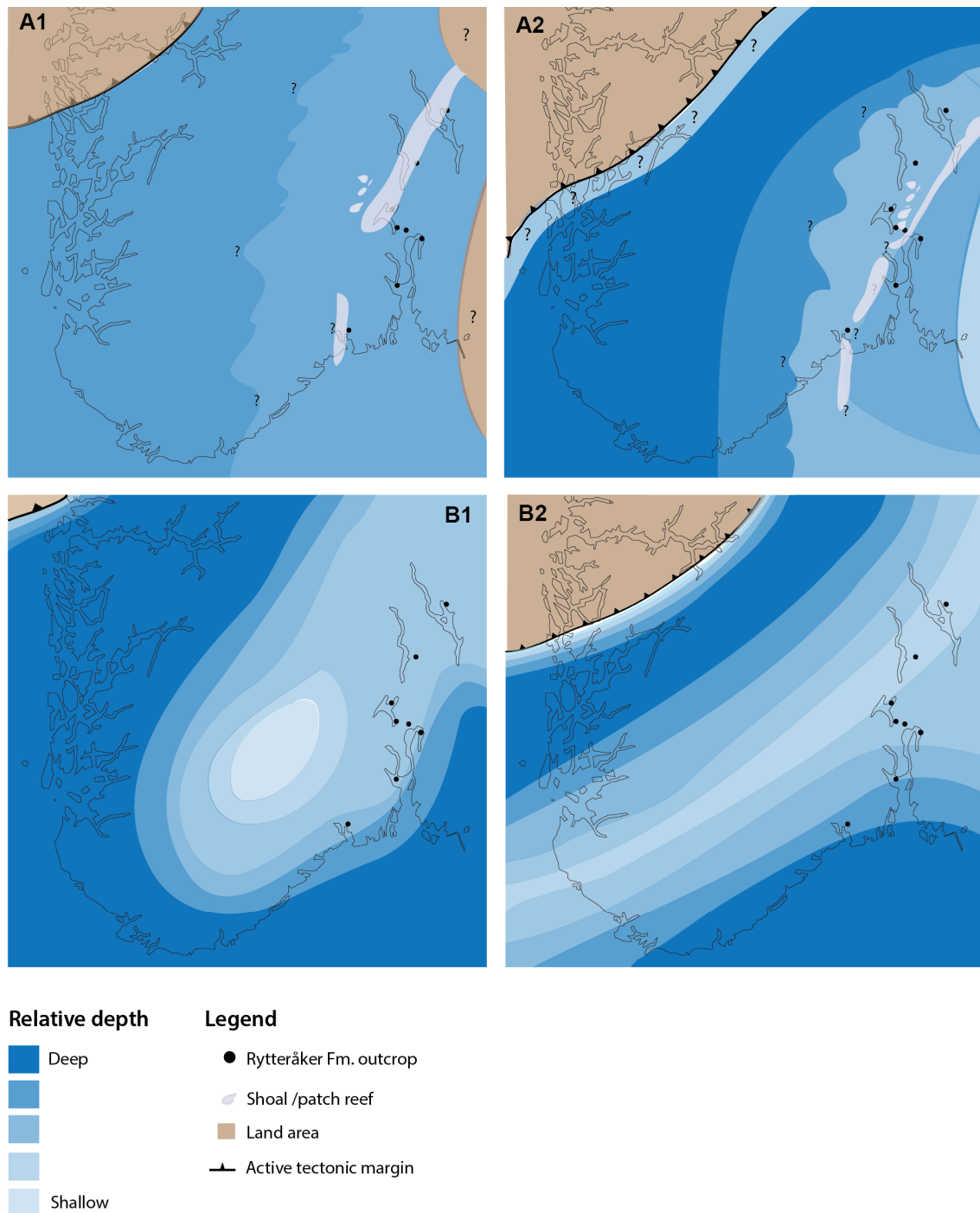


Figure 1.15. Möller model (A, top) and Baarli model (B, bottom) of the paleogeography of the Rytteråker Formation, overlain on present-day geography. Column 1 (A1 and B1): middle Aeronian (approximately). Column 2 (A2 and B2): Aeronian/Telychian transition (approximately). NB: Relative datings in the two original models/figures do not correspond precisely. Redrawn from Möller (1989; fig. 2) and Baarli et al. (2003; fig. 6b & 6c).

2 Materials and methods

2.1 Fieldwork

Samples were collected during the fall of 2020, and the spring, summer and fall of 2021, from Toverud farm (Sylling, Ringerike) and Ulvøya (inner Oslofjorden, s.e. Oslo) (see Figure 2.1). At each site, stratigraphic rock samples of between 200-1500 g were collected semi-randomly at stratigraphic intervals covering the entire outcrop, in order to capture as much lithological and biological variation as possible in the polished slabs and acetate peels. Magnetic susceptibility readings (see Section 1.3) were conducted *in situ* at regular intervals at both localities, and XRF compositional data were recorded from a separate set of samples taken from the Toverud locality. Some sporadic field observations of macrofossils (corals, stromatoporoids, large, well-preserved brachiopods etc.) were also recorded and photographed at each locality. Total numbers of sampled levels at each locality are shown in Table 2.1, and selected photographs from the field sampling procedure in Figure 2.1. The study localities and their particular procedures and concerns are described in sections 2.1 and 2.2, with some representative pictures from the fieldwork and localities shown in Figure 2.2.

2.1.1 Toverud farm, road-cutting

The Solvik and Rytteråker formations are exposed in a road cutting approximately 200 meters north-west from Toverud farm (Figure 2.1b). The locality is assumed to correspond to the locality described by Johnson (1989; fig. 2d). However, as there is some uncertainty as to whether this locality matches the one in the literature, it will be referred to in this study as Toverud 2 (TOV-2). The stratigraphic layers of the southernmost exposure are tilted roughly northwards at an 80° angle relative to the road. The base of the Rytteråker Formation was established by magnetic susceptibility measurements, and markers placed every 2 meters stratigraphically (see example in Figure 2.2a).

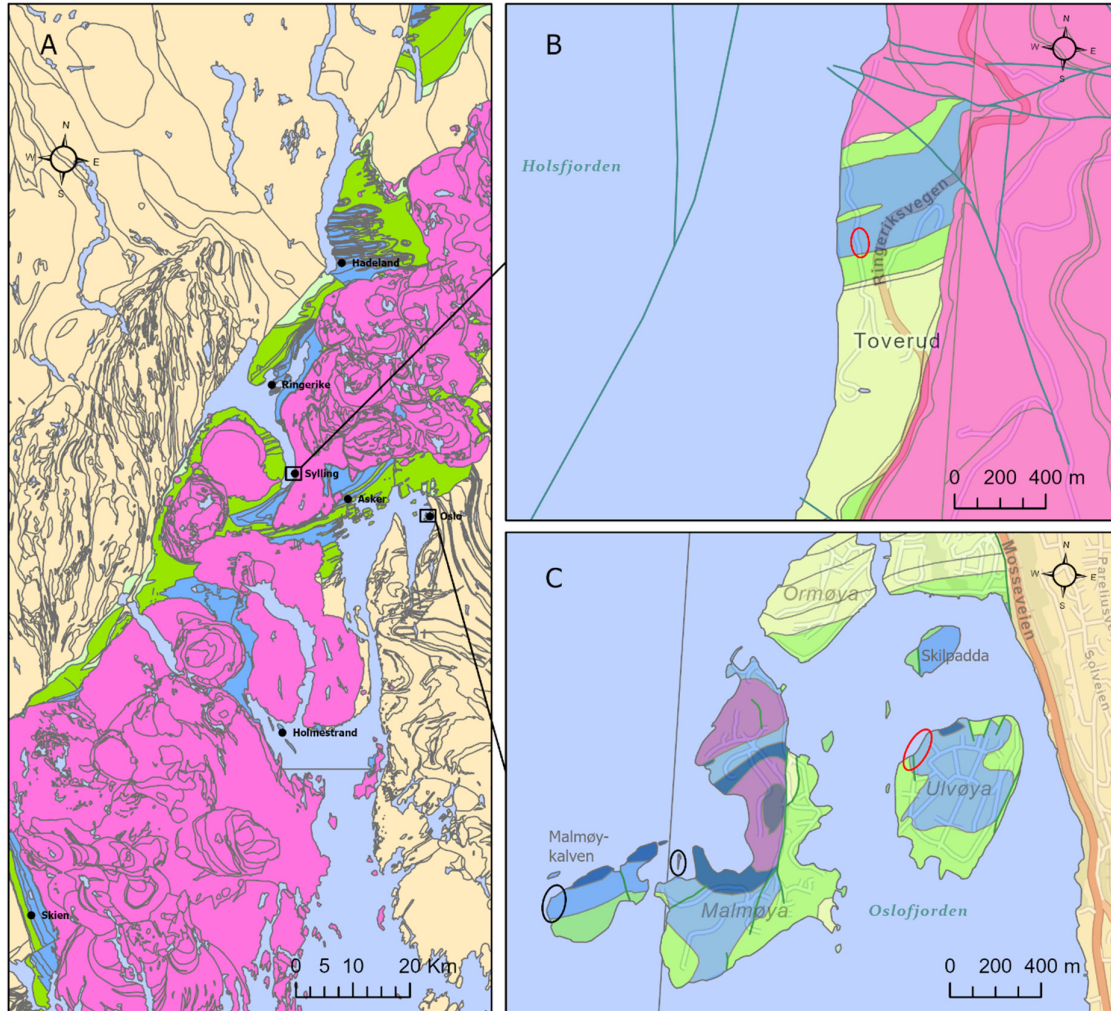
At around 38 meters above formation base, the road cutting is covered with vegetation. Further north, the Solvik Formation is exposed again. However, logs from a shoreface outcrop in Sylling suggests that the total formation thickness in the area is just above 40 meters (Johnson, 1989), implying that perhaps 2-4 meters is missing due to the coverage.

As shown in Figure 2.3, sampling at TOV-2 was done somewhat sporadically, especially in the lowest 30 meters of the section. A consequence of this is that some parts of the sequence, most notably the 5-9 and 20-29 meter intervals, are somewhat poorly covered in the sampling; which again bears on the interpretation of the sequence. A separate set of stratigraphic samples were also collected, approximately every 1 meter, to be used for XRF measurements (see Section 2.2.4).

2.1.2 Ulvøya, north-west shoreface

Rytteråker Formation outcrops are found well-exposed on the north-west shoreface of Ulvøya (Figure 2.1c), transitioning from the underlying Solvik Formation in the west, with the layers tilting northward at a 20-30° angle, lowering slightly with increasing height above formation

base. The base of the formation was established by visual assessment of lithological change from shale/siltstone to carbonate dominance.



Map A

Age

- Permo-carboniferous
- Silurian
- Ordovician
- Cambrian
- Proterozoic (basement)
- Rytteråker outcrops

Map B & C

Lithostratigraphical units

- Permo-carboniferous
- Malmøya Formation
- Skinnerbukta Formation
- Vik Formation
- Rytteråker Formation
- Solvik Formation
- Ordovician
- Proterozoic (basement)
- Fault line
- Sampling locality
- Literature locality

Figure 2.1. A: Geologic map of the central Oslo region, showing outcrops of the Rytteråker Formation described in the literature, as compiled by Möller (1989) (excluding Ringsaker and Toten, see Fig. 1.11). Fossil-bearing sedimentary rocks are found from the Cambrian, Ordovician and Silurian; Permo-Carboniferous rocks are volcanic/plutonic. B & C: sample localities in this study (red ellipses), and the localities sampled by Keilen (1985) (black ellipses). Base topographic maps (i.e. land outline) modified from Kartverket (2015, 2017), geologic maps modified from Norges geologiske undersøkelse (2022b, 2022a), with positions for the Vik Formation in map C based on Keilen (1985). Streetmap layer in maps B and C modified from ESRI et al. (2022). Maps made using ArcGis Pro [version 2.8.2.].

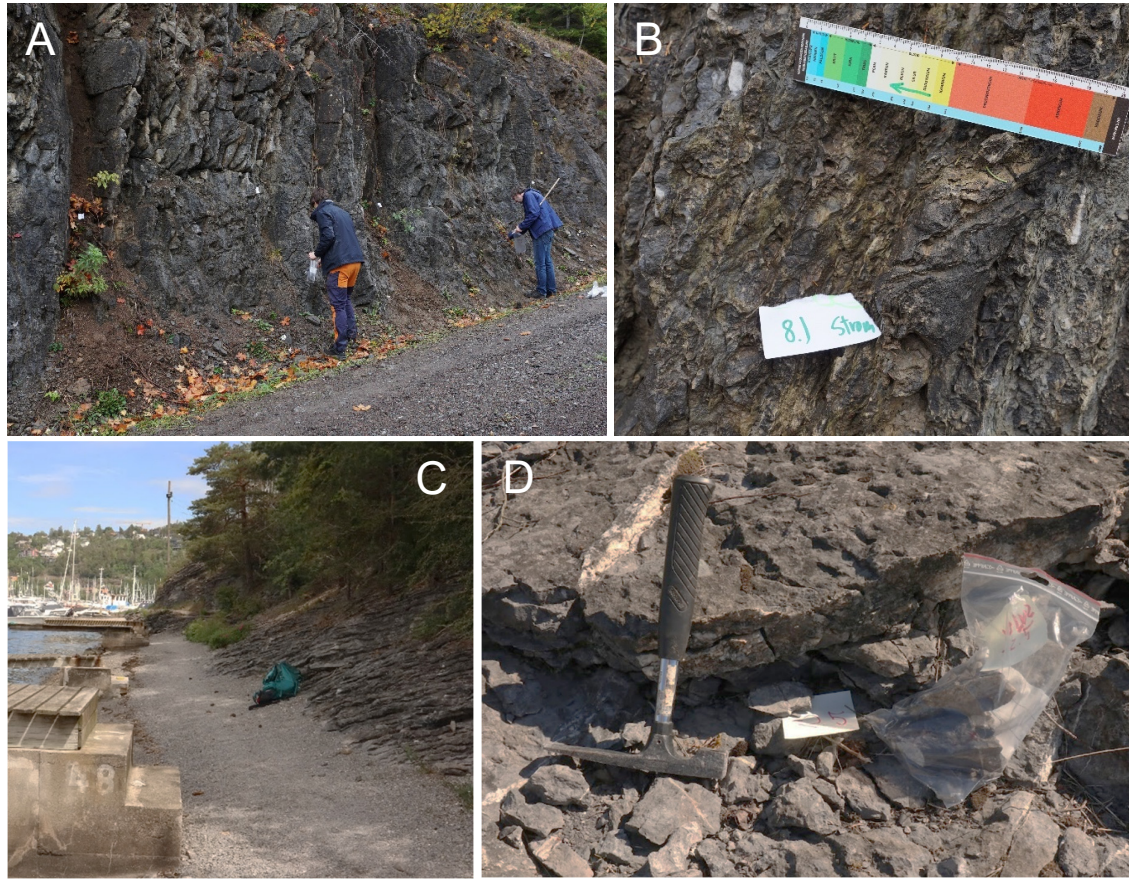


Figure 2.2. A: Study section at Toverud (TOV2), approx. middle of the Section (20 meters above base). Younger layers to the right. White post-it notes represent stratigraphic intervals of 2 meters (see text). B: Study section at Toverud Farm, field registration of macrofossil (stromatoporoid). C: Rytteråker Formation at ULV-2, approx. 25 meters below formation top, facing towards stratigraphic up (north). D: Geology hammer and sampling equipment (ULV-2, approx. 3 meters below formation top).

Approximately 10 meters above the formation base, the sequence is interrupted by a fault (shown in fig 2.1c). The formation resumes some 5 meters further north along the beach, where it continues for another 33 meters, after which it is covered by a small beach. On the other side of the beach (17 meters), what was taken to be the transition from the Rytteråker to the Vik Formation can be seen, with the Vik Formation continuing upward.

The strike and dip of the layers on both sides of the beach were measured, and based on their similarity (300/18 and 311/19), they were assumed to be contiguous. Using these values, and length of the beach, the missing interval was calculated to be approx. 2.5 meters in thickness.

On the basis of this fault line, the Ulvøya locality was divided into two sub-localities, from each side of the fault: ULV-1 (the bottom 10 meters) and ULV-2 (the top 33 meters between the fault and below the beach). Stratigraphic markers were placed every 1 meter, calculated from the base at ULV-1, and from the top (transition to Vik Formation) at ULV-2. Sampling was generally done at regular, 1 meter intervals, although somewhat more sporadically in the ULV-1 Section than the ULV-2 Section (see fig 2.3). Magnetic susceptibility readings were also conducted, and corroborated the placement of the formation base.

The composite Section of ULV-1 and ULV-2 (seen in Figure 2.3) was made by assuming that the Rytteråker sequence at Ulvøya has the same stratigraphic thickness – 70 meters – as measured at Malmøykalven and Malmøya (Keilen, 1985; Möller, 1989), due to their close proximity. This implies that approx. 28 meters of the sequence is missing due to the fault. This interpretation also rests on the assumption that the lack of exposure below the transition to the Vik Formation does not represent a second fault line, as indeed the whole interpretation of the ULV-2 locality does.

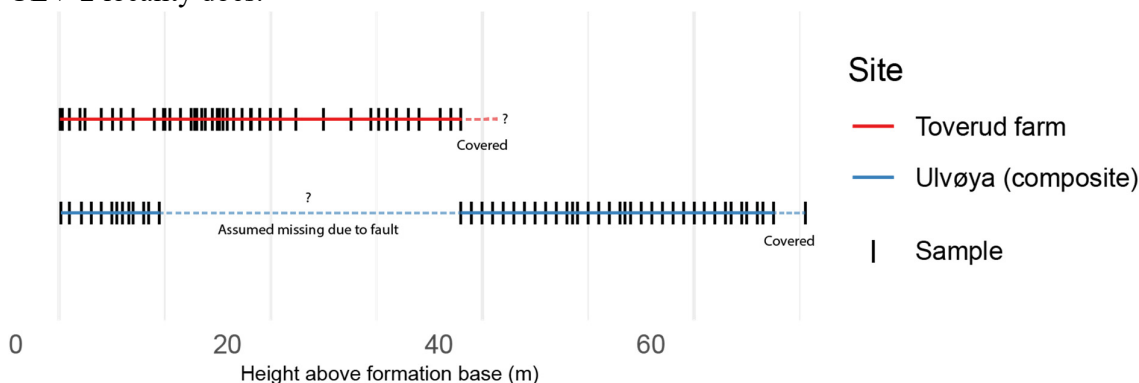


Figure 2.3. Sample positions in absolute height (m) above formation base for both localities. The composite Section from Ulvøya is composed of data from ULV-1 and ULV-2 (see text).

2.1.3 Magnetic susceptibility readings

Magnetic susceptibility readings were taken every 0.5 m through the sections at both localities, using a Terraplus KT-10 handheld susceptibility meter with a 65 mm diameter circular coil. At Ulvøya, a total of 110 measurements were taken, starting from 15 m below the formation base. At Toverud, 87 measurements were taken, starting from 5 m below the formation base. At Ulvøya, 49 measurements were taken below the fault line (ULV1), and 61 samples taken above the fault line (ULV2)

2.2 Lab work

2.2.1 Preparation of samples

As far as possible, samples from each stratigraphic level at each site were cut with a diamond saw parallel and perpendicular to bedding. After cutting, a minimum of two facets (one parallel and one perpendicular) from each stratigraphic level were polished with a Struers Knuth Rotor polishing machine to 320 grit, then scanned at 1200 dpi using a Canon 900F Mark II scanner. After scanning the slabs were further polished up to 800 grit to make acetate peels. Table 2.1 shows a summary of sampling levels, slabs and peels for the different localities. Every slab used to make an acetate peel was assigned a PMO (Paleontological Museum of Oslo) accession number (between 236.402-236.609), with the acetate peel PMOs given as single-letter extensions of these (i.e. 236.500a), similarly with the thin section PMOs (with the extension s). For a complete overview of the samples and slabs with accompanying PMO numbers, see appendix.

Table 2.1. Overview of sample positions and number of samples from each locality.

Sample types	Toverud farm (TOV-2)	Ulvøya west (ULV-1)	Ulvøya northwest (ULV-2)	Total
# sample positions	43	13	35	91
# polished slabs	95	26	76	197
# acetate peels	130	30	81	241
# thin sections	19	0	0	19

2.2.2 Acetate peels

One to four acetate peels were made per sample, preferably at least one in bedding-parallel and one in bedding-perpendicular direction, using a modified version of the method described by Wilson & Palmer (1989), shown in Figure 2.4. Generally, the acid treatment of 5% HCl for 5 seconds proved to be highly effective on the samples, presumably due to their high CaCO₃ content. This is thought to have improved the overall quality and resolution of the peels. The finished acetate peels were put into slide mounts with a 24x36 mm window. This size was chosen both for practical reasons, and because it is comparable to the slab area used in other biofacies studies with similar profiles (Klug et al., 2018). The slides were scanned with a Reflecta DigitDia 6000 Magazin-Scanner at 5000 dpi, and post-processing was done in Adobe Photoshop CS6 (version 13.0) to enhance contrast and light balance, apply sharpening (using the «smart sharpen» function, with Gaussian Blur algorithm), and convert the pictures to greyscale.

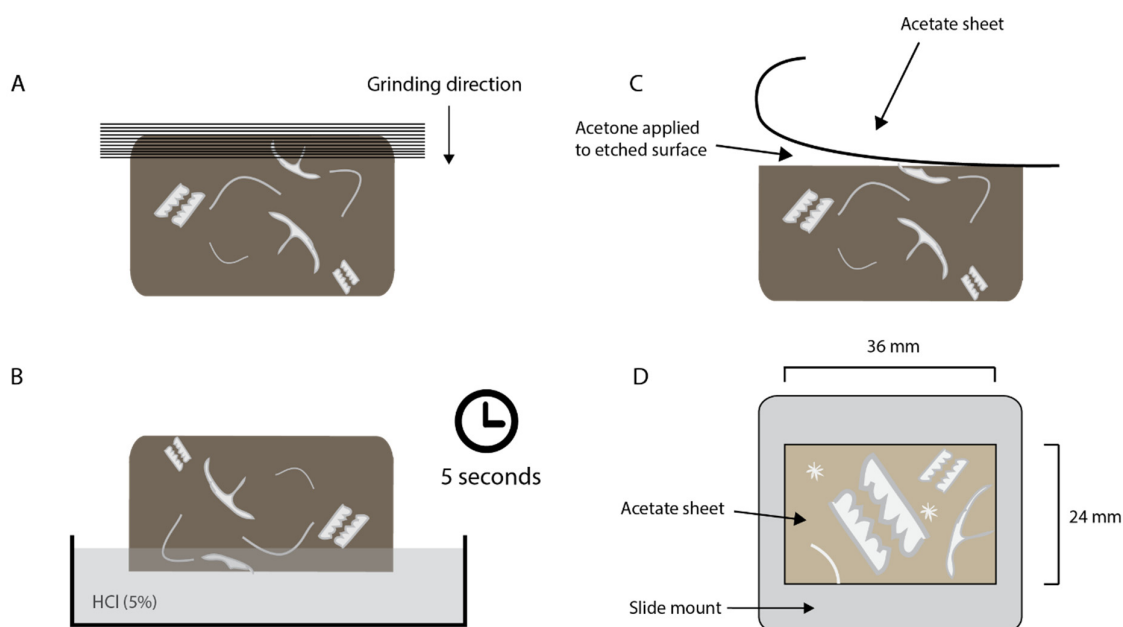


Figure 2.4. The acetate peel procedure. Figure modified from Füsün et al. (2005). A: Grinding of slab down to 800 grit size. B: application of 5% HCl to the slab for 5 seconds. C: After rinsing and drying, acetone is applied to the etched surface, and an acetate sheet is pressed down. D: After drying for 10-30 minutes, the acetate sheet is removed from the slab and fitted into a 24x34 slide mount. The etched size facing towards the front (white side).

2.2.3 Thin sections

A total of 19 thin sections were made from samples from the TOV-2 locality, based on acetate peels with observations of well-preserved, «interesting» and/or hard-to-identify bioclasts, with the purpose of comparing them with their corresponding acetate peels. Thin sections were made by Salahaldin Akhavan at the Institute for geoscience, UiO. The thin sections were scanned with a Nikon Super Cool Scan at 4000 dpi.

2.2.4 XRF scans

XRF measurements were done on 44 collected samples from Sylling, using a handheld XRF scanner (Thermo Scientific Niton XL3t GOLDD+ in the Georef All mode and with 120 s integration time). Ca, Si, Fe, Mn and Sr content was measured on a surface area of approx. 0.8 cm in diameter, and stored in a CSV file. The small size of the study area means that these measurements might be more sensitive to lateral variation than the magnetic susceptibility readings. Similarly to the magnetic susceptibility readings, the XRF values do not represent measures of the acetate peel samples themselves. Therefore, they will be interpreted separately from the acetate peel morphotaxa dataset.

2.3 Data handling and analysis

2.3.1 Subplot frequency count of acetate peels

Subplot frequency counting of the grayscale acetate peel scans and thin sections was done in ImageJ (version 1.53n1). A 40x0.15 cm² grid was overlain on the scans, using the *Grid* plugin. Presence/absence of the different morphotaxa (Table 3.3) for each plot was determined using a combination of the scanned images and optical microscopy of the acetate peels, and registered with the ImageJ MultiPoint-tool (18 parallel, color-coded counters; see Figure 2.5 for screenshot example), with one-point-count per organism group allowed within each grid cell. The measurements were subsequently exported as a data frame row to Google spreadsheets.

2.3.1.1 Choice of morphotaxa categories

18 morphotaxa categories were designated in the samples, in order to capture as much ecologically meaningful variation as possible in the samples. The straight-shelled, impunctate brachiopods, assumed to primarily represent pentamerids, were divided into thin- and thick-shelled based on the common interpretation that these represent adaptations to lower- and higher energy environments respectively (Johnson, 1989; Mørk, 1981). Similarly, the subdivision of tabulate corals into halysitids and favositids/heliolitids, is done on the basis that the two groups are broadly thought represent different ecologies, with the more “massive” and densely packed favositids and heliolitids being generally more adapted to more high-energetic environments (Scrutton, 1998), and. Isolated tabulate corallites with no identifiable affiliation were assigned as indeterminate. Syringoporid tabulate corals were not found either as macrofossils or in the thin-sections, and were subsequently not included as a category. Rough descriptions of the visual identification criteria for each group are summarized in Table 2.2 (representative examples of the morphotaxa are later presented in Section 3.1). To separate between tabulate

corallites and bryozoan zooids in cases of doubt, a practical cutoff of 1 mm diameter was used, as it is a size almost never exceeded by bryozoan zooids (Ryland et al., 1986), and tabulate corallites are often substantially bigger (Scrutton, 1998).

Table 2.2. Organism groups and identification criteria in thin sections and acetate peels.

Organism group	Identification	Abbreviation
Calcareous tubes	Calcareous tube of unknown affiliation, see PMO 236.404a.	calc_tube
Small bryozoans	Bryozoan with no clear bilateral symmetry, regular/small apertures.	bryo_small
Large bryozoans	Bryo. with no clear bilateral symmetry, irregular/large apertures	bryo_large
Bifoliate bryozoans	Bryo. with clear bilateral symmetry	bryo_bifoliate
Tentaculitoids	V-shaped, lamellar wavy shells	tentaculitoid
Favositid/heliolitid tabulate coral	Tabulate coral with "honeycomb" and/or closely spaced corallites.	tabcor_favhel
Halysitid tabulate coral	Tabulate coral with corallites in a chain.	tabcor_hal
Calcareous algae	Microbial filaments (<i>Girvanella</i> sp.)	algae
Rugose coral	Round, singular coral with radiating septa	rugcor
Trilobites	"hook" or "bumped curve" arthropod shell	trilobite
Gastropods	Swirly or "two-storied" shape, usually micritized with a calcitic lining	gastropod
Ostracods	Small curved arthropod shells, either two together with hinges or clearly delineated curved single valve	ostracod
Thick, straight-shelled brachiopod	Straight-shelled brachiopod with thick prismatic lining (i.e. <i>Borealis borealis</i>)	brach_thick
Thin, straight-shelled brachiopod	Straight-shelled brachiopod with thin or absent prismatic lining (i.e. <i>Pentamerus oblongus</i>)	brach_thin
Wavy and/or punctate brachiopod	Wavy and/or punctate brachiopod shells	brach_wavy
Crinoid	Identified either by shape ("crocodile mouth" or "donut"), or calcitic structure (single crystal).	crinoid
Stromatoporoid	Characteristic "speckled" and layered blob	strom

2.3.1.2 Data normalization

In the cases where the acetate peel or thin Section was insufficiently large to accommodate 40 subplots (or parts of the section/peel were obscured due to air bubbles, e.g.), the maximum viable number of squares below 40 was counted, and the number of squares recorded in the dataset. As a result of this, the frequencies for each morphotaxa group (i) were normalized with the following equation before data handling:

$$y_{ij} = \frac{x_{ij}}{n_j} * 40 \quad (\text{Eq. 1})$$

where n_j = number of subplots counted in the sample j . While this approach made it possible to compare plots with unequal numbers of subplots, it is important to keep in mind that it comes with some uncertainty, as it assumes that the average ratio between organism group abundances remains the same in the subplots that are not observed.

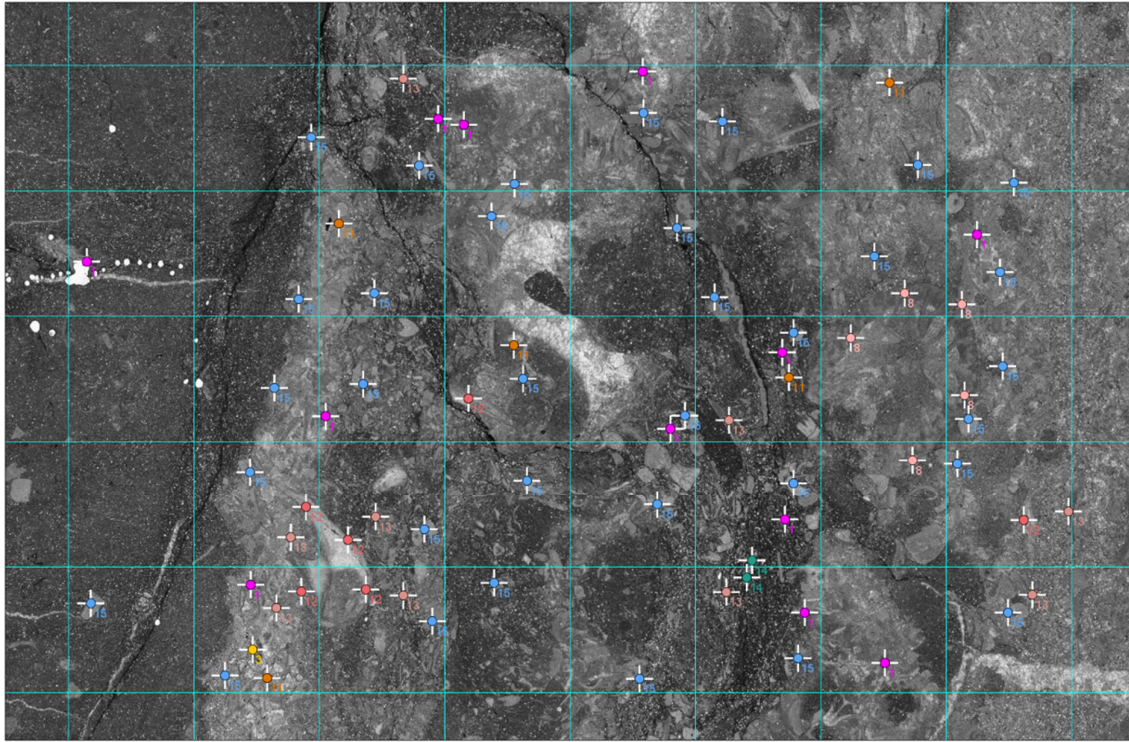


Figure 2.5. Screenshot of counting procedure (PMO 236.404a, TOV-2, 0.3 m.a.b.). Cyan lines represent the sampling grid (40 subplots), colored crosses represent different organism groups.

Especially for organisms with generally low abundances in the data (e.g. trilobites and tentaculitoids), and in plots where fossils fragments are unevenly spatially distributed (i.e. «clumped»), the effects of over- or underestimates of abundances due to this method will be the most serious. However, as no plot accommodated less than 25 subplots, and the vast majority over 35, it is assumed that the effect of this normalization is generally small.

2.3.1.1 Abundance-scale weighting

After standardizing the data to 40 subplots, 5 derived datasets were made by applying the exponential weighting function described in Økland (1986), in order to investigate the effect of subplot density and species dominance on the resulting ordination (see Section 1.2):

$$y_{ij} = x_{ij}^{\frac{\log(R)}{\log(A)}} \quad (\text{Eq. 2})$$

Where A is the range of the original abundance scale (=40), and R is the range of the new abundance scale. Five derived datasets were created using different values for R (based on Eilertsen et al., 1990; Økland, 1986): 1) $R=16$, fairly strongly emphasizing dominance, 2) $R=8$, moderately emphasizing dominance, 3) $R=4$, roughly corresponding to the length of many semi-quantitative scales widely used in present day ecology (Ohgaki, 2011), 3) $R=2$, weakly emphasizing dominance, and 4) presence-absence ($R=0$). A comparison of the different weighting functions standardized to an abundance range of 40 can be seen in Figure 2.6.

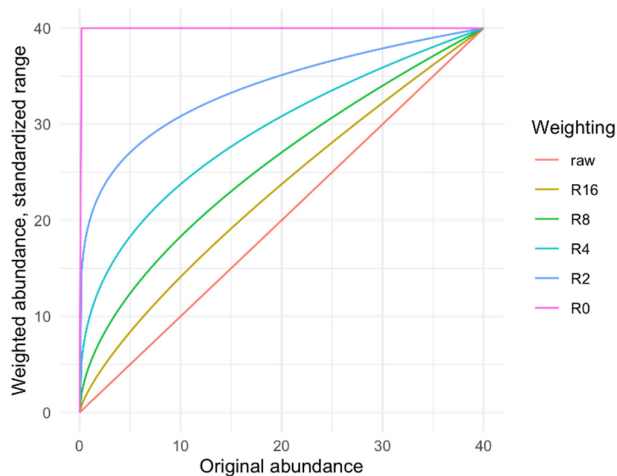


Figure 2.6. Curve-shapes of standardized, weighted abundances (y axis), plotted against the original abundances (x axis).

2.3.2 Bioturbation measurements

The degree of bioturbation in each acetate peel was estimated by drawing freehand selections in ImageJ around parts of each peel visually assessed to be bioturbated (see ex. in Figure 2.7), within the 6 cm² area of the subplot grid, or otherwise the area of the subplots counted (see Section 3.1). The total area of the selection was measured using the ImageJ «measure» tool, and divided by the area of the subplot grid to give a bioturbation fraction measurement on a scale from 0 to 1. Identification of bioturbation was primarily based on visual examples from Flügel (2004).

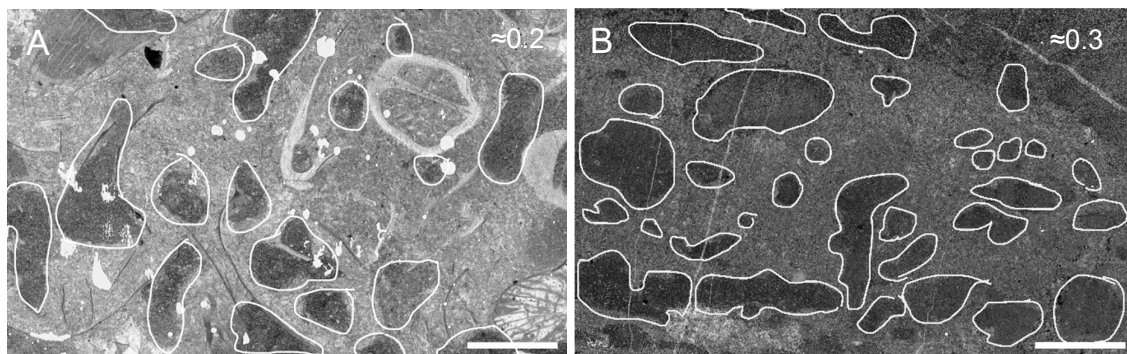


Figure 2.7. Screenshots of bioturbation measurements. White outlines represent freehand selections around bioturbated areas, and the numbers in the top right corners are the approximate fractions of the area bioturbated, as calculated. A: Acetate peel (TOV-2, PMO 236.485b). B: Acetate peel (ULV-2, PMO 236.580a). Scale bar = 5 mm.

As identification and clear delineation of trace fossils proved difficult in many peels – especially in some mudstone-dominated samples from Ulvøya with a generally uniform and undifferentiated matrix – a risk of systematic underestimation of bioturbation in these samples cannot be disregarded. Especially due to the fact that macro-scale ichnofossils were observed visually in the field, and the overall high degree of bioerosion of the bioclasts observed in the peels (as compared to most samples from TOV-2), suggesting there must have been substantial biological activity in the sediment.

2.3.3 Lithological classification

In order to provide an environmental explanatory variable to describe the overall, geological composition of the rock sample, a simple version of the Dunham carbonate classification scheme (Dunham, 1962) was applied to the counted acetate peel and thin Section samples. This was done both to provide some measure to assess the effect of sampling within temporally and spatially heterogenous sedimentary settings on any gradients observed in the ordination, as well as make it easier to interpret the results in light of previous sedimentological studies. In samples where different parts of the peel had clearly different lithologies (e.g. Figure 2.8e), the area of each lithology was measured using freehand selection and measurement in the same way as described in Section 3.2, in order to roughly calculate the fraction of different lithologies in each plot. The rationale for using the Dunham classification of carbonates rather than, for instance, the arguably more detailed Folk classification (Folk, 1962), is both due to it being simpler, thus requiring less time and previous sedimentological experience to apply, and because it is the most widely used carbonate classification system in the world – albeit in a number of variations (Lokier & Al Junaibi, 2016). It is also the system extensively used and referenced by Keilen (1985) and Möller (1987, 1989).

The delineation between the different Dunham classes is, however, prone to significant subjective bias, which has been recognized as a challenge inherent to the method (Lokier & Al Junaibi, 2016). In the case of the samples in this study, the determination of grain-support vs mud-support, and the delineation of packstone and grainstone, were particularly challenging. For instance, many of the samples here classified as packstone (e.g. figs. 2.8c or 2.8e), contain significant areas without carbonate mud, and would be classified as either poorly washed or unsorted biosparite using the Folk classification (Folk, 1962), which is partially used by Möller (1989). Thus, it is sometimes unclear if these areas should be considered grainstone «patches», or the whole sample be considered packstone on account of the presence of mud. As none of the samples were entirely mud free, this latter interpretation would imply that there are no grainstones in the dataset. However, a too liberal use of the of the former interpretation would make the delineation of packstone almost impossible. It was thus decided that the grainstone category was only to be used on samples where the break between mud-free areas and mud-containing areas is also accompanied by a clear break in lithology (as in Fig. 2.8d). This implies that grainstones are very rare, but not absent, in the dataset, and that most areas containing sparry cement (such as Fig. 2.8c the top portion of 2.8e), are classified as packstones.

Table 2.3. The Dunham classification of carbonates, as applied in this study.

Classification (Dunham, 1962)	Definition
Mudstone	<10% grains
Wackestone	>10% grains, mud supported
Packstone	>10% grains, grain supported, mud present
Grainstone	Grain supported, contains <1% mud

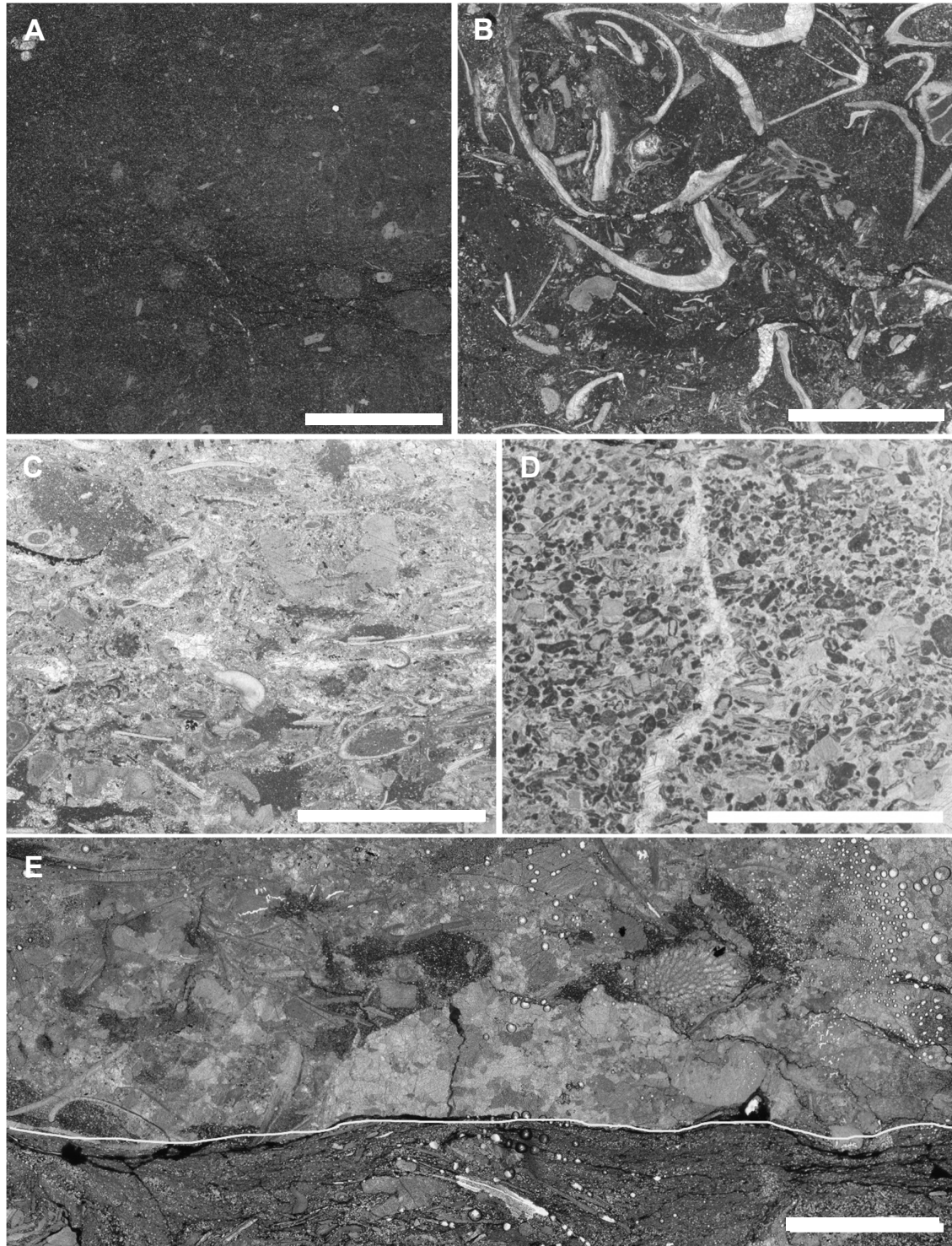


Figure 2.8. Examples of the different Dunham types observed in the peels/thin sections (screenshots of scanned images). A: Mudstone, acetate peel (ULV-1, PMO 236.525b). B: Wackestone, thin section (TOV-2, PMO 236.468s). C: Packstone, thin Section (TOV-2, PMO 236.450s). D: Grainstone, thin section (TOV-2, PMO 236.497s). E: Delineation using freehand selection (white line) between wackestone (bottom) and packstone (top), acetate peel (TOV-2, PMO 236.426a). All scale bars = 5 mm.

2.3.4 Assignment of ecological categories

The assignment of “Bushian” ecological categories (see Table 1.2) to the morphotaxa groups observed in the peels was based on the life modes which appeared to be most common in the groups in the Silurian (shown in Table 3.3). However in some cases there were more uncertainties than others: especially with regards to clades with high ecological diversity such as trilobites and ostracods, and groups of unknown taxonomic affiliation such as tentaculitoids. In these cases the ecological categories designated were based on what appeared to be the dominant forms of life within the clades in the early Silurian (Fortey, 2014; Larsson, 1979; Siveter, 1984). However, as evidence of whether surficial or semi-infaunal modes of life were most common in the period seemed inconclusive, the tiering-category of these groups was set to “surficial/semi-infaunal”.

The question of attachment versus non-attachment to the sediment was also difficult to confidently assign for a number of the sessile filter feeder categories. In the end, it was decided that the presumably pentamerid (thin- and thick valved, straight) brachiopods be designated as unattached, due to the prevalent interpretation of the *Pentamerus* genus as free-lying (Mørk, 1981; Watkins, 1994), while the tabulate corals were categorized as attached due to the evidence that most species at least required some attachment during early stages of development (Dhungana & Mitchell, 2021; Scrutton, 1998). In the case of non-pentamerid brachiopods, the mode of attachment was characterized as “sessile, unknown”.

Despite being of unknown affiliation, the calcareous tubes observed at the bottom of were assigned an infaunal tiering, due to their superficial similarity to infaunal worm tubes, but this is based largely on speculation. In all cases, the distribution of different groups resulting from these very broad categorizations should be interpreted with a great deal of caution.

2.3.5 Shell orientations

Shells reasonably identifiable as brachiopod shells were counted from the polished slabs from the TOV-2 dataset (to a total of 300 shells from 34 samples), and classified as either convex or concave up using the ImageJ multi-point tool (0 = convex up, 1 = concave up). For each sample, the area of the slab was also measured by using freehand or polygon selection, calibrated to the ruler scanned with the slab.

The polished slabs from Ulvøya contained too few clearly identifiable brachiopod shells for a statistical treatment to be viable, consequently shell orientation counts were not done on samples from ULV-1 and ULV-2.

2.3.6 Reanalysis of Malmøykalven and Jong microfossil data

Coral and stromatoporoid data from Malmøykalven and Solhaugveien (Jong, Asker) given by Keilen (1985, appendix 3) was digitized in a CSV spreadsheet. As Keilen (1985)’s other registrations, from Vallerkroken (Bærum), were incomplete with regard to lithological matrix, they were not included in the study. This was also the case with the width and height

measurements from Malmøykalven presented in Baarli et al. (1992), which were difficult to read and interpret from the raw data (Baarli, pers. comm.), and were subsequently dropped from the study.

In the dataset, the sums of registrations for growth forms and lithological matrix were each given a value of 1 per individual, meaning that where – for instance – two growth forms are registered for a single individual, each growth form received a value of 0.5. A derived dataset with abundances of each taxonomic group in each plot, as well as the average of each lithologic/morphologic variable (14 in total) for each plot was thus created with this precept.

Due to the original study only encompassing five coral/stromatoporoid groups, it was decided to be more meaningful to perform ordinations on the plot averages of these lithological/morphological variables, rather than on the abundances of the different coral/stromatoporoid groups.

2.3.7 Reanalysis of Bjerkøya bedding plane point counts

Point counts of 19 0.5x0.5 m plots (100 points in each) from 4 bedding planes at Etage 7b (assumed to correspond to the middle Section of the Rytteråker Formation, see Section 1.5), from Mørk (1978, Table 4), were digitized in CSV format. In the case where a taxa/lithology was present in the plot, but not intersected by any points, they were registered as a + in the CSV file, same as in the original table. This made it possible to create two parallel datasets where they are given a count of either 1 (i.e. outlier-inclusive) or 0 (i.e. outlier-exclusive), to assess their impact on the resulting ordination (as discussed in Section 1.2.1.2). The semiquantitative registrations of trace fossil groups in each plot are registered on an abundance scale from 0 to 3, corresponding to the number of «+» signs used in the original table.

2.4 Statistics

All data handling and statistics was done in R (version 4.0.5). All ordinations were performed with functions from the *Vegan* package (Oksanen et al., 2019), and most other statistics (e.g. correlation testing) using base R functions. Plot graphics were primarily made using the *ggplot2* package (Wickham, 2016), and other functions from the *tidyverse* and related package (primarily *dplyr* and *reshape2*) were also used for data handling (Wickham et al., 2019). Some smaller R-packages were additionally used for various minor functions (e.g. *ggimage* for displaying the fossil symbols in the ordination diagrams). In some cases (e.g. Figure 3.22), the plots were post-processed in Adobe Illustrator, for instance in order to represent missing stratigraphic sections. The following sections contain a brief description of the individual choices of ordinations and tests for the different analyses. All the R scripts used, as well as the raw data from both the novel study and the reanalyses (in CSV format), can be accessed at GitHub (<https://github.com/audunrug/Paleoecology-of-the-Rytteraker-formation-MSc-thesis-data.git>).

2.4.1 Shell orientation modelling

To assess the statistical relationship between the fraction of brachiopod shells preserved in a convex-up position and stratigraphic level, as well as their relationship to two potentially confounding variables: sample size and shell density per cm², four generalized linear models (GLM) and one linear model (LM) were made using the *glm* and *lm* functions in R respectively. Because the likelihood of convex or concave shell orientation is a binomial variable, it was modelled using a binomial GLM (adjusted for different sample sizes) as a function of stratigraphic position shell density and sample size. Sample size was modelled using a GLM with quasi-poisson distribution, due to sample size being a discrete “count” variable, and because the high overdispersion (>5) of the data made it unsuited to fit to a standard Poisson regression. Due to shell density being a continuous variable, a simple linear regression was considered sufficient for this data.

2.4.2 Abundance/diversity metrics

In order to provide some general metrics with which to describe the overall composition of morphotaxa in the samples, species richness (i.e. number of different morphotaxa in a sample), the Shannon-Wiener diversity index (Shannon’s H) and species evenness (E) were calculated for all acetate peels. These metrics are widely used to describe “ecosystem properties” in both present-day and paleoecology (Tuomisto, 2010), and were applied for the purposes of making the results of this study more comparable to the rest of the field. Even though they are not applied to true species, these metrics may still give some indication of the general diversity and disparity trends among the morphotaxa groups.

2.4.3 Ordinations

In order to enhance the reproducibility of the results, and make the different case studies as comparable as possible, all ordinations were performed using the same *vegan* functions, with similar parameters. PCA ordinations were performed using the *rda* function, with the scaling parameter set to true. CA was performed using the *cca* function. DCA was performed with the *decorana* function, while (G)NMDS was performed using the *metaMDS* function, with autotransformation of the data set to false, and the geodetic stepacross method to be applied when dissimilarity equals 1. The maximum number of NMDS runs from random starting positions was set to 300 (trymax=300), and PCA rotation of the points were conducted on the NMDS diagram resulting from the most stable solution with the lowest stress value from the multiple iterations.

As per the description of the study, all four ordination methods were applied to the raw SF morphotaxa abundance matrix from the Toverud and Ulvøya acetate peel study. For ordinations of the abundance-scale weighted datasets however, only DCA and NMDS were selected in order to make the comparison more practicable, and because these two ordination methods were deemed most likely to be the ones most appropriate for the data (see Section 1.3.2).

For the Malmøykalven/Jong dataset, PCA and NMDS were chosen as comparative ordination methods, due to the variables ordinated being more related to environmental variables rather than species abundances, and might therefore be expected to follow a more linear relationship with potential ordination axes. The contingency analysis-based methods (CA and DCA) of unimodal species optima would therefore assumed to be less fit (see Section 1.3).

For the Holmestrand bedding plane data, DCA and NMDS were chosen as comparative ordination methods, due to the dataset being more comparable to the morphotaxa abundance data set from Toverud/Ulvøya, and might be presumed to accommodate unimodal species optima along a primary gradient.

3 Results

3.1 Toverud and Ulvøya supplementary data

3.1.1 Field observations of macrofossils

While no systematic field survey was conducted, macrofossils of corals, stromatoporoids and pentamerid brachiopods were registered both at the Toverud and Ulvøya localities, although with some important variations. A short qualitative comparison of the two localities is provided in Table 3.1, with representative image examples in figures 3.1 and 3.2.

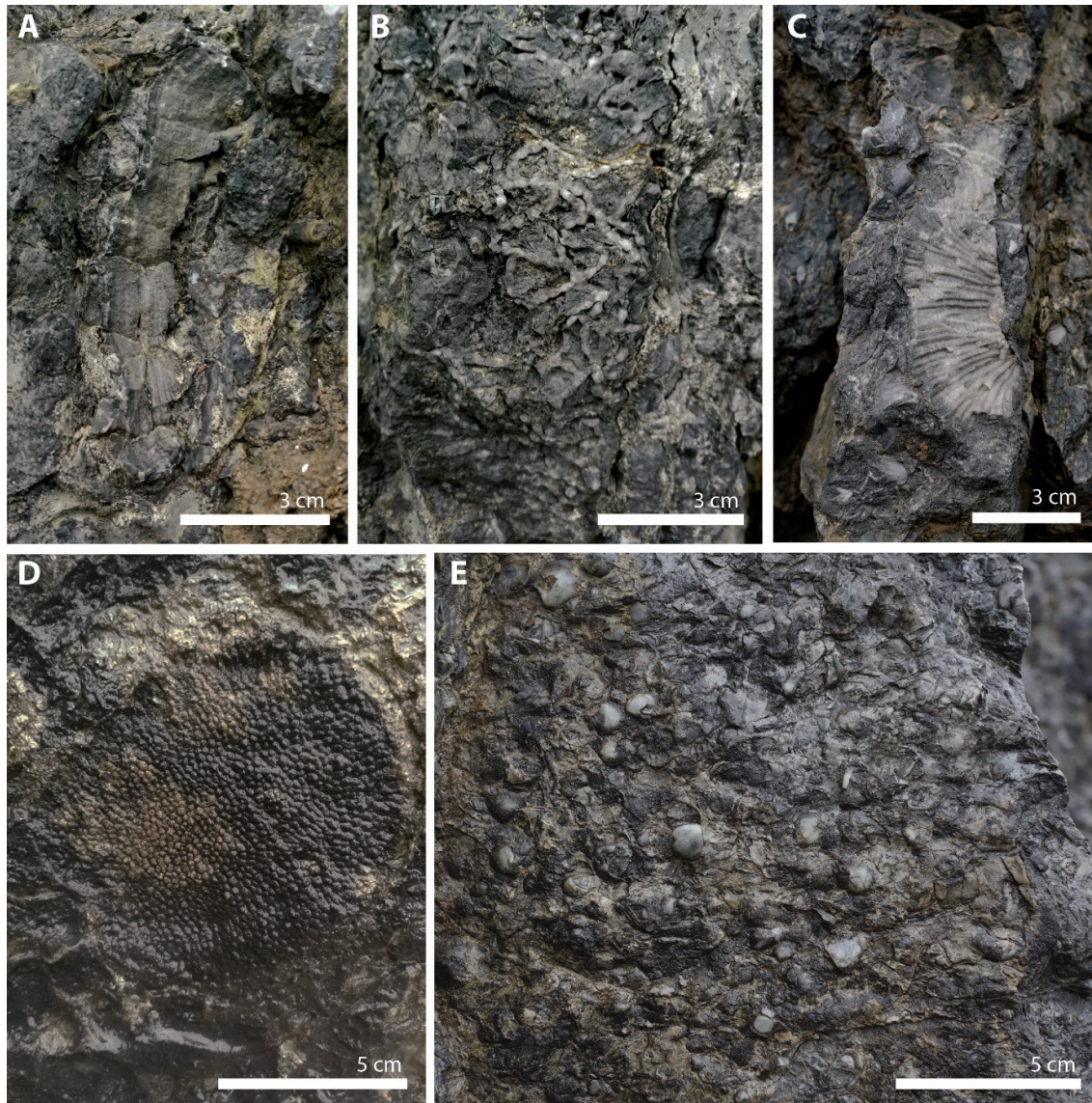


Figure 3.1. Selected macrofossil observations from the TOV2 locality. m.a.b. = meters above formation base. A: Stromatoporoid (8.8 m.a.b, left=stratigraphic up). B: Halysitid, chained tabulate coral, 17.2 m.a.b., left=stratigraphic up). C: Favositid tabulate coral (10 m.a.b., left=stratigraphic up). D: Favositid tabulate coral, top-down view of bedding plane, 26.5 m.a.b.) 2). E: “shell pavement” composed of pentamerid brachiopods (top-down view of bedding plane, 18.3 m.a.b.).

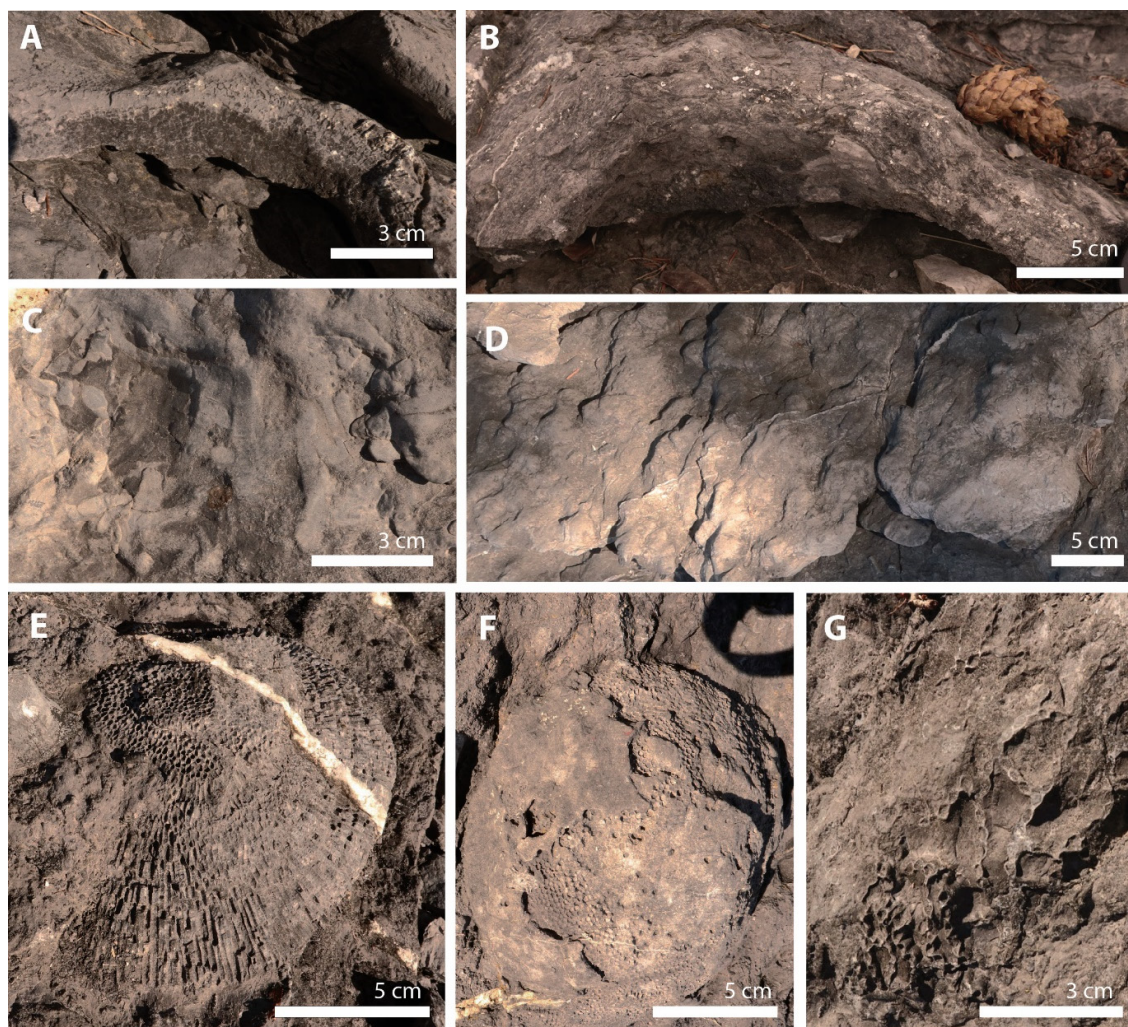


Figure 3.2. Selected macrofossil observations from the ULV2 locality. A: Tabulate coral, approx. 21 m.b.t. Up = stratigraphic up. B: Stromatoporoid, approx. 21 m.b.t. Up = stratigraphic up. C: Chondrites-like trace fossils, approx. 3 m.b.t. Top-down view of bedding plane. D: Thalassinoides-like trace fossils (approx. 12 m.b.t., top-down view of bedding plane). E: favositid colony in overturned position (ca. 3 m.b.t., top-down view of bedding plane). F: favositid colony in upright position (ca. 3 m.b.t., top-down view of bedding plane). G: Halysitid colony (ca. 3 m.b.t., top-down view of bedding plane).

The greatest qualitative difference between the localities was that the Toverud section contained several layers of clearly defined pentamerid brachiopods in the middle and upper-middle part of the section, most clearly exemplified by the “coquina” layer shown in Figure 3.1a and was generally more abundant in identifiable body fossils. Conversely, at the Ulvøya locality only a few poorly defined casts of possible large pentamerids were found (e.g. PMO 236.534 and 236.534). In large portions of the section (especially in the ULV1 locality and the middle part of ULV2), extremely few weathered-out fossils were observed. A few moderate to large favositids and stromatoporoids nevertheless occurred sporadically in the lower part of ULV2 (Fig. 3.2a and b), and in greater numbers and more clearly weathered out at the top of the ULV2 locality, directly below the beach covering (Fig. 3.2e and f), together with several halysitids (Fig. 3.2g). At least two (small) bedding planes at Ulvøya contained clearly identifiable tracefossils, one Thalassinoides-like (Fig. 3.2d) and one more Chondrites-like (Fig.

3.2c), neither of which were registered at Toverud. The corals and stromatoporoids registered at Ulvøya also seemed to generally be somewhat larger than at Toverud.

In addition to the fossil groups mentioned here, a possible large, weathered out ostracod (ca. 1 cm in diameter), and similarly sized gastropod was observed in a sample from ULV2 at 32 m.b.t. (PMO 236.553), and a large (~4 cm in diameter) gastropod was found at the base of TOV2 (PMO 236.402-3).

Table 3.1. Qualitative summary of the field macrofossil observations from each locality in the study.

Macrofossil	Toverud	Ulvøya
Favositid corals	One photographed occurrence at 10 meters (Fig. 3.1C), and several at a bedding plane at ca. 26.5 m.a.b.	Several large, well-preserved and out-weathered specimens in the upper part of ULV2, right below the beach covering (ca. 2.5-3.5 meters below the top (m.b.t.)), and one at approx. 21 m.b.t.
Halysitid corals	Found in the middle part of the section (ca. 17 m.a.b.) (Fig. 3.1B)	Some large, well-preserved and out-weathered specimens in the upper part of ULV2, right below the beach covering (ca. 2.5-3.5 meters below the top)
Heliolitid corals	One whole specimen recored at 4 m.a.b, and possibly at 26.5 m.a.b., but highly uncertain	No clear specimens.
Stromatoporoid	Found at ca. 9 and 26 m.a.b.	Some found right below the top, one large registered at 21 m.b.t. (ULV2)
Pentamerid brachiopods	Increasingly common in fossiliferous layers from around 12 m.a.b. Whole, well, preserved specimens found at around 17 and 18 m.a.b. Dominant constituents of shell-pavements between ca. 25 m.a.b. and 32 m.a.b. (Figure 3.1E)	Some isolated casts found at the middle part of ULV2, otherwise no clear occurrences.
Trace fossils	No registered occurrences	Abundant <i>Thalassinooides</i> -like trace fossils at 12 m.b.t., and a <i>Chondrites</i> -like layer at approx. 2.5-3.5 m.b.t.

3.1.2 Magnetic susceptibility readings

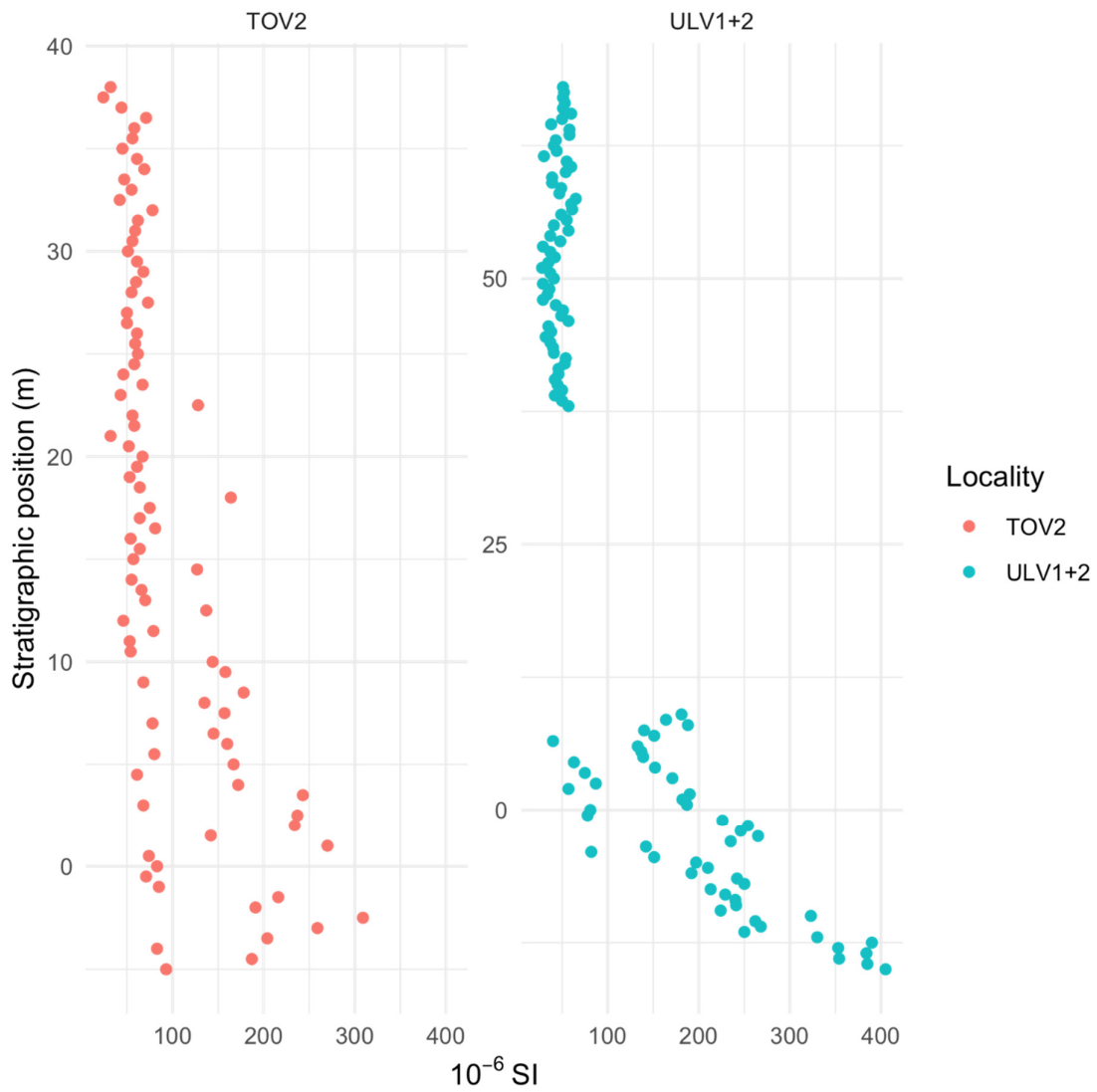


Figure 3.3. Magnetic susceptibility readings (x-axis) from the Toverud and composite Ulvøya localities (columns, color codings), plotted against stratigraphic height (y-axis), with 0 denoting the base of the Rytteråker Formation). SI = susceptibility index.

3.1.3 Toverud XRF data

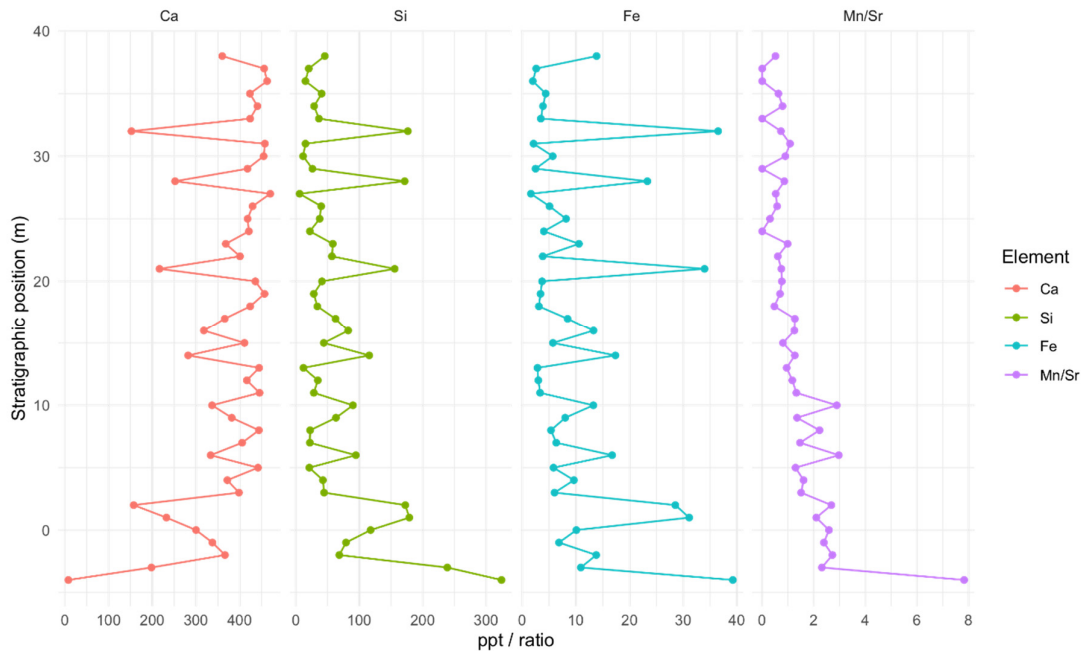


Figure 3.4. Elemental of values of Ca, Si, Fe and Mn/Sr (x-axis) plotted against stratigraphic position of samples (y-axis. 0 denote the base of the Rytteråker Formation). X-axis values for Ca, Si and Fe are in ppts, Mn/Sr values are in ratio between ppts of Mn and ppts of Sr measured.

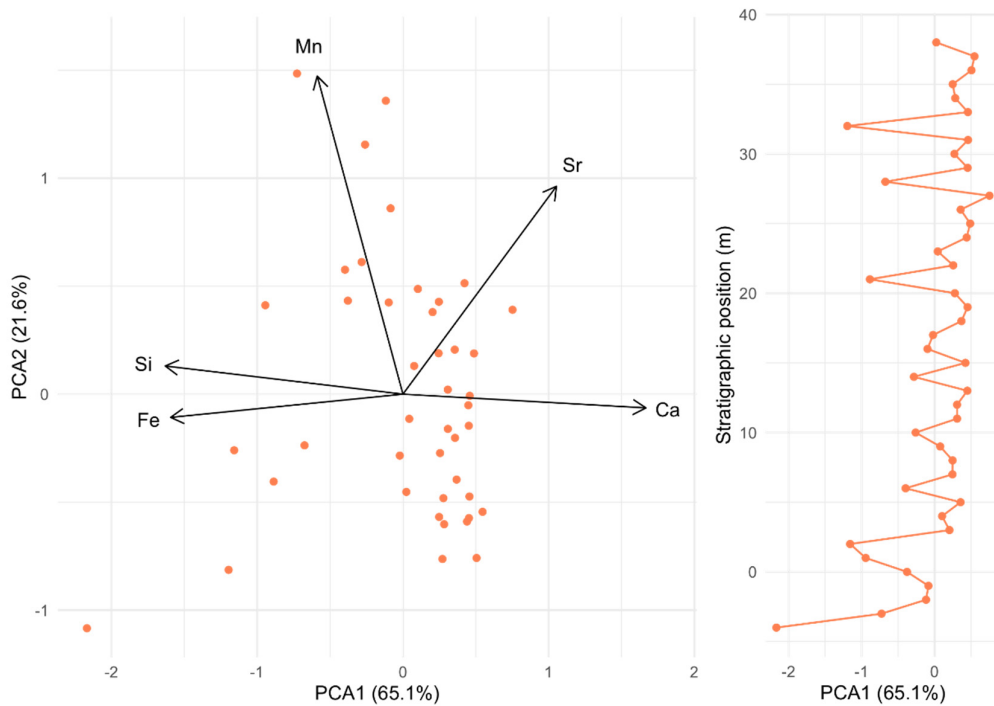


Figure 3.5 (left). 2-dimensional PCA ordination diagram of the stratigraphic samples ordinated on the ppt values of Ca, Si, Fe, Mn and Si, linearly standardized to the 0-1 range. Axes parentheses indicate the amount of variation explained by the axes eigenvalues.

Figure 3.6 (right). PCA axis 1 (x axis) plotted against stratigraphic position of samples (0 denote the base of the Rytteråker Formation)

3.1.4 TOV2 Shell orientation analysis

The result of the binomial test of convex-concave likelihood was a P value of 0.035, and a confidence interval of (see Figure 3.38). The binomial GLM model (P=0.044) for convex likelihood as a function of stratigraphic position is shown in Figure 3.39, and the result of all the models produced are shown in Table 3.2.

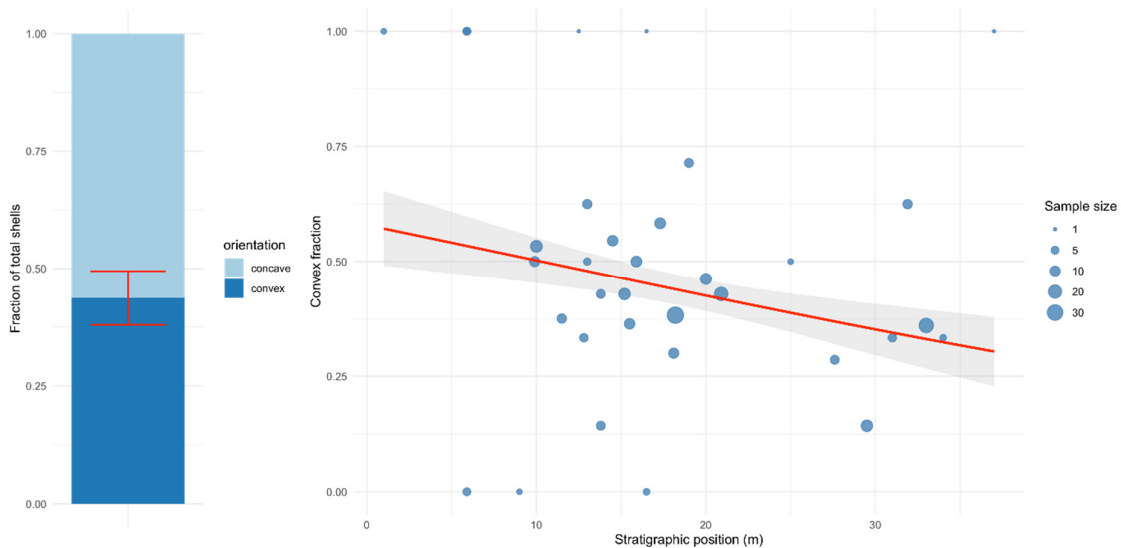


Figure 3.7 (left). Concave and convex fraction of the total shells counted in all samples (N=300). 95% confidence interval from the binomial test (P=0.035), are shown with red error bars.

Figure 3.8 (right). Binomial GLM of convex fraction as a function of stratigraphic position (Convex likelihood ~ position, see Table 3.2). Model prediction shown in red line, with 95% confidence intervals in gray. Size of the measured convex fractions (blue points) correspond to sample size (see legend).

Table 3.2. Overview of the different statistical models used to interpret the shell count data as a function of different variables ($x \sim y = x$ as a function of y). The quasipoisson model for the sample size ~ position model was chosen because of high overdispersion of the data in the model. GLM=generalized linear model (* = $P < 0.05$, ' = $P < 0.1$).

Model	Model family	Estimate	p-value
Convex likelihood ~ position	Binomial GLM	-0.031	0.044*
Convex likelihood ~ sample size	Binomial GLM	0.012	0.202
Convex likelihood ~ shell density	Binomial GLM	-0.566	0.072'
Sample size ~ position	Quasipoisson GLM	0.015	0.351
Shell density ~ position	Linear model	0.006	0.346

3.1.5 Overview of taxon morphology in acetate peels and thin sections

Plates with representative examples of the morphology of the different morphotaxa groups are shown in Figures 3.9-20. In all plates, examples from the acetate peels are juxtaposed with example from the thin sections, in order to facilitate a qualitative comparison between the two. Legend of the different morphotaxa subdivisions used in the analyses and ordination is provided in Table 3.3.

With the exception of images 3.9A & B, 3.13C & D, 3.18A & B and 3.19C & D, all images was taken with a Leica MC170 HD camera using a Leica DMLP microscope, with either 2.5x, 5x or 10x magnification, and post-processed in Leica Application Suite (version 3.4.0).

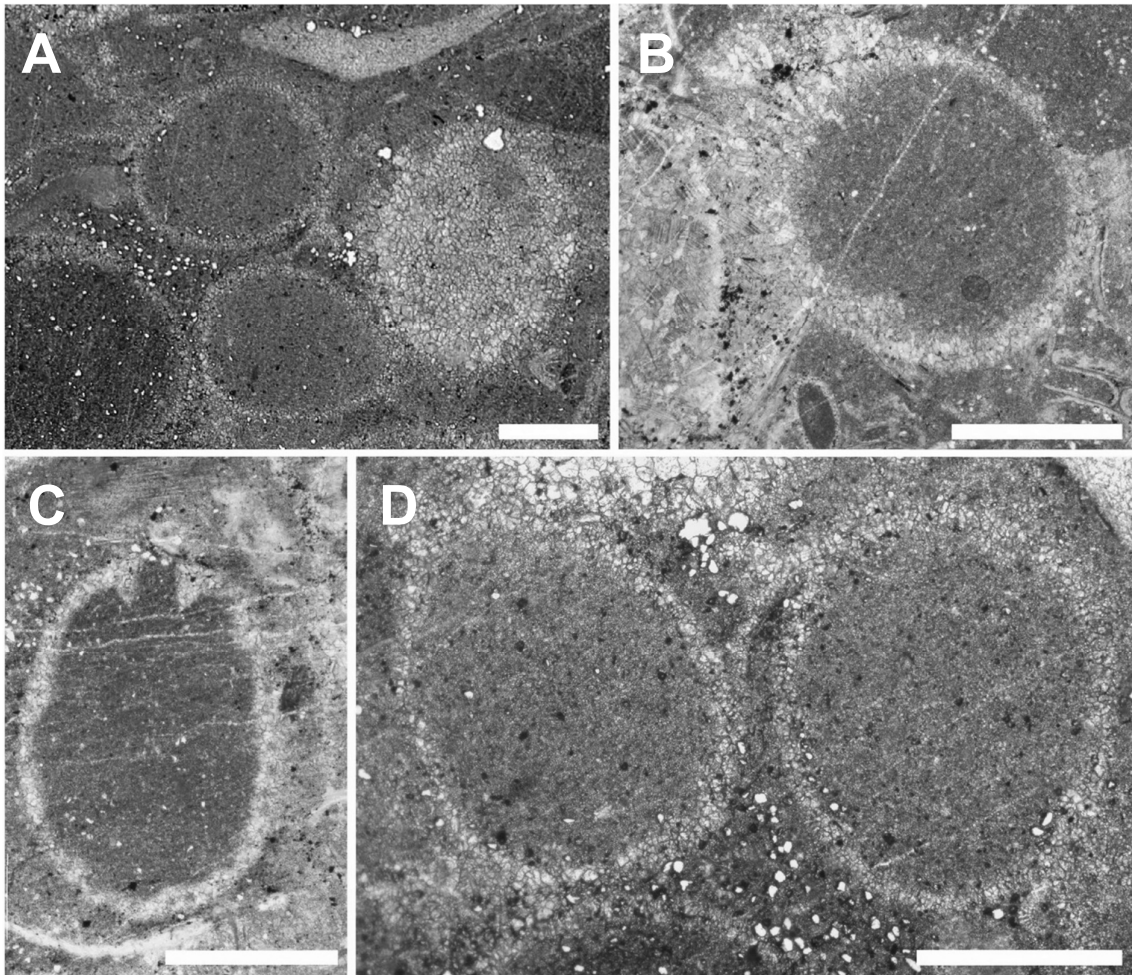


Figure 3.9. Calcareous tubes of unknown affiliation (*calc_tube*). Cross sections (presumably). A: acetate peel (PMO 236.405a). B: thin section (PMO 236.405s). C: thin section (PMO 236.405s). D: acetate peel (PMO 236.404a). Scale bars = 1 mm.

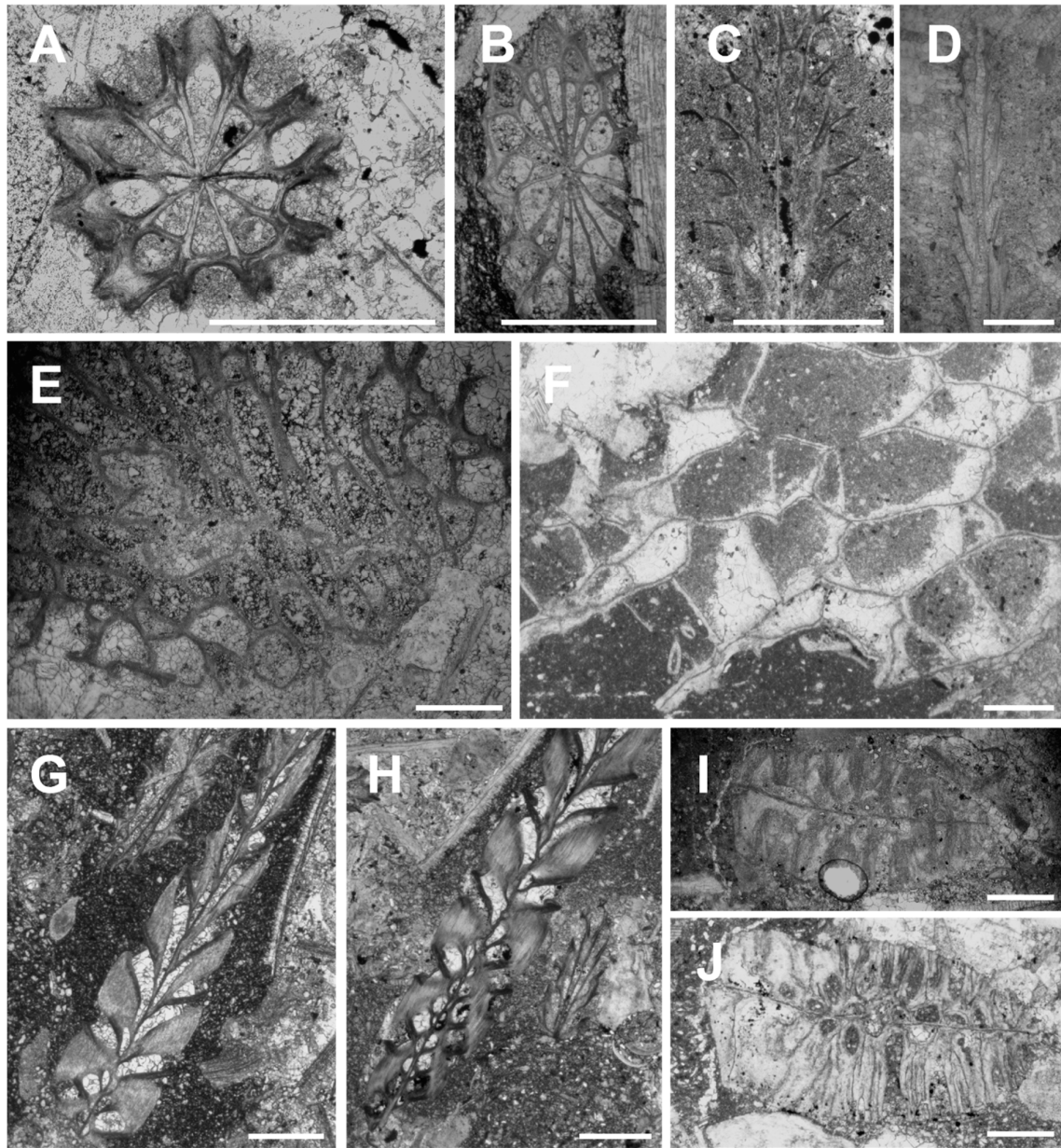


Figure 3.10. Bryozoans. A: Thin, sticklike bryozoan (bryo_small) in cross section (thin section, PMO 236.421s). B: Thin, sticklike bryozoan (bryo_small) in cross section, acetate peel (PMO 236.447a) C: Thin, sticklike bryozoan (bryo_small) in transverse section, thin section (PMO 236.405s). D: Thin, sticklike bryozoan (bryo_small) in transverse section, acetate peel (PMO 236.453a). E: Large bryozoan (bryo_large), acetate peel (PMO 236.483a). E: Large bryozoan (bryo_large), thin section (PMO 236.464s). G: Bifoliate bryozoan (bryo_bifoliate), acetate peel (PMO 236.450a). H: Bifoliate bryozoan (bryo_bifoliate), thin section (PMO 236.450s). I: Bifoliate bryozoan (bryo_bifoliate), acetate peel (PMO 236.464a). J: Bifoliate bryozoan (bryo_bifoliate), thin section (PMO 236.464s). All scale bars = 0.5 mm.

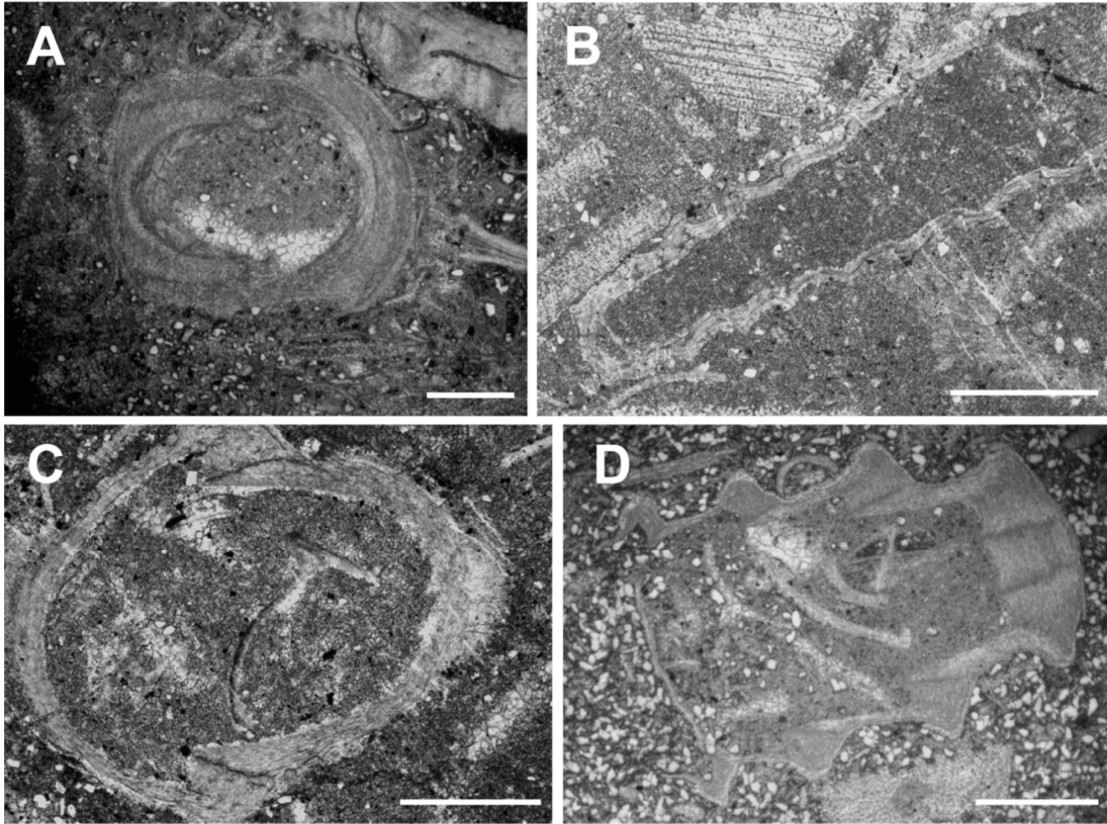


Figure 3.11. Tentaculitoids (tentaculitoids). A: cross section, acetate peel (PMO 236.414a). B: Transverse section, thin section (PMO 236.405s). C: cross section, thin section (PMO 236.405s). D: transverse section, acetate peel (PMO 236.408a). All scale bars = 0.5 mm

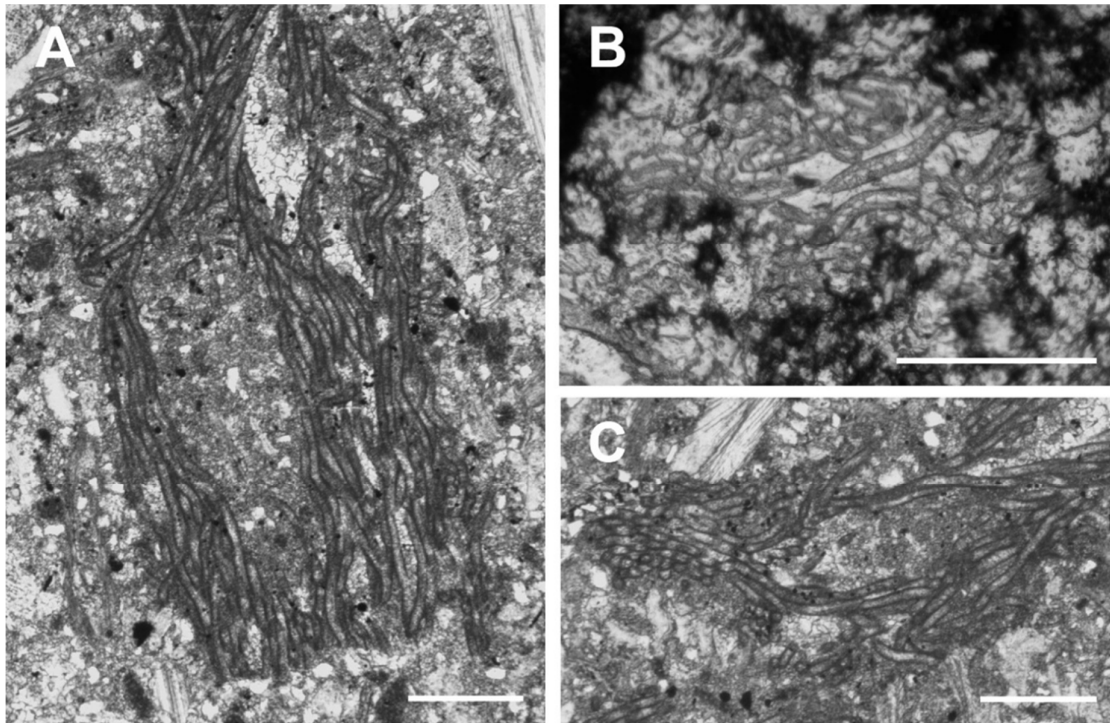


Figure 3.12. Filamentous algae (algae). A: Thin section (PMO 236.447s). B: Acetate peel (PMO 236.533b) C: Thin section (PMO 236.447s) Scale bars = 0.2 mm.

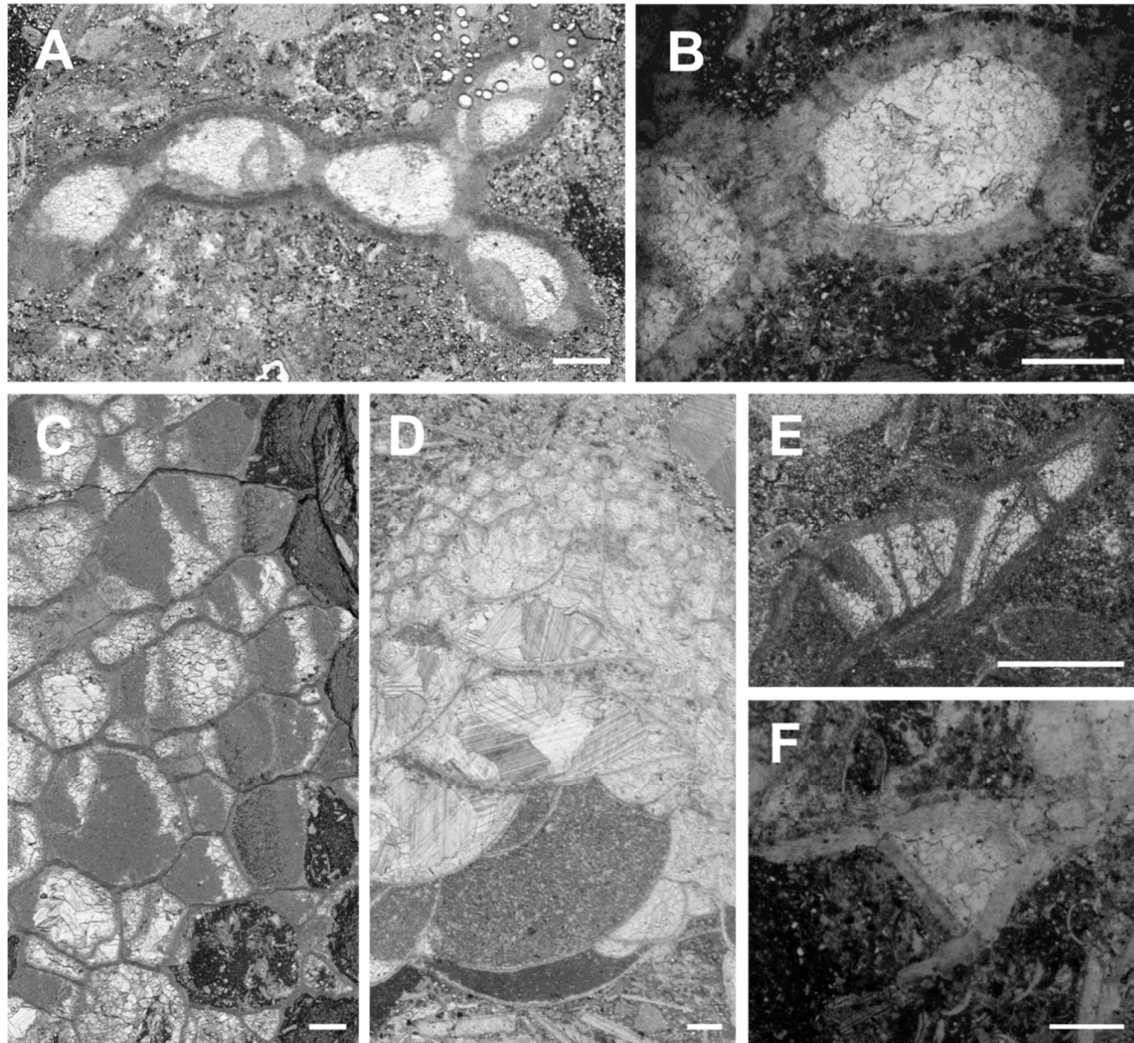


Figure 3.13. Tabulate corals. A: Halysitid coral (tabcor_hal), acetate peel (PMO 236.449a). B: Halysitid coral (tabcor_hal), thin section (PMO 236.421s). C: Favositid coral (tabcor_favhel), acetate peel (PMO 236.491a). D: Indeterminate massive, possibly heliolitid coral (tabcor_favhel), thin section (PMO 236.460s). E: Corallites of indeterminate affiliation (tabcor_indet), acetate peel (PMO 236.439a). F: Corallite of indeterminate affiliation (tabcor_indet), thin section (PMO 236.464s). Scale bars = 1 mm.

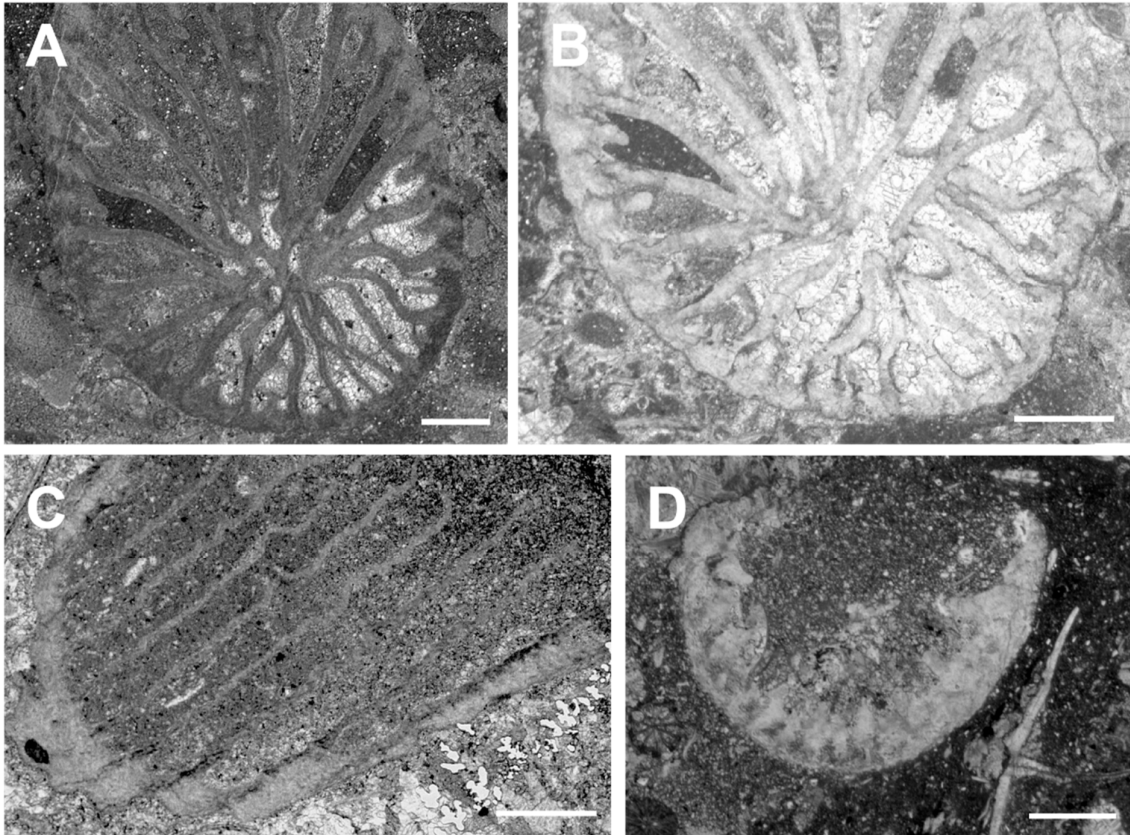


Figure 3.14. Rugose corals (rugosor) (PMO 236.417a) A: Cross section, acetate peel. B: Cross section, thin section (PMO 236.417s). C: Acetate peel (PMO 236.485b). D: Thin section (PMO 236.464s) Scale bars = 1 mm.

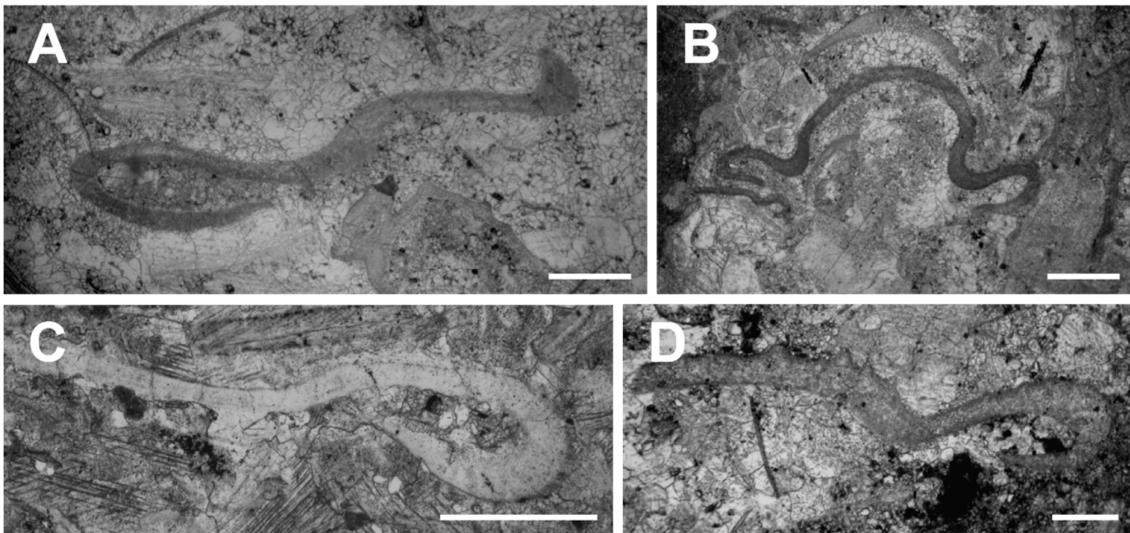


Figure 3.15. Trilobites. A: Acetate peel (PMO 236.483a). B: Acetate peel (PMO 236.417a). C: Thin section (PMO 236.462s). D: Acetate peel (PMO 236.417a). Scale bars = 0.5 mm.

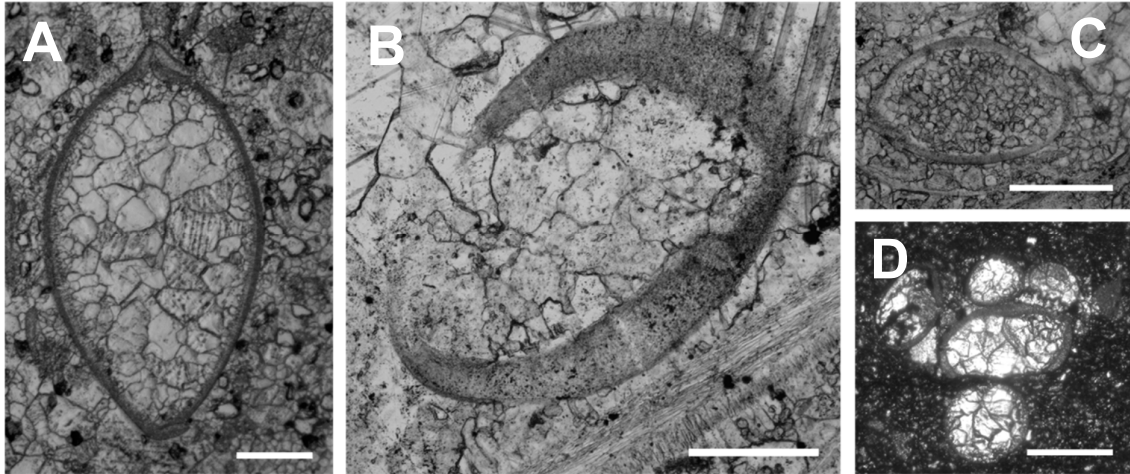


Figure 3.16. Ostracods (ostracod. A: Acetate peel (PMO 236.452a). B: Thin section (PMO 236.436s). C: Thin section (PMO 236.436s). D: Acetate peel (236.525b). Scale bars = 0.2 mm.

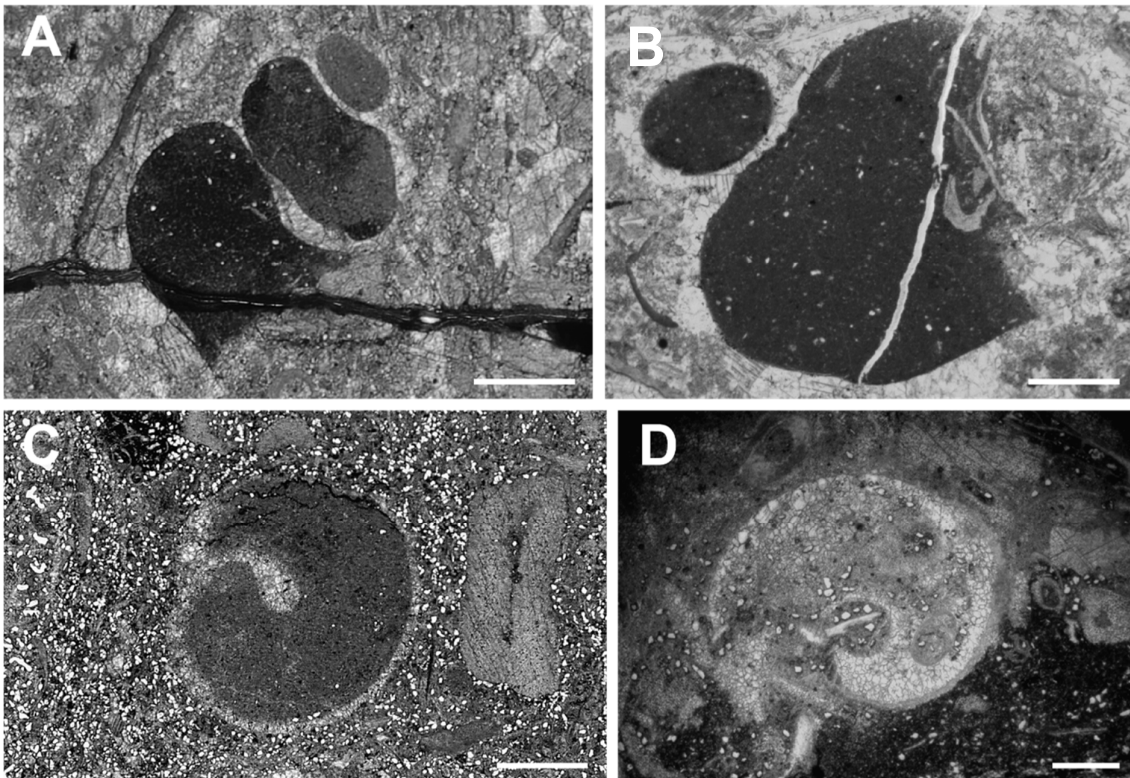


Figure 3.17. Gastropod (gastropod). A: Acetate peel (PMO 236.439a). B: Thin section (PMO 236.439s). C: Acetate peel (236.406a). D: Acetate peel (PMO 236.405a). Scale bars = 1 mm.

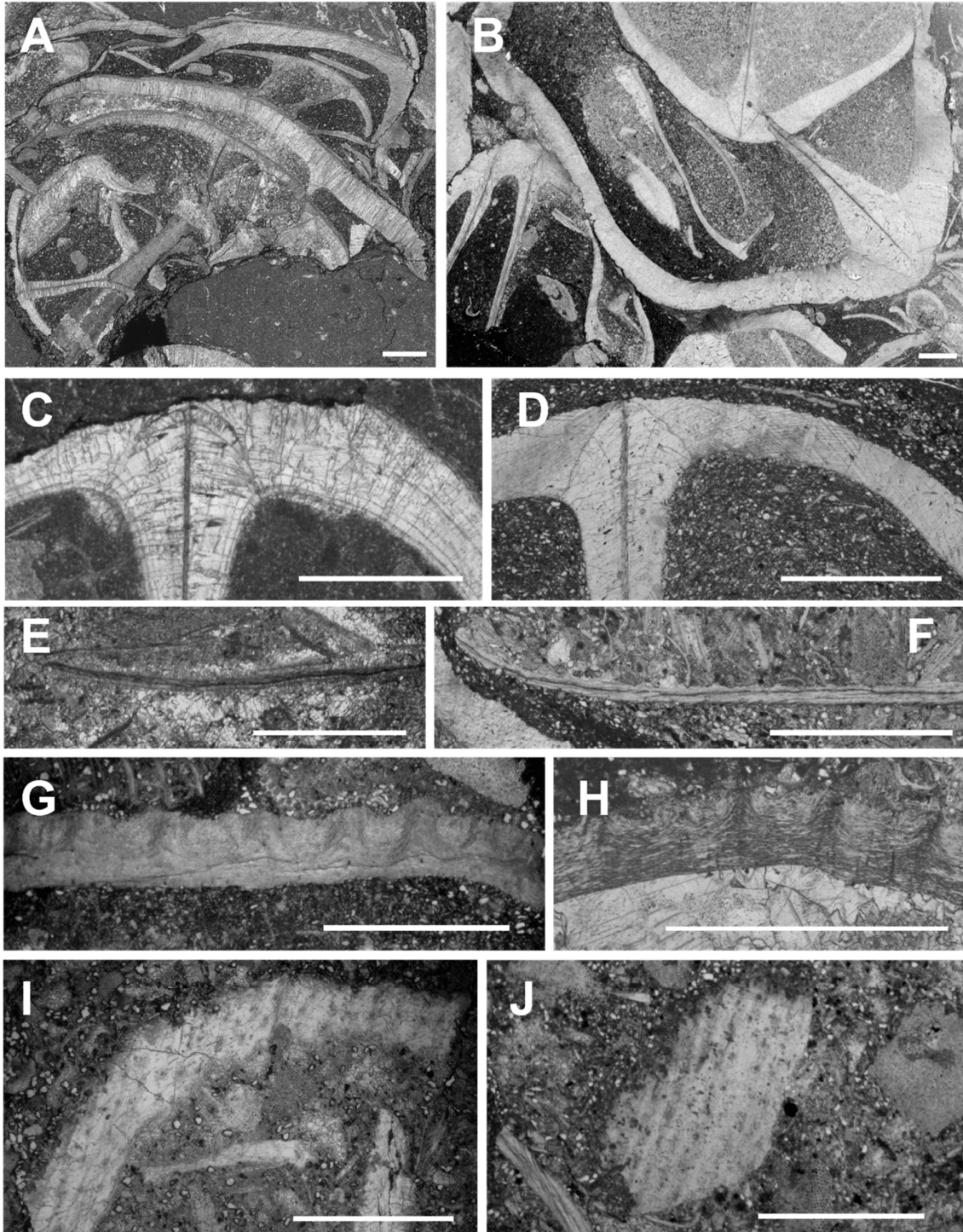


Figure 3.18. Brachiopods. A: Brachiopod packstone dominated by straight, thick-shelled walves (brach_thick), acetate peel (PMO 236.421s). B: Brachiopod packstone dominated by straight, thick-shelled walves (brach_thick), thin section (PMO 236.447a). C: Closeup of straight, thick-shelled brachiopod (brach_thick), acetate peel (PMO 236.405s). D: Closeup of straight, thick-shelled brachiopod (brach_thick), thin section (PMO 236.453a). E: Closeup of straight, thin-shelled brachiopod (brach_thin), acetate peel (PMO 236.483a). F: Closeup of straight, thin-shelled brachiopod (brach_thin), thin section (PMO 236.464s). G: Non-pentamerid brachiopod (brach_nonpent) with wavy, lamellalar shell, acetate peel (PMO 236.450a). H: Non-pentamerid brachiopod (brach_nonpent) with wavy, lamellalar shell, thin section (PMO 236.450s). I: Non-pentamerid brachiopod (brach_nonpent) with pseudopunctae, acetate peel (PMO 236.464a). J: Non-pentamerid brachiopod (brach_nonpent) with pseudopunctae, thin section. All scale bars = 1 mm.

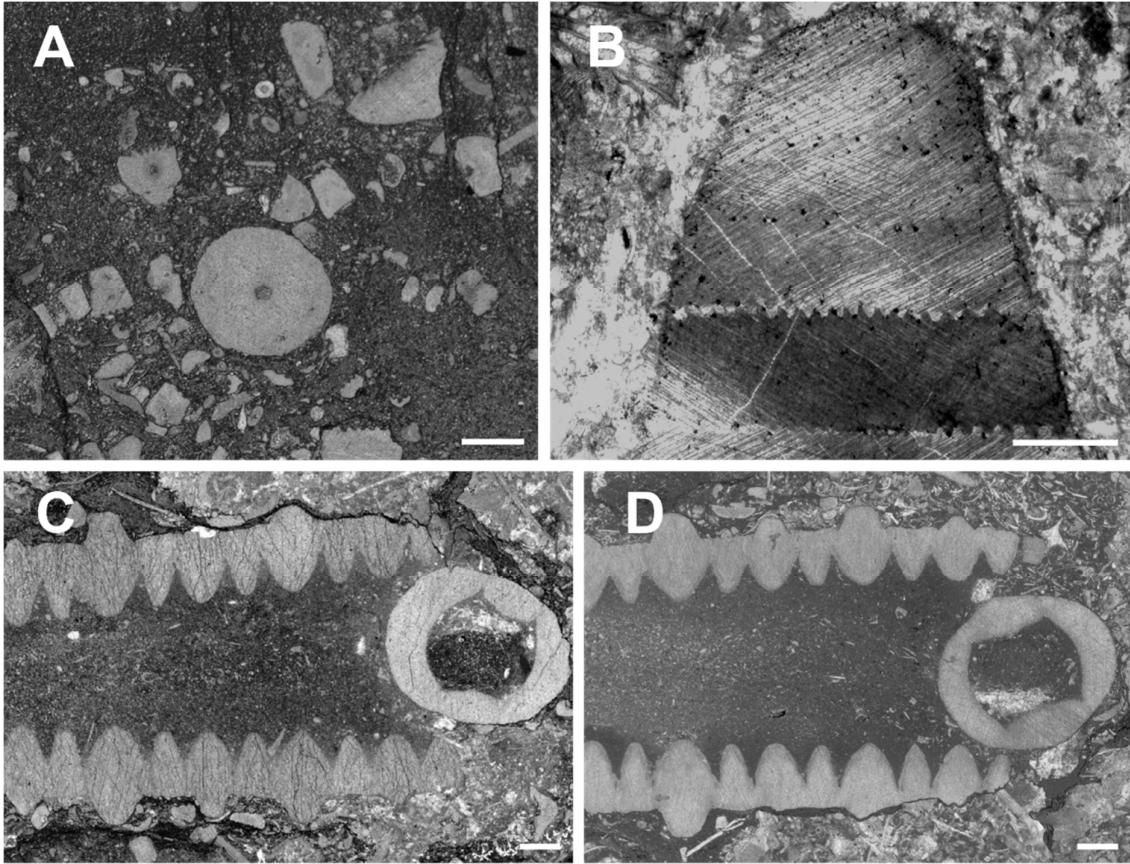


Figure 3.19. Crinoids (crinoid). A: Acetate peel (PMO 236.514a). B: Thin section, ossicle contact seams and cross-bedded crystal structure clearly visible (PMO 236.430s). C: Cross section and longitudinal section, acetate peel (236.473a). D: Cross section and longitudinal section, thin section (PMO 236.473s). Scale bars = 1 mm.

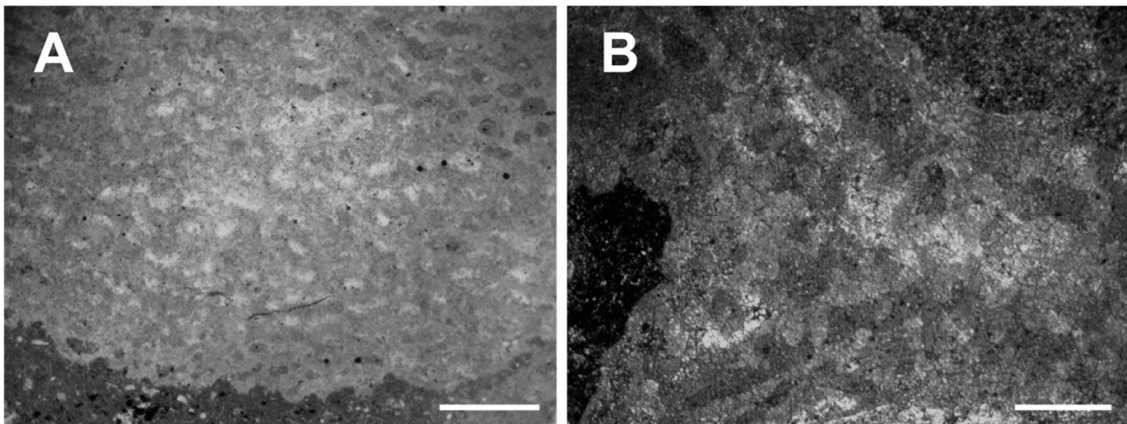



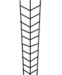
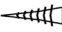















Figure 3.20. Stromatoporoids. A: Thin section peel (PMO 236.464s). B: Acetate peel (PMO 236.499b). Scale bars = 1 mm.

3.1.6 Summary of organism abundance data

Table 9 provides a general legend for the symbols used to refer to the different organism groups in the figures and ordination diagrams, with references to figures in Section 3.1.2, along with a reference to its corresponding figure in the previous section, and the approximate ecological category with regards to tiering, motility and feeding (see Section 1.2.2.3).

Table 3.3. Legend of morphotaxa in this study, with assigned ecological categories (tiering, motility, feeding), symbols used in the diagrams and corresponding figures with examples of morphology (Fig.)

Organism group	Symbol	Fig.	Tiering	Motility	Feeding
Calcareous tubes		3.9	Infaunal	Unknown	Unknown
Thin, sticklike bryozoan		3.10	Surficial	Non-motile, attached	Suspension
Large bryozoans		3.10	Surficial	Non-motile, attached	Suspension
Bifoliate bryozoans		3.10	Surficial	Non-motile, attached	Suspension
Tentaculitoids		3.11	Surficial/ semi-infaunal	Unknown	Suspension
Favositid/heliolithid tabulate coral		3.13	Surficial	Non-motile, attached	Suspension
Halysitid tabulate coral		3.13	Surficial	Non-motile, attached	Suspension
Indeterminate tabulate coral		3.13	Surficial	Non-motile, attached	Suspension
Rugose coral		3.14	Surficial/ semi-infaunal	Non-motile, attached	Suspension
Filamentous algae		3.12	Surficial	Non-motile, attached	Photosynthesis
Trilobites		3.15	Surficial/ semi-infaunal	Motile, fast	Deposit feeder
Gastropods		3.17	Surficial	Motile, slow	Herbivorous
Ostracods		3.16	ostracod	Motile, fast	Deposit feeder
Thick, straight-shelled brachiopod		3.18	Surficial	Non-motile, unattached	Suspension
Thin, straight-shelled brachiopod		3.18	Surficial	Non-motile, unattached	Suspension
Wavy and/or punctate brachiopod		3.18	Surficial	Non-motile, unknown	Suspension
Crinoid		3.19	Erect	Non-motile, attached	Suspension
Stromatoporoid		3.20	Surficial	Non-motile, attached	Suspension

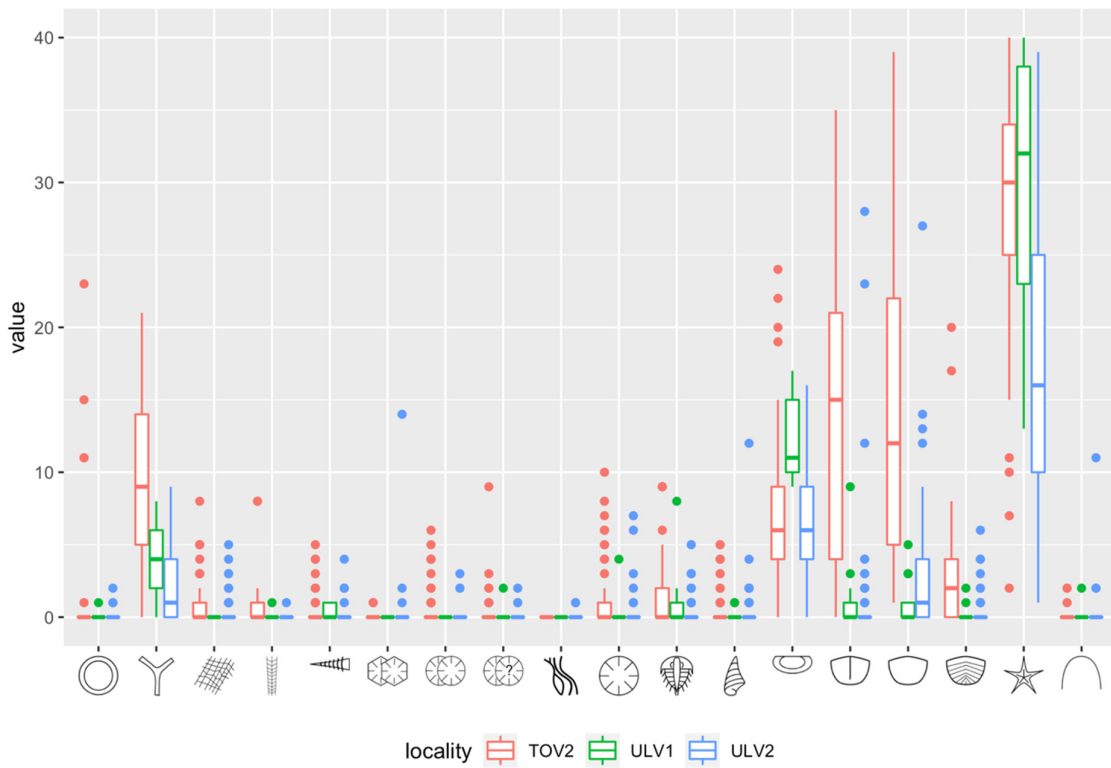
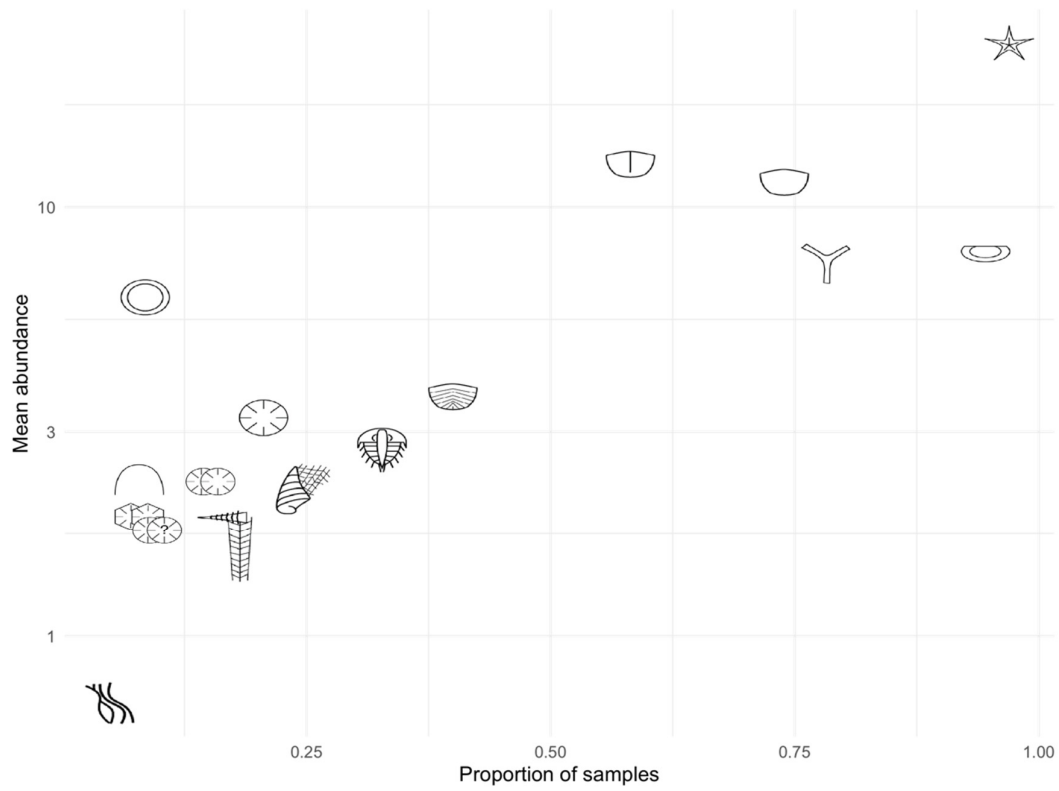


Figure 3.21 (top). Diagram showing the proportion of samples where each species occurs (x axis) and the average abundance in the plots where the species occurs (logarithmic y axis).

Figure 3.22 (bottom). Boxplot of sample abundances measured as subplot frequencies (y-axis) between the three localities (colors), for each morphotaxon (x-axis).

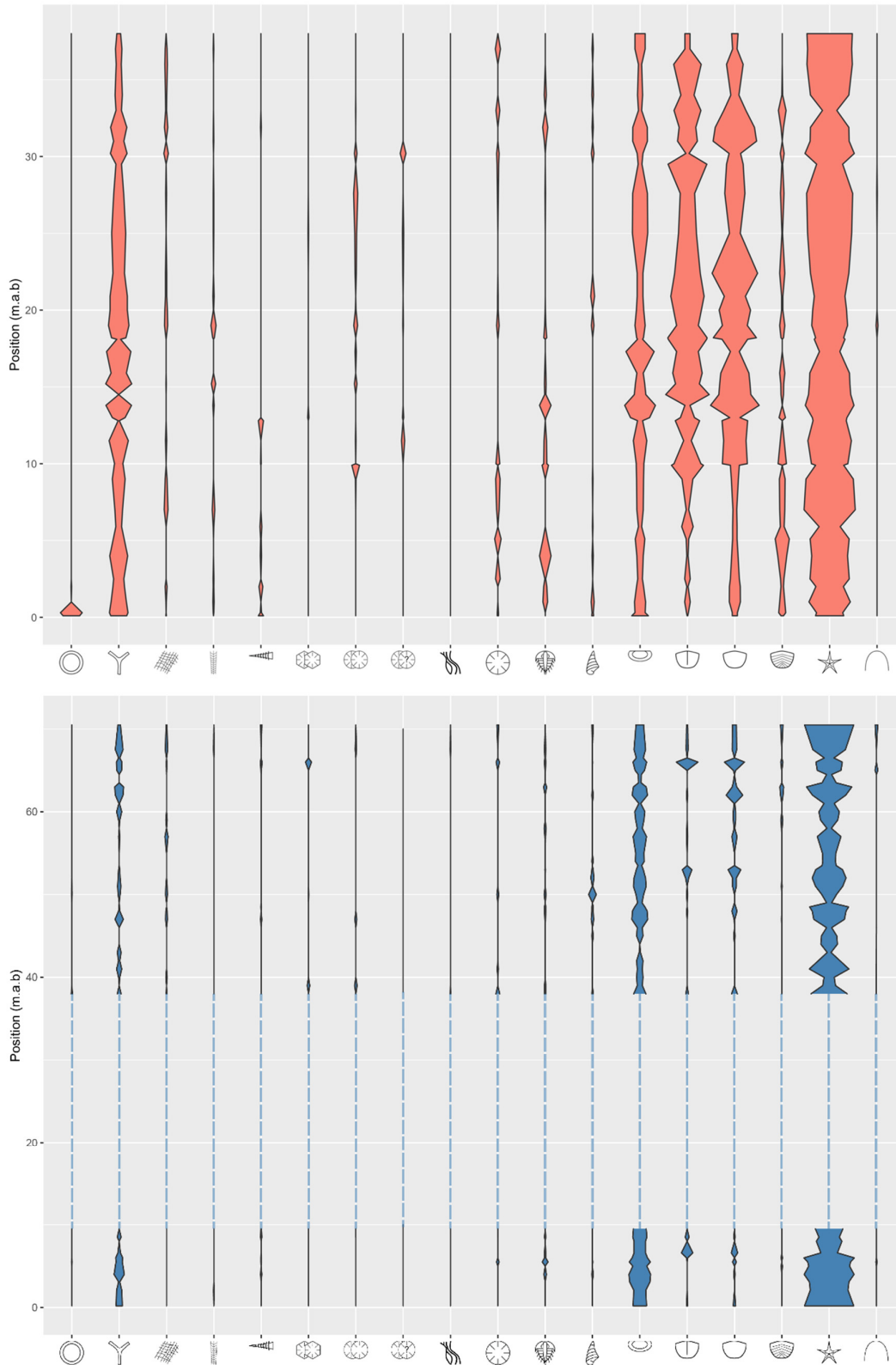


Figure 3.23 (top). Violin plot of the relative average SF abundance of the morphotaxa groups (x-axis) at each stratigraphic level (y-axis) sampled at the TOV-2 locality.

Figure 3.24 (bottom). Violin plot of the relative average SF abundance of the morphotaxa groups (x-axis) at each stratigraphic level (y-axis) sampled at the ULV-1 and ULV-2 localities. Dotted lines indicate the section assumed missing due to the fault between ULV-1 and ULV-2.

3.1.7 Diversity metrics

Boxplots of three diversity metrics (species richness, Shannon’s H and species evenness) measured for the samples from the three different localities, are shown in Figure 3.25, with results of the three one-way ANOVA tests in Table 3.4.

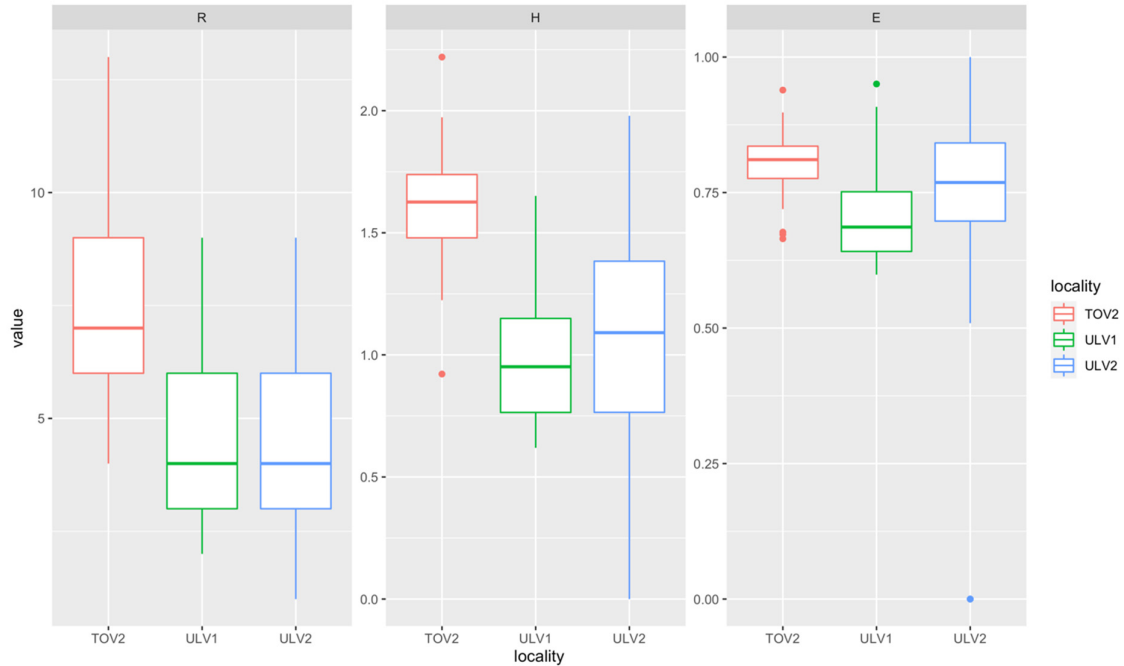


Figure 3.25. Boxplots of three diversity metrics (y-axes, columns) from samples from the three localities (x-axes). R = species richness, H = Shannon’s diversity index (Shannon’s H, E = species evenness).

Table 3.4. Results of the three one-way ANOVA test performed on the diversity metrics.

Metric	F-value	P-value
Species richness (R)	43.87	9.1×10^{-16}
Sp. diversity (Shannon’s H)	63.41	$< 2 \times 10^{-16}$
Sp. Evenness (E)	4.58	0.012

3.1.8 Ecological occupancy

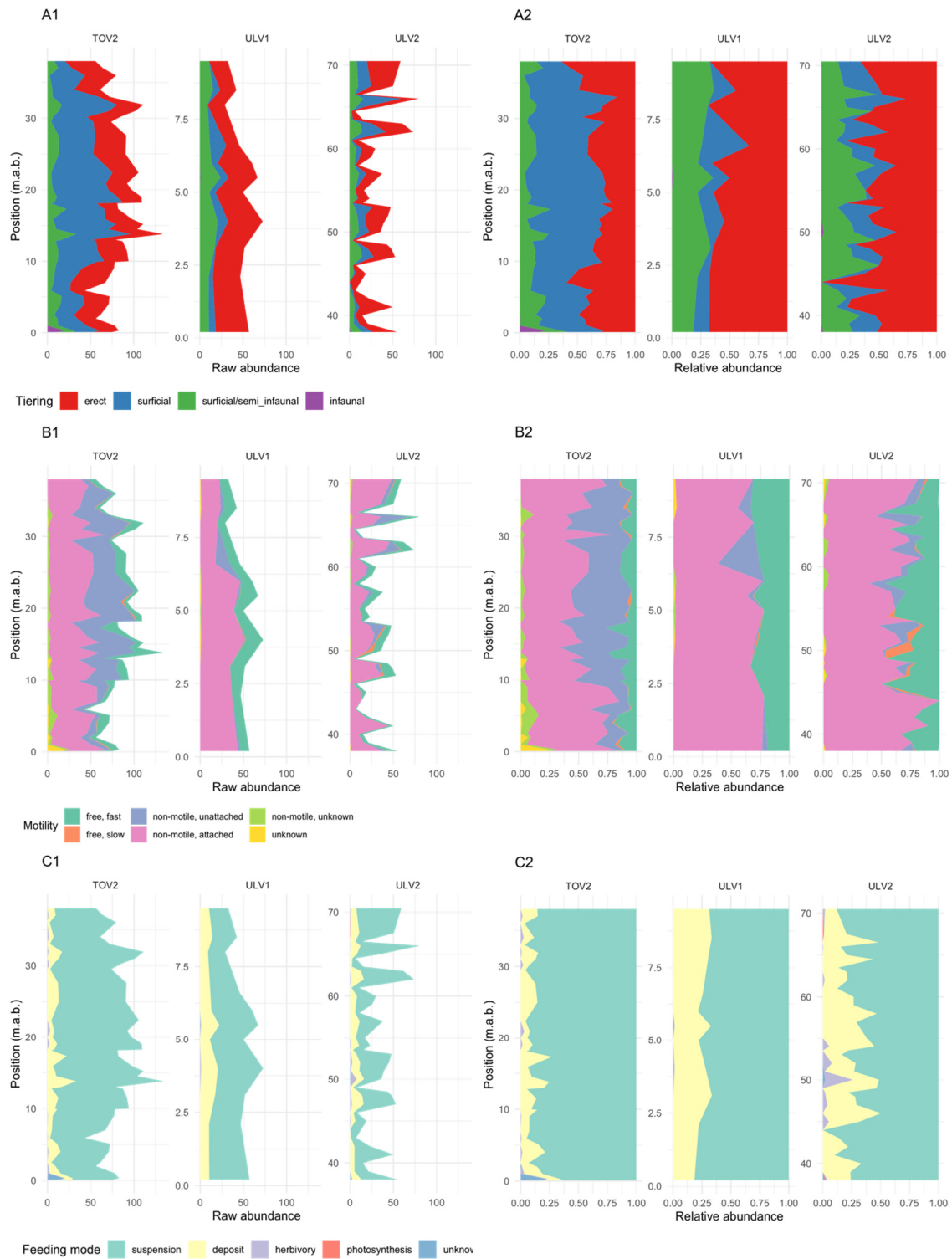


Figure 3.26. Stratigraphic overview of the different ecological categories represented in the acetate peel SF data (Table 3.2) plotted stratigraphically for the three localities, in terms of absolute abundances (left hand side, 1) and relative abundances (right hand side, 2). Top row (A): tiering. Middle row (B): Motility. Bottom row (C): Feeding mode.

3.1.9.2 CA

CA axes 1 and 2 combined explain a total of 33.08% percent of the variation in the dataset, with the first axis explaining 18.3%. For the purpose of graphical comparison between ordinations (with PCA as a reference), both axes in the CA results have been flipped in the diagram.

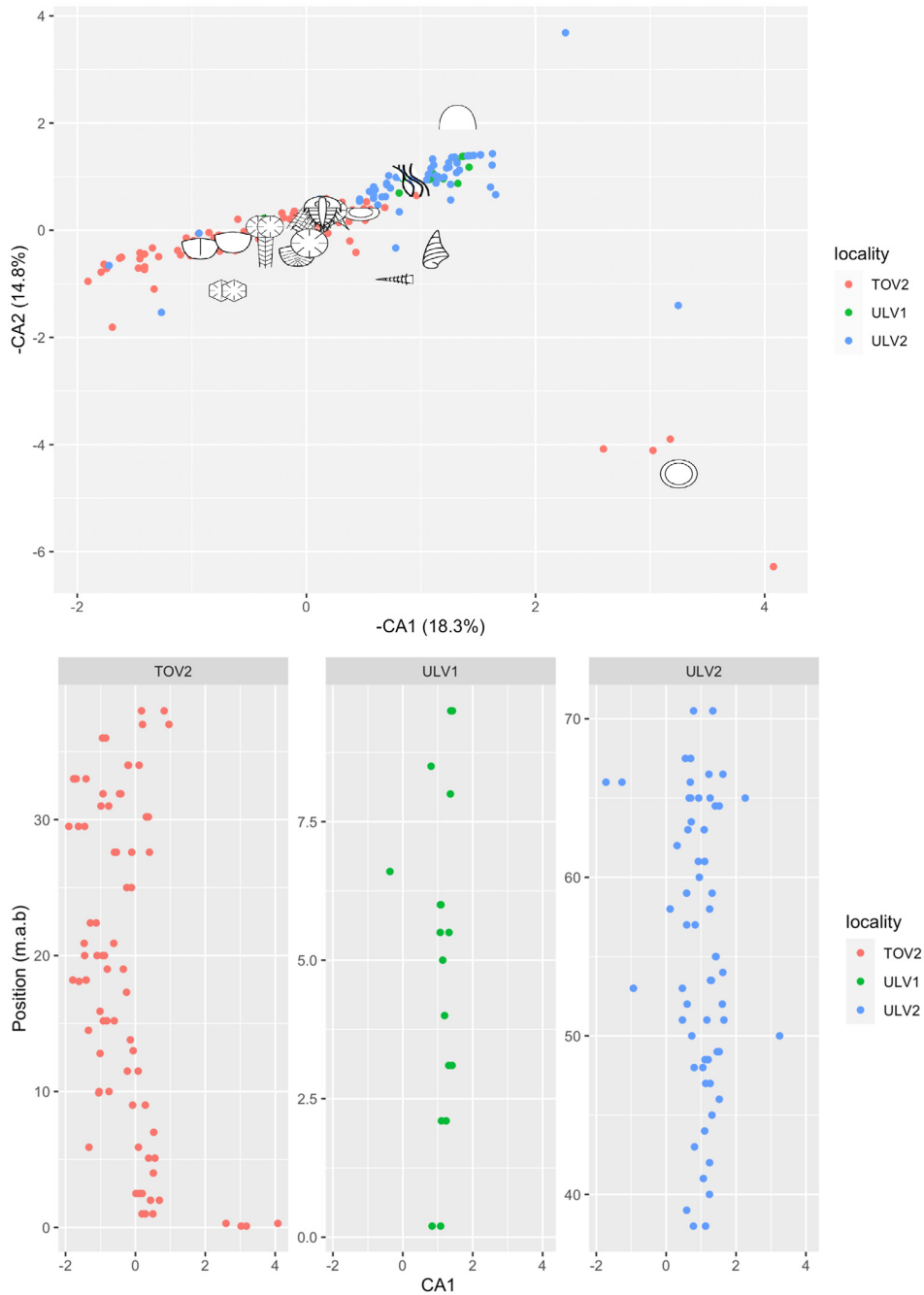


Figure 3.29 (top). CA biplot, with plot scores from the acetate peel samples color-coded by locality, and species optima (symbols) estimated as unimodal species optima by weighted calibration in the CA algorithm. X-axis = CA1, y-axis = CA2. Parentheses indicate amount of variation explained by the axes eigenvalues.

Figure 3.30 (bottom). CA axis 1 (x-axis) plotted against absolute stratigraphic position of the samples (y-axis) for the three localities, divided by study locality (columns).

3.1.9.3 DCA

The eigenvalues reported by the *decorana* function in R for DCA axis 1 and 2 were 0.236 and 0.125 respectively. However, as these bear no real statistical relationship to the total variation in the dataset, they are only meaningful in comparison with each other, and will generally not be considered in the interpretation of the ordination.

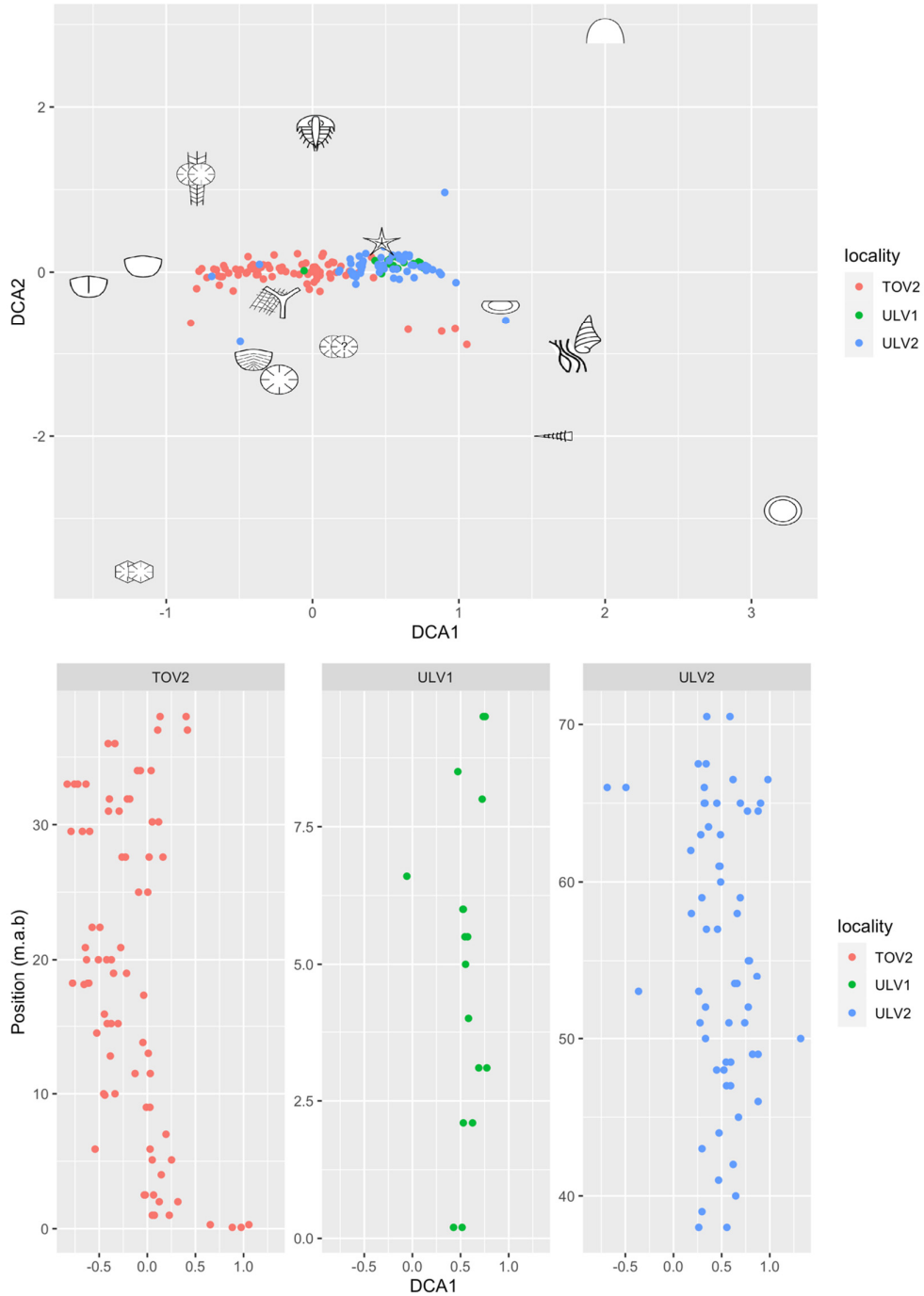


Figure 3.31 (top). DCA biplot, with plot scores from the acetate peel samples color-coded by locality, and species positions (symbols) estimated as unimodal species optima by weighted calibration in the DCA algorithm. X-axis = DCA1, y-axis = DCA2.

Figure 3.32 (bottom). DCA axis 1 (x-axis) plotted against absolute stratigraphic position of the samples (y-axis) for the three localities, divided by study locality (columns).

3.1.9.4 NMDS

The stress value of the NMDS ordination was 0.115. In order to facilitate graphical comparison with the other ordinations, ordination axis 2 is flipped in the biplot in figures 3.33 and 3.35.

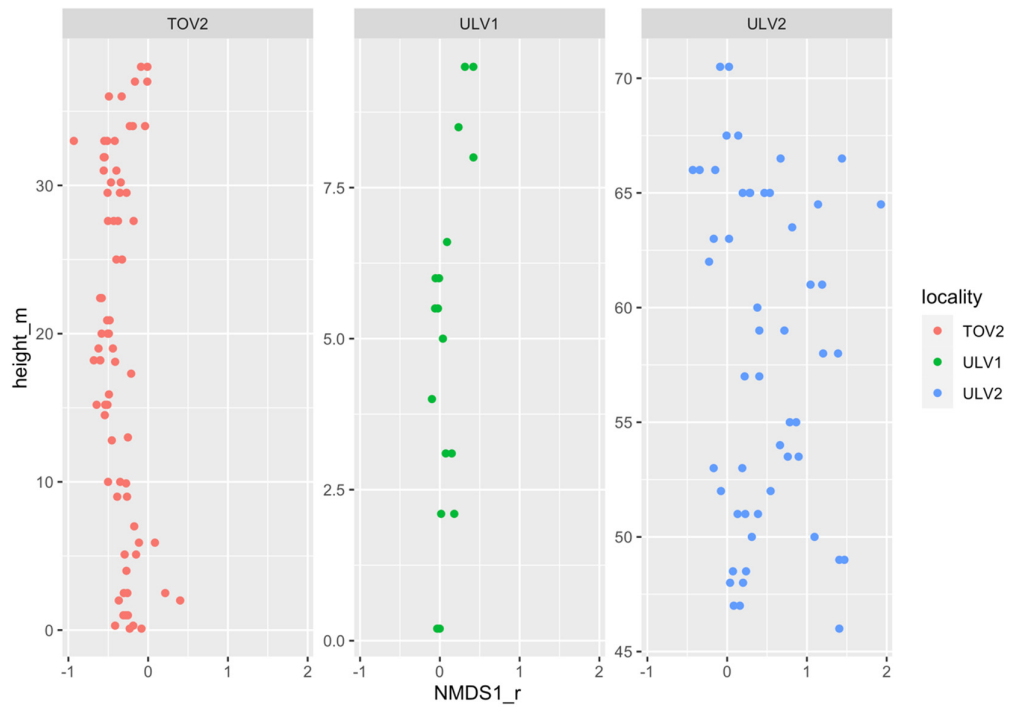
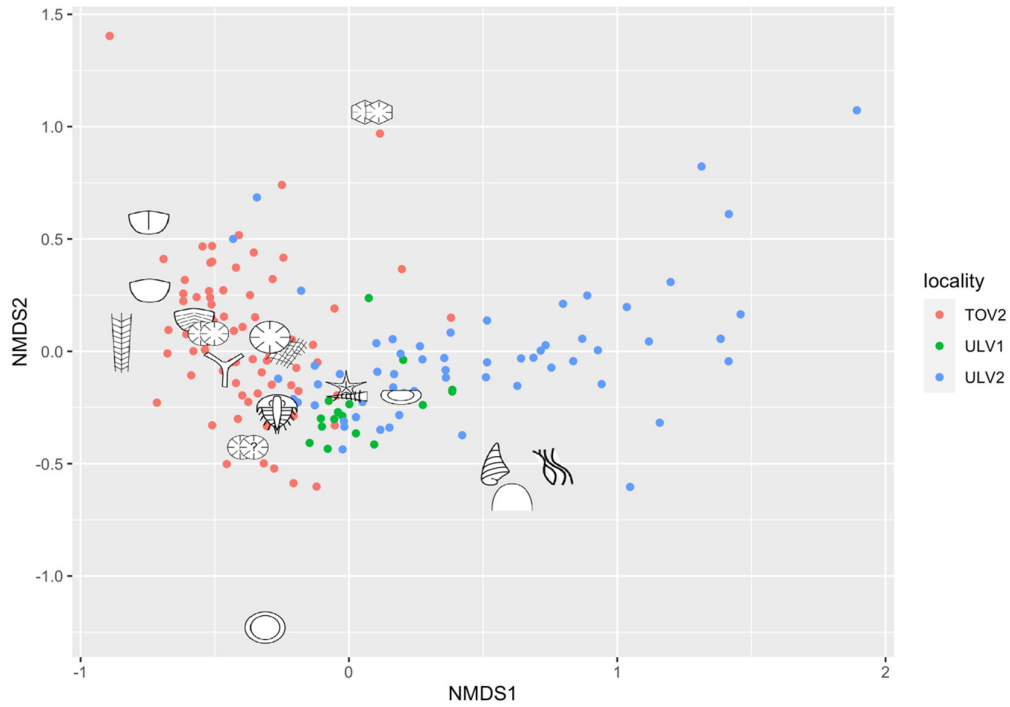


Figure 3.33 (top). Biplot of the 2-dimensional NMDS ordination (stress= 0.115), after PostMDS PCA rotation, with plot scores color-coded by locality. Species optima (symbols) fitted *a posteriori* by weighted averaging of plot scores.

Figure 3.34 (bottom). NMDS axis 1 (x-axis) plotted against absolute stratigraphic position of the samples (y-axis) for the three localities, divided by study locality (columns).

3.1.9.5 Visual comparison of plot scores

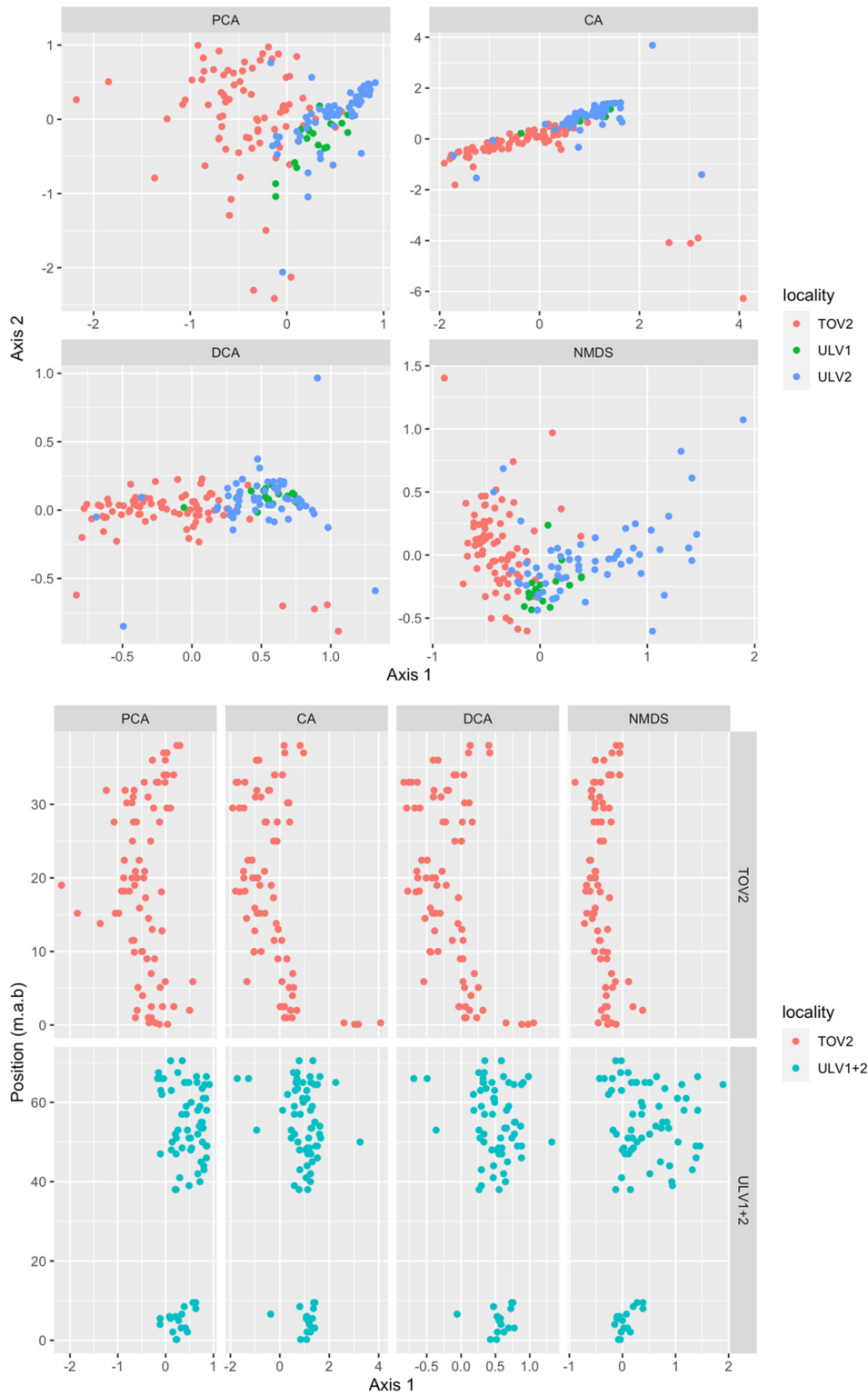


Figure 3.35 (top). Juxtaposition of plots scores along ordination axes 1 and 2 for all raw data ordinations, color coded by locality.

Figure 3.36 (bottom). Juxtaposition of ordination axis 1 plot scores (x-axis) and stratigraphic position of plots for Toverud (TOV-2) and the composite section of ULV-1 and ULV-2, with assumed missing meters added to the ULV-2 positions.

3.1.9.6 Comparison of ordinations

Table 3.5. Procrustes correlation coefficients (r) and Kendall's tau correlation coefficients of plot scores between axes 1 (τ_1) and 2 (τ_2) between the PCA, CA, DCA and NMDS ordinations. (* = $P < 0.05$, ** = $P < 0.001$).

Method 1	Method 2	r	τ_1	τ_2
PCA	CA	0.68**	0.49**	0.10
PCA	DCA	0.65**	0.51**	0.07
PCA	NMDS	0.72**	0.81**	0.60**
CA	DCA	0.83**	0.95**	0.39**
CA	NMDS	0.63**	0.59**	0.31**
DCA	NMDS	0.68**	0.61**	0.15*

Table 3.6. Outlier influence on ordination axis 1, as measured by relative core length (RCL), and the identification numbers (PMO) of the samples with the minimal and maximal score along ordination axis 1.

Axis	Relative core length	Outlier_min	Outlier_max
PCA1	0.41	236.596a	236.464a
CA1	0.43	236.405a	236.477a
DCA1	0.52	236.564a	236.485b
NMDS1	0.45	236.596a	236.485b

3.1.10 Ordination of abundance-scale weighted data

3.1.10.1 Graphical comparison

Figures 3-31 and 3-32 show the 2-dimensional plot scores of DCA and 2-dimensional NMDS ordination – respectively – of the abundance weighted data. Fig. 3.39 and 3.40 show the changes in morphotaxa optima in the 2-dimensional ordination diagrams with each ordination method, and Figs. 3.41 and 3.42 show the change in ordination scores along axis 1 plotted against stratigraphic position. It is especially important to note that the stratigraphic positions in the latter plots are *not* comparable between localities, even though they are plotted in the same diagram.

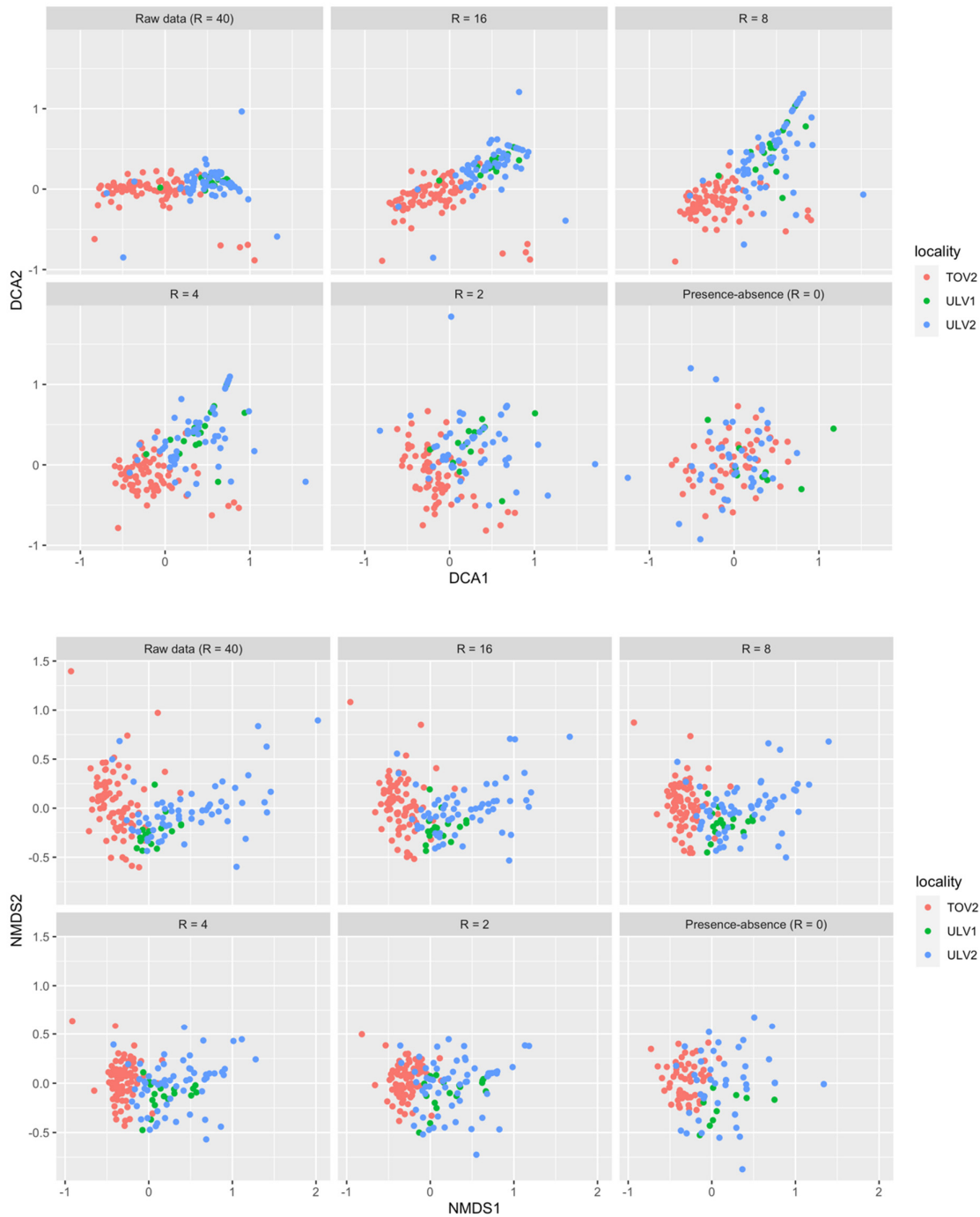


Figure 3.37. DCA plot scores with the different abundance-range weightings (grey headlines), with R indicating the total length of the abundance scale, color coded by localities. DCA axis 1 is flipped for the presence-absence weighting (R = 0), and DCA axis 2 is flipped for the the R = 8 and R = 8 weightings, in order to display the same gradient in the data across the diagrams.

Figure 3.38. NMDS plot scores with the different abundance-range weightings (grey headlines), with R indicating the total length of the abundance scale, color coded by localities. NMDS axis 2 is flipped for the presence-absence weighting (R = 0), in order to display the same gradient in the data across the diagrams.

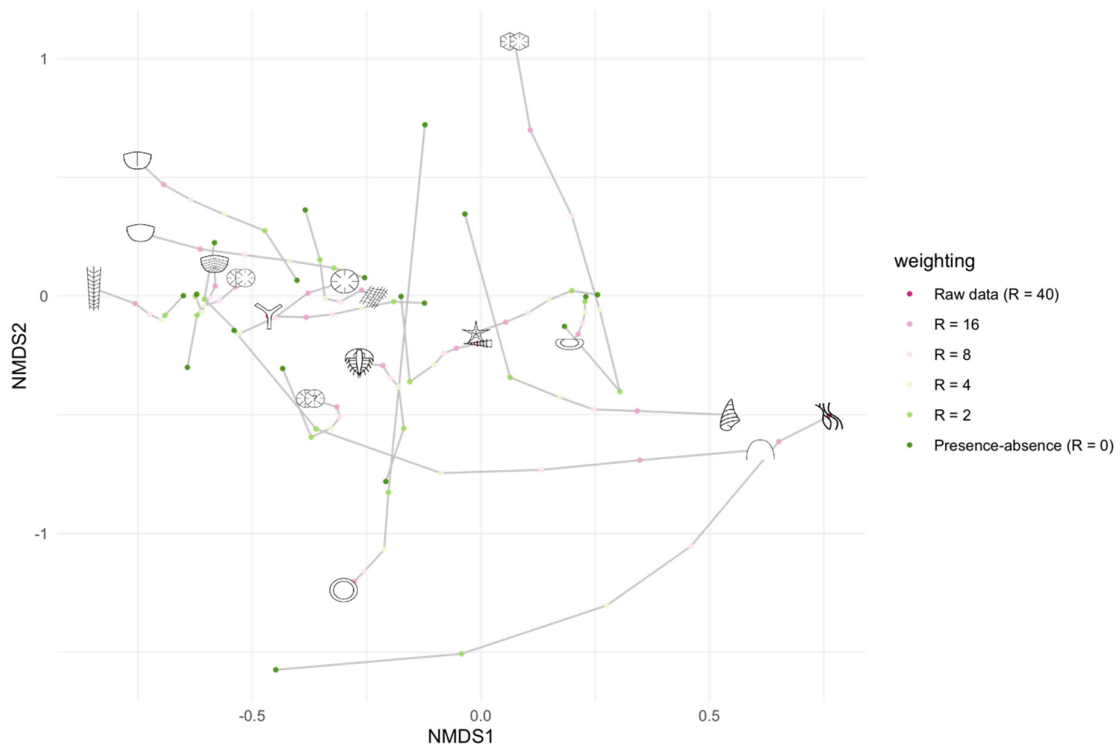
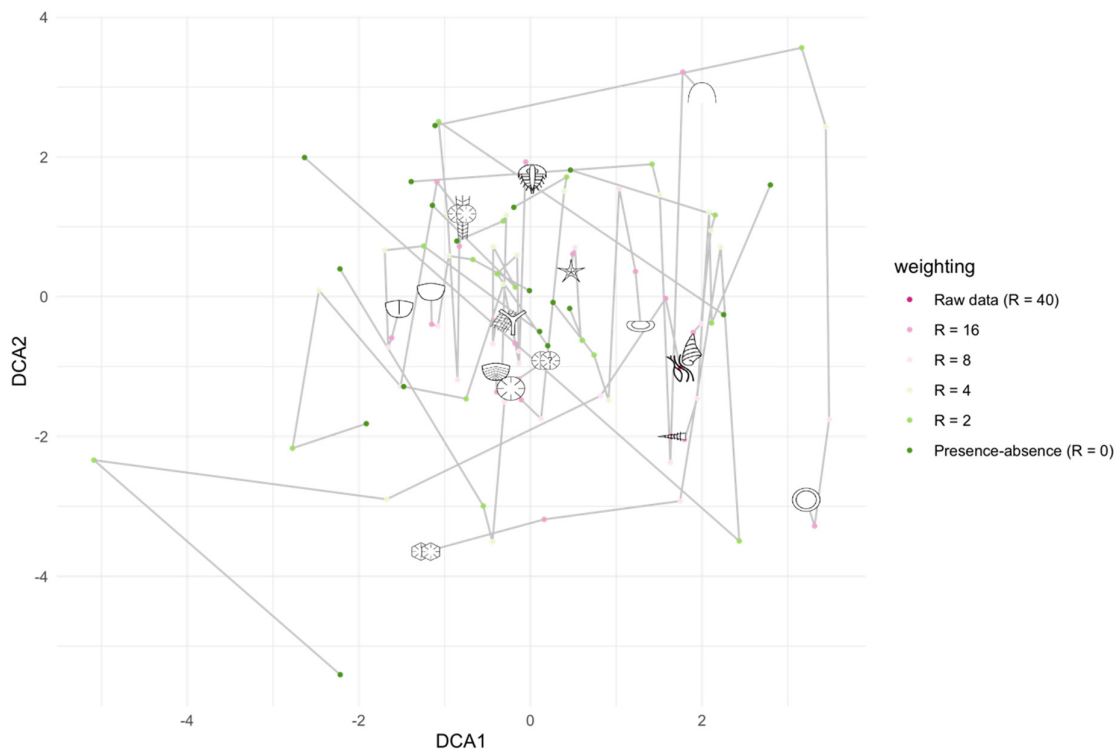


Figure 3.39. Diagram showing the change in species optima (dots) for each morphotaxon (grey line) between the different abundance-weighted DCA ordinations (color codings). The morphotaxa symbols are positioned at the optima of the raw-data ordinations (R = 40).

Figure 3.40. Diagram showing the change in species optima (dots) for each morphotaxon (grey line) between the different abundance-weighted NMDS ordinations (color codings). The morphotaxa symbols are positioned at the optima of the raw-data ordinations (R = 40).

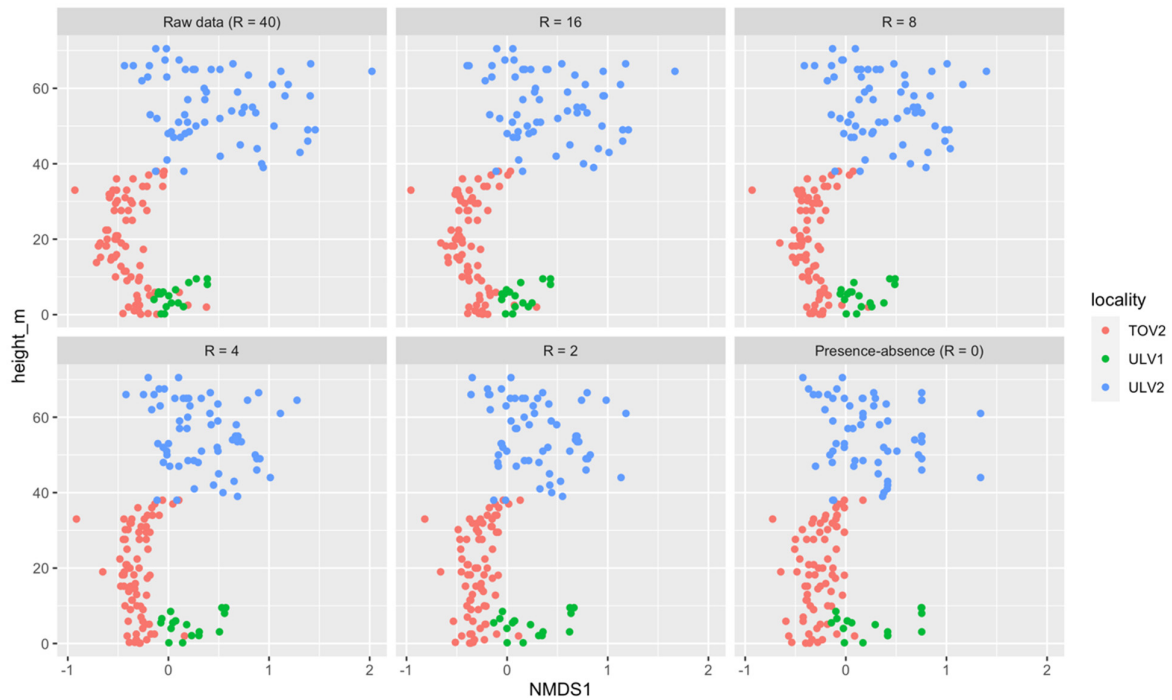
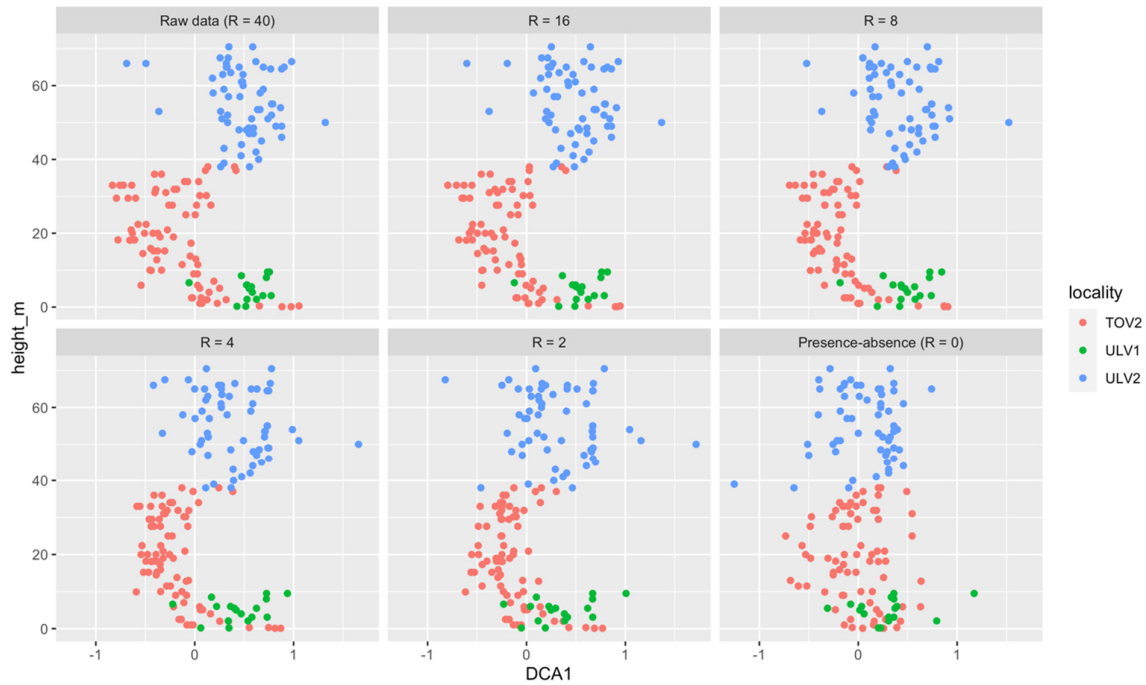


Figure 3.41 (top). DCA plot scores for axis 1 plotted against stratigraphic position under the different abundance-range weightings (grey headlines), with R indicating the total length of the abundance scale, color coded by localities. *NB: stratigraphic position is not comparable across localities.*

Figure 3.42 (bottom). NMDS plot scores for axis 1 plotted against stratigraphic position under the different abundance-range weightings (grey headlines), with R indicating the total length of the abundance scale, color coded by localities. *NB: stratigraphic position is not comparable across localities.*

3.1.10.2 Correlations between abundance weighed ordinations

Table 3.7. Procrustes correlation coefficients (r) between the parallel DCA and NMDS ordinations, Kendall's tau correlations between axes 1 (τ_1) and 2 (τ_2) of the DCA and NMDS ordinations, stress values from the NMDS ordinations and the relative core length of axis 1 for the DCA (D) and NMDS (N) ordinations (RCL1-D and RCL1-N). (* = $P < 0.01$)

Abundance range	r	τ_1	τ_2	NMDS stress	RCL1-D	RCL1-N
R ₄₀ (raw)	0.676*	0.611*	0.151	0.115	0.52	0.45
R ₁₆	0.714*	0.640*	0.204*	0.126	0.51	0.44
R ₈	0.760*	0.633*	0.007	0.140	0.48	0.45
R ₄	0.751*	0.594*	0.001	0.161	0.47	0.46
R ₂	0.588*	0.498*	0.062	0.186	0.36	0.49
R ₀ (p.a.)	0.595*	0.370*	0.397*	0.172	0.29	0.52

3.1.11 Lithological and faunistic variables measured in the plots

3.1.11.1 Between sample correlations

Because of the implicit negative correlation between the different Dunham types, as they to a large degree are mutually exclusive (the majority of the samples were designated only to a single Dunham type), between-sample correlations of these were not performed. The diversity metrics (R, H, E) are also not correlated with each other, due to their inherent relatedness. As such the correlations performed (Table 3.7) are between the faunistic and lithological variables, as well as between bioturbation and both other categories of variables.

Table 3.8. Correlation matrix (Kendall's τ) between the lithological environmental variables (* = $0.01 > Pr > 0.001$, and ** = $Pr < 0.001$).

	Bioturbation	Richness (R)	Diversity (H)	Evenness (E)
Bioturbation	—————	-0.332**	-0.352**	-0.113
Mudstone	0.354**	-0.444**	-0.395**	0.025
Wackestone	-0.011	0.236*	0.160*	-0.161*
Packstone	-0.348**	0.394**	0.417**	0.162*
Grainstone	-0.172*	-0.039	0.032	-0.067

3.1.11.2 Correlation with the ordinations

Results of the *envfit* permutation tests, and the Kendall's τ correlations between the raw data ordinations, as well as selected abundance scale-weighted DCA and NMDS ordinations are shown in table 3.9 and 3.10. Figure 3.43 show the correlation biplots with the lithological/faunistic variables which had a *envfit* permutation test P-value < 0.01 (two asterisks in Table 3.9 & 3.10).

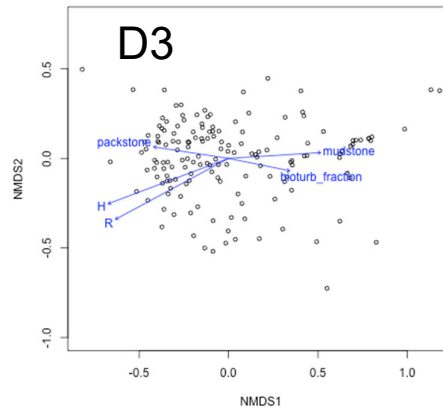
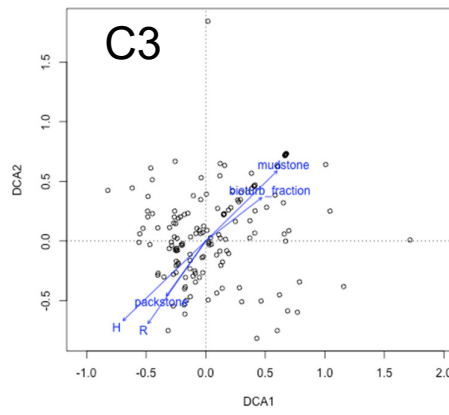
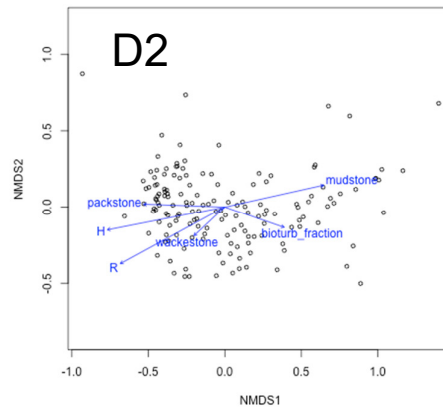
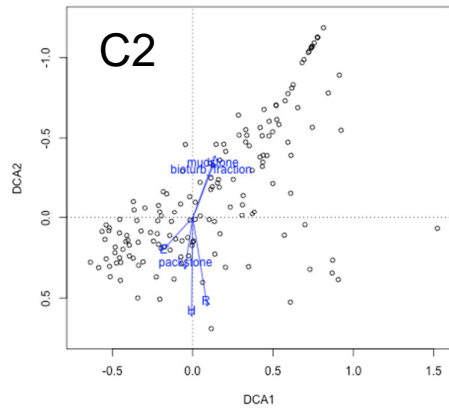
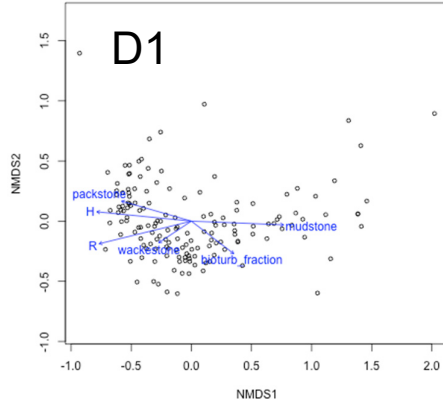
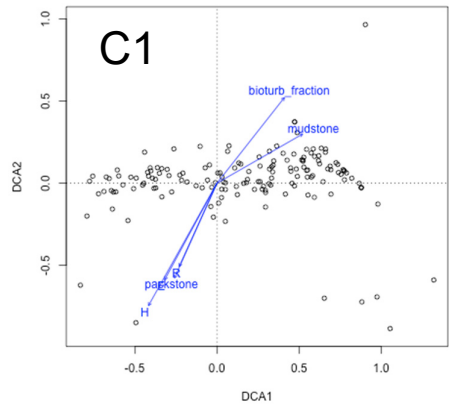
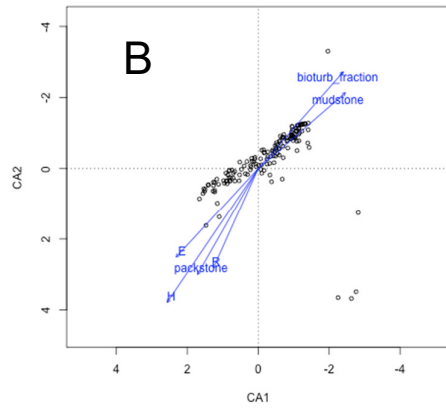
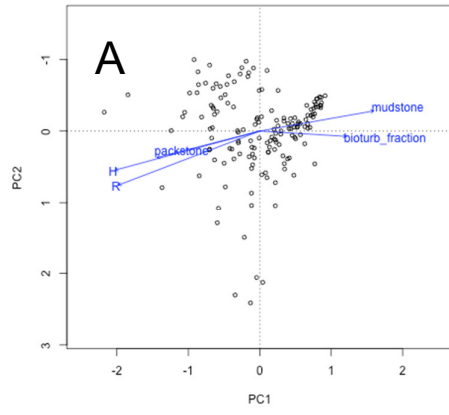
Table 3.9. Results of the *envfit* permutation tests (1000 permutations) and Kendall's τ correlation tests between the lithological/faunistic (diversity) variables and the raw-data ordinations (*= P<0.05, ** = P<0.001) τ values for the CA ordinations are flipped, to better the comparison with the axis 1 gradient observed in the other ordinations.

Variable	PCA		CA		DCA		NMDS	
	τ_1	R ²	τ_1	R ²	τ_1	R ²	τ_1	R ²
Bioturbation	0.32**	0.22**	0.29**	0.23**	0.30**	0.21**	0.32**	0.16**
Mudst.	0.50**	0.40**	0.38**	0.19*	0.40**	0.18**	0.51**	0.48**
Wackest.	-0.19*	0.03	-0.14*	0.03	-0.15*	0.05*	-0.17*	0.09**
Packst.	-0.46**	0.33**	-0.37**	0.21**	-0.38**	0.20**	-0.48**	0.30**
Grainst.	-0.01	0.01	-0.03	0.01	-0.04	0.01	-0.03	0.01
R	-0.62**	0.68**	-0.35**	0.17**	-0.37**	0.15**	-0.50**	0.51**
H	-0.64**	0.67**	-0.43**	0.37**	-0.44**	0.36**	-0.52**	0.51**
E	-0.14*	0.04*	-0.18*	0.21*	-0.16*	0.22**	-0.12*	0.03

Table 3.10. Results of the *envfit* permutation tests (1000 permutations) and Kendall's τ correlation tests between the lithological/faunistic (diversity) variables and selected abundance-weighted DCA and NMDS ordinations (R=8 and R=2. *= P<0.05, ** = P<0.001).

Variable	DCA_8		DCA_2		NMDS_8		NMDS_2	
	τ_1	R ²	τ_1	R ²	τ_1	R ²	τ_1	R ²
Bioturbation	0.28**	0.26**	0.24**	0.15**	0.33**	0.19**	0.32**	0.20**
Mudst.	0.39**	0.34**	0.37**	0.29**	0.50**	0.49**	0.44**	0.43**
Wackest.	-0.16*	0.01	-0.18*	0.02	-0.17*	0.09**	-0.17*	0.08*
Packst.	-0.37**	0.21**	-0.31**	0.13*	-0.47**	0.32**	-0.46**	0.29**
Grainst.	-0.04	0.01	-0.05	0.01	-0.02	0.01	0.01	0.01
R	-0.36**	0.61**	-0.38**	0.30**	-0.60**	0.68**	-0.77**	0.84**
H	-0.43**	0.74**	-0.43**	0.39**	-0.63**	0.69**	-0.73**	0.84**
E	-0.17*	0.12*	-0.13*	0.06*	-0.16*	0.06*	-0.11	0.04

Figure 3.43 (next page). Vector fitting of all lithological and faunistic variables with *envfit* probabilities < 0.01, to the raw-data ordinations and DCA and NMDS ordinations with an abundance-scale weighting of R = 8 and R = 4 (see Table 3.10). A: raw-data PCA ordination. B: Raw-data CA ordination. C1: Raw data DCA ordination. C2: DCA ordination with R = 8. C3: DCA ordination with R = 2. D1: Raw data NMDS ordination. D2: NMDS ordination with R = 8. D3: NMDS ordination with R = 2.



3.2 Reanalysis of Malmøykalven and Jong macrofossil data

In order to facilitate the stratigraphic comparison between the two study localities, a relative stratigraphic position for each plot was estimated by dividing the stratigraphic position (m.a.b.) by the total formational thickness reported at each locality (80m at Jong and 70m at Malmøykalven), giving an approximation of the plot position along the total thickness of the formation.

3.2.1 Coral group abundance in the plots

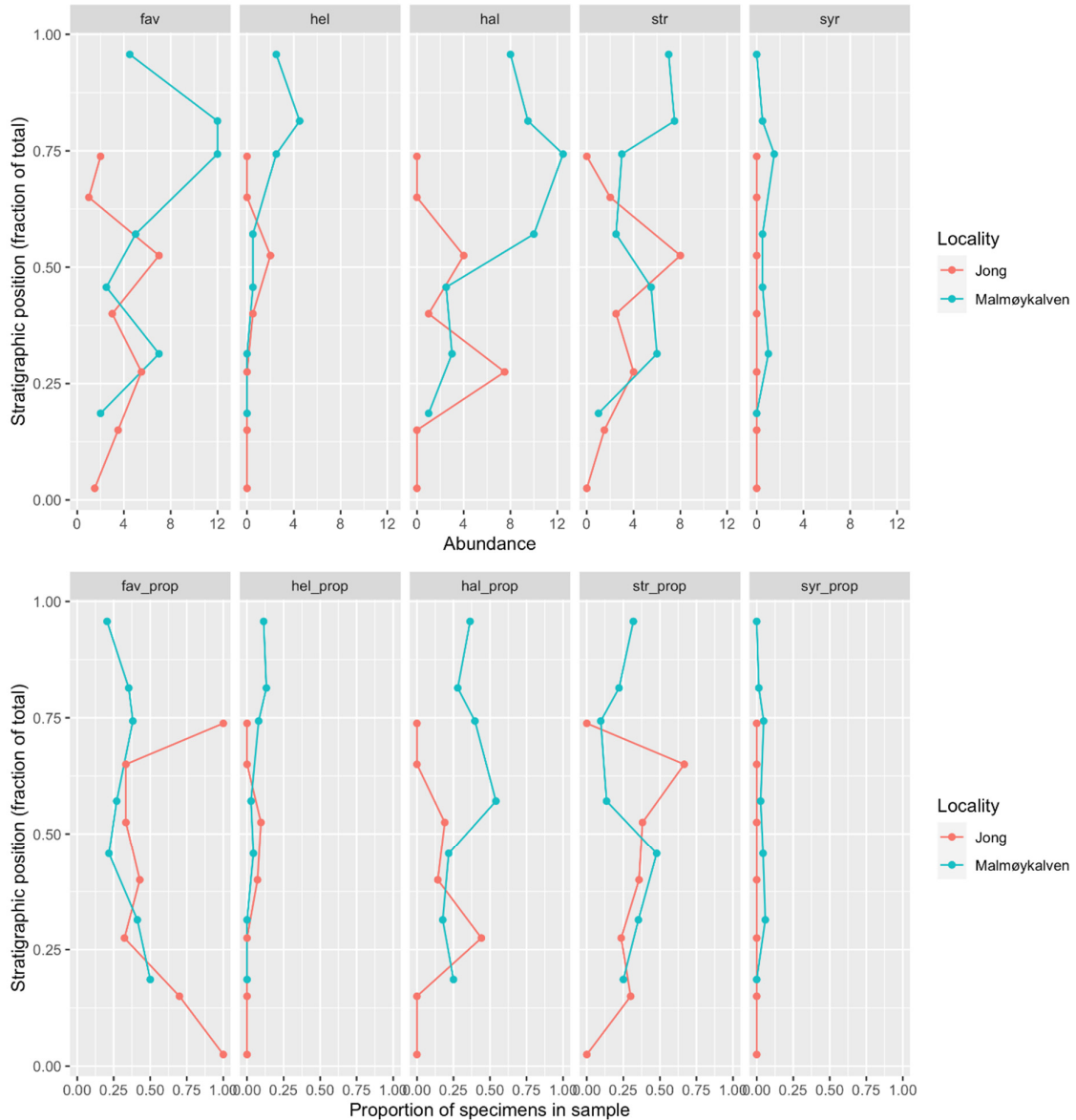


Figure 3.44 (top). Abundance of the different coral/stromatoporoid groups in the samples (x-axis), plotted against their relative stratigraphic position (as a fraction of total formational thickness at each locality) (y-axis). Fav = Favositid, Hel = Heliolitid, Hal = Halysitid. Str = stromatoprid, Syr = Syringoprid.

Figure 3.45 (bottom). Relative proportion of the different coral/stromatoporoid groups in the samples (x-axis), plotted against their relative stratigraphic position (as a fraction of total formational thickness at each locality) (y-axis). Fav = Favositid, Hel = Heliolitid, Hal = Halysitid. Str = stromatoprid, Syr = Syringoprid.

Plots of raw the abundances of the five coral/stromatoporoid taxa in each 1 x 1 normalized plot is shown in Figure 3.44, with the relative proportion of each taxon in each plot is shown in Figure 3.45.

3.2.2 Ordination of lithological matrix and growth form measurements

Ordination diagrams of PCA and 2-dimensional NMDS ordinations of the lithological and growth form averages for each 1 x 1 m normalized plot (symbol legend in Table 3.11) is shown in figures 3.46 and 3.47. The 2D NMDS ordination had a stress value of ~0.099, and the eigenvalues of PCA axis 1 and 2 explained a combined 44% of the total variation in the data. NMDS axes 1 and 2 are flipped in all the graphical representations of the ordinations, in order to facilitate comparison between corresponding gradients.

Table 3.11. Legend for the lithological and growth form variables used by Keilen (1985. Fig 4-2a, p. 73), with new symbols created for the growth form/preservational state variables.















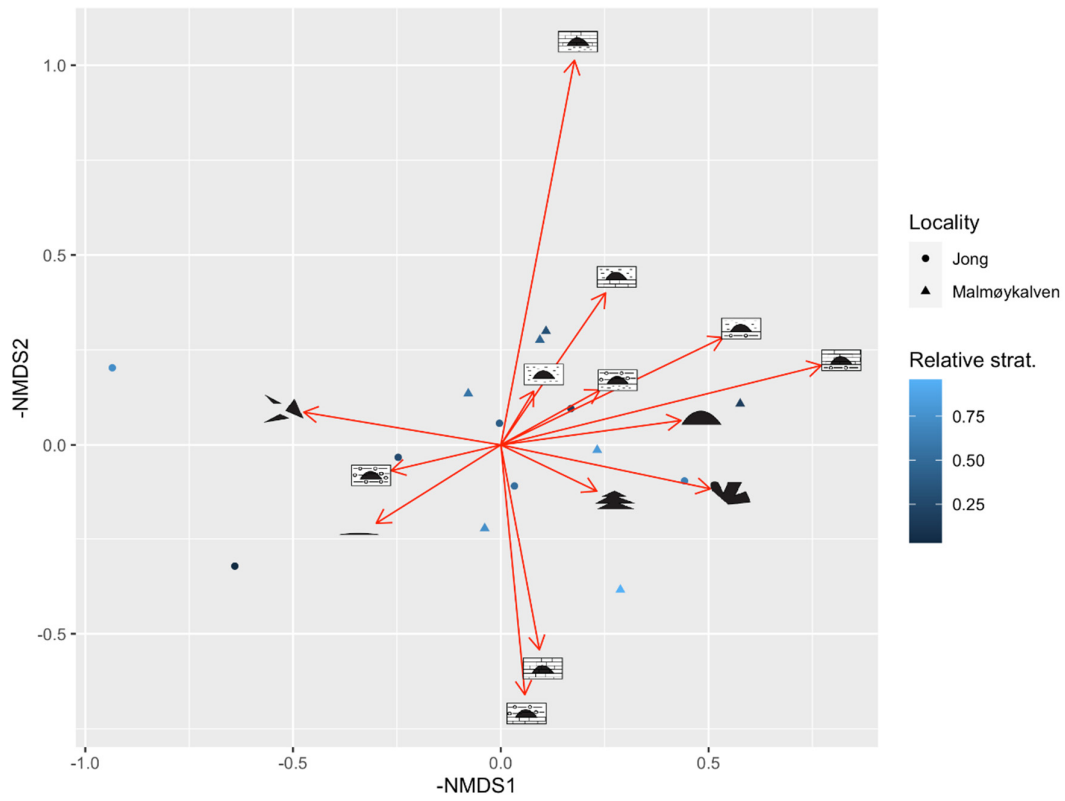
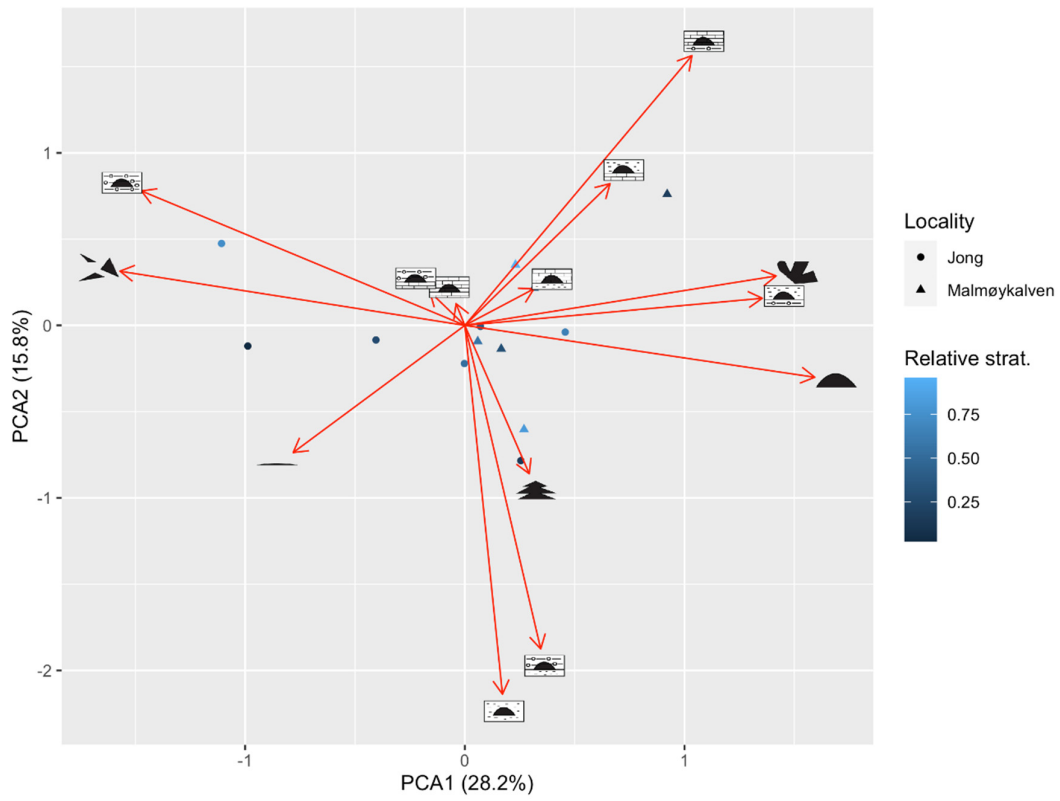
Surrounding lithology	Symbol	Growth form / preservational state	Symbol
Marl		Laminar	
Mudstone		Dome-shaped	
Wacke-, pack- or grainstone		Iregular	
Base of marl, covered in wacke-, pack- or grainstone		“Christmas tree”	
Base of wacke-, pack- or grainstone, covered in marl		Fragmented	
Base of mudstone, covered in marl			
Base of marl, covered in mudstone			
Base of wacke-, pack- or grainstone, covered in mudstone			
Base of mudstone, covered in wacke-, pack- or grainstone			

Figure 3.46 (next page, top). PCA biplot of the means of the environmental variables in each stratigraphic position, color coded by relative stratigraphic position and shape coded by locality (parentheses indicate amount of variation explained by the axes' eigenvalues). Loadings (red arrows) represent the direction of maximum increase in the lithological and growth form variables (Table 3.11).

Figure 3.47 (next page, bottom). NMDS biplot of the means of the environmental variables for corals in each stratigraphic position, color coded by relative stratigraphic position and shape coded by locality. Loadings (red arrows) represent the a posteriori estimation of the optima of the lithological and growth form variables (Table 18).



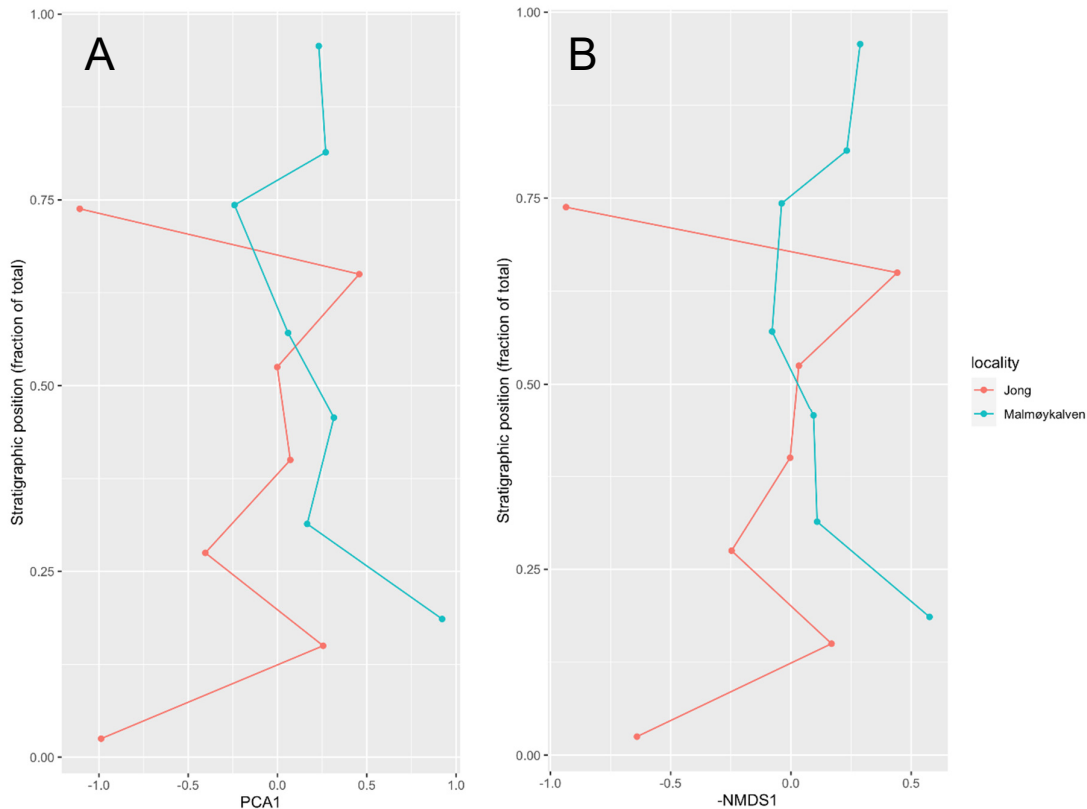


Figure 3.48. A: relationship of relative stratigraphic position to environmental PCA axis 1. B: relationship of stratigraphic position to environmental NMDS axis 1 (flipped).

3.2.3 Correlation between ordinations

The Kendall's τ coefficient between the first axes of the PCA and NMDS ordinations was 0.971, with an associated P-value of $<10^{-8}$. The Kendall's τ coefficient between the second axes was 0.009, with an associated P-value of 0.98. The Procrustes permutation test (*protest*) yielded a correlation coefficient of 0.613, with an associated P-value of 0.008.

3.2.4 Correlation between ordinations and coral abundances

The raw plot abundances of five coral/stromatoporoid taxa (standardized to unit variance) were all correlated weakly with the same direction along the gradient in axis 1 (positive for PCA and negative for NMDS) (see Figure 3.46A and B). However, none of the correlation tests (*envfit* permutation and Kendall's τ) between the plot scores and the abundances yielded a correlation that was significant to more than $P = 0.1$.

When tested against the *proportion* of the different coral/stromatoporoid taxa in each plot, the favositid and stromatoporoids however showed a moderately strong ($P < 0.05$) correlation with the axis 1 gradient in both the *envfit* permutation test and the Kendall's τ test, which was consistent across the ordinations (see Figure 3.49A2 & B2). A predominantly favositid composition was correlated with negative PCA1 values, and a higher stromatoporoid proportion with positive PCA1 values.

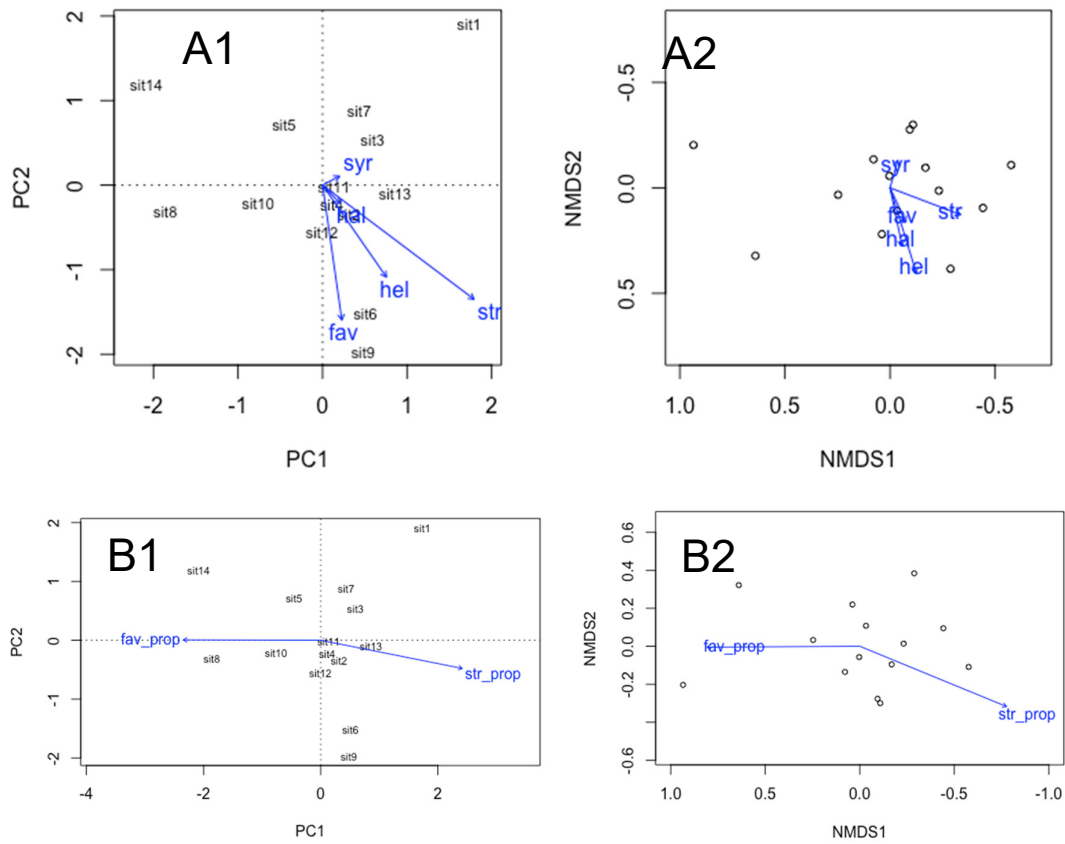


Figure 3.49. Vector fitting of abundance and proportion data for the coral. A1: fitting of standardized organism abundances to PCA axes 1 and 2 (no P-value cutoff). A2: fitting of standardized organism abundances to NMDS axes 1 and 2 (no P-value cutoff). B1: fitting of organism proportions to PCA axes 1 and 2 (only groups with $P < 0.05$). B2: Fitting of organism proportions to NMDS axes 1 and 2 (only groups with $P < 0.05$). Fav = Favositid, Hel = Heliolitid, Hal = Halysitid. Str = stromatoprid, Syr = Syringoprid.

















3.3 Reanalysis of Holmestrand bedding plane point counts

3.3.1 DCA and NMDS ordinations

Both NMDS ordinations were done in only two dimensions, as the stress values were sufficiently low (<0.2). The stress value for the outlier-inclusive NMDS ordination was 0.131, and the outlier-exclusive NMDS had a stress value of 0.136.

The morphotaxa categories employed by Mørk (1978) are to some extent overlapping with the ones used in the acetate peel study, so the symbols used to represent them (Table 3.12) are therefore largely based on the latter, with the largest change being some additional tabulate coral categories and repurposing of the tentaculitoid figure to represent cephalopods.

Table 3.12. Legend of the morphotaxa categories used by Mørk (1978, Table 4, p. 119), with corresponding symbols.

Organism group	Symbol	Organism group	Symbol
Cephalopods		Rugose corals	
Stromatoporoids		Bryozoans	
Favositids		Pentamerus oblongus	
Halycititids		Atrypids	
Heliolithids		Unidentified brachiopod	
Encrusting tabulate corals		Gastropod	
Syringoporids		Trilobites	
Indeterminate tabulate coral		Crinoids	

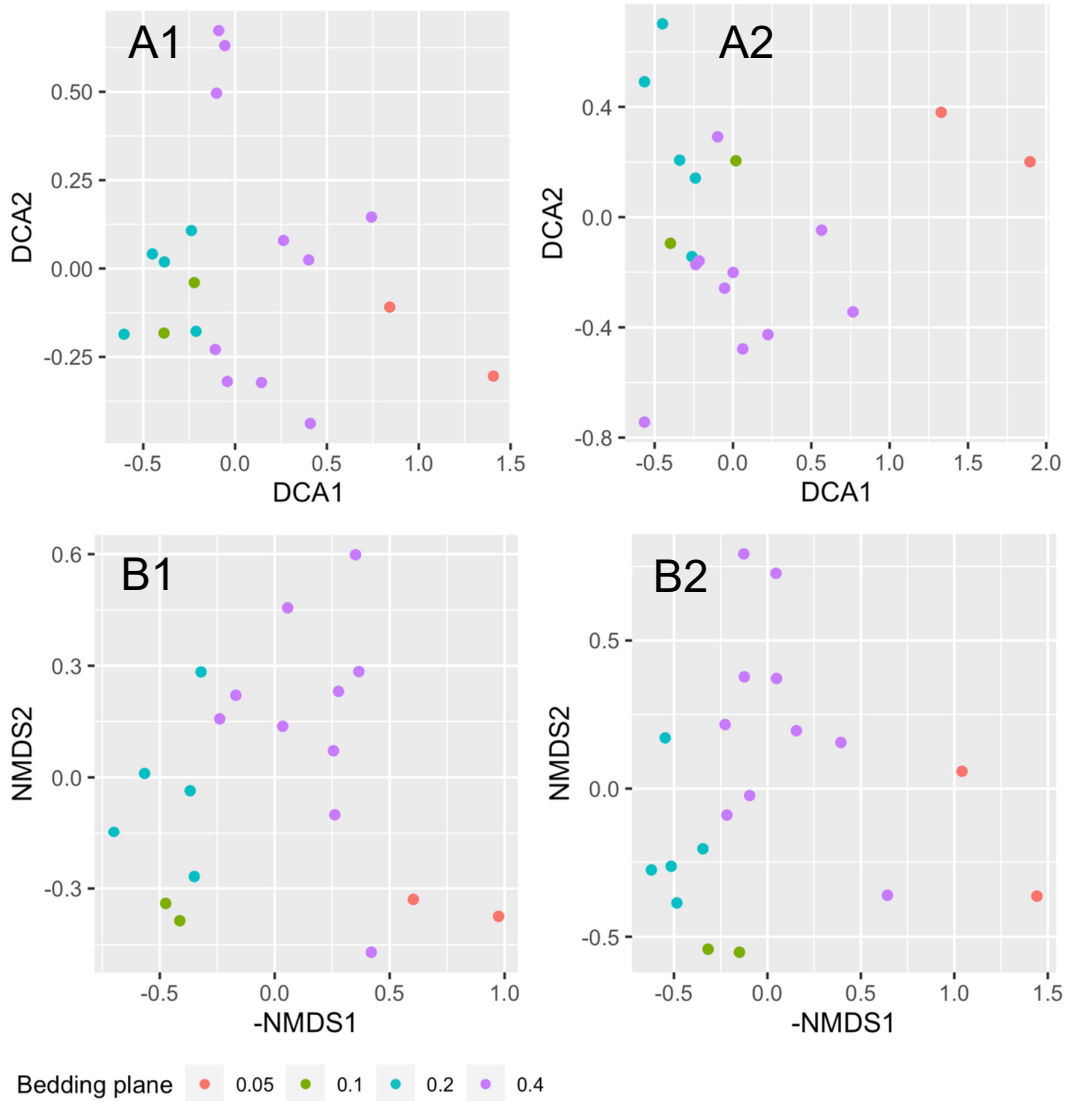


Figure 3.50. DCA and 2-dimensional NMDS ordinations of plots from the different bedding planes (colors) sampled by Mørk (1978). Names of bedding planes correspond to their measured stratigraphic position above the base of *Etagen 7b* (middle Rytteråker Formation) in meters. A1: Outlier inclusive DCA. A2: Outlier-exclusive DCA. B1: Outlier inclusive NMDS, first axis flipped to comparison easier (stress = 0.131). B2: Outlier exclusive NMDS, first axis flipped to make comparison easier (stress = 0.136).

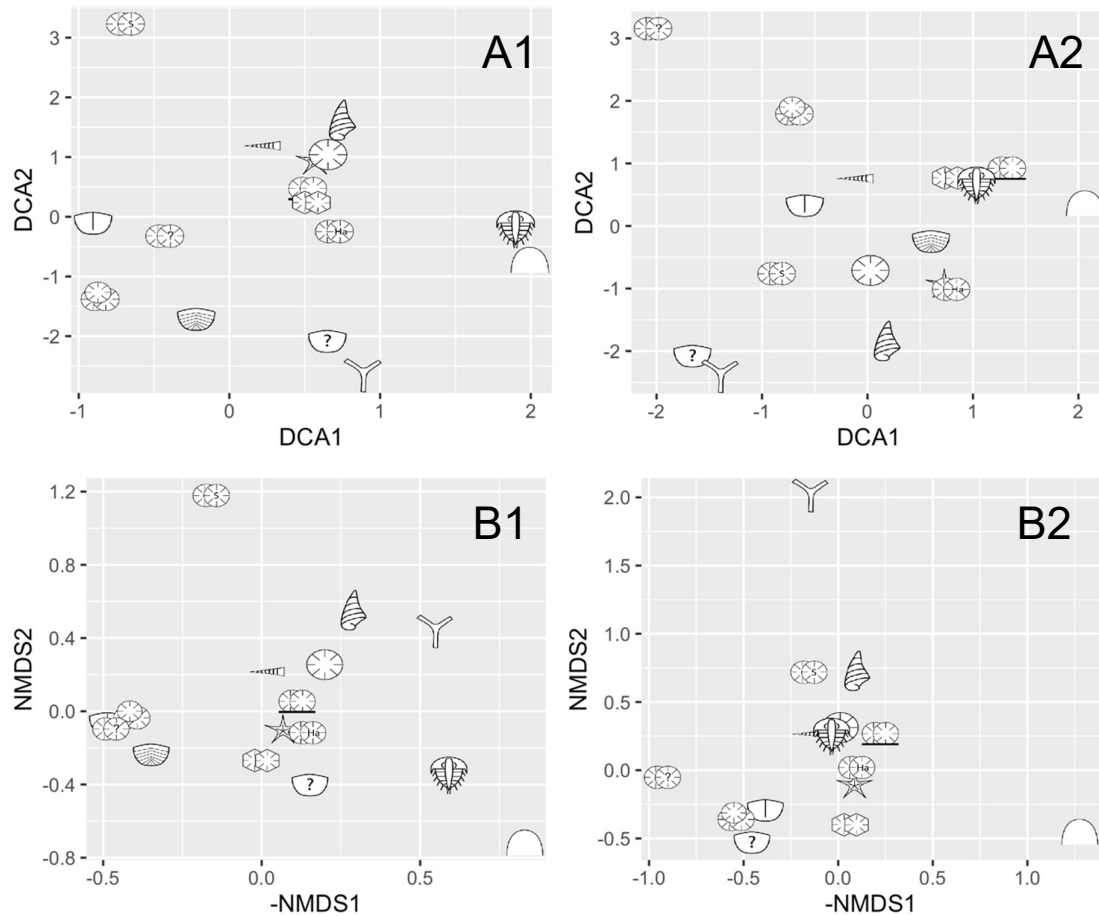


Figure 3.51. Estimated morphotaxa optima along the different ordinations A1: Outlier-inclusive DCA. A2: Outlier-exclusive DCA. B1: Outlier-inclusive NMDS, first axis flipped to make comparison easier (stress = 0.131). B2: Outlier exclusive NMDS, first axis flipped to make comparison easier (stress = 0.136).

3.3.2 Correlation between ordinations

Table 3.13. Procrustes correlation coefficients (r) and Kendall's tau correlations between axes 1 (τ_1) and 2 (τ_2) of the parallel DCA and NMDS ordinations with outlier inclusivity and –exclusivity (denoted by 1 and 0 in the names in the method column). (* = $0.01 > P > 0.001$, and ** = $P < 0.001$).

Method 1	Method 2	R ²	τ_1	τ_2
DCA_1	DCA_0	0.855**	0.684**	0.122
NMDS_1	NMDS_0	0.942**	0.696**	0.696**
DCA_1	NMDS_1	0.676**	0.801**	0.170
DCA_0	NMDS_0	0.720**	0.742**	0.252
DCA_1	NMDS_0	0.637**	0.778**	0.006
DCA_0	NMDS_1	0.663**	0.485*	0.205

3.3.3 Correlation with lithological/trace fossil variables

None of the correlation tests (*envfit* permutation and Kendall's τ) between the plot scores and the lithological / trace fossil variables yielded a correlation that was significant to more than $P = 0.015$ (the Dolminchia A trace fossil), and no correlation that was significant across multiple ordinations. As such, the correlation values are not included in this section.

4 Discussion

In this section, the most important patterns and results from the three major datasets analyzed in the study (the newly gathered data and the two reanalyses) will be summarized and discussed (sections 4.1-4.4), before being compared to each other with regards to paleoecology and methodology (Section 4.5). Lastly, a summary and conclusion about the initial research questions and hypotheses is presented in Section 4.6. For the purposes of structure and clarity, the summary and discussion of the data gathered for this study (from Toverud and Ulvøya) has been split into two parts: 1) the supplementary data (XRF measurements, magnetic susceptibility readings, shell orientation analysis and macrofossil observations), and 2) the acetate peel study (i.e. ordination of subplot frequency data and associated abundance/diversity analyses).

4.1 Toverud and Ulvøya supplementary data

4.1.1 Field macrofossil observations

As summarized in Section 3.1.1, the main qualitative difference between the two study localities in terms of field macrofossil observations was with regards to trace fossil layers and pentamerid brachiopod shell beds, which were exclusively observed in the upper part of the Ulvøya and Toverud sections respectively. The occurrence of trace fossils at Ulvøya, especially the larger, *Thalassinoides*-like beds observed in the middle-upper part of ULV-2, indicates that there must have been well-oxygenated bottom conditions with substantial biological activity at least periodically in the original paleoenvironment (Bottjer et al., 1988). Conversely, the presence of (ostensibly) pentamerid shell beds in the Toverud section seems to be indicative either that the ecosystem at least periodically was dominated by these organisms, and/or that storm events leading to rapid deposition of a large number of these individuals periodically occurred, as suggested by Johnson (1989). The shell beds also seem to appear somewhat more frequently with increasing stratigraphic position in the middle of the section, up to around 25-26 m.a.b., possibly implying that storm events occurred more frequently in this interval (again in accordance with Johnson, 1989).

The presence of stromatoporoid, favositid and halysitid macrofossils at both Toverud and Ulvøya would nevertheless seem to place the two localities very broadly within a similar range of depths – possibly within the photic zone, depending on the association between tabulate corals and symbiotic algae (see Section 1.4.3.2). The untested impression of the corals/stromatoporoids from the Ulvøya section as generally larger and more dome-shaped than the ones recorded at Toverud (although the size and shape of the favositid corals in the upper part of the TOV-2 section were generally hard to discern), would also seem to suggest that they lived in a less energetic, possibly deeper environment than the corals at Toverud.

A general increase in the abundance of coral macrofossils seen in the upper part of the ULV-2 section could further be interpreted as evidence of a transition to a more productive – possibly

more photoenergetic or nutrient rich – environment. The upside-down deposition of corals near the top (i.e. Fig. 3.2e), also seems to suggest at least some current action. One study of stromatoporoid and tabulate coral sizes from Malmøykalven further indicated that an increase in their mean width was generally positively correlated (although only slightly) with increasing stratigraphic position (Baarli et al., 1992), further supporting the interpretation of the Rytteråker Formation in this area as progressing into a more suitable environment for tabulate corals to grow larger.

However, it is again important to keep in mind that the macrofossil observations in this study were *not* systematic, nor comprehensive. They do not include all macrofossils from the two localities, and might therefore be biased. As such, we should tread carefully when using the conclusions here to interpret the other data and analyses.

4.1.2 Magnetic susceptibility readings

Although the middle section at Ulvøya is missing due to faulting (presumably), the magnetic susceptibility logs from the two localities (Fig. 3.43) nevertheless show a highly similar signal overall. The SI values in both cases go from being higher and more variable at the base of the formation (at $100\text{-}300 \times 10^{-6}$ SI) to stabilizing at around 50×10^{-6} SI in the middle of the section (around 15-20 meters at TOV-2, and somewhere in the missing section at Ulvøya). The sampling at Ulvøya, which extended 10 m further below the formation base than at Toverud, also shows an increase in susceptibility further below the formation base, to around 400×10^{-6} SI, further supporting this trend.

Magnetic susceptibility strength is most commonly used as a proxy for siliciclastic (i.e. terrigenous) influence on lithified sediment (da Silva et al., 2012; Whalen & Day, 2008). Thus, these results fit with the notion of the Rytteråker Formation as a representing gradual transition from a siliciclastic-dominated (the Solvik and Sælabonn formations) to carbonate dominated marine environment. A development like this could either be due to reduced input of siliciclastic material from land, an increase in abundance in carbonate-producing organisms overtaking and “diluting” said input, or a combination of both (da Silva et al., 2012). In either scenario, the development would nevertheless seem to fit quite well with a hypothetical change from a Primo to Secundo oceanic/climatic state as described in Section 1.4.1.1, which is hypothesized to have caused both reduced weathering from land and more favorable conditions for shallow-water carbonate producing organisms (Aldridge et al., 1993).

Using MS as a proxy for water depth – which has also been attempted in several studies – seems to be highly dependent on the depositional environment in a carbonate setting (da Silva & Boulvain, 2006). One study of carbonate platforms and reefs from the middle Devonian of Belgium found that MS values, in the range recorded at Toverud and Ulvøya, positively correlated with decreasing water depth (or closeness to the shore) in an onshore-offshore slope. However, they were *negatively* correlated with decreasing depth in slopes leading up to carbonate mounds and atolls (da Silva et al., 2012). The values recorded in the lower part of the Rytteråker Formation could therefore be seen as fitting either an offshore depth-increase or

a shallowing-up to a carbonate shoal/bank environment. However, the leading interpretation of the Rytteråker Formation in the literature – as a predominantly shallowing-up sequence in a shoal-barrier system (see Section 1.5.6), does intuitively seem to make the latter scenario more plausible.

The small “dip” in MS values (down to at around $25 \cdot 10^{-6}$ SI) at the top of the TOV-2 section (at 38 m.a.b.), may also be worth noting in this context. It coincides with the “grainstone unit” reported by Johnson, 1989, as well as the TOV-2 samples with the clearest examples of grainstone lithology in the acetate peels/thin sections (e.g. PMO 236.497), supporting the hypothesis that this interval represents the “purest” carbonate environment in the section.

However, these topmost values are also not extremely different from the MS values measured in the rest of the top half of the section. Overall, the similarity and relative “stability” of the low SI values observed in the upper 60% of both localities suggest that the MS values are *primarily* indicative of the transition from a siliciclastic to carbonate-dominated environment – whatever the cause, and any relationship to water depth is in that case secondary and more uncertain.

4.1.3 Toverud XRF data

The Toverud XRF data seem largely to confirm the results from the MS readings. Apart from occasional “spikes”, Si and Fe, proxies for siliciclastic input, generally decrease from the base of the formation to the top, while Ca (i.e. carbonate content) increases (Fig. 3.4). The PCA ordination of the elemental readings also summarizes this pattern, giving a PCA axis 1 (Fig. 3.6) that very closely resembles the Ca log (and the inverse of Fe and Si logs) in Fig. 3.40, although slightly more “smoothed”.

The ratio of Mn to Sr, commonly used as a proxy of the degree of post-depositional diagenetic alteration of the rocks (Derry et al., 1992; Ganai et al., 2018), also shows a decreasing upwards trend (Fig. 3.4). This also fits with the interpretation of the sequence becoming more “pure” carbonate, meaning it also becomes less permeable to the ion transport needed to exchange Sr with Mn atoms, and therefore less metamorphosed (Brand & Veizer, 1980).

Overall, the XRF values should however be interpreted with a substantial amount of reservation. As the measurements were only done on a small area of the samples (8 mm diameter window), they may – as mentioned in Section 2.2.4 – be highly susceptible to lateral variations. Particularly the spikes recorded in the Ca, Si and Fe logs might very well be the result of such fluctuations.

4.1.4 Toverud shell orientation analysis

The binomial testing of the shell orientation data (Fig. 3.38) indicated that the fraction of brachiopod shells in a concave-up orientation in the TOV-2 locality as a whole was weakly statistically significantly lower than 0.5 ($P=0.035$). When modelled as a function of stratigraphic position, the likelihood of concave-up orientation was also significantly (albeit

only slightly) positively correlated with stratigraphic height (Fig. 3.39), with the model prediction ranging from a 0.4 concave likelihood at the formation base, to ca. 0.65 at around 34 m.a.b. The additional modelling (Table 3.10) revealed no significant or systematic relationship between the other sample-related variables (sample size and shell density) and stratigraphic position, implying the trend observed in Fig. 3.39 is not due to indirect correlation with underlying variables. However, the binomial GLM model of convex likelihood as a function of shell density was borderline statistically significant ($P = 0.072$), with a highly negative model estimate. This indicates that the concentration of shell valves per cm^2 might also be a second independent predictor for the likelihood of a concave-up orientation.

Results from experimental taphonomy, as well as other paleontological shell-orientation studies, suggest that brachiopod valves almost always settle in a concave-up position after being suspended in the water column, due to the position of the center of gravity in the shell (Simoes et al., 2005). Preservation of this pattern in the fossilized sediment, then, suggests an absence of bioturbation and influence from currents after deposition. Studies have found that concave-up shells are often associated with storm-deposited (i.e. tempestite) assemblages (Fürsich & Oschmann, 1993; Kidwell et al., 1986), as brachiopod shells in these cases are assumed to have been suspended by underwater turbulence and quickly buried in the sediment. Conversely, a predominantly *convex*-up shell assemblage may be interpreted as a result of prolonged exposure to a biologically active and/or current-rich sea floor, giving the shells time to be overturned to a more stable hydrodynamic state as the result of physical forcing or bioturbation before being buried (Simoes et al., 2005). Storm-deposited and rapidly buried brachiopod assemblages have also been connected to denser packing of the shells (Y. Li & Rong, 2007).

In this context, the results of the Toverud shell orientation analysis seem to suggest a higher degree of storm-deposition with increasing stratigraphic position. This fits with the assertion of Johnson (1989), which posited that storm deposition and tempestite shell-beds are more frequent with increasing stratigraphic height up to the grainstone unit at approx. 38 m.a.b., which Johnson interpreted as evidence of a marine shallowing.

Even though the samples measured for the shell-orientation analysis were not collected systematically from “corresponding” layers (i.e. only shell-beds or non-shell beds), one might argue that the likelihood of sampling a storm-layer – if sampling at random – would increase if they are more frequent as a function of stratigraphic height. However, the fact that more shells are typically preserved in a better condition with storm deposition than with gradual deposition (Fürsich & Oschmann, 1993), might also be an important bias to keep in mind when discussing these results.

Another potentially confounding factor might be the fact that thick, calcified shell valves (i.e. *Borealis borealis*-like valves) are more common in slabs from the upper part of the section (as they are in e.g. PMO 236.478). Their larger weight and center of gravity might conceivably have made them more inclined to settle in a concave-up position regardless of depositional circumstances, and harder to overturn by currents or bioturbation. Still, Johnson (1989) also

interprets this “thickening” of the brachiopod valves as an eco-morphological response to shallower, more storm-exposed habitat, meaning that they nevertheless could be a sign of increased wave-action and storm frequency.

4.2 Toverud and Ulvøya acetate peel study

4.2.1 Comparison with thin sections

As illustrated by Figures 3-7 to 3-18, the different organism groups were overall relatively easy to identify both in the thin section and acetate peels. Although the cross-bedded crystal-calcite structure of the crinoid ossicles, and to a lesser degree the thick-valved brachiopods, was more pronounced in the thin sections (e.g. 3-19b versus 3-19a), the delineation of the groups themselves was not significantly more difficult in the peels. Arthropod (i.e. ostracod and trilobite) shells generally appeared somewhat darker in the peels than the thin section (as in 3-15a vs 3-15c), which in some cases made them *more* easy to distinguish from e.g. brachiopod shells than in the thin sections. Most other morphotaxa appeared to be relatively similar in the two substrates. The micro-granular structure characteristic of tabulate corallite walls (Scrutton, 1998) was also generally distinguishable in both peels and thin sections (see Fig. 3.13).

The only organism group which was more clearly present and identified in greater abundance in the thin sections, were the filamentous algae (i.e. *Girvanella* sp). This might be partially due to chance, and to the fact that the small size of the algal filaments makes them hard to identify in the first place. However, in the few cases where they were identified in the acetate peels (as seen in Fig. 3.12b), they were very hard to distinguish from the micritic matrix. As such, there seems to be a decent chance that filamentous algae could generally have been more prevalent in the samples if a thin-section-study had been conducted. Other than this, the only real difference between the two substrates was that some more post-processing of images was required for the acetate peels.

4.2.2 Morphotaxa abundances and diversity

4.2.2.1 Abundance-occupancy relationships

As seen in Figure 3.16, the relationship between taxon frequencies (proportion of samples) and mean subplot frequency (SF) abundances in all acetate peels appears to follow an approximately positive, log-linear trend – with some significant deviations. Ostracods, like crinoids, appear in nearly all samples, but at a significantly lower mean abundance (7.3, as opposed to 22.5 for crinoids). Conversely, thick-valved, straight shelled brachiopods have a notably high mean abundance in samples where they are present (second only to crinoids), despite only being present in 55% of the samples. However, the most striking outlier to the log-linear trend are the calcareous tubes of unknown affiliation, which occur in only 12% of the plots (mainly at the base of TOV-2, see Fig. 3.18), but in a relatively considerable mean abundance (4.9). Overall, the taxa that appear in more than 50% of the plots (crinoids, ostracods, bryozoans, thin- and thick-valved straight-shelled brachiopods), seem to form a somewhat distinct cluster in the right-hand side of the diagram, with mean abundances from

ca. 8 to 22, while the rest of the taxa cluster in the lower left-hand side with mean abundances generally ranging between 2 to 5.

A positive relationship between species' abundance and occupancy appears to be a fundamental pattern in ecology, with log-linearity also being a common relationship between them (Buckley & Freckleton, 2010). Our species abundances overall thus appear to behave relatively similar to what one might expect in a more "standard" multivariate analysis of species-level abundances (i.e. van Son et al., 2014), although the outliers should warrant some caution when interpreting them as such.

In terms of the ordination of samples, the abundance-occupancy results might be assumed to influence the ordination methods in different ways. The CA/DCA algorithm in particular has been recognized as particularly susceptible to plots with low occupancy and medium- to high abundances, due to its statistical basis in contingency analysis (van Son & Halvorsen, 2014), while an NMDS ordination based on Bray-Curtis dissimilarity might be expected to place less emphasis on rare species, being instead based on overall (percent) dissimilarities between the samples (see Section 1.3).

4.2.2.2 Relationship to locality and stratigraphy

When broken down by locality (Fig. 3.17), there is a consistent difference between the boxplots of morphotaxa abundances between the TOV-2 and the two Ulvøya localities. Even though the median abundance in the majority of taxa is 0 for all localities, the former locality generally has a much higher incidence of nearly every taxon. The only exceptions are ostracods and crinoids, where the ULV-1 locality has a higher median abundance than both ULV-2 and TOV-2, and filamentous algae, which only had one occurrence in the peels (at ULV-2). The TOV-2 dominance is the most evident in the case of bryozoans and the three brachiopod categories, where the TOV-2 data has a consistent range of high to medium abundances in all plots, and the Ulvøya localities only a few, sporadic abundances, registered as outliers in the boxplots.

When viewed against their stratigraphic position (Figs. 3-18 & 3-19), the abundances of most taxa generally do not seem to be very clearly structured stratigraphically within each locality. However, a notable exception to this is the aforementioned calcareous tubes at TOV-2, as well as the two straight-shelled brachiopod categories from the same locality, which both show a distinct increase in abundance at around 10 m.a.b., after which, with some fluctuation, there is consistently higher abundance in the upper part of the sequence – with the possible exception of the highest 1-2 meters. "Fluctuations" in abundance between close stratigraphic levels also seem to be more frequent at ULV-2 than the other localities – perhaps most clearly seen in the crinoid counts. This is perhaps not surprising, as ULV-2 was unique among the localities with several samples containing almost no discernible fossil fragments (i.e. at 24 m.b.t)

4.2.2.3 Diversity metrics

The general differences in abundance between the localities inferred from figures 3-? are largely confirmed by the boxplots of diversity metrics (Fig. 3.20) and their associated one-way ANOVA-tests (Table 3.3). For all three diversity metrics measured, the samples from the TOV-2-locality consistently had a higher mean and median than the two Ulvøya localities, the largest and most significant difference between the localities being in terms of Simpson's H, closely followed by species richness (S). The ANOVA test of species evenness gave a much lower, and only moderately significant result (F-value) for the SS explained by the locality means.

As Shannon's H takes into account both species evenness and richness, this indicates that the difference between morphotaxa diversity across localities is the result of richness rather than evenness, although the latter was also somewhat lower at ULV1 and -2 (Fig. 3.20).

4.2.3 Ecological occupancy

As can be seen in Fig. 3.24, the three localities are for the most part dominated by the same ecological categories. Non-motile suspension feeders – particularly crinoids, brachiopods and bryozoans, constitute the majority of all SF registrations across stratigraphy and locality, while free-moving, surficial and semi-infaunal deposit feeders (primarily represented by ostracods) remain the second largest constituent with a different mode of both feeding and motility, consistently making up about 10-25% of the SF registrations. All other modes of feeding and tiering remain consistently very low in both sections. The biggest outliers to this are a small peak in organisms with infaunal tiering and otherwise unknown life modes (i.e. calcareous tubes) at the base of the Toverud section, and a similar minor peak in slow-moving herbivores (i.e. gastropods) in the middle of the ULV-2 section – neither of which will be considered as significant trends in the rest of this discussion.

There are however some distinct differences between the three localities. Most notably, the Toverud section consistently has a larger proportion of *surficial* and to a lesser degree also unattached (i.e. pentamerid brachiopod) filter feeders – attributable mostly to bryozoans and pentamerid brachiopods. This trend is also most clear in the middle of the section, where the abundances of brachiopods are greatest. Conversely, both Ulvøya sections, but particularly ULV-2, have a higher proportion of *erect* filter feeders (i.e. crinoids), as well as a higher proportion of potentially semi-infaunal deposit feeders (primarily ostracods). The proportions between these also fluctuate more between the stratigraphic levels in the ULV-2 section than the other sections.

When looking at the raw abundances (left hand side of Fig. 3.26), the difference in proportions between the localities seems to be primarily due to the fact that the ULV-1 and ULV-2 sections have fewer overall surficial (i.e. brachiopod, bryozoan etc.) registrations, while the raw number of SF registrations of crinoids and ostracods are roughly comparable between the three sections.

In a very broad sense, these results generally seem to fit well with the general conception of the ecospace utilization of the “Paleozoic fauna” (Bush, Bambach, et al., 2007, see also Section

1.4), in that epifaunal suspension feeding is the dominant mode of life. The relative dominance of erectly tiered filter-feeders (i.e. crinoids) at the ULV-2 locality might conceivably also be seen as a sign of less favorable conditions for lower-tiered suspension feeders like pentamerid brachiopods, indicating a possibly deeper or calmer (i.e. less nutrient-carrying currents) environment.

The interpretation of these patterns is however quite speculative, and comes with major interpretative biases and challenges. The assignment of a single ecological category to each morphotaxa group is only based on what appears to be the most common and/or likely mode of life for species in the group given the literature on their diversity and adaptations in similar environmental settings in the Silurian (see Section 2.3.4). This means that there is no guarantee that the life modes assigned accurately match the lifestyle of the actual species. This is perhaps particularly true for groups like ostracods and trilobites, which contain within them a large variety of ecological adaptations and life modes (Fortey, 2014; Siveter, 1984). However, since the ecological categories used here are so broad and general, it is assumed that they for the most part will be reasonably useful for describing very broad-scale trends like in the previous paragraph.

Secondly, it is also important to keep in mind that the SF counting method is *not* a proxy for biomass the way point-counting is, and it supposes no inherent proportionality between the groups. Therefore, the notion of “abundance” and especially *proportional* abundance in this context should generally be taken with a grain of salt.

4.2.4 Comparison of raw-data ordinations

4.2.4.1 Sample scores in the ordination diagrams

In all four raw-data ordinations, the majority of the plots from the Toverud locality clustered separately from the two Ulvøya localities along one end of ordination axis 1. The ULV-1 samples generally dispersed along the middle of axis 1, while the ULV-2 points occupied the other end of axis 1 (right-hand side in the diagrams). As the Kendall’s τ correlation test statistic for axis 1 (Table 3.4) was strong (≥ 0.49) and highly significant between every ordination, it implies that this clustering is likely a real property of the data and not a result of stochasticity or statistical artefacts. The relatively high explanatory power of axis 1 in both the PCA and CA ordinations, when considering the number of samples ordinated, also seems to support this.

Ordination axis 2 showed less overall similarity between ordinations, with only three τ -tests indicating a significant correspondence, and generally with a lower correlation coefficient than for axis 1. When comparing the ordination diagrams visually (as in Fig. 3.29), the sample scores seem to broadly sort into two main geometric patterns with respect to the configuration of axis 2. In the PCA and NMDS ordinations, the samples form a curve-shape in axis 2 – perhaps most evident in the NMDS diagram. In the CA and DCA ordinations, a more “line”-shaped configuration occurs, either slightly slanted (CA) or straight along axis 1 (DCA), with a few distinct clusters of outlier plots (mainly from the TOV-2 locality) in the lower corner (the ULV-2 side of axis 1). These observations are underpinned by the fact that NMDS-PCA, and CA-

DCA – respectively – were the most highly correlated with each other in terms of correlation coefficients (Table 3.4), both in the case of axis 1 and 2, and overall Procrustes (r) similarity. These patterns will be discussed further in the following sections.

4.2.4.2 PCA and NMDS pattern

The curve-shape in the NMDS and PCA ordinations clearly resemble a polynomial distortion axis (i.e. horseshoe/arch effect, see Section 1.3). As such, this pattern seems to imply that there is only one real – or at least only one strong – species-compositional gradient in the ordinations (the one seen along axis 1), and that this gradient is sufficiently long to be distorted by the ordination algorithms. However, there can also be seen one major difference between the NMDS and PCA results along axis 1. Even though their order is similar, (ref. their Kendall's τ similarity) the *spread* of scores along axis 1 (and to a lesser degree axis 2) in the PCA diagram is much higher on the left-hand (TOV-2) side of axis 1, approximately double, than that of the ULV-2 side, while almost the exact opposite is the case in the NMDS diagram. Here, the ULV-2 plot scores have a much higher spread along axis 1 than the other localities.

A likely cause for this discrepancy is the fact that, as discussed in sections 4.2.1-2, the average abundances, species richness and diversity are generally substantially higher in the TOV-2 samples than the ULV-2 samples – a “skewness” that then has different consequences for the two ordination procedures. The PCA algorithm attempts to find the direction of maximum increase in abundance in species, which is generally greater – and more variable - for TOV-2 data, meaning it will be “interpreted” as the direction of maximum increase for most taxa. The NMDS sample scores, however, are only based on Bray-Curtis similarity (i.e. percent dissimilarity) between samples, meaning that in samples with very few species present in low abundances – such as many ULV-2 samples – slight variations in species abundances between these could result in a very large degree of dissimilarity, somewhat disproportionately to the more “robust” TOV-2 samples. For instance, the Bray-Curtis dissimilarity between a sample with 10 crinoid fragments and one with 2, and no other species, would be 0.8 – even though they are identical in terms of species shared, and the absolute difference in abundance is the same as e.g. between two samples with 32 and 40 crinoid fragments respectively (which would have a Bray-Curtis dissimilarity of 0.2).

This explanation also seems to be supported by the distribution of species scores/loadings (i.e. symbol position) in the two methods. In the PCA diagram especially, all species optima are either on the TOV2 side of axis one or in the middle (at 0), meaning they do not contribute to the structuring of axis 1. In the NMDS diagram, the majority of species optima calculated by weighted averaging also occur within the TOV2 “cloud”, or at the transition between the Ulvøya and Toverud samples (with a few notable exceptions, see Section 4.2.4.6).

4.2.4.3 CA and DCA pattern

That the results of the CA and DCA methods are very similar is perhaps not surprising, since they are essentially versions of the same method, with the same algorithmic basis. Overall,

these two ordinations appear to handle the overall difference in abundance between the localities “better” in the sense that the spread of plot scores along axis 1 is more even with these methods, and there is no clear sign of an arch effect in either diagram. The slanted line in the CA diagram might *potentially* be taken as a sign of an arch-trend in combination with the outliers in the lower left-hand corner, but this interpretation seems somewhat speculative.

When looking at the estimated morphotaxa optima, the cause of the outlier cluster in the right-hand corner is apparent as the result of the samples having high abundances of the unknown calcareous tubes (see Section 4.2).. This largely confirms the hypothesis in Section 4.2.2 that the CA and DCA methods are more “vulnerable” to outliers resulting from low occupancy/high abundance than the other methods. When looking at the distribution of morphotaxa optima in the ordination diagrams overall, low-occupancy and low- to medium abundance taxa (like gastropods, stromatoporoids, favositid/heliolitid corals and tentaculitids), generally also appear to be more dispersed along the first and second axis than in the PCA and NMDS ordinations – especially in the DCA diagram. However, the non-linear rescaling of the DCA method *does* seem to dampen the severity of the outlier effect on the sample scores somewhat – reflected both in the distance between the points observed visually, as well as the relative core length of axis 1. The absence of a “slant” in the main TOV2-ULV1 (Peters, 2008) gradient is also likely attributable to the detrending performed by the DCA algorithm.

4.2.4.4 Outlier influence

The total outlier influence on axis 1, as measured through relative core length (Table 3.5) was relatively similar among the ordinations, with the DCA standing out with a slightly higher RCL (0.52) than the other methods. The RCL values for all methods are, however, low compared to other ordination-based studies of recent species-data where the metric is used (Liu et al., 2008; van Son & Halvorsen, 2014). This implies that all the ordinations are substantially impacted by outliers. The PCA ordination had the lowest RCL, closely followed by CA and NMDS, all three within the 0.42-0.45 range, meaning that in the case of these ordination methods, more than half of the length of axis 1 is occupied by only 10 percent of the plots.

The nature and cause of the outliers seem however to be somewhat different between the different ordination methods, even though some of the “outermost” samples are the same (i.e. between DCA and NMDS). In the case of PCA and NMDS, it appears to be mainly caused by the aforementioned “spreading out” of the sample scores on the right and left-hand side of axis 1, respectively. While in the case of CA and DCA, it seems mostly to be due to the clustering resulting from the calcareous tubes and other outliers, as discussed.

4.2.4.5 Similarities between morphotaxa optima

In terms of the relationship between sample scores and morphotaxa optima/loadings, some patterns were nevertheless present in all the ordination methods. Of all the morphotaxa, the two straight-shelled (i.e. pentamerid-like) brachiopod categories are consistently the most or second most (in the PCA) associated with direction of axis 1 associated with the TOV-2 locality, and

gastropods, stromatoporoid and filamentous algae are consistently the most associated with the ULV-2 side of the axis. Many of the other morphotaxa optima appear to be mostly associated with the middle of the TOV-2 side of axis 1, especially the bryozoans, corals and wavy/punctate (i.e. non-pentamerid) brachiopods. Others are more associated with the transitional area between the two localities (i.e. the middle of axis 1), primarily ostracods, crinoids, trilobites and tentaculitids. However, the variability in placement of these latter taxa is also generally greater, especially with regard to placement in axis 2 – suggesting that they have a less “stable” association in the ordination diagram than e.g. the pentamerid brachiopods.

When framed in terms of ecological occupancy, it appears that the general trends discussed in Section 4.2.3 are reflected in the clustering of species optima along axis 1, as the optima of the surficial, non-motile filter feeders are consistently more associated with the TOV-2 side of axis 1.

4.2.4.6 Relationship between stratigraphic position and ordination axis 1 scores

In the case of the TOV-2 locality, a similar stratigraphic development trend in axis 1 is observed with all ordination methods (Fig. 3.36). Namely a more or less gradual, leftward shift in the sample scores beginning at around the 5-10 m.a.b. mark, to a “left maximum” at approx. 20 m.a.b., followed by a gradual, slight to moderate rightward shift most clear from around 33 m.a.b. Sample scores along axis 1 also appear to become somewhat more dispersed (i.e. fluctuating more between stratigraphically close samples), in the topmost 15 meters of the section – a trend that is perhaps most clear in the DCA ordination.

The variation in axis 1 scores with regards to the TOV-2 stratigraphy between the ordinations seems mostly attributable to the method-specific distortions discussed in the previous sections. The CA (and to a lesser extent DCA) are especially “marked” by the calcareous tube-outliers at the base of the formation, while the PCA produces some significant left-ward outliers around the 15-19 m.a.b. interval, and the spacing of the NMDS TOV-2 sample scores is more dense. The curved “left-then-right” pattern is nevertheless prominent in all diagrams, most clearly pronounced in the DCA ordination, and the least clearly pronounced in the NMDS ordination. This last point is probably connected with the “skewness” in dispersal between the localities discussed in Section 4.2.4.2.

With the two Ulvøya localities, no clear directional stratigraphic trends in axis 1 seem to be present across the ordination methods in the same way as with TOV-2. Plot scores generally seem to be more dispersed in the ULV-2-section than the ULV-1 section, but this trend, again, appears to be highly dependent on the choice of ordination method – e.g. as the NMDS method disperses the points considerably more than the other methods (again, see Section 4.2.4.2).

4.2.5 Effect of abundance-scale weighting on DCA and NMDS ordinations

4.2.5.1 Plot scores in the ordination diagrams

The abundance-scale weighting of the data seems at first glance to affect the DCA ordinations (Fig. 3.37) more profoundly than the NMDS ordination (Fig. 3.38). With decreasing abundance-weighting, the DCA plot scores appear to shift from a line parallel to axis 1 into a more slanted, stretched out and eventually more cloud-like configuration, with the distinction between the Toverud and Ulvøya clusters becoming progressively less clear. Some outliers, like the TOV-2 cluster at the right-hand side, become less clearly separated from the rest of the points, while other points (mainly from the ULV-2 locality), appear to become more outlying (as in R=2). With the presence-absence ordinations, the greatest shift in plot scores occurs, causing the distinction between the clusters to disappear more or less entirely.

In the NMDS ordinations, changes are less severe. The points generally appear to migrate gradually towards the center of the diagram with decreasing abundance ranges, retaining but slightly obscuring the distinction between the TOV-2 and ULV-2 cluster. As with DCA, the greatest shift towards there being just “one big cloud” seems to occur with the presence-absence weighting, but not nearly to the degree it does in the DCA. The progressive change in NMDS sample scores generally seems to both slightly reduce the prominence of the arch-structure observed in the raw-data ordination, and to a lesser extent also the skew in sample score distributions on the ULV-2 side of axis 1 discussed in Section 4.2.4.2, although the TOV-2 cluster also seems to become denser at the same time.

Interestingly, the effect of abundance-scale weighting on the relative core length of the axes was nearly opposite between the methods, with the DCA RCL becoming consistently lower with each abundance-scale, “shortening” to 0.29 in the presence-absence ordination, while the NMDS RCL increases slightly, up to 0.52 in the presence-absence ordination. Even so, with the exception of R=2 and the presence-absence weighting, the DCA ordination still has a higher RCL than the NMDS, although the difference between them is slight (<0.07).

In terms of correlation testing, the weak- to intermediate weightings (R=16 to R=4) resulted in a higher Procrustes r-correlation between the ordinations than the raw data weightings, and in the case of the R=8 and R=4 weightings also higher than between raw NMDS and PCA. The R=16 and R=8 weightings had a higher Kendall’s τ -value for axis 1 than the raw data as well (see Table 3.7). Examining the diagrams visually also seems to confirm this: the shape of the “slanted” cloud in the DCA R=8 and R=4 diagrams is overall relatively similar to a rotated version of the point-clouds in the corresponding NMDS diagrams, indicating that a moderate weighting of the abundance scale produces a more similar pattern in the ordinations.

This fits with the conclusion of Son & Halvorsen (2014), that a lower emphasis on the quantitative properties of abundance data (i.e. weighting to a shorter abundance-range) might potentially help dampen the effect of method-specific outliers on ordinations, thus providing more robustly comparable diagrams. This seems to be most true for the NMDS ordinations, given the differences in RCL development. Additionally, the substantial shift in sample scores

for both ordinations – and especially DCA – between the low ($R = 2$) weighted and presence-absence data and subsequent loss of similarity between the ordinations in terms of r and τ -correlation, suggests that at least some measure of quantitative information about species' occurrences is necessary for robustly producing the structures seen in both the other weighted-data ordinations as well as the raw-data ordinations.

4.2.5.2 Species scores in the ordination diagrams

Similarly to the sample scores, the species optima in the DCA ordinations (Fig. 3.39) generally changed more, as well as more “erratically”, than the NMDS species optima (Fig. 3.40) – which to a larger extent followed more continuous “paths” mostly towards the center of the ordination diagram. This again somewhat seems to support the notion that the NMDS ordination is more “robust” in the face of less emphasis on quantitative aspect of the data. However, the radically different ways in which the species optima are calculated between the method is likely also a major reason for why the DCA scores are somewhat more “unstable” than NMDS (as they are calculated as part of the ordination algorithm rather than *a posteriori*).

The “optima-paths” in both ordinations nevertheless also have some important similarities. In both Figs 3-39 and 3-40, the morphotaxa with high abundances that were most consistently associated with the TOV-2 side of axis 1 (primarily the pentamerid brachiopods), gradually seem to migrate towards the center, and other morphotaxa with high abundances generally did not move very much. On the other hand, species with *low* abundances that were mostly associated with the center of the ULV-2 cluster, generally had larger and more erratic “jumps” between ordinations (especially in the DCA), in many cases ending up on the opposite side of axis 1 in the lower abundance-scale weightings. This supports the assertion that the low-abundance-occupancy taxa are not strongly associated with the structure of axis 1 in any way. A lower emphasis on the quantitative aspects of the data will also give these taxa more “weight” in the configuration of sample scores, and might thus conceivably lead them to become greater “confounding factors” on the ordinations. However, this seems mostly to be a problem with the presence-absence weightings. The fundamental differences in how species optima are calculated and emphasized between the two methods are also likely of equal or perhaps even greater importance in this respect.

4.2.5.3 Relationship between stratigraphy and ordination axis 1

In both the DCA and NMDS ordinations, the distinct “curve-shape” formed by the sample scores in the TOV-2 section remains more or less intact with all abundance-scale weightings except the presence-absence weighting – and in the case of NMDS also the $R=2$ weighting. Generally, the curve-shape seems to become less distinct quicker in the NMDS with intermediate weightings. In the intermediate weightings ($R=8$ and $R=4$), the points in both ordinations also cluster *more* densely along the curve shape, with fewer outliers than in the raw data ordinations. Additionally, the “rightward turn” in the top third of the section seems to become slightly greater, with the basal leftward turn becoming comparably less pronounced.

All in all, these results suggest that the stratigraphic changes in axis 1 from the Toverud section represent a robust pattern in the ordinations, although perhaps slightly more robust in the DCA ordination. In an extension of this, it also seems to imply that the shifting in magnitude between the left-ward shift in the lower half of the section is likely more connected to quantitative differences within and between the faunal groups than the topmost, rightward shift.

In terms of the Ulvøya stratigraphy, no equally clear trends were observed. Still, in the intermediate weightings, the ULV-2 point cloud appeared more similar and between the ordinations than with the raw data. It also seemed to slightly contain a more leftward shift in the upper sample scores, although still very dispersed and not nearly as clear as in the Toverud section.

4.2.6 Relationship to lithological and faunistic diversity variables

4.2.6.1 Between-sample correlations

The results of the correlation tests in Table 3.8 show a strong and significant positive correlation between the bioturbation fraction of the peels and the amount of mudstone in the samples. Conversely, there is a similarly strong negative correlation between bioturbation and packstone and less significantly wackestone, on the other. Species richness and H-diversity were also significantly positively correlated with packstone lithology – and to a lesser extent wackestone, and highly negatively correlated with mudstone and bioturbation. Interestingly, grainstone lithology was not significantly correlated with any environmental variable.

When interpreting these results however, it is important to keep in mind the prospect of several underlying correlations. In addition to the factors mentioned in Section 3.1.11, the inherent definitions of the lithology types – as containing more or less grains or fossil fragments – naturally makes especially the mudstone indicative of a very low concentration of fossils. The more fossil dense lithologies in particular might conversely be assumed to have less available substrate for bioturbation compared to a mudstone matrix. Additionally, as species richness is a component of Shannon's H diversity index, it is also not surprising that the two are correlated with the same lithologies. Still, the results of the correlations reveal that these two latter assumptions do *not* fit with the grainstone-influenced samples. Additionally, that the mudstone-dominated samples generally are correlated with a significant amount of bioturbation, is an important indication that the paleo-seafloor at the Ulvøya locality nevertheless was biologically active.

4.2.6.2 Fit with the ordinations

When correlated against both ordination axis 1 (τ) and the ordinations as a whole (R^2), the positive and negative correlations described in the previous section appear to be highly correlated with the TOV2-ULV2 gradient in axis 1 in both the raw-data and abundance-scale weighted ordinations. In all ordinations, there is a high positive correlation between wackestone, packstone, species richness, diversity and the TOV-2 side of axis 1, and a corresponding positive correlation with bioturbation fraction, mudstone dominance with the

ULV-2 side of axis 1. Species evenness was only slightly significantly correlated with the left side of axis 1 in around half of the ordinations, and grainstone lithology was not correlated with any ordinations. To a large degree, these results fit well with the results from the diversity metrics discussed in Section 4.2.2.3. Furthermore, it strongly implies that the disparity in species richness and diversity between Toverud and Ulvøya is largely due by prevalence of fossil-poor, mudstone-dominated samples in the latter locality.

Although the distribution of correlation significant was highly corresponding across ordinations, there were also some differences in the *strength* of these correlations. Among the raw-data ordinations (Table 3.10), species richness and diversity in particular were consistently more strongly associated the PCA and NMDS plot configuration than the CA and DCA. However, this changes in the intermediately (R=8) abundance-scale weighted DCA, which shows a much higher R² correlation between these metrics higher than the raw-data NMDS. Generally, both the intermediate abundance-weighted DCA and NMDS seem to be either similarly or more strongly correlated with the most significant environmental/faunistic variables from the raw-data ordinations, and with more similar correlation coefficients between across ordinations. This seems to suggest that a moderate de-emphasizing of the quantitative abundances not only confirms the robustness of the environmental variable correlations, but also to some extent converges on a more similarly structured configuration, which is also implied by the samples-score correlation in Section 4.2.5.

4.2.7 Ordination axis 1 as a complex ecological and preservational gradient

Based on the discussion in the previous sections, and Section 4.2.6 in particular, the most plausible interpretation of ordination axis 1 is, in my opinion, that it simultaneously represents a real coenocline of faunal change from a quieter shelf- or lagoonal environment to a more energetic and storm-influenced shell bank environment, as well as a gradient in the *preservation* of organisms as skeletal fragments in the samples, controlled by the depositional environment. More specifically, the preservation gradient is interpreted as a distortion and in some cases perhaps also damage of the structure of the underlying “real” coenocline, most clearly evident in the case of the Ulvøya samples and the disparities between the Toverud and Ulvøya localities.

The main argument for the interpretation of axis 1 as representing a “real” coenocline, is the fact that the axis 1 sample scores from the Toverud locality in all ordinations show a clear and consistent stratigraphic trend. This becomes especially apparent when fitting a smoothing function to the distribution of the points (as in Figure 4.1). When viewed against the distribution of morphotaxa optima along axis 1 (e.g. Figure 3.31), as well as the raw sample abundances plotted stratigraphically (Figure 4.2), this gradient relatively clearly seems to mirror an initial transition to an environment dominated by thin- and thick-shelled pentamerid brachiopods, represented by the most “leftward” sample scores – back to a less heavily brachiopod-dominated environment. As the samples throughout Toverud section are all generally fossil rich, mainly consisting of wacke-, pack- and grainstones, it is assumed that this trend is not significantly influenced by depositional bias, and therefore represents a “real” trend in the

organism diversity captured stratigraphically. The fact that grainstone content in the samples was not correlated with axis 1 in any systematic way, especially supports the interpretation that fossil density in and of itself is not indicative of any faunal gradient in the section. Other than the pentamerid brachiopods, the Toverud axis 1 sample scores do not seem to correspond strongly – either positively or negatively – with the abundances in any other taxa, with the possible exception of small-stick like bryozoans (see Fig. 4.2, also Fig. 3.22). This supports the interpretation that these groups are the ones primarily responsible for the strongest and most consistent coenocline at the Toverud section.

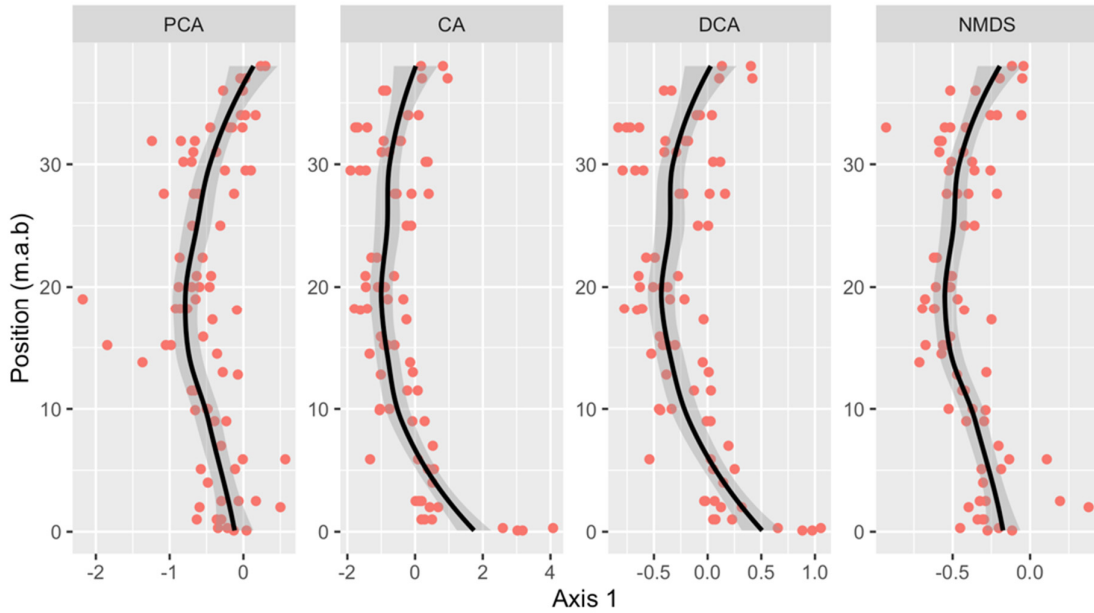


Figure 4.1. Ordination axis 1 sample scores from the TOV-2 section plotted against stratigraphic height (red points), with a smoothed curve (LOESS function, black line, uncertainty estimates indicated by shaded area).

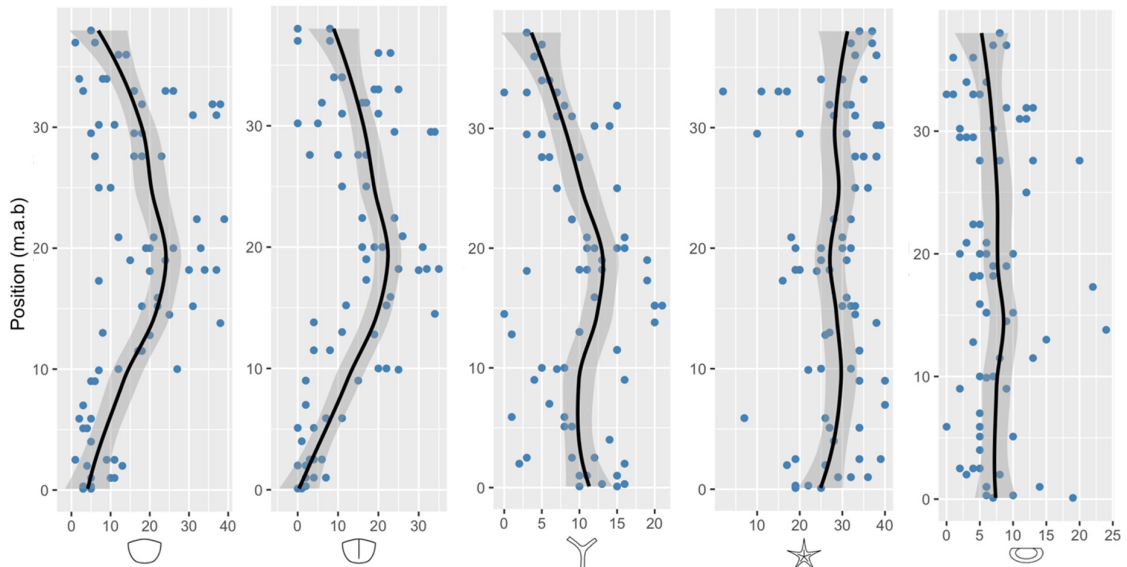


Figure 4.2. Subplot frequency abundances (x-axis) of the five morphotaxa with highest occupancy in the TOV-2 section, plotted stratigraphically (blue points) with a smoothing curve fitted (LOESS function, black line,

uncertainty estimates indicated by shaded area). From left to right: straight, thin-shelled brachiopods; straight, thick-shelled brachiopods; small, stick-like bryozoans; crinoids; ostracods.

The interpretation of this faunal gradient as relating to an environmental gradient of increasing and decreasing storm frequency, rests on three main observations. Firstly, pentamerid brachiopods in general – and the pentamerid faunas of the Oslo region in particular – have long been associated with periodically storm-dominated carbonate platforms (Baarli et al., 1999; Johnson, 1989; Mørk, 1981). Secondly, both the field observations of shell pavements (Section 4.1.1) and shell orientation modelling (Section 4.1.4) seem to support the notion that storm deposition of large number of densely packed brachiopod shells becomes more frequent with increasing stratigraphic position above the base in the lower half of the section (as proposed by Johnson, 1989). Thirdly, the “shifting back” of the faunal gradient to an ostensibly more quiet-water configuration with fewer pentamerid brachiopods in the top 8-10 meters of the section, also coincides with – and is likely partially caused by – an appearance of grainstones dominated by fecal peloids in the acetate peels – especially in the topmost 2-3 meters (e.g. PMO ???). Fecal peloids are generally thought to be deposited in energetically quiet, warm-water environments (Flügel, 2004), thus supporting the interpretation that their appearance is a sign of reduced storm frequency. This last interpretation therefore conflicts somewhat with Johnson’s interpretation of the Toverud Rytteråker Formation section as representing a continuous shallowing-up, increasingly storm-influenced environment up to the grainstone layer at 38 m.

The question of whether the “back and forth” gradient in storm frequency proposed here corresponds to an equivalent shallowing-deepening of the depositional environment, is however not as straightforward to answer. In an idealized, open shelf-shore environment, the frequency of storm events stirring the seafloor would be directly correlated with decreasing depth relative to the shoreline. However, if the Rytteråker Formation – as Möller (1989) suggests – represents a complex underwater topography with a more “sheltered” lagoonal basin to the east, this need not be the case. Especially the purest carbonate grainstones in the topmost part of the formation might very well have been deposited in protected, relatively shallow waters, as they bear at least a superficial resemblance to what has been interpreted as shallow hardgrounds from contemporaneous Silurian strata from Gotland (Alvaro et al., 2007).

One possible further confounding factor on the relationship between the life depth of organisms and storm-frequency of the environment, is the prospect of downslope transport before burial, as an increase in storm burial might conceivably lead to a greater degree of transport. However, Johnson (1989) estimated the effect of storm-induced transport to be low to moderate throughout the section at Toverud. Möller (1989) also concludes that the only (possible) signs of long-distance transport by turbidity currents significant enough to obscure the general ecological signal in the Rytteråker Formation, are found in the Skien district.

Other environmental factors than depth and storm frequency might also have influenced the faunal distribution of the sequence. Notably, Jin (2008) proposed sea-water *temperature* as the most credible explanation for the distributions of different brachiopod faunas in the Rytteråker-contemporaneous biota of Anticosti Island, Canada. Specifically, a predominantly pentamerid-

dominated fauna was interpreted as being associated with warmer water conditions, while stricklandiid brachiopods – which are abundant in the formations underlying the Rytteråker Formation (Baarli, 1981; Baarli et al., 1999; Baarli & Johnson, 1988) – were connected to cooler waters. This interpretation is also interesting to consider, given that the deposition of the Rytteråker Formation appears to broadly coincide with an oceanic $\delta^{18}\text{O}$ -excursion in Baltica (see Figure 1.7) indicative of warming. The possible connection between the increased carbonate production and a “Secundo” oceanic state as discussed in Section 4.1.2, would also fit with a warming interval, according to the ocean-state hypothesis (Aldridge et al., 1993). The fact that non-pentamerid brachiopods are more or less only present in the basal 10-15 meters of the Toverud section (and not in the top section), could therefore conceivably both be explained by them being adapted to a more siliciclastic and/or a cooler environment, than is common in the rest of the section.

However, as the basal trend in non-pentamerids is not distinct from the topmost trend in the primary gradient in the ordinations, storm frequency – possibly in connection to depositional depth – still seems to be the most plausible environmental explanation for this trend. Although one should be careful when making the comparison, this interpretation also does not seem to be unrealistic given our understanding of present-day benthic ecosystems. In the present day outer Oslo Fjord for instance, periodic physical forcing (i.e. storm frequency) was recognized through ordination as the environmental variable most strongly associated with the primary benthic coenoclines observed by van Son et al. (2014).

The main argument for the existence of a significant *preservational* bias affecting the structure of axis 1, is the large disparity in morphotaxa diversity, richness and abundance between the Toverud and Ulvøya localities, which especially in the PCA and NMDS ordinations leads to distortion of the sample scores in ordination axis 1 (see Section 4.2.4.1-3). Based on the generally significant prevalence of bioturbation in the fossil-poor, mudstone-dominated samples from the Ulvøya section, it also seems unlikely that the scattered, low abundances from this locality accurately reflect a corresponding lack of biological activity in the original paleoenvironment. Rather, it seems better explained by the Ulvøya locality representing a much more energetically quiet and possibly deeper depositional environment, where a substantially lower degree of storm-deposition has resulted in fewer easily identifiable, fragmented fossil remains. This interpretation seems to be supported by both the macrofossil field observations and the MS readings discussed in previous sections, which seem to imply a productive carbonate environment with several large coral and stromatoporoid fossils.

A more energetically quiet environment might possibly also have meant that organismal remains persisted on the seafloor for a longer time before burial and were more frequently bioeroded, reworked or otherwise dissolved or destroyed before their final burial than at Toverud. This inference is also tentatively supported by the prevalence of bioerosion in nearly all the Ulvøya samples.

The cause of this preservational bias and thus the overall separation between the Toverud and Ulvøya clusters along axis 1, seems nevertheless likely to be structured by the *same*

environmental gradient in storm frequency, or at least more generally rapid, energetic deposition of the organisms – as structures the main coenocline within the Toverud section. However, the much more “noisy” and unstructured stratigraphic signal *within* both Ulvøya sections, especially at ULV-2, suggests that the acetate-peel sampling design is incapable to capture any meaningful coenoclines here due to the lack of appropriate deposition, even as e.g. the macrofossil observations and MS readings would suggest a changing environment. While fossiliferous peels containing abundant crinoids and ostracods *are* produced from Ulvøya, they are found much more infrequently than at Toverud, resulting in the large back-and forth fluctuations seen in the stratigraphic plots. The very rare non-crinoid or ostracod fossils observed in the Ulvøya samples often also appear more complete than at Toverud – again implying that a random sampling of 30x20 mm slab sections from the outcrop might be much less efficient in capturing the “ambient” abundances of different organism groups in the environment here, than at Toverud. The fact that stratigraphic sampling was conducted somewhat more randomly at Ulvøya than Toverud (see Section 2.1), probably also did not help in this regard, and is a source of error to keep in mind, that could have additionally inflated the disparity in preservation between Toverud and Ulvøya localities apparent in the peels.

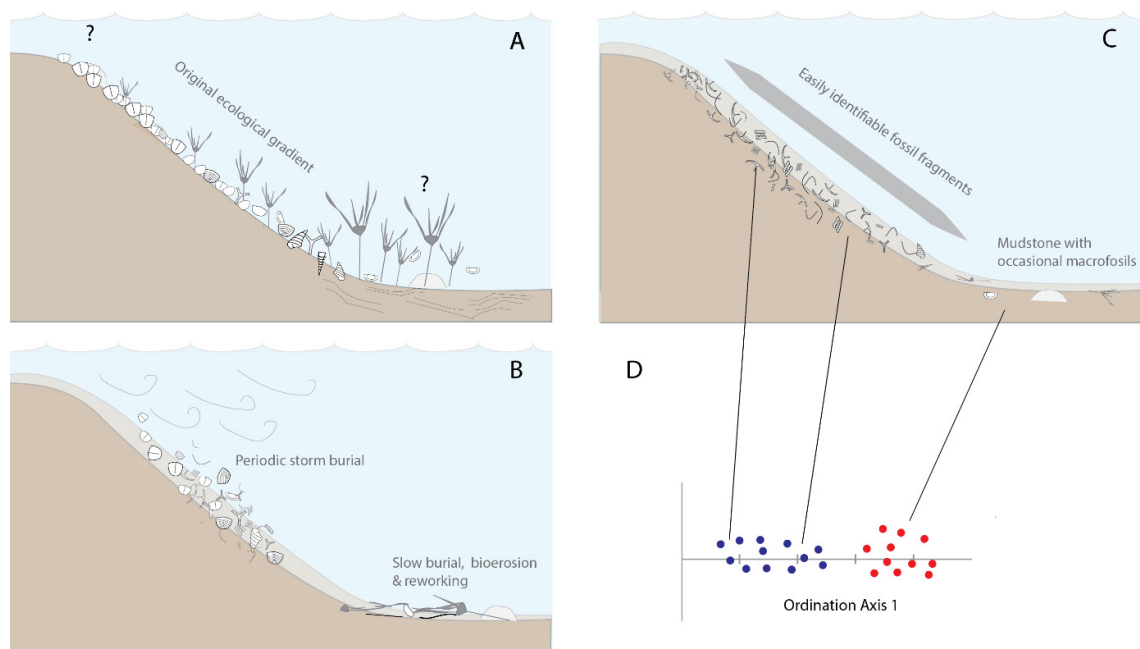


Figure 4.3. Conceptual model of potential preservational bias leading to “distortion” of the ecological gradient observed in the ordinations. A: original paleoenvironment with a depth and/or wave-energy related faunal gradient. B: Burial of organisms through storm / wave action in the upper part of the section (roughly corresponding to the Toverud section), and slower burial further down (roughly corresponding to the Ulvøya section). C: Skeletal debris is more dispersed in the lithological matrix in the upper part of the section than in the lower, leading to D: a stronger faunal gradient signal from random acetate peel samples in the upper part of the section (blue points) than at the bottom).

This notion of a greater “information loss” in the Ulvøya acetate peels could potentially also be explained partially by the fact that stylolithization, pressure dissolution seams and sparite microfractures also seems to be more common there, although they also occur at Toverud. These structures might indicate a higher degree of diagenetic alteration and pressure dissolution

of the sediment at Ulvøya post-deposition (Flügel, 2004). If they do, they might potentially also partially explain some of the patterns of abundances observed in the ULV-2 peels. Namely, Flügel (2004) suggests that *crinoid* fragments, in particular, might be more resistant to pressure dissolution than fragments of other organisms. Still, the comparative dominance of crinoids in the Ulvøya section could potentially also be a sign of a real coenocline, as high crinoid abundances have generally also been associated with quieter, deeper soft-substrate conditions, e.g. in the Vik Formation overlaying the Rytteråker Formation (Baarli, 1990). Some representative examples of the differences in preservation between the Ulvøya and Toverud section are shown in Fig. 4.3. Furthermore, a conceptual model of how this partially conflicting preservation-ecological gradient might arise in the data is attempted shown in Figure 4.4.

A moderate de-emphasizing of the quantitative abundance of taxa seems to help in some degree to ameliorate the effects of this preservational disparity in the ordinations, especially in the case of NMDS. However, it also come with its share of trade-offs, as discussed in Section 4.2.5, and does not result in a significantly clearer stratigraphic trend within the Ulvøya section. On the other hand, I will argue that this discussion clearly shows the utility of applying multiple parallel ordinations when the data are skewed and “noisy” – as they are this case. The fact that the Ulvøya section (especially ULV-2) produced far less consistent stratigraphic axis 1 scores among the ordinations than the Toverud section, is for instance an argument for these results being less robust and more contingent on the ordination method than at the latter locality.

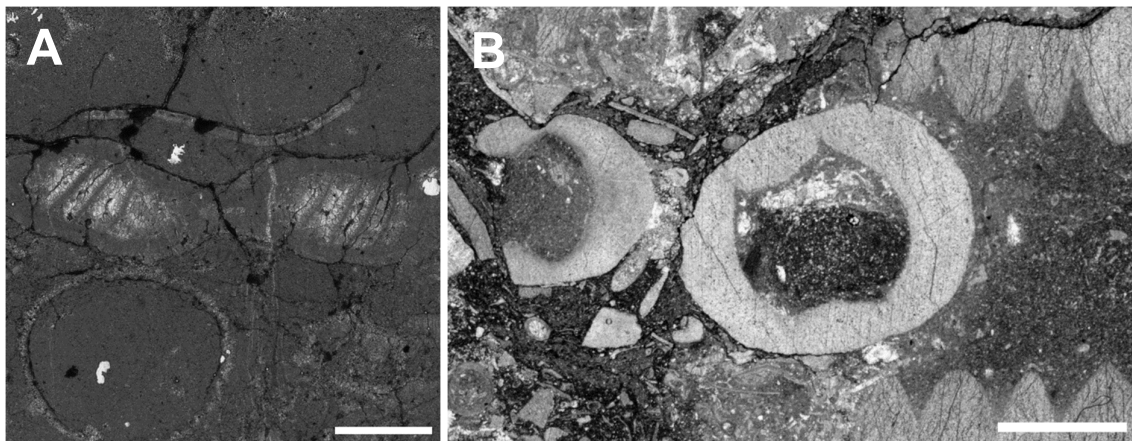


Figure 4.4. Examples of the difference in the preservation of a halysitid tabulate coral and (possible) calcareous tube near the middle of the Ulvøya section (A, PMO 236.533a), and preservation of crinoids in the middle of the Toverud section (B, PMO 236.473a). Scalebars = 2 mm.

4.3 Malmøykalven and Jong macrofossils

4.3.1 Stratigraphic abundances and proportions

As shown in figures 3.44-45, the raw and proportional abundances of the different coral/stromatoporoid groups vary significantly both stratigraphically and between the localities. Overall, the Malmøykalven locality seems to be more fossil rich than the Jong locality, especially with regards to halysitids, heliolithids and syringoporids – and favositids in the topmost stratigraphic plots. The stratigraphic trend in the Malmøykalven sections seems to

broadly tend towards greater diversity with stratigraphic height, but this trend is far from clear, and seems to be subject to significant variation between the plots.

The Jong locality on the other hand seems to be dominated mostly by stromatoporoids and favositids in low- to moderate abundances compared to Malmøykalven – with the stratigraphically lowest and highest Jong plots containing only 2-3 favositids, and no other fossil groups.

4.3.2 PCA and NMDS gradients

In both ordination diagrams, a packe-wacke-stone lithology, fragmentation and laminar growth form of the corals were all strongly associated with one end of axis 1 (the left in the diagrams), and a dome-shaped or irregular growth form, along with marl or mudstone surrounding lithology on a base of grainstone, with the other (right). Both the overall Procrustes correlation and the Kendall's τ for axis 1 support the interpretation that this gradient is robust across the two ordinations. The environmental variable loadings in axis 2 seem on the other hand to be more inconsistent among the ordinations, suggesting no robust pattern there. The significant disparity between the amount of variation explained by axis 1 and 2 in the PCA ordination also seems to support this interpretation.

Laminar growth forms among Paleozoic tabulate corals are typically interpreted as an eco-morphological response to higher-energy, more wave-intense conditions, and more dome-shaped forms as a response to quieter water (Scrutton, 1998). Both a higher probability of fragmentation and – as previously discussed – packe-/wackstone lithology, are generally associated with high-energy deposition and storm events, as discussed in the original study (Keilen, 1985). These results therefore seem to suggest that ordination axis 1 in both ordinations relatively unambiguously represents a gradient from low energy (left-hand side) to higher energy / more storm-exposed conditions (right hand side) in the plots sampled.

Stratigraphically (Figure 3.48), the axis 1 ordination scores seem to separate more clearly between localities than sample levels, with the majority of the Malmøykalven plots grouping to the right (i.e. less energetic) side of the Jong plots. Still, the stratigraphic development in the samples from the Malmøykalven section also seems to indicate a slight leftward shift in the middle of the section, towards more fragmented, laminar growth forms (i.e. higher energy conditions), and a shift back towards the right-hand side near the top of the sampled section – perhaps most clearly in the NMDS than the PCA. In the case of the Jong section however, the trend is more chaotic and much less clear. The top and bottom plots appear as significant leftward outliers on ordination axis 1, while the rest of the plots seem to suggest a more unstructured fluctuation around the middle of axis 1. As the total number of specimens in the top- and bottom plots are very low (between 1-3), their plot positions should be interpreted with a great deal of caution, as it could have been more susceptible to random chance than the others.

When looking at the raw and proportional organism abundances fitted to the ordinations, some trends were also consistent across the methods. In the case of the raw abundances, all fitted optima were associated with the right hand-side of axis 1, somewhat more strongly in the PCA than in the NMDS. Although this trend was not very statistically significant, it is highly interesting, as it implies that the side of axis 1 associated with quieter, lower-energy environments is actually skewed towards a *higher* abundance of all coral and stromatoporoid morphotaxa. This appears to be the reverse of the trend in diversity observed and interpreted from the acetate peel ordinations. It also more generally implies that the ordinations might have suffered from some of the same abundance-skewnesses as the acetate peel ordinations, had the organism plot data been used as the bases for the ordinations.

The fact that the proportional abundances of favositids and stromatoporoids were highly significantly associated with the left and right side of axis 1 respectively, is also noteworthy, although it should probably be interpreted more carefully. Even though the two points furthest to the left (the top and bottom samples from Jong) have a 100% favositid percentage, they have – as mentioned – also very small sample sizes, meaning this could again just as easily be due to chance than any other factor (and note that the favositid species optimum is on the right hand side in Figs. 3.49A & B). Still, it provides some tentative indications that favositid corals could perhaps have been more tolerant to – or at least are more easily identifiable in – high-energetic environments in the Rytteråker Formation, especially when compared to stromatoporoids.

4.4 Holmestrand bedding plane study

In all the ordinations, plots from the four bedding planes separated into three more or less distinct clusters in a similar pattern along ordination axis 1 (Fig. 3.50). The 0.05 m bedding plane clustering in the right-hand side, the 0.4 m plane in the middle section, and the 0.1 m and 0.2 m planes together on the left-hand side. This separation of the bedding planes seems to be somewhat more distinct in the two outlier-inclusive ordinations, than the outlier-exclusive. Furthermore, a slight arch effect also seems to be present in axis 2 of both NMDS diagrams, perhaps slightly more pronounced in the outlier-exclusive ordination. Axis 2 is also far less similar between all the ordinations, only significantly similar between the two NMDS variants (Table 3.13), further implying that it does not represent a robust gradient in this axis. The correlation testing further revealed that while the two DCA and NMDS variants (outlier exclusive and outlier-inclusive) were most similar to each other overall (as measured by *envfit* similarity), the two outlier-inclusive ordinations were the strongest correlated with each other in terms of axis 1 plot scores, implying that this dataset decision was more important than ordination method for robustly recovering the primary gradient in the data.

That the relative stratigraphic positions of the bedding planes do not structure their position along ordination axis 1 is perhaps not that surprising, since they are stratigraphically adjacent. This however makes it all the more interesting that plots from the same bedding planes mostly *do* cluster together along axis 1. Presuming that axis 1 represent a “true” coenocline in the data, this implies that there nevertheless is some underlying environmental/faunal gradient that varies between the bedding planes, primarily more so than between the plots overall.

When looking at the morphotaxa optima (Figure 3.51), this axis 1 gradient appears to be characterized by the span from a stromatoporoid and trilobite-characterized assemblage to an environment characterized by brachiopods (primarily pentamerid) and heliolitid tabulate corals. Interestingly, development seems to partially mirror the distribution of species optima seen in axis 1 of the acetate peel ordination – especially when considering the trend in pentamerids. This trend however seems to be most clear in the outlier-inclusive ordinations, where the morphotaxa optima are also generally more dispersed along axis 1, and less clear in the outlier-exclusive ordinations

The fact that none of the trace fossil or lithological matrix variables were consistently, significantly correlated with any of the ordinations, suggest that they are also not associated with this gradient. In this regard it is important to keep in mind that the lithological matrix values were also counted alongside the morphotaxa in the point-intersection grid (as points where no fossils were present) in the original study. Therefore, the separation of the two into one species and one environmental dataset will entail some inherent correlation. The fact that the lithological variables nevertheless were not associated with the faunal gradient, seems to suggest that the prevalence of lithological matrix over fossil fragments was less important for the distribution of the species in this case, as in the acetate peel study.

When it comes to potential environmental variables underlying the gradient between the bedding planes, there are few concrete proxies to interpret from these data alone. However, the presence of a relatively strong coenocline with an optimum of pentamerid brachiopods in one end, that seems to in some ways resemble the gradient in the TOV-2 section, *is* tempting to interpret as a sign that the same environmental factors – namely storm- or high energy deposition – also were important for structuring this environment. This interpretation would also be a credible explanation for why temporally and spatially adjacent bedding-planes cluster distinctly different from each other. As storm-deposition occurs only episodic and irregularly and in itself also has a large influence on the burial and bedding, it is natural that it also varies significantly from bedding plane to bedding plane. This also fits with Mørk (1978)'s interpretation of the data: that increasing storm-frequency underpins the transition to a more fossil-rich, pentamerid environment from the underlying sections.

All in all, the results from the Holmestrand re-analysis indicate that both the DCA and NMDS ordination methods are successful in discerning a faunal gradient in axis 1 between adjacent bedding-planes in the middle Rytteråker Formation in data not originally intended for gradient analysis. The results also suggest that the inclusion of point-count “outliers” (i.e. species that are present in the plots but not counted in a point-intersection), generally seems to result in a stronger and more interpretable coenocline than only counting point-intersections. Thus, this dataset decision seems to be at least as important to the results as the choice of ordination method, perhaps even more so, and should probably be accounted for alongside choice of ordination method in future corresponding point-count studies.

4.5 Comparison between studies

4.5.1 Methodological results

In all three case studies discussed here, the use of comparative, multiple parallel ordinations on the data sets resulted in the identification of primary, more or less robust coenoclines in axis 1, through both visual and statistical correlations of the diagrams. The lack of real gradients in the higher axes – i.e. axis 2 – was subsequently also confirmed through low correlation between the different methods, and in some cases also by the presence of polynomial distortion artefacts. Even though the two literature reanalyses were far more limited than the novel study, the comparative ordination was therefore nevertheless highly valuable in all cases.

Disparities between samples with regards to overall fossil abundances and taxon richness also presented some similar challenges to interpreting the ordination-based gradient analysis in both the acetate peel and coral macrofossil study (albeit with different environmental interpretations). In both cases, using multiple different ordination methods in parallel and assessing the results in light of the underlying properties of the methods made it easier to identify and understand these disparities and their inherent properties. Even though the difference in how disparities manifested in the methods seem to be somewhat more pronounced in the Toverud/Ulvøya study than in the re-analysis.

The question of *which* ordination method performed “best” overall in terms of capturing “un-skewed” and ecologically interpretable gradients from the datasets, seems however to be very difficult to answer. Both because the context of the studies and properties of the data are so varied, and because the two literature re-analyses only employed two ordination methods each, and different combinations each time. The only ordination method applied in all studies was NMDS, which performed moderately well in all cases. This could in and of itself be taken as an argument for its versatility in many different settings. However, distortions due to sample size and -richness disparities observed in the NMDS ordinations also suggest careful interpretation and comparison to other methods. DCA also performed well in both cases where species-abundance-like data was supplied (Toverud/Ulvøya and Holmestrand study), although the method in both cases seemed to be susceptible to changes in quantitative abundance-weighting and inclusion of point outliers – slightly more so than NMDS.

Overall, it would seem that which ordination methods are “right” is dependent on the properties of the data and what one wants to do with them. And in this case of the two re-analyses, the ordination methods chosen generally seem to have been appropriate. That is: DCA and NMDS in parallel when dealing with species-abundance-like data, and PCA and NMDS in tandem when ordinating environmental sample data.

In summary, these results all highlight the need for ordination results to be interpreted both in the light of the inherent strengths and weaknesses of the methods used. Additionally, both in-sample environmental variables and supplementary proxy information about the paleoenvironment and/or the taxa sampled are also needed in order to assess whether the gradients observed are ecologically interpretable.

4.5.2 Paleocological results

In this respect, the primary, faunal/environments gradients recovered in ordination axis 1 in the three studies provide both some common and some contrasting implications about the paleoenvironment of the Rytteråker Formation. Crucially, they *all* seem to indicate high-energy deposition – perhaps primarily through storm events – as the primary environmental factor structuring the coenoclines observed in the data.

The coenoclines observed in the Toverud/Ulvøya and Holmestrand ordinations (at least with the outlier-inclusive data), seem to indicate a similar coenocline structured largely by pentamerid brachiopods in one end and stromatoporoids in the other, despite the significant difference in study design and sampling area. As mentioned this coenocline seems – at least based on the supplementary environmental data from the Toverud/Ulvøya localities – best explained by a gradient in high energy deposition and storm frequency. In the Toverud/Ulvøya study, this gradient however also seems to have resulted in a significant preservation skewness and distorted in terms of overall richness and fossil content between the two localities sampled, with bioturbation and mudstone content being indicative of the more fossil poor ULV-2 locality. However, in the Holmestrand study, such a distortion seems not to be clearly present, as neither of the ordination axes were significantly correlated either with the abundances of any of the sedimentary matrix categories, nor the trace fossils.

In the Malmøykalven/Jong reanalysis, being primarily based on environmentally interpretable properties of the corals, the gradient related to depositional energy is even more easily interpretable in the first axis of the ordination. However, as the fitted optima of all coral and macrofossil taxa are mostly associated with the side of axis 1 quiet-energy conditions, the data appear to be skewed in the opposite way to the Toverud/Ulvøya study, meaning that quieter-water conditions are indicative of an overall increase in the preservation and/or proliferation of all organism groups. This again seems to partially support the interpretation from the Ulvøya data that quiet water conditions allow more complete macrofossils to be preserved at a larger, more dispersed spatial scale, at the expense of the fauna of the paleoenvironment being well represented “ambiently” in the lithological matrix.

Still, the very large number of coral and stromatoporoid macrofossils recorded throughout the Malmøykalven section by Keilen (1985) when compared to the – admittedly highly sporadic and non-comprehensive – macrofossil survey at the Ulvøya locality, is also striking. While it could partially be due to human error and the, again, completely sporadic approach to macrofossil observation at Ulvøya, it still seems that the Malmøykalven locality was overall substantially richer in coral and stromatoporoid macrofossils than the very close-lying Ulvøya section. This indicates that a small-scale spatial variation in the sampling area in this locality could potentially have a large impact on the interpretation of the paleoenvironment drawn.

Collectively, I will argue that the results of these three studies paint a picture of a complex, regionally varied and dynamic marine ecosystem around the Aeronian-Telychian boundary in the Oslo Region, where storm frequency – likely at least to some degree directly related to

depositional depth – was the primary controlling factor both of the benthic ecosystem and its taphonomic preservation. In isolation, three studies can be seen to indicate a roughly east-west gradient in increasing storm frequency in the central Oslo region – ranging from crinoid-ostracod and coral/stromatoporoid characterized quiet water ecosystems in the Oslo area, to more pentamerid-dominated shell bank environments at Sylling, Holmestrand and Asker. Ordination scores from both the Toverud section and to a lesser extent Malmøykalven, also appear to show a gradual increase in storm-frequency/high energy up to the middle of the formation, and a gradual return to quieter conditions in the top. A trend which could potentially be seen as indicative of a regional change in sea-level, although the trend is not consistent in all the ordinations.

4.6 Summary and conclusion

To summarize the most important results of the discussion, I will here return to the introductory research hypotheses outlined in Section 1.2.3, and attempt to give a brief summary of their most central points, as well as the most important sources of error and bias in the study. Finally, I will end with some perspectives on future research.

4.6.1 Viability of novel sampling strategy and study design

Both the choice of using acetate peels as a sampling substrate as opposed to thin sections, and the choice of the subplot frequency counting (SF) method, seem to have been successful given the framework of this study. Apart from the filamentous algae, skeletal fragments were overall equally – and in some cases even slightly more – distinguishable from each other in the acetate peels than in the thin sections. The only difference being that some more post-processing of images was required for the acetate peels. At least for the purposes of delineating the generalized morphotaxa categories applied here, the method seems to be a more efficient way to capture minor biofacies variations in “pure” limestone lithologies with a larger number of samples at lower cost, than thin sections.

With many rare taxa in the peels and large size differences between them, it also seems reasonable to assume that the SF method captured more faunal variation in the acetate peels, at a lower time-cost, than e.g. point counting would have done. The abundance-occupancy relationships produced were also fairly comparable to those produced by recent ecological surveys with higher taxonomic resolution and more detailed sampling, suggesting that they are generally interpretable as ecologically meaningful (see Section 4.2.2.1). Even though an outlier-inclusive point-count (as in the Holmestrand bedding plane data) would have resulted in the same qualitative representation of taxa, it would likely have emphasized the abundances of large, common taxa like crinoids more significantly, and missed smaller individuals. To see a future study comparing the results of these two counting methods on a dataset similar to the acetate peel data used here, would however be very interesting.

As evidenced by the differing results from the two study localities, the acetate peel-SF-study design *does* however seem to require a certain density of evenly dispersed, disarticulated fossil

material in the rocks sampled in order to produce easily interpretable coenoclines. It seems in this context therefore relatively well suited for capturing gradients in a (presumably) higher-energy / more storm-frequented carbonate stratigraphy like the Toverud section, while less suited for a more energetically quiet, mudstone-dominated locality characterized by dispersed and less disarticulated macrofossils, like the Ulvøya section. In the latter case, larger-scale macrofossil sampling in the field – as evidenced by the coral/stromatoporoid study from the Malmøykalven locality – might yield a larger and more meaningful data basis.

When it comes to the use of high-level morphotaxa groups, the most “species-like” (i.e. the pentamerid brachiopods) were the ones most clearly supporting a coenocline in the data, lending support to the argument that higher taxonomic resolutions are generally preferable to lower taxonomic resolutions (Forcino, Stafford, et al., 2012). Still, researchers have argued that the most important factor for determining whether higher taxa are useful as surrogates for genera or species is 1) to what degree ecological niches are conserved within the higher taxon, and 2) the number of species represented by each higher taxon in the study (Rosser, 2017). Therefore, in the scope of the very broad-stroke ecological trends examined in this study, too detailed a taxonomic resolution might also not be too meaningful either. This could be seen as indicated by the fact that the subdivision of (ostensibly) pentamerid brachiopods into thin- and thick shelled variants had no impact on the ecological signal of the groups. The trade-off between ecological differentiation of species, the ecological scope and goals of the study, as well as to what level it is practically feasible to identify organisms within a given study design, is complex and context-dependent, and could probably be considered in even more detail when designing a future study.

4.6.2 Utility of multiple parallel ordination approach

All in all, the Multiple Parallel Ordinations (MPO) approach seems to have been a highly useful tool for discerning and confirming a primary, relatively robust faunal gradient from both the newly sampled Toverud/Ulvøya dataset, as well as the two reanalyses. In the Toverud/Ulvøya ordinations, this gradient was most prevalent in the stratigraphic development of the Toverud section, where it was primarily characterized by a transition from a more mixed and partially more fossil-poor fauna characterized by an abundance of erect suspension-feeders and semi-infaunal and epifaunal deposit feeders, to shell-bank fauna characterized by epifaunal filter feeders, mainly in the form of pentamerid brachiopods. The gradient was consistent both across ordination methods and abundance-weighting regimes, and the DCA and NMDS methods appear to have been marginally better at capturing it in a meaningful and ecologically interpretable way. However, distortions due to sample-size disparities and faunal abundance outliers impacted all ordination methods, albeit in different ways – again supporting the argument that multiple parallel ordinations are necessary for properly understanding and describing the gradients observed. A moderate de-emphasizing of quantitative abundances also seemed to ameliorate some of the distortions – especially in the case of NMDS – and make the different ordination methods converge more similar configurations. It should therefore also be considered for future studies.

More or less the same gradient also seems to be captured and confirmed through parallel ordination-reanalysis of the Holmestrand data, although the ecospace-occupation of the different morphotaxa was not considered in detail there. In the Malmøykalven/Jong macrofossil reanalysis, a primary environmental gradient in the preservation and growth forms of tabulate corals was similarly also identified through parallel ordination. As such, both of these examples provide in my opinion strong arguments for the utility of comparative multivariate gradient analysis as a useful tool for extracting potentially new information from historical datasets not originally intended for gradient analysis.

4.6.3 Ordination-based evidence for a depth-controlled ecocline in the Rytteråker Formation

However, as evidenced in particular from the Toverud/Ulvøya and Malmøykalven/Jong studies, the results of this study seem more to suggest *high-energy deposition and storm frequency* as the primary environmental factors underlying the morphotaxa turnover of the gradient, rather than depositional depth directly, as originally hypothesized. Frequency of storm-associated layers would probably at least in some cases also be applicable as a proxy for depositional depth, but not necessarily, as the proposed complex shelf-lagoonal topography of the Aeronian-Telychian Oslo Region could also have allowed for shallower, storm-protected environments. This seems for instance to be a possibility near the top of the Toverud section. Storm deposition being a discontinuous environmental variable with high, short-scale high temporal variability, also fits well with the Holmestrand bedding plane reanalysis, as well as the significant fluctuations along the primary gradient between adjacent stratigraphic levels at Toverud and Ulvøya. Any long-term gradual change in sea-level associated with a higher *frequency* of storm layers (Baarli, 1988; Johnson, 1989), would in any case be a more abstracted, removed interpretation of the gradient actually captured in this study, rather than a direct interpretation of the gradient itself.

It also does not seem unlikely that other environmental factors such as siliciclastic input, seawater temperature and a change in ocean-circulation states also influenced the ecological gradients in the epicontinental seaway where the Rytteråker Formation was deposited – even though these were not as clearly captured in the ordination gradients. In any case, using, say, ordination axis 1 as a direct proxy for depositional depth, as Miller et al. (2001) and to a lesser extent Hennebert and Lees (1991) do, seems to be highly uncertain and inappropriate in the cases examined here. If anything, the results in this thesis provide an indication of how the nature of spatiotemporal faunal gradients observed in the fossil record – even when they are structured by comparable environmental factors – may be highly sensitive both in terms of locality, short-scale temporal variations and sampling design. A challenge that has also been addressed in previous studies (Holland, 2005). Nevertheless, comparative gradient analyses by way of multiple ordinations seems at least in this case to indicate one common environmental factor responsible for a primary gradient of faunal change. Even though the faunal responses to the gradient themselves – as evidenced from the differing results from the bedding plan/acetate peel and the coral macrofossil study – seems to be highly dependent on both the study design, which organism groups are looked at, smaller-scale fluctuation and likely also

the local “baseline” conditions of the paleoenvironment. This interpretation does not come across as all that unreasonable either, in my opinion. After all, we have no real reason to believe that the benthic ecosystems of the Silurian – although significantly taxonomic and ecologically different from today – would necessarily have less of a multi-layered, locally determined, and complex response to a changing climate and sea level, than any modern marine ecosystem.

4.6.4 Sources of error and bias

Numerous potential sources of error, bias and uncertainty permeate both the sampling, data analysis and statistics in this study, some of which have already been touched upon. In the case of the Toverud and Ulvøya acetate peel dataset, the process of identifying the different morphotaxa from fragmented and disarticulated fossil debris is perhaps the most significant human source of error, as the process includes a very substantial degree of subjectivity, uncertainty and opportunity for misidentification. In a substantial number of cases, fossil fragments were not assignable to any morphotaxa category, either due to disarticulation or dissolution, or that they had an unknown affiliation (and were too rare to include as their own category), meaning they were not represented in the dataset. The same goes for the identification of bioturbation and designation to lithological (Dunham) categories, which was often times difficult, and always included a large subjective component as well.

As previously mentioned, the minor, but not insignificant differences in the semi-randomness of the stratigraphic sampling between the Toverud and Ulvøya localities could potentially also be a source of bias in the dataset. The Toverud sampling was done prior to the final working out of the study design of this thesis, and fossil-rich layers were likely sampled somewhat more often here out of “interest” than at Ulvøya, where the “random” 1 m interval was adhered to more strictly. Unfortunately no explicit logs of the Toverud sampling strategy were kept either. Concerns like these should probably be considered more thoroughly beforehand in a future study.

4.7 Future perspectives

To further our understanding of the marine ecosystems of the Early Silurian generally, and the paleoecology of the Rytteråker Formation in particular, a number of approaches to future studies could prove fruitful. In my opinion, an especially intriguing and potentially highly relevant avenue to further explore through multivariate gradient analysis, would be the prospective similarities between the underlying mechanistic factors structuring ecological gradients in Rytteråker Formation (or other Silurian formations) and modern-day benthic ecoclines. The fact that the environmental factor of “storm frequency/high-energy deposition” implicated in this study superficially seems to be very similar to the “periodic physical forcing” factor identified by van Son et al (2014) as important for present-day soft substrate ecosystems in the Oslo Fjord, is highly intriguing. The question of to what degree this and other environmental drivers are *really* comparable through time, could therefore be pertinent to explore. A good place to start for a future study could for instance be with Van Son et al (2014)’s hypothesis of periodic *hypoxia* as the compound environmental factor most associated with the *opposite* end of the primary coenocline to physical forcing (and in their interpretation

primarily deeper water). Examining the impact of fine-scale changes in bottom oxygenation conditions and possibly also paleotemperature proxies on faunal gradients through comparative gradient analyses in Paleozoic of the Oslo Region (or comparable localities), would potentially make us able to place these past ecosystems more meaningfully in a comparative framework with present ecosystems and their changing environments. Not only that: looking specifically at environmental factors like oxygenation and paleotemperature could also be highly valuable for understanding and connecting the regional fauna of the Oslo region to larger-scale trends in biogeochemistry, climate change and ocean chemistry in the early Silurian, thereby enhancing our knowledge of the ecological dynamics of the period in its own right.

In order to properly investigate these or related dynamics in the Paleozoic ecosystems of the Oslo region however, a larger scale study where more care is taken to integrate fossil data from both field and lab studies at different scales qualitatively and quantitatively, and with more information of the sedimentary contexts and scales of the sampling, would be necessary. Crucially, more – and more precise – paleoenvironmental proxies such as $\delta^{13}\text{C}$ and $\delta^{18}\text{O}$ isotopes (if the sediment is not too metamorphized) and a more comprehensive description of bioturbation fabrics both in the micro- and macroscale, would be vital in order to more accurately interpret the prospective relationships between fauna and environment. Integrating some of the tools and approaches from the relatively novel field of paleoecological niche modelling (paleoENM), such as its framework for creating environmental proxy variables from stratigraphic logs (Myers et al., 2015), could potentially be very useful in this regard. Not to mention that a paleoENM study, i.e. of some potentially ecologically important brachiopod species in the Oslo region, could be highly interesting in its own right.

In the case of the Rytteråker Formation specifically, I think it could be very interesting to conduct a more comprehensive gradient analysis study particularly on the sections in the Asker and Bærum district – which was originally also planned for this study but cut due to time constraints. The stratigraphic development of the Rytteråker Formation in this district seems to be particularly varied, including both bioturbated mudstones, shell-banks and even bioherms – and showing a substantial degree of local spatial variation (Möller, 1989). It could therefore be a well-suited study system to explore many environmental dynamics and factors related to faunal turnover and change, within a comparative ordination framework.

There are also a number of more purely methodological and technical factors that might improve future studies. For instance, using more advanced image recognition and -analysis software may help in alleviating some of the biases, irreproducibility and imprecision of lithology and bioturbation measurement used in this study. Especially in the case of bioturbation, image recognition software tools like those developed by Dorador and Rodríguez-Tovar (2014), could be helpful in identifying and delineating bioturbated fabrics more reliably and in a more reproducible manner than the human eye.

New, dynamic approaches to ordination like the model-based framework developed by van der Veen et al. (2021) – which is designed to accommodate individual (unequal) species niche widths in ordination gradients, might also be very interesting to explore in future studies.

Potentially, it might be more equipped to face potential challenges of unequal taxonomic resolutions producing unequal niche widths. However, these methods are also typically more “data hungry” than traditional ordination methods, and somewhat more mathematically advanced (van der Veen et al., 2021), meaning they would have to be applied with care and knowledge.

Finally, a more general and subtle research trend to which I hope this thesis might also contribute to, is for the language of gradient analysis to take its place even more comfortably within paleoecology. Both literally in terms of the methods and analyses employed, but also in a broader conceptual sense. To paraphrase the philosopher Ludwig Wittgenstein: The limits of our language are, to a large extent, also the limits of our world. And faced with the formidable task of piecing together and making sense of the creatures and ecosystems in Earth's deepest past through the tiny keyhole of the fossil record – both in light of our present predicaments and on the past's own terms – I believe it will be a great strength to strive towards making our world of scientific thought as large, rich and nuanced as the very complex, wondrous Earth system we set out to study.

References

- Aberhan, M., & Kiessling, W. (2012). *Phanerozoic Marine Biodiversity: A Fresh Look at Data, Methods, Patterns and Processes*. https://doi.org/10.1007/978-90-481-3428-1_1
- Aldridge, R., Jeppsson, L., & Dornig, K. (1993). Early silurian oceanic episodes and events. *Journal of the Geological Society*, *150*, 501–513. <https://doi.org/10.1144/gsjgs.150.3.0501>
- Alroy, J. (2004). Are Sepkoski's evolutionary faunas dynamically coherent? *Evolutionary Ecology Research*, *6*.
- Alroy, J. (2010). The shifting balance of diversity among major marine animal groups. *Science*, *329*(5996), 1191–1194. <https://doi.org/10.1126/science.1189910>
- Alroy, J. (2015). A simple way to improve multivariate analyses of paleoecological data sets. *Paleobiology*, *41*(3), 377–386. <https://doi.org/10.1017/pab.2014.21>
- Alroy, J., Aberhan, M., Bottjer, D. J., Foote, M., Fürsich, F. T., Harries, P. J., Hendy, A. J. W., Holland, S. M., Ivany, L. C., Kiessling, W., Kosnik, M. A., Marshall, C. R., McGowan, A. J., Miller, A. I., Olszewski, T. D., Patzkowsky, M. E., Peters, S. E., Villier, L., Wagner, P. J., ... Visaggi, C. C. (2008). Phanerozoic trends in the global diversity of marine invertebrates. *Science*, *321*(5885), 97–100. <https://doi.org/10.1126/science.1156963>
- Alroy, J., Marshall, C., Bambach, R., Bezusko, K., Foote, M., Fürsich, F. T., Hansen, T., Holland, S., Ivany, L., Jablonski, D., Jacobs, D., Jones, D. C., Kosnik, M., Lidgard, S., Low, S., Miller, A., Novack-Gottshall, P., Olszewski, T., Patzkowsky, M., ... Webber, A. (2001). Effects of sampling standardization on estimates of Phanerozoic marine diversification. *Proceedings of the National Academy of Sciences of the United States of America*. <https://doi.org/10.1073/pnas.111144698>
- Alvaro, J.-J., Aretz, M., Boulvain, F., Munnecke, A., Vachard, D., & Vennin, E. (2007). Fabric transitions from shell accumulations to reefs: An introduction with Palaeozoic examples. *Geological Society, London, Special Publications*, *275*. <https://doi.org/10.1144/GSL.SP.2007.275.01.01>
- Amati, L., & Westrop, S. R. (2006). Sedimentary facies and trilobite biofacies along an Ordovician shelf to basin gradient, Viola Group, South-Central Oklahoma. *PALAIOS*, *21*(6), 516–529.
- Austin, M. P. (1985). Continuum concept, ordination methods, and niche theory. *Annual Review of Ecology and Systematics*, *16*, 39–61.
- Ayoub-Hannaa, W., Huntley, J. W., & Fürsich, F. T. (2013). Significance of Detrended Correspondence Analysis (DCA) in palaeoecology and biostratigraphy: A case study from the Upper Cretaceous of Egypt. *Journal of African Earth Sciences*, *80*, 48–59. <https://doi.org/10.1016/j.jafrearsci.2012.11.012>
- Azmy, K., Veizer, J., Jin, J., Copper, P., & Brand, U. (2006). Paleobathymetry of a Silurian shelf based on brachiopod assemblages: An oxygen isotope test. *Canadian Journal of Earth Sciences*, *43*(3), 281–293. <https://doi.org/10.1139/e05-109>
- Baarli, B. G. (1981). *En analyse av fossil-samfunn og faciesvariasjoner i Solvikformasjonen (Undersilur) i Oslo og Asker* [Cand. scient.]. University of Oslo.
- Baarli, B. G. (1988). Bathymetric co-ordination of proximity: Trends and level-bottom communities: A case study from the Lower Silurian of Norway. *PALAIOS*, *3*(6), 577–586. <https://doi.org/10.2307/3514446>
- Baarli, B. G. (1990a). Depositional environments in the Telychian stage (Silurian) of the central Oslo region, Norway. *Geological Journal*, *25*(2), 65–79. <https://doi.org/10.1002/gj.3350250202>
- Baarli, B. G. (1990b). Peripheral bulge of a foreland basin in the Oslo Region during the Early Silurian. *Palaeogeography, Palaeoclimatology, Palaeoecology*, *78*(1–2), 149.
- Baarli, B. G., & Johnson, M. (1988). Biostratigraphy of key brachiopod lineages from the Llandovery Series (Lower Silurian) of the Oslo Region. *Norsk Geologisk Tidsskrift*, *68*, 259–274.
- Baarli, B. G., Johnson, M., & Antoshkina, A. (2003). Silurian stratigraphy and paleogeography of Baltica. *New York State Museum Bulletin*, *493*, 3–34.
- Baarli, B. G., Johnson, M., & KEILEN, H. (1992). Size and shape distribution of level-bottom tabulate corals and stromatoporoids (Silurian). *Lethaia*, *25*, 269–282. <https://doi.org/10.1111/j.1502-3931.1992.tb01396.x>
- Baarli, B. G., Keilen, H. B., & Johnson, M. E. (1999). Silurian communities of the Oslo region, Norway. In A. J. Boucot & J. D. Lawson (Eds.), *Paleocommunities: A case study from the Silurian and Lower Devonian* (pp. 327–349). Cambridge University Press.
- Bambach, R. K., Knoll, A. H., & Sepkoski, J. J. (2002). Anatomical and ecological constraints on Phanerozoic animal diversity in the marine realm. *Proceedings of the National Academy of Sciences*, *99*(10), 6854–6859. <https://doi.org/10.1073/pnas.092150999>
- Barbacka, M., Kustatscher, E., & Bodor, E. R. (2019). Ferns of the Lower Jurassic from the Mecsek Mountains (Hungary): Taxonomy and palaeoecology. *Paläontologische Zeitschrift*, *93*(1), 151–185. <https://doi.org/10.1007/s12542-018-0430-8>
- Beals, E. W. (1973). Ordination: Mathematical elegance and ecological naivete. *Journal of Ecology*, *61*(1), 23–35. <https://doi.org/10.2307/2258914>

- Bennington, J. B., & Bambach, R. K. (1996). Statistical testing for paleocommunity recurrence: Are similar fossil assemblages ever the same? *Palaeogeography, Palaeoclimatology, Palaeoecology*, *127*(1–4), 107–133. [https://doi.org/10.1016/s0031-0182\(96\)00090-9](https://doi.org/10.1016/s0031-0182(96)00090-9)
- Bialik, O. M., Jarochowska, E., & Grossowicz, M. (2021). Ordination analysis in sedimentology, geochemistry and palaeoenvironment—Background, current trends and recommendations. *The Depositional Record*, *7*(3), 541–563. <https://doi.org/10.1002/dep2.161>
- Bonelli Jr., J. R., Brett, C. E., Miller, A. I., & Bennington, J. B. (2006). Testing for faunal stability across a regional biotic transition: Quantifying stasis and variation among recurring coral-rich biofacies in the Middle Devonian Appalachian Basin. *Paleobiology*, *32*(1), 20–37. Scopus. <https://doi.org/10.1666/05009.1>
- Bottjer, D. J., Droser, M. L., & Jablonski, D. (1988). Palaeoenvironmental trends in the history of trace fossils. *Nature*, *333*(6170), 252–255. <https://doi.org/10.1038/333252a0>
- Boucot, A. J. (1975). *Evolution and extinction rate controls* (Vol. 1). Elsevier.
- Boucot, A. J. (1981). *Principles of benthic marine paleoecology*. Academic Press.
- Boucot, A. J., & Lawson, J. D. (1999). *Paleocommunities: A case study from the Silurian and Lower Devonian*. Cambridge University Press.
- Brand, U., & Veizer, J. (1980). Chemical diagenesis of a multicomponent carbonate system; 1, Trace elements. *Journal of Sedimentary Research*, *50*(4), 1219–1236. <https://doi.org/10.1306/212F7BB7-2B24-11D7-8648000102C1865D>
- Brown, R. J. (1986). SEM examination of carbonate microfacies using acetate peels. *Journal of Sedimentary Petrology*, *56*(4), 538.
- Bruton, D. L., Gabrielsen, R. H., & Larsen, B. T. (2010). The Caledonides of the Oslo Region, Norway—Stratigraphy and structural elements. *Norwegian Journal of Geology*, *90*(3), 93–121.
- Buckley, H. L., & Freckleton, R. P. (2010). Understanding the role of species dynamics in abundance–occupancy relationships. *Journal of Ecology*, *98*(3), 645–658. <https://doi.org/10.1111/j.1365-2745.2010.01650.x>
- Bush, A. M., & Bambach, R. K. (2011). Paleoecologic megatrends in marine metazoa. *Annual Review of Earth and Planetary Sciences*, *39*(1), 241–269. <https://doi.org/10.1146/annurev-earth-040809-152556>
- Bush, A. M., Bambach, R. K., & Daley, G. M. (2007). Changes in theoretical ecospace utilization in marine fossil assemblages between the mid-Paleozoic and late Cenozoic. *Paleobiology*, *33*(1), 76–97.
- Bush, A. M., Bambach, R. K., & Erwin, D. H. (2011). Ecospace utilization during the Ediacaran radiation and the Cambrian eco-explosion. In M. Laflamme, J. D. Schiffbauer, & S. Q. Dornbos (Eds.), *Quantifying the Evolution of Early Life: Numerical Approaches to the Evaluation of Fossils and Ancient Ecosystems* (pp. 111–133). Springer Netherlands. https://doi.org/10.1007/978-94-007-0680-4_5
- Bush, A. M., & Brame, R. I. (2010). Multiple paleoecological controls on the composition of marine fossil assemblages from the Frasnian (Late Devonian) of Virginia, with a comparison of ordination methods. *Paleobiology*, *36*(4), 573–591. <https://doi.org/10.1666/07022.1>
- Bush, A. M., Kowalewski, M., Hoffmeister, A. P., Bambach, R. K., & Daley, G. M. (2007). Potential paleoecologic biases from size-filtering of fossils: Strategies for sieving. *PALAIOS*, *22*(6), 612–622.
- Calner, M. (2008). Silurian global events – at the tipping point of climate change. In A. M. T. Elewa (Ed.), *Mass Extinction* (pp. 21–57). Springer. https://doi.org/10.1007/978-3-540-75916-4_4
- Ceballos, G., Ehrlich, P. R., Barnosky, A. D., García, A., Pringle, R. M., & Palmer, T. M. (2015). Accelerated modern human-induced species losses: Entering the sixth mass extinction. *Science Advances*. <https://doi.org/10.1126/sciadv.1400253>
- Chahouki, M. A. Z. (2013). Classification and ordination methods as a tool for analyzing of plant communities. In *Multivariate Analysis in Management, Engineering and the Sciences*. IntechOpen. <https://www.intechopen.com/chapters/undefined/state.item.id>
- Cherns, L., Wheeley, J. R., & Wright, V. P. (2011). Taphonomic bias in shelly faunas through time: Early aragonitic dissolution and its implications for the fossil record. In P. A. Allison & D. J. Bottjer (Eds.), *Taphonomy: Process and Bias Through Time* (pp. 79–105). Springer Netherlands. https://doi.org/10.1007/978-90-481-8643-3_3
- Christie, M., Holland, S. M., & Bush, A. M. (2013). Contrasting the ecological and taxonomic consequences of extinction. *Paleobiology*, *39*(4), 538–559.
- Cisne, J. L., & Rabe, Bruce. (1978). Coenocorrelation: Gradient analysis of fossil communities and its applications in stratigraphy. *Lethaia*, *11*(4), 341–364. <https://doi.org/10.1111/j.1502-3931.1978.tb01893.x>
- Clapham, M. E. (2011). Ordination methods and the evaluation of Ediacaran communities. In *Topics in Geobiology* (pp. 3–21). Springer. https://doi.org/10.1007/978-94-007-0680-4_1

- Cocks, L. R. M., & Torsvik, T. H. (2005). Baltica from the late Precambrian to mid-Palaeozoic times: The gain and loss of a terrane's identity. *Earth-Science Reviews*, 72(1), 39–66. <https://doi.org/10.1016/j.earscirev.2005.04.001>
- Cohen, K. M., Finney, S. C., Gibbard, P. L., & Fan, J.-X. (2013). The ICS international chronostratigraphic chart. *Episodes*, 36(3), 199–204.
- Copper, P. (2002). Silurian and Devonian Reefs: 80 Million Years of Global Greenhouse between two Ice Ages. In W. Klessling, E. Flügel, & J. Golonka (Eds.), *Phanerozoic Reef Patterns* (Vol. 72). Society for Sedimentary Geology. <https://pubs.geoscienceworld.org/sepm/books/book/1123/chapter/10559112/Silurian-and-Devonian-Reefs80-Million-Years-of>
- Cramer, B. D., Brett, C. E., Melchin, M. J., Männik, P., Kleffner, M. A., McLaughlin, P. I., Loydell, D. K., Munnecke, A., Jeppsson, L., Corradini, C., Brunton, F. R., & Saltzman, M. R. (2011). Revised correlation of Silurian Provincial Series of North America with global and regional chronostratigraphic units and $\delta^{13}\text{C}$ chemostratigraphy. *Lethaia*, 44(2), 185–202. <https://doi.org/10.1111/j.1502-3931.2010.00234.x>
- Cramer, B. D., & Saltzman, M. R. (2007). Fluctuations in epeiric sea carbonate production during Silurian positive carbon isotope excursions: A review of proposed paleoceanographic models. *Palaeogeography, Palaeoclimatology, Palaeoecology*, 245(1), 37–45. <https://doi.org/10.1016/j.palaeo.2006.02.027>
- da Silva, A.-C., & Boulvain, F. (2006). Upper Devonian carbonate platform correlations and sea level variations recorded in magnetic susceptibility. *Palaeogeography, Palaeoclimatology, Palaeoecology*, 240(3), 373–388. <https://doi.org/10.1016/j.palaeo.2006.02.012>
- da Silva, A.-C., Dekkers, M. J., Mabille, C., & Boulvain, F. (2012). Magnetic susceptibility and its relationship with paleoenvironments, diagenesis and remagnetization: Examples from the Devonian carbonates of Belgium. *Studia Geophysica et Geodaetica*, 56(3), 677–704. <https://doi.org/10.1007/s11200-011-9005-9>
- Dale, M. B. (1975). On objectives of methods of ordination. *Vegetatio*, 30(1), 15–32. <https://doi.org/10.1007/BF02387874>
- Davies, J. R., Waters, R. A., Molyneux, S. G., Williams, M., Zalasiewicz, J. A., & Vandenbroucke, T. R. A. (2016). Gauging the impact of glacioeustasy on a mid-latitude early Silurian basin margin, mid Wales, UK. *Earth-Science Reviews*, 156, 82–107. <https://doi.org/10.1016/j.earscirev.2016.02.004>
- Dean, C. D., Allison, P. A., Hampson, G. J., & Hill, J. (2019). Aragonite bias exhibits systematic spatial variation in the Late Cretaceous Western Interior Seaway, North America. *Paleobiology*, 45(4), 571–597. <https://doi.org/10.1017/pab.2019.33>
- Dean, M. T., Owen, A. W., Bowdler-Hicks, A., & Akhurst, M. C. (2010). Discriminating faunal assemblages and their palaeoecology based on museum collections: The Carboniferous Hurler and Index limestones of western Scotland. *Scottish Journal of Geology*, 46, 45–57. <https://doi.org/10.1144/0036-9276/01-399>
- Derry, L. A., Kaufman, A. J., & Jacobsen, S. B. (1992). Sedimentary cycling and environmental change in the Late Proterozoic: Evidence from stable and radiogenic isotopes. *Geochimica et Cosmochimica Acta*, 56(3), 1317–1329. [https://doi.org/10.1016/0016-7037\(92\)90064-P](https://doi.org/10.1016/0016-7037(92)90064-P)
- Dhungana, A., & Mitchell, E. G. (2021). Facilitating corals in an early Silurian deep-water assemblage. *Palaeontology*, 64(3), 359–370. <https://doi.org/10.1111/pala.12527>
- Dirzo, R., Young, H. S., Galetti, M., Ceballos, G., Isaac, N. J. B., & Collen, B. (2014). Defaunation in the Anthropocene. *Science*. <https://doi.org/10.1126/science.1251817>
- Dorador, J., & Rodríguez-Tovar, F. J. (2014). Quantitative estimation of bioturbation based on digital image analysis. *Marine Geology*, 349, 55–60. <https://doi.org/10.1016/j.margeo.2014.01.003>
- Droser, M., Bottjer, D., Sheehan, P., & Mcghee, G. R. (2000). Decoupling of taxonomic and ecologic severity of Phanerozoic marine mass extinctions. *Geology*, 28(8), 675–678. [https://doi.org/10.1130/0091-7613\(2000\)28<675:DOTAES>2.0.CO;2](https://doi.org/10.1130/0091-7613(2000)28<675:DOTAES>2.0.CO;2)
- Droser, M. L., Bottjer, D. J., & Sheehan, P. M. (1997). Evaluating the ecological architecture of major events in the Phanerozoic history of marine invertebrate life. *Geology*, 25(2), 167. [https://doi.org/10.1130/0091-7613\(1997\)025<0167:eteaom>2.3.co;2](https://doi.org/10.1130/0091-7613(1997)025<0167:eteaom>2.3.co;2)
- Dunham, R. J. (1962). Classification of carbonate rocks according to depositional textures. In W. E. Ham (Ed.), *Classification of Carbonate Rocks—A Symposium* (pp. 108–121). American Association of Petroleum Geologists. <http://archives.datapages.com/data/specpubs/carbona2/data/a038/a038/0001/0100/0108.htm>
- Edinger, E. N., Copper, P., Risk, M. J., & Atmojo, W. (2002). Oceanography and reefs of recent and Paleozoic tropical epeiric seas. *Facies*, 47, 127–149. <https://doi.org/10.1007/BF02667710>
- Eilertsen, O., Økland, R. H., Økland, T., & Pedersen, O. (1990). Data manipulation and gradient length estimation in DCA ordination. *Journal of Vegetation Science*, 1(2), 261–270. <https://doi.org/10.2307/3235663>

- Flügel, E. (2004). *Microfacies of Carbonate Rocks: Analysis, Interpretation and Application* (1st ed.). Springer.
- Folk, R. L. (1962). Spectral subdivision of limestone types. In W. E. Ham (Ed.), *Classification of Carbonate Rocks—A Symposium* (pp. 62–84). American Association of Petroleum Geologists.
<http://archives.datapages.com/data/specpubs/carbona2/data/a038/a038/0001/0050/0062.html>
- Foote, M., Crampton, J. S., Beu, A. G., & Nelson, C. S. (2015). Aragonite bias, and lack of bias, in the fossil record: Lithological, environmental, and ecological controls. *Paleobiology*, *41*(2), 245–265.
<https://doi.org/10.1017/pab.2014.16>
- Forcino, F. L., Barclay, K., Schneider, C. L., Linge-Johnsen, S., & Leighton, L. R. (2013). The influence of dataset decisions on paleocommunity results: Comparison of different categorizations of two datasets from Devonian carbonate units. *Palaeogeography, Palaeoclimatology, Palaeoecology*, *386*, 479–491.
<https://doi.org/10.1016/j.palaeo.2013.06.016>
- Forcino, F. L., Leighton, L. R., Twerdy, P., & Cahill, J. F. (2015). Reexamining sample size requirements for multivariate, abundance-based community research: When resources are limited, the research does not have to be. *PLOS ONE*, *10*(6), e0128379. <https://doi.org/10.1371/journal.pone.0128379>
- Forcino, F. L., Richards, E. J., Leighton, L. R., Chojnacki, N., & Stafford, E. S. (2012). The sensitivity of paleocommunity sampling strategy at different spatiotemporal scales. *Palaeogeography, Palaeoclimatology, Palaeoecology*, *313–314*, 246–253. <https://doi.org/10.1016/j.palaeo.2011.12.002>
- Forcino, F. L., Ritterbush, K. A., & Stafford, E. S. (2015). Evaluating the effectiveness of the Mantel test and Procrustes randomization test for exploratory ecological similarity among paleocommunities. *Palaeogeography Palaeoclimatology Palaeoecology*, *426*, 199–208.
<https://doi.org/10.1016/j.palaeo.2015.03.023>
- Forcino, F. L., & Stafford, E. S. (2020). The influence of collection method on paleoecological datasets: In-place versus surface-collected fossil samples in the Pennsylvanian Finis Shale, Texas, USA. *PLOS ONE*, *15*(2), e0228944. <https://doi.org/10.1371/journal.pone.0228944>
- Forcino, F. L., Stafford, E. S., & Leighton, L. R. (2012). Perception of paleocommunities at different taxonomic levels: How low must you go? *Palaeogeography, Palaeoclimatology, Palaeoecology*, *365–366*, 48–56.
<https://doi.org/10.1016/j.palaeo.2012.09.011>
- Forcino, F. L., Stafford, E., Warner, J., Webb, A., Leighton, L., Schneider, C., Michlin, T., Palazzolo, L., Morrow, J., & Schellenberg, S. A. (2010). Effects of data categorization on paleocommunity analysis: A case study from the Pennsylvanian Finis Shale of Texas. *Palaios*, *25*, 144–157.
<https://doi.org/10.2110/palo.2009.p09-011r>
- Fortey, R. (2014). The palaeoecology of trilobites. *Journal of Zoology*, *292*(4), 250–259.
<https://doi.org/10.1111/jzo.12108>
- Fürsich, F., & Oschmann, W. (1993). Shell beds as tools in basin analysis: The Jurassic of Kachchh, western India. *Journal of The Geological Society - J GEOL SOC*, *150*, 169–185.
<https://doi.org/10.1144/gsjgs.150.1.0169>
- Ganai, J. A., Rashid, S. A., & Romshoo, S. A. (2018). Evaluation of terrigenous input, diagenetic alteration and depositional conditions of Lower Carboniferous carbonates of Tethys Himalaya, India. *Solid Earth Sciences*, *3*(2), 33–49. <https://doi.org/10.1016/j.sesci.2018.03.002>
- Gauch Jr., H. G., & Whittaker, R. H. (1972). Coenocline simulation. *Ecology*, *53*(3), 446–451.
<https://doi.org/10.2307/1934231>
- Greenacre, M. J. (2010). Correspondence analysis. *WIREs Computational Statistics*, *2*(5), 613–619.
<https://doi.org/10.1002/wics.114>
- Gushulak, C. A. C., & Jin, J. S. (2017). Post-extinction recovery and diversification of reef-dwelling brachiopod communities: Examples from the lower Silurian of Hudson Bay Basin, Canada. *Palaeogeography Palaeoclimatology Palaeoecology*, *485*, 605–621. <https://doi.org/10.1016/j.palaeo.2017.07.016>
- Gutteridge, P. (1985). Grain-size measurement from acetate peels. *Journal of Sedimentary Petrology*, *55*(4), 595–596.
- Hendy, A., J. W. (2013). Spatial and stratigraphic variation of marine paleoenvironments in the middle-upper Gatun Formation, Isthmus of Panama. *Palaios*, *28*(4), 210–227. <https://doi.org/10.2110/palo.2012.p12-024r>
- Hennebert, M., & Lees, A. (1991). Environmental gradients in carbonate sediments and rocks detected by correspondence analysis: Examples from the Recent of Norway and the Dinantian of southwest England. *Sedimentology*, *38*(4), 623–642. <https://doi.org/10.1111/j.1365-3091.1991.tb01012.x>
- Hill, M. O. (1974). Correspondence analysis: A neglected multivariate method. *Journal of the Royal Statistical Society. Series C (Applied Statistics)*, *23*(3), 340–354. <https://doi.org/10.2307/2347127>
- Hill, M. O., & Gauch, H. G. (1980). Detrended correspondence analysis: An improved ordination technique. *Vegetatio*, *42*(1), 47–58. <https://doi.org/10.1007/BF00048870>
- Hoffman, A. (1979). Community paleoecology as an epiphenomenal science. *Paleobiology*, *5*(4), 357–379.

- Holland, S. M. (2005). The Signatures of Patches and Gradients in Ecological Ordinations. *PALAIOS*, 20(6), 573–580.
- Holland, S. M., Miller, A. I., Meyer, D. L., & F. Dattilo, B. (2001). The detection and importance of subtle biofacies within a single lithofacies: The Upper Ordovician Kope Formation of the Cincinnati, Ohio Region. *Palaios*, 16, 205–217.
- Hotelling, H. (1933). Analysis of a complex of statistical variables into principal components. *Journal of Educational Psychology*, 24(6), 417–441. <https://doi.org/10.1037/h0071325>
- Hounslow, M. W., Ratcliffe, K. T., Harris, S. E., Nawrocki, J., Wojcik, K., Montgomery, P., & Woodcock, N. H. (2021). The Telychian (early Silurian) oxygenation event in northern Europe: A geochemical and magnetic perspective. *Palaeogeography Palaeoclimatology Palaeoecology*, 567, 110277. <https://doi.org/10.1016/j.palaeo.2021.110277>
- Huang, B., Harper, D. A. T., Rong, J. Y., & Zhan, R. B. (2017). Brachiopod faunas after the end Ordovician mass extinction from South China: Testing ecological change through a major taxonomic crisis. *Journal of Asian Earth Sciences*, 138, 502–514. <https://doi.org/10.1016/j.jseae.2017.02.043>
- Huang, B., Jin, J., & Rong, J. Y. (2018). Post-extinction diversification patterns of brachiopods in the early-middle Llandovery, Silurian. *Palaeogeography Palaeoclimatology Palaeoecology*, 493, 11–19. <https://doi.org/10.1016/j.palaeo.2017.12.025>
- Huang, B., Zhan, R. B., & Wang, G. X. (2016). Recovery brachiopod associations from the lower Silurian of South China and their paleoecological implications. *Canadian Journal of Earth Sciences*, 53(7), 674–679. <https://doi.org/10.1139/cjes-2015-0193>
- Jeppson, L. (1997). The anatomy of the mid-Early Silurian Ireviken Event. *Paleontological Events : Stratigraphic, Ecological, and Evolutionary Implications*, 451–492.
- Jeppson, L., & Calner, M. (2002). The Silurian Mulde Event and a scenario for secundo-secundo events. *Earth and Environmental Science Transactions of the Royal Society of Edinburgh*, 93. <https://doi.org/10.1017/S0263593300000377>
- Jeppsson, L. (1990). An oceanic model for lithological and faunal changes tested on the Silurian record. *Journal of the Geological Society*, 147(4), 663–674. <https://doi.org/10.1144/gsjgs.147.4.0663>
- Jeppsson, L. (1996). Recognition of a probable secundo-primario event in the Early Silurian. *Lethaia*, 29(4), 311–315. <https://doi.org/10.1111/j.1502-3931.1996.tb01666.x>
- Jia-Yu, R., & Harper, D. A. T. (1999). Brachiopod survival and recovery from the latest Ordovician mass extinctions in South China. *Geological Journal*, 34(4), 321–348. [https://doi.org/10.1002/\(SICI\)1099-1034\(199911/12\)34:4<321::AID-GJ809>3.0.CO;2-I](https://doi.org/10.1002/(SICI)1099-1034(199911/12)34:4<321::AID-GJ809>3.0.CO;2-I)
- Jin, J. (2008). Environmental control on temporal and spatial differentiation of Early Silurian pentameride brachiopod communities, Anticosti Island, eastern Canada. *Canadian Journal of Earth Sciences*, 45, 159–187. <https://doi.org/10.1139/E07-045>
- Johnson, M. E. (1989). Tempestites recorded as variable Pentamerus layers in the lower Silurian of southern Norway. *Journal of Paleontology*, 63(2), 195–205.
- Johnson, M. E. (2006). Relationship of Silurian sea-level fluctuations to oceanic episodes and events. *GFF*, 128(2), 115–121. <https://doi.org/10.1080/11035890601282115>
- Johnson, M. E., Baarli, B. G., Nestor, H., Rubel, M., & Worsley, D. (1991). Eustatic sea-level patterns from the Lower Silurian (Llandovery Series) of southern Norway and Estonia. *GSA Bulletin*, 103(3), 315–335. [https://doi.org/10.1130/0016-7606\(1991\)103<0315:ESLPFT>2.3.CO;2](https://doi.org/10.1130/0016-7606(1991)103<0315:ESLPFT>2.3.CO;2)
- Kartverket. (2015). *N250 kartdata* [Map]. Kartkatalogen, Geonorge.
- Kartverket. (2017). *N50 kartdata* [Map]. Kartkatalogen, Geonorge.
- Keilen, H. B. (1985). *Tabulate koraller og avsetningsmiljøet i Rytteråkerformasjonen, silur, Oslo og Bærum* [Cand. scient. thesis]. University of Oslo.
- Kenrick, P., Wellman, C. H., Schneider, H., & Edgecombe, G. D. (2012). A timeline for terrestrialization: Consequences for the carbon cycle in the Palaeozoic. *Philosophical Transactions of the Royal Society B: Biological Sciences*, 367(1588), 519–536. <https://doi.org/10.1098/rstb.2011.0271>
- Kiær, J. (1908). *Das Obersilur im Kristianiagebiete: Eine stratigraphisch-faunistische Untersuchung*. Published by commission by Jacob Dybwad. https://urn.nb.no/URN:NBN:no-nb_digibok_2009042212002
- Kidwell, S. M., Fürsich, F. T., & Aigner, T. (1986). Conceptual framework for the analysis and classification of fossil concentrations. *PALAIOS*, 1(3), 228–238. <https://doi.org/10.2307/3514687>
- Klug, C., Samankassou, E., Pohle, A., De Baets, K., Franchi, F., & Korn, D. (2018). Oases of biodiversity: Early Devonian palaeoecology at Hamar Laghdad, Morocco. *Neues Jahrbuch Für Geologie Und Paläontologie - Abhandlungen*, 290(1–3), 9–48. <https://doi.org/10.1127/njgpa/2018/0772>
- Landing, E., & Johnson, M. (Eds.). (1998). *Silurian cycles linkages of dynamic stratigraphy with atmospheric, oceanic, and tectonic cycles*. New York State Museum.
- Larsson, K. (1979). Silurian tentaculitids from Gotland and Scania. *Fossils and Strata*, 11.
- Legendre, P., & Legendre, L. (1998). *Numerical Ecology* (2nd ed.). Elsevier.

- Legendre, P., & Legendre, L. (2012). Ordination in reduced space. In P. Legendre & L. Legendre (Eds.), *Developments in Environmental Modelling* (Vol. 24, pp. 425–520). Elsevier. <https://doi.org/10.1016/B978-0-444-53868-0.50009-5>
- Li, Q.-N., Zhang, C., & Cao, M. (2022). An ordinal weighted EDM model for nonmetric multidimensional scaling. *Asia-Pacific Journal of Operational Research*, 39(03), 2150033. <https://doi.org/10.1142/S0217595921500330>
- Li, Y., & Rong, J. (2007). Shell concentrations of Early Silurian virgianid brachiopods in northern Guizhou: Temporal and spatial distribution and tempestite formation. *Chinese Science Bulletin*, 52(12), 1680–1691. <https://doi.org/10.1007/s11434-007-0224-y>
- Liu, H., Økland, T., Halvorsen, R., Gao, J., Liu, Q., Eilertsen, O., & Bratli, H. (2008). Gradients analyses of forests ground vegetation and its relationships to environmental variables in five subtropical forest areas, S and SW China. *Sommerfeltia*, 32(1), 3–196. <https://doi.org/10.2478/v10208-011-0012-6>
- Lokier, S. W., & Al Junaibi, M. (2016). The petrographic description of carbonate facies: Are we all speaking the same language? *Sedimentology*, 63(7), 1843–1885. <https://doi.org/10.1111/sed.12293>
- López, G. I. (2013). Walther's Law of Facies. In W. J. Rink & J. Thompson (Eds.), *Encyclopedia of Scientific Dating Methods* (pp. 1–2). Springer Netherlands. https://doi.org/10.1007/978-94-007-6326-5_30-1
- Mahecha, M. D., Martínez, A., Lischeid, G., & Beck, E. (2007). Nonlinear dimensionality reduction: Alternative ordination approaches for extracting and visualizing biodiversity patterns in tropical montane forest vegetation data. *Ecological Informatics*, 2(2), 138–149. <https://doi.org/10.1016/j.ecoinf.2007.05.002>
- Mamet, S. D., Young, N., Chun, K. P., & Johnstone, J. F. (2016). What is the most efficient and effective method for long-term monitoring of alpine tundra vegetation? *Arctic Science*, 2(3), 127–141. <https://doi.org/10.1139/as-2015-0020>
- McGhee, G. R., Clapham, M. E., Sheehan, P. M., Bottjer, D. J., & Droser, M. L. (2013). A new ecological-severity ranking of major Phanerozoic biodiversity crises. *Palaeogeography, Palaeoclimatology, Palaeoecology*, 370, 260–270. <https://doi.org/10.1016/j.palaeo.2012.12.019>
- McGhee, G. R., Jr, Sheehan, P. M., Bottjer, D. J., & Droser, M. L. (2012). Ecological ranking of Phanerozoic biodiversity crises: The Serpukhovian (early Carboniferous) crisis had a greater ecological impact than the end-Ordovician. *Geology*, 40(2), 147–150. <https://doi.org/10.1130/G32679.1>
- McGowan, A. J., & Smith, A. B. (2008). Are global Phanerozoic marine diversity curves truly global? A study of the relationship between regional rock records and global Phanerozoic marine diversity. *Paleobiology*, 34(1), 80–103.
- McKerrow, W. S. (Ed.). (1978). *The Ecology of fossils: An illustrated guide* (1st ed.). Duckworth.
- McLaughlin, P. I., Emsbo, P., Brett, C. E., Bancroft, A. M., Desrochers, A., & Vandenbroucke, T. R. A. (2019). The rise of pinnacle reefs: A step change in marine evolution triggered by perturbation of the global carbon cycle. *Earth and Planetary Science Letters*, 515, 13–25. <https://doi.org/10.1016/j.epsl.2019.02.039>
- Mead, A. (1992). Review of the development of multidimensional scaling methods. *Journal of the Royal Statistical Society. Series D (The Statistician)*, 41(1), 27–39. <https://doi.org/10.2307/2348634>
- Melchin, M. J., Mitchell, C. E., Holmden, C., & Štorch, P. (2013). Environmental changes in the Late Ordovician–early Silurian: Review and new insights from black shales and nitrogen isotopes. *GSA Bulletin*, 125(11–12), 1635–1670. <https://doi.org/10.1130/B30812.1>
- Miller, A. I., Holland, S. M., Meyer, D. L., & Dattilo, B. F. (2001). The use of faunal gradient analysis for intraregional correlation and assessment of changes in sea-floor topography in the type Cincinnati. *The Journal of Geology*, 109(5), 603–613. <https://doi.org/10.1086/321965>
- Minchin, P. (1987). An evaluation of the relative robustness of techniques for ecological ordination. *Vegetatio*, 69(1–3), 89–107. <https://doi.org/10.1007/BF00038690>
- Möller, N. K. (1987). A lower silurian transgressive carbonate succession in Ringerike (Oslo region, Norway). *Sedimentary Geology*, 51(3), 215–247. [https://doi.org/10.1016/0037-0738\(87\)90049-2](https://doi.org/10.1016/0037-0738(87)90049-2)
- Möller, N. K. (1989). Facies analysis and palaeogeography of the Rytteråker Formation (lower Silurian, Oslo region, Norway). *Palaeogeography, Palaeoclimatology, Palaeoecology*, 69, 167–192. [https://doi.org/10.1016/0031-0182\(89\)90163-6](https://doi.org/10.1016/0031-0182(89)90163-6)
- Mørk, A. (1978). *En stratigrafisk, sedimentologisk og paleoøkologisk undersøkelse av de undersiluriske sedimenter (6c-7b) med hovedvekt på Bjerkøya ved Holmestrand* [Cand. real]. University of Oslo.
- Mørk, A. (1981). A reappraisal of the lower Silurian brachiopods *Borealis* and *Pentamerus*. *Palaeontology*, 24(3), 537–553.
- Munnecke, A., Calner, M., Harper, D. A. T., & Servais, T. (2010). Ordovician and Silurian sea–water chemistry, sea level, and climate: A synopsis. *Palaeogeography, Palaeoclimatology, Palaeoecology*, 296(3), 389–413. <https://doi.org/10.1016/j.palaeo.2010.08.001>
- Myers, C. E., Stigall, A. L., & Lieberman, B. S. (2015). PaleoENM: Applying ecological niche modeling to the fossil record. *Paleobiology*, 41(2), 226–244. <https://doi.org/10.1017/pab.2014.19>

- North American Commission on Stratigraphic Nomenclature. (2005). North American Stratigraphic Code. *AAPG Bulletin*, 89(11), 1547–1591. <https://doi.org/10.1306/07050504129>
- Novack-Gottshall, P. M. (2007). Using a theoretical ecospace to quantify the ecological diversity of Paleozoic and modern marine biotas. *Paleobiology*, 33(2), 273–294. <https://doi.org/10.1666/06054.1>
- Ohgaki, S.-I. (2011). Semi-quantitative Survey Methods and the Utility of Relative Abundance. *Japanese Journal of Benthology*, 66(1), 33–39. <https://doi.org/10.5179/benthos.66.33>
- Økland, R. H. (1986). Rescaling of ecological gradients. I. Calculation of ecological distance between vegetation stands by means of their floristic composition. *Nordic Journal of Botany*, 6(5), 651–660. <https://doi.org/10.1111/j.1756-1051.1986.tb00464.x>
- Økland, R. H. (1990). Vegetation ecology: Theory, methods and applications with reference to Fennoscandia. *Sommerfeltia*, 1(s1), 1–238. <https://doi.org/10.2478/som-1990-0003>
- Økland, R. H. (1996). Are ordination and constrained ordination alternative or complementary strategies in general ecological studies? *Journal of Vegetation Science*, 7(2), 289–292. <https://doi.org/10.2307/3236330>
- Økland, R. H. (2007). Wise use of statistical tools in ecological field studies. *Folia Geobotanica*, 42(2), 123. <https://doi.org/10.1007/BF02893879>
- Økland, R. H., Økland, T., & Rydgren, K. (2001). Vegetation-environment relationships of boreal spruce swamp forests in Østmarka Nature Reserve, SE Norway. *Sommerfeltia*, 29(1), 1–1. <https://doi.org/10.2478/som-2001-0001>
- Oksanen, J., Blanchet, F. G., Friendly, M., Kindt, R., Legendre, P., McGlinn, D., Minchin, P. R., O’Hara, R. B., Simpson, G. L., Solymos, P., Stevens, M. H. H., Szoecs, E., & Wagner, H. (2019). *vegan: Community Ecology Package*. <https://CRAN.R-project.org/package=vegan>
- Patzkowsky, M. E., & Holland, S. M. (2016). Biotic invasion, niche stability, and the assembly of regional biotas in deep time: Comparison between faunal provinces. *Paleobiology*, 42(3), 359–379. <https://doi.org/10.1017/pab.2016.1>
- Pearson, K. (1901). LIII. On lines and planes of closest fit to systems of points in space. *The London, Edinburgh, and Dublin Philosophical Magazine and Journal of Science*, 2(11), 559–572. <https://doi.org/10.1080/14786440109462720>
- Peres-Neto, P. R., & Jackson, D. A. (2001). How well do multivariate data sets match? The advantages of a Procrustean superimposition approach over the Mantel test. *Oecologia*, 129(2), 169–178. <https://doi.org/10.1007/s004420100720>
- Peters, S. E. (2007). The problem with the Paleozoic. *Paleobiology*, 33(2), 165–181.
- Peters, S. E. (2008). Environmental determinants of extinction selectivity in the fossil record. *Nature*, 454(7204), 626–629. <https://doi.org/10.1038/nature07032>
- Prosser, C. W., Skinner, K. M., & Sedivec, K. K. (2003). Comparison of 2 techniques for monitoring vegetation on military lands. *Journal of Range Management*, 56(5), 446–454. <https://doi.org/10.2307/4003835>
- Rojas, A., Calatayud, J., Kowalewski, M., Neuman, M., & Rosvall, M. (2021). A multiscale view of the Phanerozoic fossil record reveals the three major biotic transitions. *Communications Biology*, 4(1). <https://doi.org/10.1038/s42003-021-01805-y>
- Rosser, N. (2017). Shortcuts in biodiversity research: What determines the performance of higher taxa as surrogates for species? *Ecology and Evolution*, 7(8), 2595–2603. <https://doi.org/10.1002/ece3.2736>
- Rothman, D. (2017). Thresholds of catastrophe in the Earth system. *Science Advances*, 3(9). <https://doi.org/10.1126/sciadv.1700906>
- Ryland, J. S., Warner, G. F., Harper, J. L., Rosen, B. R., & White, J. (1986). Growth and form in modular animals: Ideas on the size and arrangement of zooids. *Philosophical Transactions of the Royal Society of London. B, Biological Sciences*, 313(1159), 53–76. <https://doi.org/10.1098/rstb.1986.0025>
- Saeedi, H., Warren, D., & Brandt, A. (2022). The Environmental Drivers of Benthic Fauna Diversity and Community Composition. *Frontiers in Marine Science*, 9. <https://www.frontiersin.org/articles/10.3389/fmars.2022.804019>
- Schmidt, D. N. (2018). Determining climate change impacts on ecosystems: The role of palaeontology. *Palaeontology*, 61(1), 1–12. <https://doi.org/10.1111/pala.12335>
- Scrutton, C. T. (1998). The Palaeozoic corals, II: Structure, variation and palaeoecology. *Proceedings of the Yorkshire Geological Society*, 52(1), 1–57. <https://doi.org/10.1144/pygs.52.1.1>
- Sepkoski, J. J. (1981). A factor analytic description of the Phanerozoic marine fossil record. *Paleobiology*, 7(1), 36–53. <https://doi.org/10.1017/S0094837300003778>
- Servais, T., Owen, A. W., Harper, D. A. T., Kröger, B., & Munnecke, A. (2010). The Great Ordovician Biodiversification Event (GOBE): The palaeoecological dimension. *Palaeogeography, Palaeoclimatology, Palaeoecology*, 294(3), 99–119. <https://doi.org/10.1016/j.palaeo.2010.05.031>

- Shi, G. (1993). Multivariate data-analysis in paleoecology and paleobiogeography—A review. *Palaeogeography Palaeoclimatology Palaeoecology*, 105(3–4), 199–234. [https://doi.org/10.1016/0031-0182\(93\)90084-V](https://doi.org/10.1016/0031-0182(93)90084-V)
- Simoës, M., Rodrigues, S., Leme, J., & Bissaro Júnior, M. C. (2005). The settling pattern of brachiopod shells: Stratigraphic and taphonomic implications to shell bed formation and paleoecology. *Brazilian Journal of Geology (Former Revista Brasileira de Geociências)*, 35, 383–391. <https://doi.org/10.25249/0375-7536.2005353383391>
- Simpson, G. L., Oksanen, J., & Rodriguez-Sanchez, F. (2021). *coenocliner: Coenocline Simulation (0.2-3)*. <https://CRAN.R-project.org/package=coenocliner>
- Siveter, D. J. (1984). Ecology of silurian ostracodes. In M. G. Bassett & J. D. Lawson (Eds.), *Autecology of Silurian Organisms*. The Palaeontological Association.
- Sneltorp, S. K. (2020). Pentamerus. In *Store norske leksikon*. <http://snl.no/Pentamerus>
- Speden, I. G. (1966). Paleocology and the study of fossil benthic assemblages and communities. *New Zealand Journal of Geology and Geophysics*, 9(4), 408–423. <https://doi.org/10.1080/00288306.1966.10422485>
- Stemans, P., Hérissé, A. L., Melvin, J., Miller, M. A., Paris, F., Verniers, J., & Wellman, C. H. (2009). Origin and radiation of the earliest vascular land plants. *Science (New York, N.Y.)*, 324(5925), 353. <https://doi.org/10.1126/science.1169659>
- Størmer, L. (1953). The Middle Ordovician of the Oslo Region, Norway. 1. Introduction to stratigraphy. *Norsk Geologisk Tidsskrift*, 31, 37–142.
- ter Braak, C. J. F. (1985). Correspondence Analysis of incidence and abundance data: Properties in terms of a unimodal response model. *Biometrics*, 41(4), 859–873. <https://doi.org/10.2307/2530959>
- ter Braak, C. J. F., & Looman, C. W. N. (1986). Weighted averaging, logistic regression and the Gaussian response model. *Vegetatio*, 65(1), 3–11. <https://doi.org/10.1007/BF00032121>
- ter Braak, C. J. F., & Prentice, I. C. (1988). A theory of gradient analysis. In *Advances in Ecological Research* (pp. 271–317). Elsevier. [https://doi.org/10.1016/s0065-2504\(08\)60183-x](https://doi.org/10.1016/s0065-2504(08)60183-x)
- Thuy, B., Eriksson, M. E., Kutscher, M., Lindgren, J., Numberger-Thuy, L. D., & Wright, D. F. (2022). Miniaturization during a Silurian environmental crisis generated the modern brittle star body plan. *Communications Biology*, 5(1), 14. <https://doi.org/10.1038/s42003-021-02971-9>
- Tornabene, C., Martindale, R. C., Wang, X. T., & Schaller, M. F. (2017). Detecting photosymbiosis in fossil Scleractinian corals. *Scientific Reports*, 7, 9465. <https://doi.org/10.1038/s41598-017-09008-4>
- Trotter, J. A., Williams, I. S., Barnes, C. R., Männik, P., & Simpson, A. (2016). New conodont $\delta^{18}\text{O}$ records of Silurian climate change: Implications for environmental and biological events. *Palaeogeography, Palaeoclimatology, Palaeoecology*, 443(1), 34–48. <https://doi.org/10.1016/j.palaeo.2015.11.011>
- Tuomisto, H. (2010). A consistent terminology for quantifying species diversity? Yes, it does exist. *Oecologia*, 164(4), 853–860. <https://doi.org/10.1007/s00442-010-1812-0>
- Turvey, S. T. (2005). Early Ordovician (Arenig) trilobite palaeoecology and palaeobiogeography of the South China Plate. *Palaeontology*, 48, 519–547. <https://doi.org/10.1111/j.1475-4983.2005.00468.x>
- Tyler, C. L., & Kowalewski, M. (2014). Utility of marine benthic associations as a multivariate proxy of paleobathymetry: A direct test from recent coastal ecosystems of North Carolina. *PLOS ONE*, 9(4), e95711. <https://doi.org/10.1371/journal.pone.0095711>
- van der Veen, B., Hui, F. K. C., Hovstad, K. A., Solbu, E. B., & O'Hara, R. B. (2021). Model-based ordination for species with unequal niche widths. *Methods in Ecology and Evolution*, 12(7), 1288–1300. <https://doi.org/10.1111/2041-210x.13595>
- van Son, T. C., & Halvorsen, R. (2014). Multiple parallel ordinations: The importance of choice of ordination method and weighting of species abundance data. *Sommerfeltia*, 37(1), 1–37. <https://doi.org/10.2478/som-2014-0001>
- van Son, T. C., Halvorsen, R., Norling, K., Bakke, T., Kaurin, M., & Melsom, F. (2014). Identification of fine-scale marine benthic ecoclines by multiple parallel ordination. *Journal of Marine Biology*, 2014, e462529. <https://doi.org/10.1155/2014/462529>
- Wagner, H. H. (2004). Direct multi-scale ordination with canonical correspondence analysis. *Ecology*, 85(2), 342–351. <https://doi.org/10.1890/02-0738>
- Wartenberg, D., Ferson, S., & Rohlf, F. (1987). Putting things in order: A critique of detrended correspondence analysis. *American Naturalist - AMER NATURALIST*, 129. <https://doi.org/10.1086/284647>
- Watkins, R. (1994). Evolution of Silurian Pentamerid communities in Wisconsin. *PALAIOS*, 9(5), 488–499. <https://doi.org/10.2307/3515138>
- Watkins, R. (1996). Skeletal composition of Silurian benthic marine faunas. *PALAIOS*, 11(6), 550–558. <https://doi.org/10.2307/3515190>
- Webber, A. J. (2002). High-resolution faunal gradient analysis and an assessment of the causes of meter-scale cyclicity in the type Cincinnati Series (Upper Ordovician). *PALAIOS*, 17(6), 545–555. [https://doi.org/10.1669/0883-1351\(2002\)017<0545:HRFGAA>2.0.CO;2](https://doi.org/10.1669/0883-1351(2002)017<0545:HRFGAA>2.0.CO;2)

- Whalen, M. T., & Day, J. E. (Jed). (2008). Magnetic susceptibility, biostratigraphy, and sequence stratigraphy: Insights into Devonian carbonate platform development and basin infilling, Western Alberta, Canada. In L. Simo (Ed.), *Controls on Carbonate Platform and Reef Development* (pp. 291–314). Society for Sedimentary Geology.
<https://pubs.geoscienceworld.org/sepm/books/book/1134/chapter/10564438/Magnetic-Susceptibility-Biostratigraphy-and>
- Whittaker, R. H. (1967). Gradient analysis of vegetation. *Biological Reviews*, 42(2), 207–264.
<https://doi.org/10.1111/j.1469-185X.1967.tb01419.x>
- Wickham, H. (2016). *ggplot2: Elegant Graphics for Data Analysis*. Springer-Verlag New York.
<https://ggplot2.tidyverse.org>
- Wickham, H., Averick, M., Bryan, J., Chang, W., McGowan, L. D., François, R., Grolemund, G., Hayes, A., Henry, L., Hester, J., Kuhn, M., Pedersen, T. L., Miller, E., Bache, S. M., Müller, K., Ooms, J., Robinson, D., Seidel, D. P., Spinu, V., ... Yutani, H. (2019). Welcome to the tidyverse. *Journal of Open Source Software*, 4(43), 1686. <https://doi.org/10.21105/joss.01686>
- Wilson, M. A., & Palmer, T. J. (1989). Preparation of acetate peels. In R. M. Feldmann, R. E. Chapman, & J. T. Hannibal (Eds.), *Paleotechniques* (pp. 142–145). Paleontological Society.
- World Street Map*. (2022). [Map].
https://basemaps.arcgis.com/arcgis/rest/services/World_Basemap_v2/VectorTileServer
- Worsley, D., Aarhus, N., Bassett, M. G., Howe, M. P. A., Mørk, A., & Olaussen, S. (1983). The Silurian Succession of the Oslo Region. *Norges Geologiske Undersøkelser*, 384, 60.
- Yue, L., & Kershaw, S. (2003). Reef reconstruction after extinction events of the latest Ordovician in the Yangtze platform, South China. *Facies*, 48(1), 269–284. <https://doi.org/10.1007/BF02667544>
- Zapalski, M. K. (2014). Evidence of photosymbiosis in Palaeozoic tabulate corals. *Proceedings of the Royal Society B: Biological Sciences*, 281(1775), 20132663. <https://doi.org/10.1098/rspb.2013.2663>
- Zapalski, M. K., & Berkowski, B. (2019). The Silurian mesophotic coral ecosystems: 430 million years of photosymbiosis. *Coral Reefs*, 38(1), 137–147. <https://doi.org/10.1007/s00338-018-01761-w>
- Zdealveindy. (2014). *Comparison of Correspondence Analysis and Detrended Correspondence Analysis on example (ideal) data*. Own work. <https://commons.wikimedia.org/wiki/File:CA-vs-DCA-made-by-vegan.png>
- Zhang, S., Jowett, D. M. S., & Barnes, C. R. (2017). Hirnantian (Ordovician) through Wenlock (Silurian) conodont biostratigraphy, bioevents, and integration with graptolite biozones, Cape Phillips Formation slope facies, Cornwallis Island, Canadian Arctic Islands. *Canadian Journal of Earth Sciences*, 54(9), 936–960. <https://doi.org/10.1139/cjes-2017-0023>
- Ziegler, A. M., Cocks, L. R. M., & Bambach, R. K. (1968). Composition and structure of Lower Silurian marine communities. *Lethaia*, 1(1), 1-. <https://doi.org/10.1111/j.1502-3931.1968.tb01724.x>

Appendix

This appendix contains an overview of the polished slabs and acetate peels collected for this thesis. The rest of the raw data, analyses and R-scripts can be accessed publicly at GitHub via this link: <https://github.com/audunrug/Paleoecology-of-the-Rytteraker-formation-MSc-thesis-data.git>.

Supplementary table 1. Overview of acetate peel samples. Height = meters above formation base, with the exception of the ULV-2 section, where it denotes meters below formation top. Orientation denotes whether the acetate peel was taken parallel to bedding (parallel) or perpendicular to bedding (cross-long = longest side perpendicular, cross-short = shortest side perpendicular). Scanned = whether the acetate peel was scanned and digitized. SF-count = whether the acetate peel has been counted for the morphotaxa study. Thin section = whether a corresponding thin section has been made from the area of the slab represented in the acetate peel.

locality	PMO	height	orientation	scanned	SF-count	thin section	comment
TOV_2	236.403a	-0,2	cross-long	x			Gastropod dominated
TOV_2	236.402a	-0,2	cross-short	x			Gastropod dominated
TOV_2	236.412a	0,1	cross-short	x	x		
TOV_2	236.413a	0,1	parallel	x	x		
TOV_2	236.404a	0,3	unknown	x	x		
TOV_2	236.405a	0,3	unknown	x	x	x	
TOV_2	236.406a	1,0	cross-long	x	x		
TOV_2	236.406b	1,0	cross-long	x	x	x	
TOV_2	236.407a	1,0	parallel	x	x		
TOV_2	236.408a	2,0	cross-short	x	x		
TOV_2	236.409a	2,0	parallel	x	x		
TOV_2	236.410a	2,5	parallel	x	x		
TOV_2	236.410b	2,5	parallel	x	x	x	
TOV_2	236.411a	2,5	cross-long	x	x		
TOV_2	236.411b	2,5	cross-long	x			
TOV_2	236.414a	4,0	cross-short	x	x		
TOV_2	236.415a	4,0	parallel	x			
TOV_2	236.416a	5,1	unknown	x	x		
TOV_2	236.417a	5,1	unknown	x	x	x	
TOV_2	236.418a	5,9	cross-long	x	x		
TOV_2	236.418b	5,9	cross-long				Identical to 236.418a
TOV_2	236.419a	5,9	parallel	x	x		
TOV_2	236.419b	5,9	parallel	x			
TOV_2	236.425a	5,9	unknown	x			
TOV_2	236.424a	5,9	unknown				
TOV_2	236.420a	7,0	parallel	x			
TOV_2	236.421a	7,0	cross-short	x	x	x	
TOV_2	236.423a	9,0	parallel	x	x		
TOV_2	236.422a	9,0	cross-long	x	x		
TOV_2	236.422b	9,0	cross-long	x		x	

TOV_2	236.426a	9,9	cross-short	x		
TOV_2	236.427a	9,9	parallel	x		
TOV_2	236.427b	9,9	parallel	x	x	x
TOV_2	236.428a	9,9	parallel	x		
TOV_2	236.429a	10,0	cross-long	x	x	
TOV_2	236.429b	10,0	cross-long	x		
TOV_2	236.430a	10,0	parallel	x		
TOV_2	236.430b	10,0	parallel	x	x	x
TOV_2	236.431a	10,5	unknown	x		
TOV_2	236.432a	11,5	cross-short	x	x	
TOV_2	236.433a	11,5	cross-short	x		
TOV_2	236.433b	11,5	cross-short	x	x	
TOV_2	236.434a	11,5	cross-long	x		
TOV_2	236.435a	12,5	cross-short	x		
TOV_2	236.436a	12,5	parallel	x		
TOV_2	236.438a	12,8	cross-short	x	x	
TOV_2	236.437a	12,8	parallel	x		
TOV_2	236.440a	13,0	parallel	x		
TOV_2	236.440b	13,0	parallel	x	x	
TOV_2	236.439a	13,0	cross-long	x		x
TOV_2	236.439b	13,0	cross-long	x		
TOV_2	236.441a	13,5	unknown	x		
TOV_2	236.442a	13,8	cross-short	x	x	
TOV_2	236.441a	13,8	cross-long	x		
TOV_2	236.444b	14,5	unknown	x		
TOV_2	236.445a	14,5	unknown	x		
TOV_2	236.444a	14,5	unknown	x		
TOV_2	???	14,5	unknown	x		Missing slab
TOV_2	236.443a	14,5	cross-short	x	x	
TOV_2	236.446a	14,5	unknown	x		
TOV_2	236.446b	14,5	unknown	x		
TOV_2	236.463a	14,5	unknown	x		
TOV_2	236.447a	15,0	cross-short	x		
TOV_2	236.447b	15,0	parallel	x		x
TOV_2	236.448a	15,0	parallel	x		
TOV_2	236.448b	15,0	parallel	x		
TOV_2	236.450a	15,2	cross-short	x	x	
TOV_2	236.450b	15,2	cross-long	x	x	x
TOV_2	236.449a	15,2	parallel	x	x	x
TOV_2	236.451a	15,5	parallel	x		
TOV_2	236.451b	15,5	parallel	x		
TOV_2	236.452a	15,5	cross-short	x		
TOV_2	236.453a	15,9	parallel	x	x	
TOV_2	236.454a	15,9	cross-long	x		

TOV_2	236.454b	15,9	cross-long	x			
TOV_2	236.455a	16,5	cross-short	x			
TOV_2	236.456a	16,5	cross-long	x			
TOV_2	236.457a	17,3	parallel	x	x		
TOV_2	236.457b	17,3	parallel	x			
TOV_2	236.457c	17,3	parallel	x			
TOV_2	236.458a	17,3	cross-long	x			
TOV_2	236.458b	17,3	cross-short	x			
TOV_2	236.459a	18,1	parallel	x			
TOV_2	236.459b	18,1	parallel	x			
TOV_2	236.460a	18,1	cross-short	x	x		x
TOV_2	236.461a	18,2	cross-long	x	x		
TOV_2	236.462a	18,2	parallel	x	x		
TOV_2	236.462b	18,2	parallel	x	x		
TOV_2	236.464a	19,0	parallel	x	x		x
TOV_2	236.465a	19,0	cross-short	x	x		
TOV_2	236.468a	20,0	parallel	x	x		x
TOV_2	236.466a	20,0	cross-long	x	x		
TOV_2	236.466b	20,0	cross-long	x	x		
TOV_2	236.467a	20,0	parallel	x	x		
TOV_2	236.468a	20,0	parallel	x			Missing slab
TOV_2	???	20,0	cross-long	x			Missing slab
TOV_2	236.470a	20,9	parallel	x	x		
TOV_2	236.469a	20,9	cross-short	x	x		
TOV_2	236.472a	22,4	parallel	x	x		
TOV_2	236.471a	22,4	cross-short	x	x		
TOV_2	236.473a	25,0	cross-short	x	x		x
TOV_2	236.474a	25,0	parallel	x	x		
TOV_2	236.476a	27,6	parallel	x			
TOV_2	236.476b	27,6	parallel	x	x		
TOV_2	236.475a	27,6	cross-short	x	x		
TOV_2	236.475b	27,6	cross-short	x	x		
TOV_2	236.475c	27,6	cross-long	x	x		
TOV_2	236.477a	29,5	parallel	x	x		x
TOV_2	236.477b	29,5	parallel	x	x		
TOV_2	236.478a	29,5	cross-short	x	x		
TOV_2	236.478b	29,5	cross-short	x			
TOV_2	236.479a	30,2	cross-short	x	x		
TOV_2	236.480a	30,2	parallel	x	x		
TOV_2	236.481a	31,0	parallel	x	x		
TOV_2	236.482a	31,0	cross-short	x	x		
TOV_2	236.483a	31,9	parallel	x	x		
TOV_2	236.484a	31,9	cross-long	x	x		
TOV_2	236.484b	31,9	cross-long	x	x		x

TOV_2	236.485a	33,0	parallel	x	x		
TOV_2	236.485b	33,0	parallel	x	x		
TOV_2	236.486a	33,0	cross-long	x	x		
TOV_2	236.486b	33,0	cross-short	x	x		
TOV_2	236.487a	34,0	parallel	x			Dom. by rugose coral
TOV_2	236.488a	34,0	parallel	x	x		
TOV_2	236.488b	34,0	parallel	x	x		
TOV_2	236.489a	34,0	cross-short	x	x		
TOV_2	236.490a	36,0	cross-short	x			Dom. by favositid
TOV_2	236.491a	36,0	cross-short	x			Dom. by favositid
TOV_2	236.492a	36,0	parallel	x	x	x	
TOV_2	236.493a	36,0	parallel	x	x		
TOV_2	236.493b	36,0	parallel				
TOV_2	236.495a	37,0	cross-long	x	x		
TOV_2	236.494a	37,0	cross-short	x	x		
TOV_2	236.497a	38,0	cross-short	x	x	x	
TOV_2	236.496a	38,0	parallel	x	x		
ULV_1	236.500a	0,2	unknown	x	x		
ULV_1	236.501a	0,2	unknown	x	x		
ULV_1	236.502a	0,2	unknown	x			
ULV_1	236.503a	1,0	cross-short				
ULV_1	236.504a	1,0	parallel				
ULV_1	236.504b	1,0	parallel				
ULV_1	236.505a	2,1	cross-long	x	x		
ULV_1	236.506a	2,1	cross-short	x	x		
ULV_1	236.507a	3,1	parallel	x	x		
ULV_1	236.508a	3,1	cross-short	x	x		
ULV_1	236.509a	4,0	parallel				
ULV_1	236.509b	4,0	parallel				
ULV_1	236.510a	4,0	cross-short	x	x		
ULV_1	236.511a	5,0	parallel	x	x		
ULV_1	236.512a	5,5	cross-short	x	x		
ULV_1	236.513a	5,5	parallel	x	x		
ULV_1	236.514a	6,0	cross-long	x	x		
ULV_1	236.515a	6,0	cross-long	x	x		
ULV_1	236.516a	6,6	unknown	x	x		
ULV_1	236.517a	7,0	parallel				
ULV_1	236.518a	7,0	cross-short				
ULV_1	236.519a	8,0	parallel				
ULV_1	236.520a	8,0	parallel	x	x		
ULV_1	236.520b	8,0	cross-short				
ULV_1	236.521a	8,5	parallel				
ULV_1	236.522a	8,5	cross-short	x	x		
ULV_1	236.523a	9,5	cross-long	x			

ULV_1	236.524a	9,5	parallel	x	x
ULV_1	236.525a	9,5	cross-long	x	
ULV_1	236.525b	9,5	cross-long	x	x
ULV_2	236.533a	-32,0	cross-short	x	
ULV_2	236.533b	-32,0	cross-short	x	x
ULV_2	236.534a	-32,0	parallel	x	x
ULV_2	236.535a	-32,0	parallel	x	
ULV_2	236.536a	-31,0	cross-short	x	
ULV_2	236.537a	-31,0	parallel	x	x
ULV_2	236.538a	-31,0	parallel	x	
ULV_2	236.539a	-30,0	parallel	x	x
ULV_2	236.540a	-30,0	cross-short	x	
ULV_2	236.540b	-30,0	cross-short	x	
ULV_2	236.541a	-29,0	cross-short	x	x
ULV_2	236.542a	-29,0	parallel	x	
ULV_2	236.543a	-28,0	parallel	x	x
ULV_2	236.544a	-28,0	cross-short	x	
ULV_2	236.545a	-27,0	cross-short	x	
ULV_2	236.546a	-27,0	parallel	x	x
ULV_2	236.547a	-26,0	parallel	x	x
ULV_2	236.548a	-26,0	parallel	x	x
ULV_2	236.549a	-25,0	parallel	x	x
ULV_2	236.550a	-25,0	cross-short	x	
ULV_2	236.551a	-24,0	cross-short	x	
ULV_2	236.552a	-24,0	parallel	x	x
ULV_2	236.553a	-23,0	cross-short	x	x
ULV_2	236.554a	-23,0	cross-short	x	
ULV_2	236.555a	-23,0	parallel	x	x
ULV_2	236.556a	-21,5	cross-long	x	x
ULV_2	236.557a	-21,5	cross-short	x	x
ULV_2	236.558a	-22,0	parallel	x	
ULV_2	236.559a	-22,0	cross-short	x	x
ULV_2	236.560a	-22,0	cross-long	x	x
ULV_2	236.561a	-21,0	cross-short	x	
ULV_2	236.562a	-21,0	parallel	x	x
ULV_2	236.563a	-21,0	parallel	x	x
ULV_2	236.564a	-20,0	cross-short	x	x
ULV_2	236.565a	-20,0	parallel	x	x
ULV_2	236.566a	-19,0	cross-long	x	x
ULV_2	236.567a	-19,0	parallel	x	x
ULV_2	236.568a	-19,0	cross-short	x	x
ULV_2	236.569a	-18,0	parallel	x	x
ULV_2	236.570a	-18,0	cross-short	x	x
ULV_2	236.571a	-17,0	cross-short	x	x

Dom. by rugose coral

ULV_2	236.572a	-17,0	parallel	x	x
ULV_2	236.573a	-16,5	cross-short	x	x
ULV_2	236.574a	-16,5	parallel	x	x
ULV_2	236.575a	-16,0	cross-short	x	x
ULV_2	236.576a	-15,0	parallel	x	x
ULV_2	236.577a	-15,0	cross-short	x	x
ULV_2	236.578a	-14,0	cross-short		
ULV_2	236.579a	-14,0	parallel		
ULV_2	236.580a	-13,0	cross-short	x	x
ULV_2	236.581a	-13,0	parallel	x	x
ULV_2	236.582a	-12,0	cross-short	x	x
ULV_2	236.583a	-12,0	parallel	x	x
ULV_2	236.584a	-11,0	parallel	x	x
ULV_2	236.585a	-11,0	parallel	x	x
ULV_2	236.586a	-10,0	parallel		
ULV_2	236.587a	-10,0	cross-short	x	x
ULV_2	236.588a	-9,0	parallel	x	x
ULV_2	236.589a	-9,0	parallel	x	x
ULV_2	236.590a	-8,0	parallel	x	x
ULV_2	236.591a	-8,0	cross-long		
ULV_2	236.592a	-7,0	parallel	x	x
ULV_2	236.593a	-7,0	cross-short	x	x
ULV_2	236.594a	-6,5	parallel		
ULV_2	236.595a	-6,5	cross-short	x	x
ULV_2	236.596a	-5,5	parallel	x	x
ULV_2	236.597a	-5,5	cross-short	x	x
ULV_2	236.598a	-5,0	cross-short	x	x
ULV_2	236.598b	-5,0	cross-short	x	x
ULV_2	236.599a	-5,0	cross-short	x	x
ULV_2	236.599b	-5,0	parallel	x	x
ULV_2	236.600a	-4,0	parallel	x	x
ULV_2	236.601a	-4,0	cross-short	x	x
ULV_2	236.602a	-4,0	parallel	x	x
ULV_2	236.603a	-4,0	cross-short	x	x
ULV_2	236.604a	-3,5	parallel	x	x
ULV_2	236.605a	-3,5	cross-short	x	x
ULV_2	236.606a	-2,5	cross-short	x	x
ULV_2	236.607a	-2,5	parallel	x	x
ULV_2	236.608a	0,5	unknown	x	x
ULV_2	236.609a	0,5	unknown	x	x
SUM	244			225	157

Supplementary table 2. Overview of polished slabs used to make acetate peels and conduct the brachiopod shell orientation analysis. Height = meters above formation base, with the exception of the ULV-2 section, where it denotes meters below formation top. Orientation denotes whether the acetate peel was taken parallel to bedding (parallel) or perpendicular to bedding (cross). # peels = the number of acetate peels with PMO numbers made from the slab. Shell orientation analysis = whether the slab was used for the brachiopod shell orientation analysis.

locality	PMO	height	orientation	# peels	Shell orientation analysis
236.402	TOV2	-0,2	cross	1	
236.403	TOV2	-0,2	cross	1	
236.404	TOV2	0,3	unknown	1	
236.405	TOV2	0,3	unknown	1	
236.406	TOV2	1,0	cross	2	x
236.407	TOV2	1,0	parallel	1	
236.408	TOV2	2,0	cross	1	
236.409	TOV2	2,0	parallel	1	
236.410	TOV2	2,5	parallel	2	
236.411	TOV2	2,5	cross	2	
236.412	TOV2	0,1	cross	1	
236.413	TOV2	0,1	parallel	1	
236.414	TOV2	4,0	cross	1	
236.415	TOV2	4,0	parallel	1	
236.416	TOV2	5,1	unknown	1	
236.417	TOV2	5,1	unknown	1	
236.418	TOV2	5,9	cross	2	x
236.419	TOV2	5,9	parallel	2	x
236.420	TOV2	7,0	parallel	1	
236.421	TOV2	7,0	cross	1	
236.422	TOV2	9,0	cross	2	x
236.423	TOV2	9,0	parallel	1	
236.424	TOV2	5,9	unknown	1	
236.425	TOV2	5,9	unknown	1	
236.426	TOV2	9,9	cross	1	x
236.427	TOV2	9,9	parallel	2	
236.428	TOV2	9,9	parallel	1	
236.429	TOV2	10,0	cross	2	x
236.430	TOV2	10,0	parallel	2	
236.431	TOV2	10,5	unknown	1	
236.432	TOV2	11,5	cross	1	x
236.433	TOV2	11,5	cross	2	
236.434	TOV2	11,5	cross	1	
236.435	TOV2	12,5	cross	1	x
236.436	TOV2	12,5	parallel	1	
236.437	TOV2	12,8	parallel	1	
236.438	TOV2	12,8	cross	1	x

236.439	TOV2	13,0	cross	2	x
236.440	TOV2	13,0	parallel	2	x
236.441	TOV2	13,8	cross	1	x
236.442	TOV2	13,8	cross	1	x
236.443	TOV2	14,5	unknown	1	x
236.444	TOV2	14,5	unknown	2	
236.445	TOV2	14,5	unknown	1	
236.446	TOV2	14,5	unknown	2	
236.447	TOV2	15,0	both	2	
236.448	TOV2	15,0	parallel	2	
236.449	TOV2	15,2	parallel	1	
236.450	TOV2	15,2	cross	2	x
236.451	TOV2	15,5	parallel	2	
236.452	TOV2	15,5	cross	1	x
236.453	TOV2	15,9	parallel	1	
236.454	TOV2	15,9	cross	2	x
236.455	TOV2	16,5	cross	1	x
236.456	TOV2	16,5	cross	1	x
236.457	TOV2	17,3	parallel	3	
236.458	TOV2	17,3	cross	2	x
236.459	TOV2	18,1	parallel	2	
236.460	TOV2	18,1	cross	1	x
236.461	TOV2	18,2	cross	1	x
236.462	TOV2	18,2	parallel	2	
236.463	TOV2	14,5	unknown	1	
236.464	TOV2	19,0	cross	1	
236.465	TOV2	19,0	parallel	1	x
236.466	TOV2	20,0	cross	2	x
236.467	TOV2	20,0	parallel	1	
236.468	TOV2	20,0	parallel	1	
236.469	TOV2	20,9	cross	1	x
236.470	TOV2	20,9	parallel	1	
236.471	TOV2	22,4	cross	1	
236.472	TOV2	22,4	parallel	1	
236.473	TOV2	25,0	cross	1	x
236.474	TOV2	25,0	parallel	1	
236.475	TOV2	27,6	cross	3	x
236.476	TOV2	27,6	parallel	2	
236.477	TOV2	29,5	parallel	2	
236.478	TOV2	29,5	cross	2	x
236.479	TOV2	30,2	cross	1	
236.480	TOV2	30,2	parallel	1	
236.481	TOV2	31,0	parallel	1	
236.482	TOV2	31,0	cross	1	x

236.483	TOV2	31,9	parallel	1	
236.484	TOV2	31,9	cross	2	x
236.485	TOV2	33,0	parallel	2	
236.486	TOV2	33,0	cross	2	x
236.487	TOV2	34,0	parallel	1	
236.488	TOV2	34,0	parallel	2	
236.489	TOV2	34,0	cross	1	x
236.490	TOV2	36,0	cross	1	
236.491	TOV2	36,0	cross	1	
236.492	TOV2	36,0	parallel	1	
236.493	TOV2	36,0	parallel	2	
236.494	TOV2	37,0	cross	1	x
236.495	TOV2	37,0	cross	1	
236.496	TOV2	38,0	parallel	1	
236.497	TOV2	38,0	cross	1	
236.500	ULV1	0,2	unknown	1	
236.501	ULV1	0,2	unknown	1	
236.502	ULV1	0,2	unknown	1	
236.503	ULV1	1,0	cross-short	1	
236.504	ULV1	1,0	parallel	2	
236.505	ULV1	2,1	cross	1	
236.506	ULV1	2,1	cross-short	1	
236.507	ULV1	3,1	parallel	1	
236.508	ULV1	3,1	cross	1	
236.509	ULV1	4,0	parallel	2	
236.510	ULV1	4,0	cross	1	
236.511	ULV1	5,0	parallel	1	
236.512	ULV1	5,5	cross	1	
236.513	ULV1	5,5	parallel	1	
236.514	ULV1	6,0	cross	1	
236.515	ULV1	6,0	cross	1	
236.516	ULV1	6,6	unknown	1	
236.517	ULV1	7,0	parallel	1	
236.518	ULV1	7,0	cross	1	
236.519	ULV1	8,0	parallel	1	
236.520	ULV1	8,0	parallel	2	
236.521	ULV1	8,5	parallel	1	
236.522	ULV1	8,5	cross	1	
236.523	ULV1	9,5	cross	1	
236.524	ULV1	9,5	parallel	1	
236.525	ULV1	9,5	cross	2	
236.533	ULV2	-32	cross	2	
236.534	ULV2	-32	parallel	1	
236.535	ULV2	-32	parallel	1	

236.536	ULV2	-31	cross	1
236.537	ULV2	-31	parallel	1
236.538	ULV2	-31	parallel	1
236.539	ULV2	-30	parallel	1
236.540	ULV2	-30	cross	2
236.541	ULV2	-29	cross	1
236.542	ULV2	-29	parallel	1
236.543	ULV2	-28	parallel	1
236.544	ULV2	-28	cross	1
236.545	ULV2	-27	cross	1
236.546	ULV2	-27	parallel	1
236.547	ULV2	-26	cross	1
236.548	ULV2	-26	parallel	1
236.549	ULV2	-25	parallel	1
236.550	ULV2	-25	cross	1
236.551	ULV2	-24	cross	1
236.552	ULV2	-24	parallel	1
236.553	ULV2	-23	parallel	1
236.554	ULV2	-23	cross	1
236.555	ULV2	-23	cross	1
236.556	ULV2	-21,5	cross	1
236.557	ULV2	-21,5	parallel	1
236.558	ULV2	-22	parallel	1
236.559	ULV2	-22	cross	1
236.560	ULV2	-22	cross	1
236.561	ULV2	-21	cross	1
236.562	ULV2	-21	parallel	1
236.563	ULV2	-21	parallel	1
236.564	ULV2	-20	parallel	1
236.565	ULV2	-20	cross	1
236.566	ULV2	-19	cross	1
236.567	ULV2	-19	parallel	1
236.568	ULV2	-19	cross	1
236.569	ULV2	-18	parallel	1
236.570	ULV2	-18	cross	1
236.571	ULV2	-17	cross	1
236.572	ULV2	-17	parallel	1
236.573	ULV2	-16,5	cross	1
236.574	ULV2	-16,5	parallel	1
236.575	ULV2	-16	cross	1
236.576	ULV2	-15	parallel	1
236.577	ULV2	-15	cross	1
236.578	ULV2	-14	cross	1
236.579	ULV2	-14	parallel	1

236.580	ULV2	-13	cross	1
236.581	ULV2	-13	parallel	1
236.582	ULV2	-12	cross	1
236.583	ULV2	-12	parallel	1
236.584	ULV2	-11	parallel	1
236.585	ULV2	-11	cross	1
236.586	ULV2	-10	parallel	1
236.587	ULV2	-10	cross	1
236.588	ULV2	-9	parallel	1
236.589	ULV2	-9	parallel	1
236.590	ULV2	-8	cross	1
236.591	ULV2	-8	cross	1
236.592	ULV2	-7	parallel	1
236.593	ULV2	-7	cross	1
236.594	ULV2	-6,5	parallel	1
236.595	ULV2	-6,5	cross	1
236.596	ULV2	-5,5	parallel	1
236.597	ULV2	-5,5	cross	1
236.598	ULV2	-5	cross	2
236.599	ULV2	-5	parallel	2
236.600	ULV2	-4	cross	1
236.601	ULV2	-4	parallel	1
236.602	ULV2	-4	parallel	1
236.603	ULV2	-4	cross	1
236.604	ULV2	-3,5	parallel	1
236.605	ULV2	-3,5	cross	1
236.606	ULV2	-2,5	cross	1
236.607	ULV2	-2,5	parallel	1
236.608	ULV2	0,5	unknown	1
236.609	ULV2	0,5	unknown	1
236.402	TOV2	-0,2	cross	1
236.403	TOV2	-0,2	cross	1
236.404	TOV2	0,3	unknown	1
236.405	TOV2	0,3	unknown	1
236.406	TOV2	1,0	cross	2
236.407	TOV2	1,0	parallel	1
236.408	TOV2	2,0	cross	1
236.409	TOV2	2,0	parallel	1
236.410	TOV2	2,5	parallel	2
SUM	199			
